

2012

# New Rotaxane Ligands for Metal Complexes and Frameworks

Darren Mercer  
*University of Windsor*

Follow this and additional works at: <http://scholar.uwindsor.ca/etd>

---

## Recommended Citation

Mercer, Darren, "New Rotaxane Ligands for Metal Complexes and Frameworks" (2012). *Electronic Theses and Dissertations*. Paper 394.

This online database contains the full-text of PhD dissertations and Masters' theses of University of Windsor students from 1954 forward. These documents are made available for personal study and research purposes only, in accordance with the Canadian Copyright Act and the Creative Commons license—CC BY-NC-ND (Attribution, Non-Commercial, No Derivative Works). Under this license, works must always be attributed to the copyright holder (original author), cannot be used for any commercial purposes, and may not be altered. Any other use would require the permission of the copyright holder. Students may inquire about withdrawing their dissertation and/or thesis from this database. For additional inquiries, please contact the repository administrator via email ([scholarship@uwindsor.ca](mailto:scholarship@uwindsor.ca)) or by telephone at 519-253-3000ext. 3208.

# New Rotaxane Ligands for Metal Complexes and Frameworks

By

Darren J. W. Mercer

A Dissertation  
submitted to the Faculty of Graduate Studies  
through the Department of Chemistry and Biochemistry  
in Partial Fulfillment of the Requirements for  
the Degree of Doctor Philosophy at the  
University of Windsor

Windsor, Ontario, Canada

2011

© Darren J. W Mercer 2011

All Rights Reserved

## **Declaration of Co-Authorship / Previous Publication**

### **I. Co-Authorship Declaration**

The collaborations in this thesis are as follows: In all cases, the key ideas, primary contributions, experimental designs, data analysis and interpretation, were performed by the author. In chapters 3 and 4, Joseph Yacoub prepared one the rotaxanes as part of an undergraduate project supervised by the author and Stephanie Loeb carried out two of the X-ray crystal structure solutions. In chapter 5, Nicholas Vukotic collected X-ray data for two of the compounds.

I am aware of the University of Windsor Senate Policy on Authorship and I certify that I have properly acknowledged the contribution of other researchers to my thesis, and have obtained written permission from each of the co-authors to include the above material in my thesis.

I certify that, with the above qualification, this thesis, and the research to which it refers, is the product of my own work.

## II. Declaration of Previous Publication

This thesis includes 3 original papers that have been previously published/submitted for publication in peer reviewed journals, as follows:

Thesis Chapter	Publication	Publication status
Chapter 2	Darren J. W. Mercer and Stephen J. Loeb “Complexes of a [2]rotaxane ligand with terminal terpyridine groups”, <i>Dalton Trans.</i> , <b>2011</b> , 40, 6385.	published
Chapter 3/4	Darren J. W. Mercer, Joseph Yacoub, Stephanie K. Loeb and Stephen J. Loeb “The effect of decorating 24-crown-8 wheels on the structures of [2]pseudorotaxane, [2]rotaxane and metal organic rotaxane frameworks”, <i>Chem. Sci.</i>	in progress
Chapter 5	Darren J. W. Mercer, V. Nicholas Vukotic and Stephen J. Loeb, “Linking [2]rotaxane wheels to create a new type of metal organic rotaxane Framework” <i>Chem. Commun.</i> <b>2011</b> , 47, 896-898.	published

I certify that I have obtained a written permission from the copyright owner to include the above published material in my thesis. I certify that the above material describes work completed during my registration as graduate student at the University of Windsor.

I declare that, to the best of my knowledge, my thesis does not infringe upon anyone’s copyright nor violate any proprietary rights and that any ideas, techniques, quotations, or any other material from the work of other people included in my thesis, published or otherwise, are fully acknowledged in accordance with the standard referencing practices.

I declare that this is a true copy of my thesis, including any final revisions, as approved by my thesis committee and the Graduate Studies office, and that this thesis has not been submitted for a higher degree to any other University or Institution.

## ABSTRACT

The focus of this thesis is the incorporation of the 1,2-bis(pyridinium)ethane motif into new [2]rotaxane ligands for the purpose of developing new metal organic rotaxane frameworks (MORFs). Both new stoppers that can act as ligands as well as new crown ethers with appended donors were synthesized and these components combined to create new [2]rotaxane ligands and eventually new MORFs.

Chapter 2, looks at the synthesis and coordination chemistry of a [2]rotaxane containing terpyridine stoppers. The [2]rotaxane was shown to form mixed ligand complexes with  $\text{Ru}^{\text{II}}$ ,  $\text{Ag}^{\text{I}}$ ,  $\text{Zn}^{\text{II}}$ , and  $\text{Pd}^{\text{II}}$ . The complexes were studied in solution by NMR, and UV/vis spectroscopy and mass spectrometry and in the solid state by X-ray crystallography.

Chapter 3 and 4, focuses on the synthesis of new tetrasubstituted dibenzo-24-crown-8 ethers and their inclusion into [2]pseudorotaxanes and [2]rotaxanes. The new [2]pseudorotaxanes and [2]rotaxanes were characterized in solution by NMR spectroscopy and mass spectrometry and in the solid state by X-ray crystallography. The new crown ethers were then used for the development of [2]rotaxane ligands and metal-organic rotaxane frameworks. The complexes were studied in solution by NMR, and UV/vis spectroscopy and mass spectrometry and in the solid state by X-ray crystallography.

Chapter 5, focuses on a new class of MORFs in which donor groups have been incorporated on to the crown ethers which allows for the [2]rotaxane ligands to link through the wheel rather than axles to propagate the coordination polymer. The highlight was formation of a coordination complex with  $\text{Cd}^{\text{II}}$  that is a 2-periodic, metal-organic

rotaxane framework. The synthesis and characterization of all the species were studied by NMR spectroscopy and mass spectrometry in solution and in the solid state by X-ray crystallography.

Chapter 6, looks at ways to combine chelating axles with coordinating crown ethers to form unique “combo” [2]rotaxane ligands capable of forming two independent frameworks by virtue of having coordinating groups on both components of the rotaxane. A new stopper based on a the polydentate ligand bis(2-pyridylmethyl)amine was developed for this purpose. “Combo” [2]rotaxane ligands were prepared and characterized in solution by NMR spectroscopy and mass spectrometry.

This work is dedicated to my mother, father, and my sister  
Thank you for always believing in me.



## **Acknowledgements**

First and foremost, I would like to thank my supervisor Dr. Steve Loeb for the guidance and patience over the years.

To my co-workers in the Loeb group past and present, especially: Dr. Kelong Zhu, Nick V. Vukotic, Nissa Frank, Michael Bolla, Elizabeth Viljoen, Dr. Nadim Noujeim, Dr. Sapna Sharma, and Dr. Natalie Suhan,

To the many people outside of the Loeb group and throughout chemistry department especially Ronan San Juan for proof reading my thesis, Mike Miller, and else of the Carmichael group.

Special thanks go out to Dr. Hilary Jenkins giving me a chance in her a lab at St. Mary's University. In addition to Dr. Matt Revington, Mr. Mike Fuerth, and Dr. Shuangquan Zhang were a tremendous help in acquiring the NMR and ESI-MS data, respectively.

Finally, I would like to thank my family for all the love and support they have given me over the years.

## Table of Contents

Declaration of Co-Authorship / Previous Publication.....	iv
Abstract.....	vi
Dedication.....	viii
Acknowledgements.....	ix
List of Figures and Schemes.....	xv
List of Tables.....	xxiii
List of Abbreviations.....	xxviii
<b>Chapter 1 Background.....</b>	<b>1</b>
<b>1.1</b> Origins of Supramolecular Chemistry.....	<b>2</b>
<b>1.2</b> Interpenetrated and Interlocked Compounds.....	<b>3</b>
<b>1.2.1</b> Pseudorotaxanes.....	<b>3</b>
<b>1.2.2</b> Measuring Association Constants.....	<b>6</b>
<b>1.2.3</b> Rotaxanes.....	<b>8</b>
<b>1.2.4</b> Early Attempts at the Synthesis of Interlocked Molecules.....	<b>8</b>
<b>1.2.5</b> Synthesis of Rotaxane Using Molecular Recognition Templates.....	<b>10</b>
<b>1.3</b> Polymeric Frameworks.....	<b>14</b>
<b>1.3.1</b> Coordination Polymers.....	<b>14</b>
<b>1.3.2</b> Metal Organic Frameworks.....	<b>17</b>
<b>1.3.3</b> Metal Organic Rotaxane Frameworks.....	<b>19</b>
<b>1.4</b> Scope of this Thesis.....	<b>26</b>
<b>Reference.....</b>	<b>27</b>

<b>Chapter 2 A [2]Rotaxane Ligand with Terminal Terpyridine Groups.....</b>	<b>32</b>
<b>2.1 Introduction.....</b>	<b>32</b>
<b>2.2 Results and Discussion.....</b>	<b>35</b>
<b>2.2.1 Terpyridine based ligands.....</b>	<b>35</b>
<b>2.2.2 Labile metal complexes.....</b>	<b>38</b>
<b>2.2.3 Inert metal complexes.....</b>	<b>41</b>
<b>2.3 Conclusions.....</b>	<b>49</b>
<b>2.4 Experimental.....</b>	<b>50</b>
<b>2.4.1 General Methods.....</b>	<b>50</b>
<b>Synthesis 4-tolyterpyridine.....</b>	<b>50</b>
<b>Synthesis bromo-4-tolyterpyridine.....</b>	<b>51</b>
<b>Synthesis [2.2][OTf]<sub>4</sub>.....</b>	<b>52</b>
<b>Synthesis [2.2-DB24C8][OTf]<sub>4</sub>.....</b>	<b>54</b>
<b>Synthesis [(Ru(terpy))<sub>2</sub>(2.2-DB24C8)][OTf]<sub>8</sub>.....</b>	<b>56</b>
<b>Synthesis [(Ru(terpy))<sub>2</sub>(2.2)][OTf]<sub>8</sub>.....</b>	<b>57</b>
<b>Synthesis [(Ag(MeCN))<sub>2</sub>(2.2-DB24C8)][OTf]<sub>6</sub>.....</b>	<b>59</b>
<b>Synthesis [(Pd(MeCN))<sub>2</sub>(2.2-DB24C8)][OTf]<sub>8</sub>.....</b>	<b>60</b>
<b>Synthesis [(Zn(H<sub>2</sub>O))<sub>3</sub>(2.2-DB24C8)][OTf]<sub>8</sub>.....</b>	<b>62</b>
<b>Reference.....</b>	<b>62</b>
<b>Chapter 3 The Effect of Crown Ether Substitution on the 1,2-Bis(pyridinium)ethane-24-Crown-8 Templating Motif.....</b>	<b>65</b>
<b>3.1 Introduction.....</b>	<b>65</b>
<b>3.2 Results and Discussion.....</b>	<b>67</b>
<b>3.2.1 Synthesis of tetrakis-substituted crown ethers.....</b>	<b>67</b>

<b>3.2.2</b>	Synthesis of [2]rotaxanes via alkylation.....	77
<b>3.2.3</b>	Synthesis of [2]rotaxanes through acylation.....	84
<b>3.3</b>	Conclusion.....	87
<b>3.4</b>	Experimental.....	88
<b>3.4.1</b>	General Methods.....	88
	Synthesis <b>TB-DB24C8</b> .....	89
	Synthesis <b>TP-DB24C8</b> .....	90
	Synthesis <b>TE-DB24C8</b> .....	92
	Synthesis [ <b>3.4</b> ▬ <b>TP-DB24C8</b> ][OTf] <sub>4</sub> .....	94
	Synthesis [ <b>3.4</b> ▬ <b>TE-DB24C8</b> ][OTf] <sub>4</sub> .....	95
	Synthesis [ <b>3.6</b> ▬ <b>TP-DB24C8</b> ][BF <sub>4</sub> ] <sub>2</sub> .....	97
	Synthesis [ <b>3.6</b> ▬ <b>TE-DB24C8</b> ][BF <sub>4</sub> ] <sub>2</sub> .....	98
	<b>Reference</b> .....	100
<b>Chapter 4</b>	<i>Effects of Crown Ether Substituents on [2]Rotaxane Ligands, Complexes and Metal-Organic Frameworks</i> .....	101
<b>4.1</b>	Introduction.....	101
<b>4.2</b>	Results and Discussion.....	102
<b>4.2.1</b>	Synthesis of Tollylterpy [2]Rotaxane.....	102
<b>4.2.2</b>	Synthesis of a 2-D polyrotaxane.....	112
<b>4.3</b>	Conclusion.....	116
<b>4.4</b>	Experimental.....	116
<b>4.4.1</b>	General Methods.....	116
	Synthesis [ <b>4.2</b> ▬ <b>TE-DB24C8</b> ][OTf] <sub>4</sub> .....	117
	Synthesis [(Ru(terpy)) <sub>2</sub> ( <b>4.2</b> ▬ <b>TE-DB24C8</b> )] [OTf] <sub>8</sub> .....	118

Synthesis [(Cd(H <sub>2</sub> O)) <sub>2</sub> ( <b>2.1</b> )( <b>4.3cTP-DB24C8</b> )] [BF <sub>4</sub> ] <sub>8</sub> .....	120
<b>Reference</b> .....	121
<b>Chapter 5</b> <i>Linking [2]Rotaxane Wheels to Create a New Type of Metal-Organic Rotaxane Framework</i> .....	122
<b>5.1</b> Introduction.....	122
<b>5.2</b> Results and Discussion.....	123
<b>5.2.1</b> Chelating [2]rotaxane.....	123
<b>5.2.2</b> Polymeric rotaxane.....	130
<b>5.3</b> Conclusion.....	138
<b>5.4</b> Experimental.....	138
<b>5.4.1</b> General Methods.....	138
Synthesis <b>TO-DB24C8</b> .....	139
Synthesis <b>T<sup>4</sup>P-DB24C8</b> .....	140
Synthesis <b>T<sup>3</sup>P-DB24C8</b> .....	142
Synthesis [ <b>5.2cTO-DB24C8</b> ] [BF <sub>4</sub> ] <sub>2</sub> .....	144
Synthesis [ <b>5.2cT<sup>4</sup>P-DB24C8</b> ] [BF <sub>4</sub> ] <sub>2</sub> .....	146
Synthesis [ <b>5.2cT<sup>3</sup>P-DB24C8</b> ] [BF <sub>4</sub> ] <sub>2</sub> .....	148
Synthesis [(Cd(MeCN) <sub>2</sub> (H <sub>2</sub> O)) <sub>2</sub> ( <b>5.2cTO-DB24C8</b> )] [BF <sub>4</sub> ] <sub>6</sub> .....	149
Synthesis [Cd <sub>2</sub> Cl <sub>4</sub> (H <sub>2</sub> O)) <sub>4</sub> ( <b>5.2cT<sup>3</sup>P-DB24C8</b> )] [BF <sub>4</sub> ] <sub>2</sub> .....	151
<b>Reference</b> .....	151
<b>Chapter 6</b> <i>[2]Rotaxane Ligands with Donors on Both the Axle and Wheel</i> .....	152
<b>6.1</b> Introduction.....	152
<b>6.2</b> Results and Discussion.....	153
<b>6.2.1</b> Synthesis of bis(2-pyridylmethyl)amine.....	153

<b>6.2.2</b>	Synthesis of a <b>BPMA</b> stoppered [2]rotaxane.....	157
<b>6.2.3</b>	[2]Rotaxane ligands with donors on both the axle and wheel.....	164
<b>6.3</b>	Conclusion.....	166
<b>6.4</b>	Experimental.....	167
<b>6.4.1</b>	General Methods.....	167
	Synthesis <b>BPMA</b> .....	167
	Synthesis <b>MeO<sub>2</sub>-BzBPMA</b> .....	169
	Synthesis [Re(CO) <sub>3</sub> ( <b>MeCO<sub>2</sub>-BzBPMA</b> )] [OTf].....	171
	Synthesis <b>HCO<sub>2</sub>-BzBPMA</b> .....	172
	Synthesis [ <b>6.2</b> - <b>DB24C8</b> ] [OTf] <sub>2</sub> .....	174
	Synthesis [ <b>6.2</b> ] [OTf] <sub>2</sub> .....	175
	Synthesis [(Re(CO <sub>3</sub> )) <sub>2</sub> ( <b>6.2</b> - <b>DB24C8</b> )] [OTf] <sub>4</sub> .....	177
	Synthesis [(Re(CO <sub>3</sub> )) <sub>2</sub> ( <b>6.2</b> )] [OTf] <sub>4</sub> .....	178
	Synthesis [(Ag) <sub>x</sub> ( <b>6.2</b> - <b>DB24C8</b> )] [OTf] <sub>x</sub> .....	180
	Synthesis [(Cd) <sub>x</sub> ( <b>6.2</b> - <b>DB24C8</b> )] [OTf] <sub>x</sub> .....	181
	Synthesis [ <b>6.2</b> - <b>T<sup>3</sup>P-DB24C8</b> ] [OTf] <sub>2</sub> .....	183
	<b>Reference</b> .....	184
<b>Chapter 7</b>	<i>Future Directions</i> .....	186
<b>Vita Auctoris</b> .....		189

## List of Figures and Schemes

Figure 1.1	Structures of crown ethers.	2
Figure 1.2	Structure of a cryptand.	2
Figure 1.3	Cartoon representation of [2]pseudorotaxane formation.	3
Figure 1.4	The first interpenetrated molecular species.	4
Figure 1.5	A [2]pseudorotaxane that relies on electron rich and electron poor aromatics.	4
Figure 1.6	A hydrogen bonding [2]pseudorotaxane.	5
Figure 1.7	An anion binding template.	5
Figure 1.8	Sauvage used metal ion as templates for [n]pseudorotaxane formation.	6
Figure 1.9	Second-sphere interaction to form [2]pseudorotaxane.	6
Figure 1.10	Cartoon representation of [2]rotaxane.	8
Figure 1.11	Harrison's "statistical slipping" methodology.	9
Figure 1.12	"Directed" synthesis of a [2]rotaxane.	10
Figure 1.13	Cartoon illustration of the threading/capping method.	10
Figure 1.14	Example of a [2]rotaxane formed by the threading/capping process.	11
Figure 1.15	Cartoon representation of clipping.	11
Figure 1.16	Example of the clipping process in the formation [2]rotaxane.	12
Figure 1.17	Cartoon illustration of slippage of a [2]rotaxane.	12
Figure 1.18	Example of a [2]rotaxane formed by slippage.	13
Figure 1.19	The use of transition a metals for templatation by Sauvage.	13
Figure 1.20	A [2]rotaxane formed using Leigh's "active metal" template coupling of alkyl chains.	14

Figure 1.21	Schematic representation of the networks that CPs can form, where E are donor atoms.	15
Figure 1.22	Diamond-like network of $\text{Cu}[\text{CC}_6\text{H}_5\text{CN}]_4\text{BF}_4$ .	16
Figure 1.23	A representation of the cubic arrangement of SBU and linkers in MOF-5 where blue blocks are M-O-C clusters and the black lines are the organic linkers.	18
Figure 1.24	Representation of a mixed linker system.	19
Scheme 1.1	Kim framework with diaminoalkane, axle, and cucbituril (CB[6]) wheel.	20
Figure 1.25	A polyrotaxane.	20
Figure 1.26	(top) A 1D framework and (bottom) a 2D grid with 1,2-bis(4,4'-dipyridinium) ethane, thread and <b>DB24C8</b> wheel (bottom).	21
Figure 1.27	N-oxide axles developed to form 3D networks.	22
Figure 1.28	3-D Framework using a 1,2-bis(4,4'-dipyridinium-N-oxide)ethane axle and <b>DB24C8</b> wheels.	22
Figure 1.29	Extended axle used for the neutral 1-D MORFs.	23
Figure 1.30	1-D Framework with 1,2-bis(4,4'-dipyridinium)ethane axle, <b>DSDB24C8</b> wheel and $\text{Cu}_2\text{BnO}_4$ linker.	23
Figure 1.31	A negatively charged [2]pseudorotaxane linker.	24
Figure 1.32	Stoddart's macrocyclic polyether linkers that form a MOF-5 type structure use to "dock" $\text{PQT}^{2+}$ .	25
Figure 1.33	Stoddart's macrocyclic polyether used to form a framework containing a [2]catenane.	25
Figure 1.34	Schematic representations of the binding mode of Sessler's MORF where the pink balls are the Zn(II) ions, black lines are the axle, and rectangles are the wheels.	26
Figure 2.1	Rotaxane ligand $[\mathbf{2.1} \subset \mathbf{DB24C8}]^{2+}$ .	32
Figure 2.2	Rotaxane formation via metal coordination.	33
Figure 2.3	Rotaxane formation via porphyrin coordination.	33



Figure 2.4	2,2':6',2''-Terpyridine group ligand utilized as stopper for a [2]rotaxane.	34
Figure 2.5	Bis(2-pyridylmethyl)amine utilized as a stopper for a [2]rotaxane.	34
Scheme 2.1	i) 1:1MeOH/H <sub>2</sub> O, NaOH, ii) excess NH <sub>4</sub> OAc, reflux.	35
Scheme 2.2	i) NBS, BnO <sub>2</sub> , CCl <sub>4</sub> , reflux.	35
Scheme 2.3	i) [2.1][OTf] <sub>2</sub> , <b>DB24C8</b> , <b>Br-tolyterpy</b> in MeNO <sub>2</sub> /NaOTf(aq) at RT for 168 h.	36
Figure 2.6	Comparison of the <sup>1</sup> H NMR shifts of (a) [2.2⊂ <b>DB24C8</b> ][OTf] <sub>4</sub> , and (b) [2.2][OTf] <sub>4</sub> in CD <sub>3</sub> CN at 500 MHz.	37
Scheme 2.4	i) 2 equivalents of Ag(OTf) or Pd(MeCN) <sub>4</sub> [BF <sub>4</sub> ] <sub>2</sub> or Zn(H <sub>2</sub> O) <sub>6</sub> [OTf] <sub>2</sub> in MeCN for 24 h at RT.	39
Figure 2.7	A ball-stick representation of the cationic portion of the X-ray crystal structure of [(Zn(H <sub>2</sub> O) <sub>3</sub> ) <sub>2</sub> (2.2⊂ <b>DB24C8</b> )] <sup>8+</sup> . The complex occupies a crystallographic centre of symmetry. All hydrogen atoms, except those on the coordinated water molecules, all anions and all solvent molecules have been omitted for clarity. (Zn = blue-gray, O = red, N = blue, C = black, H = white; wheel bonds = silver, axle bonds = gold).	40
Scheme 2.5	i) Ru(terpy)Cl <sub>3</sub> , 1:1 EtOH/H <sub>2</sub> O, reflux, 24h.	42
Figure 2.8	<sup>1</sup> H NMR spectrum of [(Ru(terpy)) <sub>2</sub> (2.2⊂ <b>DB24C8</b> )] <sup>8+</sup> at 500MHz.	43
Figure 2.9	Ball-and-stick representation of the cationic portion of the X-ray crystal structure of [(Ru(terpy)) <sub>2</sub> (2.2⊂ <b>DB24C8</b> )] <sup>8+</sup> . The complex occupies a crystallographic centre of symmetry. All anions and all solvent molecules have been omitted for clarity. (Ru = blue-gray, O = red, N = blue, C = black, H = white; wheel bonds = silver, axle bonds = gold).	45
Figure 2.10	Schematic energy level diagram of an octahedral metal complex showing possible transitions.	47
Figure 2.11	UV/Vis spectra of complex [Ru(terpy) <sub>2</sub> (2.2)] <sup>8+</sup> (---) and [Ru(terpy) <sub>2</sub> (2.2⊂ <b>DB24C8</b> )] <sup>8+</sup> (—) at concentration of 1.0 x 10 <sup>-5</sup> M in CH <sub>3</sub> CN.	48
Figure 3.1	[2]Pseudorotaxane with [( <b>Bn</b> ) <sub>2</sub> NH <sub>2</sub> ⊂ <b>DEDB24C8</b> ] <sup>+</sup> .	66

Figure 3.2	Structural formula of the [2]pseudorotaxane studied by Liu.	66
Scheme 3.1	i) $(\text{CH}_2\text{O})_n$ , $\text{CHCl}_3/\text{AcOH}$ , $\text{HBr}$ , $60^\circ\text{C}$ 48h.	67
Scheme 3.2	i) <b>TP-DB24C8</b> , $\text{PhOH}$ or $4\text{-EtO}_2\text{CPhOH}$ , $\text{K}_2\text{CO}_3$ , $\text{MeCN}$ , $\text{N}_2$ , $\Delta$ 120h.	68
Figure 3.3	Crystal structure of <b>TP-DB24C8</b> . (O = red, C = black, wheel bonds = silver).	69
Scheme 3.3	i) $\text{MeCN}$ , $\Delta$ 72h ii) $\text{NaOTf}_{(\text{aq})}$ .	70
Scheme 3.4	i) benzyl bromide in $\text{MeNO}_2$ , $\text{NaOTf}_{(\text{aq})}$ , for 72 h.	70
Figure 3.4	Cartoon representation of the new addition interactions observed in the crystal of [2]rotaxane. The black dash lines indicate new secondary interactions.	74
Figure 3.5	A ball-stick representation of the cationic portion of the X-ray crystal structure of $[\mathbf{3.2}\subset\text{TP-B24C8}]^{2+}$ . The complex occupies a crystallographic centre of symmetry. All hydrogen atoms, all anions, and all solvent molecules have been omitted for clarity. (O = red, N = blue, C = black; wheel bonds = silver, axle bonds = gold).	75
Figure 3.6	A ball-stick representation of the cationic portion of the X-ray crystal structure of $[\mathbf{3.3}\subset\text{TE-DB24C8}]^{4+}$ . The complex occupies a crystallographic centre of symmetry. All hydrogen atoms, all anions, and all solvent molecules have been omitted for clarity. (O = red, N = blue, C = black; wheel bonds = silver, axle bonds = gold).	76
Scheme 3.5	i) $[\mathbf{2.1}][\text{OTf}]_2$ , <b>TP-DB24C8</b> or <b>TE-DB24C8</b> i) 4- <i>t</i> -butylbenzyl bromide, $\text{CH}_3\text{CN}$ , RT 96 h ii) $\text{MeNO}_2/\text{NaOTf}_{(\text{aq})}$ at RT for 24 h.	77
Figure 3.7	Comparison of the $^1\text{H}$ NMR shifts of (a) <b>TP-DB24C8</b> (b) $[\mathbf{3.4}][\text{OTf}]_4$ , and (c) $[\mathbf{3.4}\subset\text{TP-DB24C8}][\text{OTf}]_4$ in $\text{CD}_3\text{CN}$ at 500 MHz.	78
Figure 3.8	Comparison of the $^1\text{H}$ NMR shifts of (a) <b>TE-DB24C8</b> (b) $[\mathbf{3.4}][\text{OTf}]_4$ , and (c) $[\mathbf{3.4}\subset\text{TE-DB24C8}][\text{OTf}]_4$ in $\text{CD}_3\text{CN}$ at 500 MHz.	78
Figure 3.9	Cartoon representation of the new additional interactions observed in the crystal structure of [2]rotaxanes. The black dash lines indicating new secondary interactions.	81

Figure 3.10	A ball-stick representation of the cationic portion of the X-ray crystal structure of $[3.4\text{-TP-DB24C8}]^{4+}$ . The complex occupies a crystallographic centre of symmetry. All hydrogen atoms, all anions, and all solvent molecules have been omitted for clarity. (O = red, N = blue, C = black; wheel bonds = silver, axle bonds = gold).	82
Figure 3.11	A ball-stick representation of the cationic portion of the X-ray crystal structure of $[3.4\text{-TE-DB24C8}]^{4+}$ . The complex occupies a crystallographic centre of symmetry. All hydrogen atoms, all anions, and all solvent molecules have been omitted for clarity. (O = red, N = blue, C = black; wheel bonds = silver, axle bonds = gold).	83
Scheme 3.6	i) $[3.5][\text{BF}_4]_2$ <b>TP-DB24C8</b> or <b>TE-DB24C8</b> i) 4- <i>tert</i> -butylbenzoic anhydride, ${}^n\text{Bu}_3\text{P}$ (cat.), MeCN/ $\text{CH}_2\text{Cl}_2$ for 72 h.	84
Figure 3.12	Comparison of the ${}^1\text{H}$ NMR shifts of (a) <b>TP-DB24C8</b> (b) $[3.6][\text{BF}_4]_2$ , and (c) $[3.6\text{-TP-DB24C8}][\text{BF}_4]_2$ in $\text{CD}_3\text{CN}$ at 500 MHz.	85
Figure 3.13	Comparison of the ${}^1\text{H}$ NMR shifts of (a) <b>TE-DB24C8</b> (b) $[3.6][\text{BF}_4]_2$ , and (c) $[3.6\text{-TE-DB24C8}][\text{BF}_4]_2$ in $\text{CD}_3\text{CN}$ at 500 MHz.	85
Scheme 4.1	i) $\text{Cd}(\text{OTf})_2$ in $\text{MeNO}_2$ .	101
Scheme 4.2	i) $[4.1\text{-TE-DB24C8}]^{2+}$ , <b>Br-tolyterpy</b> in $\text{MeNO}_2/\text{NaOTf}(\text{aq})$ at RT for 168 h.	102
Figure 4.1	Comparison of the ${}^1\text{H}$ NMR spectra of <b>TE-DB24C8</b> , $[4.2\text{-TE-DB24C8}][\text{OTf}]_4$ , and $[2.2][\text{OTf}]_4$ , and in $\text{CD}_3\text{CN}$ at 500 MHz.	103
Figure 4.2	Additional interaction observed in the crystal of $[4.2\text{-TE-DB24C8}]^{4+}$ . The black dash lines indicates a new secondary interaction.	105
Figure 4.3	Ball-and-stick representation of the cationic portion of the X-ray crystal structure of $[4.2\text{-TE-DB24C8}]^{4+}$ . The complex occupies a crystallographic centre of symmetry. All anions and all solvent molecules have been omitted for clarity. (Ru = blue-gray, O = red, N = blue, C = black; wheel bonds = silver, axle bonds = gold).	106
Scheme 4.3	i) $\text{Ru}(\text{Terpy})\text{Cl}_3$ , 1:1 EtOH/ $\text{H}_2\text{O}$ , reflux, 24h.	107
Figure 4.4	${}^1\text{H}$ NMR spectrum of $[\text{Ru}(\text{terpy})]_2(4.2\text{-TE-DB24C8})[\text{OTf}]_8$ at 500MHz.	108

Figure 4.5	Ball-and-stick representation of the cationic portion of the X-ray crystal structure of $[(\text{Ru}(\text{terpy}))_2(\mathbf{4.2}\text{-}\mathbf{TE}\text{-}\mathbf{DB24C8})]^{8+}$ . (Ru = blue-gray, O = red, N = blue, C = black; wheel bonds = silver, axle bonds = gold).	110
Figure 4.6	UV/Vis spectra of complex $[(\text{Ru}(\text{terpy}))_2(\mathbf{2.2})]^{8+}$ (---) and $[(\text{Ru}(\text{terpy}))_2(\mathbf{2.2}\text{-}\mathbf{DB24C8})]^{8+}$ (— —) and $[(\text{Ru}(\text{terpy}))_2(\mathbf{4.2}\text{-}\mathbf{TE}\text{-}\mathbf{DB24C8})]^{8+}$ (—) at concentration of $1.0 \times 10^{-5}$ M in $\text{CD}_3\text{CN}$ .	111
Scheme 4.4	i) $\text{MeNO}_2$ , excess <b>TP-DB24C8</b> .	113
Figure 4.7	Ball and stick representation of the coordination sphere of the metal centre in $[(\text{Cd}(\text{H}_2\text{O}))_2(\mathbf{2.1})(\mathbf{4.2}\text{-}\mathbf{TP}\text{-}\mathbf{DB24C8})]^{8+}$ . (Key: blue= $\mathbf{2.2}^{2+}$ , red = crown, green = water).	114
Figure 4.8	A space-filling model showing four square-grids of $[(\text{Cd}(\text{H}_2\text{O}))_2(\mathbf{2.2})(\mathbf{4.3}\text{-}\mathbf{TP}\text{-}\mathbf{DB24C8})]^{8+}$ . $\text{MeNO}_2$ solvent molecules and anions are omitted for clarity.	115
Figure 4.9	Comparing MORFs with <b>DB24C8</b> (left) and <b>TP-DB24C8</b> (right).	115
Figure 5.1	An example of the axle used in the construction of MORFs.	122
Figure 5.2	Stang's acceptor and donor crown ethers.	123
Figure 5.3	Steel's oxine type chelating ligand.	123
Scheme 5.1	i) $\text{NaH}$ , oxine, THF, stirred 2 h ii) <b>TB-DB24C8</b> , $\Delta$ 36 h.	124
Scheme 5.2	i) 3 eq. $[\mathbf{3.5}]^{2+}$ , 1 eq. <b>TO-DB24C8</b> , 9 eq. 3,5-dimethylbenzoic anhydride, ${}^n\text{Bu}_3\text{P}$ (cat.), $\text{MeCN}/\text{CH}_2\text{Cl}_2$ for 72 h.	125
Figure 5.4	Ball-and stick presentation of $[(\text{Cd}(\text{MeCN})_2(\text{H}_2\text{O}))_2(\mathbf{5.2}\text{-}\mathbf{TO}\text{-}\mathbf{DB24C8})]^{6+}$ , with H-atoms and anions omitted for clarity. (Colour key: Cd = teal, O = red, N = blue, C = dark gray, axle = gold bonds, wheel = silver bonds).	128
Figure 5.5	The crown ether and the Cd(II) coordination sphere to emphasize the metal ligand bonding (the axle omitted for clarity).	129
Scheme 5.3	i) $\text{NaH}$ , 3-py or 4-py, DMF, rt 2 h ii) <b>TB-DB24C8</b> , $60^\circ\text{C}$ , 36 h.	130
Scheme 5.4	i) 3 eq. $[\mathbf{5.1}]^{2+}$ , 1eq. <b>T<sup>4</sup>P-DB24C8</b> or <b>T<sup>3</sup>P-DB24C8</b> , 9 eq. 3,5-dimethylbenzoic anhydride, ${}^n\text{Bu}_3\text{P}$ (cat.), $\text{MeCN}/\text{CH}_2\text{Cl}_2$ for 72 h.	131

Figure 5.6	Ball-and-stick representation of $[\mathbf{5.2}\text{-T}^4\mathbf{P}\text{-DB24C8}]^{2+}$ (anions and H-atoms are omitted for clarity. Colour key: O = red, N = blue, C = dark gray; axle = gold bonds, wheel = silver bonds).	134
Figure 5.7	Son's bis(pyridylether) ligand that can form polymers.	135
Figure 5.8	Shows a ball and stick representation of $[\text{Cd}_2\text{Cl}_4(\text{H}_2\text{O})_4(\mathbf{5.2}\text{-T}^3\mathbf{P}\text{-DB24C8})]^{2+}$ showing how the 3-pyridyl groups each coordinate to a different Cd(II) ion. All counterions and all solvent molecules have been omitted for clarity. (Colour key: Cd = teal, Cl = green, O = red, N = blue, C = dark gray; axle = gold bonds, wheel = silver bonds).	136
Figure 5.9	A space filling model of the complete 2-periodic network. All non-coordinating anions have been omitted for clarity. (colour key: Cd = teal, Cl = green, axle = blue, wheel = red).	137
Figure 6.1	The new stopper based [2]rotaxane with bis(2-pyridylmethyl)amine.	152
Figure 6.2	Leigh "combo" chelating ligand.	153
Scheme 6.1	i) EtOH, ii) $\text{NaBH}_4$ , reflux.	154
Scheme 6.2	i) $\text{Et}_3\text{N}$ , THF, reflux, 2h ii) 2M $\text{NaOH}_{(\text{aq})}$ , MeOH.	154
Scheme 6.3	i) $\text{M}(\text{CO})_5\text{Br}$ , AgOTf, MeOH, 60 min (M = Mn or Re) ii) $\text{Re}(\text{CO})_5[\text{MeOH}]\text{OTf}$ , <b>MeCO<sub>2</sub>-BzBPMA</b> , 60 min.	155
Figure 6.3	A ball-stick representation of the cationic portion of the X-ray crystal structure of $[(\text{Mn}(\text{CO})_3(\mathbf{MeCO}_2\text{-BzBPMA}))]^+$ . All hydrogen atoms, all anions and all solvent molecules have been omitted for clarity. (Mn = blue-gray, O = red, N = blue, C = black, ligands bonds = gold).	157
Scheme 6.4	i) <b>DB24C8</b> , <b>HCO<sub>2</sub>-BzBPMA</b> , DCC, $^n\text{Bu}_3\text{P}$ (cat.), MeCN for 72 h.	158
Figure 6.4	Comparison of the $^1\text{H}$ NMR shifts of (a) $[\mathbf{6.2}\text{-DB24C8}][\text{OTf}]_2$ , and (b) $[\mathbf{6.2}][\text{OTf}]_2$ in $\text{CD}_3\text{CN}$ at 500 MHz.	159
Scheme 6.5	i) $[\text{Re}(\text{CO})_5(\text{MeOH})][\text{OTf}]$ in MeOH, reflux, 1h	160
Figure 6.5	$^1\text{H}$ NMR spectrum of $[(\text{Re}(\text{CO})_3)_2(\mathbf{6.2}\text{-DB24C8})][\text{OTf}]_4$ at 500MHz.	161
Scheme 6.6	i) 2 equivalents of Ag(OTf) or $[\text{Cd}(\text{H}_2\text{O})_6][\text{BF}_4]_2$ in MeCN for 24 h at RT.	162

Scheme 6.6	i) <b>T<sup>3</sup>P-DB24C8</b> , <b>HCO<sub>2</sub>-BzBPMA</b> , DCC, <sup>n</sup> Bu <sub>3</sub> P (cat.), MeCN for 72h.	164
Figure 6.6	Possible coordination of the “combo” rotaxane ligand.	166
Figure 7.1	Possible “double” network that [ <b>6.2-DB24C8</b> ][OTf] <sub>2</sub> will form upon coordination where M = Cd(II) or Ag(I).	186
Figure 7.2	Sulfur donor “combo” rotaxane ligand.	187
Figure 7.3	Possible mixed donor [2]rotaxane system that could be made	188

## List of Tables

Table 2.1	Comparison of the chemical shifts of the dumbbell <b>[2.2][OTf]<sub>4</sub></b> , and <b>[2]rotaxane, [2.2-DB24C8][OTf]<sub>4</sub></b> .	37
Table 2.2	A comparison of the <sup>1</sup> H NMR chemical shifts for dumbbell <b>[2.2][OTf]<sub>4</sub></b> , <b>[2]rotaxane ligand [2.2-DB24C8][OTf]<sub>4</sub></b> and complexes <b>[(Ru(terpy)<sub>2</sub>)(2.2)][OTf]<sub>8</sub></b> , <b>[(Ru(terpy)<sub>2</sub>)(2.2-DB24C8)][OTf]<sub>5</sub></b> .	44
Table 2.3	The bite angle of complex <b>[(Ru(terpy)<sub>2</sub>)(2.2-DB24C8)]<sup>8+</sup></b> as compared to other <b>[Ru(terpy)<sub>2</sub>]<sup>2+</sup></b> based complexes.	46
Table 2.4	UV/Vis data for complex <b>[Ru(terpy)<sub>2</sub>(2.2)]<sup>8+</sup></b> , <b>[Ru(terpy)<sub>2</sub>(2.2-DB24C8)]<sup>8+</sup></b> and a few other selected ruthenium(II) complexes.	49
Table 2.5	<sup>1</sup> H NMR spectroscopic data in CD <sub>3</sub> CN.	51
Table 2.6	<sup>1</sup> H NMR spectroscopic data in CD <sub>3</sub> CN.	52
Table 2.7	<sup>1</sup> H NMR spectroscopic data for <b>[2.2][OTf]<sub>4</sub></b> in CD <sub>3</sub> CN.	53
Table 2.8	<sup>1</sup> H NMR spectroscopic data for <b>[2.2-DB24C8][OTf]<sub>4</sub></b> in CD <sub>3</sub> CN.	55
Table 2.9	<sup>1</sup> H NMR spectroscopic data for <b>[2.2-DB24C8][OTf]<sub>4</sub></b> in CD <sub>3</sub> NO <sub>2</sub> .	55
Table 2.10	<sup>1</sup> H NMR spectroscopic data for <b>[(Ru(terpy)<sub>2</sub>)(2.2-DB24C8)][OTf]<sub>8</sub></b> in CD <sub>3</sub> CN.	57
Table 2.11	<sup>1</sup> H NMR spectroscopic data for <b>[(Ru(terpy)<sub>2</sub>)(2.2)][OTf]<sub>8</sub></b> in CD <sub>3</sub> CN.	58
Table 2.12	<sup>1</sup> H NMR spectroscopic data for <b>[(Ag(MeCN))<sub>2</sub>(2.2-DB24C8)][OTf]<sub>6</sub></b> in CD <sub>3</sub> CN.	60
Table 2.13	<sup>1</sup> H NMR spectroscopic data for <b>[(Pd(MeCN))<sub>2</sub>(2.2-DB24C8)][OTf]<sub>8</sub></b> in CD <sub>3</sub> NO <sub>2</sub> .	61
Table 3.1	Comparison of the chemical shifts of the wheels <b>TB-DB24C8</b> , <b>TP-DB24C8</b> , and <b>TE-DB24C8</b> in CD <sub>2</sub> Cl <sub>2</sub> .	68
Table 3.2	<sup>1</sup> H NMR chemical shifts for the axles and <b>[2]pseudorotaxanes</b> undergoing slow exchange.	70
Table 3.3	K <sub>a</sub> (M <sup>-1</sup> ) and ΔG (kJ mol <sup>-1</sup> ) values for the <b>[2]pseudorotaxane</b> formed between <b>TP-DB24C8</b> , <b>TE-DB24C8</b> and <b>3.1-3.3</b> and <b>2.1</b> at 298K.	72

Table 3.4	Complete listing of $\Delta H^\circ$ (kJ mol <sup>-1</sup> ) and $\Delta S^\circ$ (J mol <sup>-1</sup> K <sup>-1</sup> ) values for [2]pseudorotaxanes in CD <sub>3</sub> CN.	72
Table 3.5	Hydrogen bonds parameter in the crystal structure of [2]pseudorotaxane [ <b>3.2</b> ⊂ <b>TP-DB24C8</b> ][OTf] <sub>2</sub> .	73
Table 3.6	Hydrogen bonds parameters in the crystal structure of [2]rotaxane [ <b>3.4</b> ⊂ <b>TE-DB24C8</b> ][OTf] <sub>4</sub> .	74
Table 3.7	<sup>1</sup> H NMR assignments for [ <b>3.4</b> ][OTf] <sub>4</sub> , [ <b>3.4</b> ⊂ <b>TP-DB24C8</b> ][OTf] <sub>4</sub> , and [ <b>3.4</b> ⊂ <b>TE-DB24C8</b> ][OTf] <sub>4</sub> in CH <sub>3</sub> CN.	79
Table 3.8	Comparison of the chemical shifts of the [2]rotaxanes [ <b>3.4</b> ⊂ <b>TP-DB24C8</b> ][OTf] <sub>4</sub> and [ <b>3.4</b> ⊂ <b>TE-DB24C8</b> ][OTf] <sub>4</sub> in CD <sub>3</sub> CN.	79
Table 3.9	<sup>1</sup> H NMR assignments for [ <b>3.6</b> ][BF <sub>4</sub> ] <sub>2</sub> , [ <b>3.6</b> ⊂ <b>TP-DB24C8</b> ][BF <sub>4</sub> ] <sub>2</sub> , and [ <b>3.6</b> ⊂ <b>TE-DB24C8</b> ][BF <sub>4</sub> ] <sub>2</sub> in CH <sub>3</sub> CN.	86
Table 3.10	Comparison of the chemical shifts of the [2]rotaxanes [ <b>3.6</b> ⊂ <b>TP-DB24C8</b> ][BF <sub>4</sub> ] <sub>2</sub> and [ <b>3.6</b> ⊂ <b>TE-DB24C8</b> ][BF <sub>4</sub> ] <sub>2</sub> in CD <sub>3</sub> CN.	87
Table 3.11	<sup>1</sup> H-NMR spectroscopic data for <b>TB-DB24C8</b> in CDCl <sub>3</sub> .	89
Table 3.12	<sup>1</sup> H-NMR spectroscopic data for <b>TB-DB24C8</b> in CD <sub>2</sub> Cl <sub>2</sub> .	89
Table 3.13	<sup>1</sup> H-NMR spectroscopic data for <b>TP-DB24C8</b> in CD <sub>2</sub> Cl <sub>2</sub> .	90
Table 3.14	<sup>1</sup> H-NMR spectroscopic data for <b>TP-DB24C8</b> in CD <sub>3</sub> CN.	91
Table 3.15	<sup>13</sup> C-NMR spectroscopic data for <b>TP-DB24C8</b> in CD <sub>2</sub> Cl <sub>2</sub> .	91
Table 3.16	<sup>1</sup> H-NMR spectroscopic data for <b>TE-DB24C8</b> in CD <sub>2</sub> Cl <sub>2</sub> .	92
Table 3.17	<sup>1</sup> H-NMR spectroscopic data for <b>TE-DB24C8</b> in CD <sub>3</sub> CN.	93
Table 3.18	<sup>13</sup> C-NMR spectroscopic data for <b>TE-DB24C8</b> in CD <sub>2</sub> Cl <sub>2</sub> .	93
Table 3.19	<sup>1</sup> H-NMR spectroscopic data for [ <b>3.4</b> ⊂ <b>TP-DB24C8</b> ] <sup>4+</sup> in CD <sub>3</sub> CN.	95
Table 3.20	<sup>1</sup> H-NMR spectroscopic data for [ <b>3.4</b> ⊂ <b>TE-DB24C8</b> ] <sup>4+</sup> in CD <sub>3</sub> CN.	96
Table 3.21	<sup>1</sup> H-NMR spectroscopic data for [ <b>3.6</b> ⊂ <b>TP-DB24C8</b> ] <sup>2+</sup> in CD <sub>3</sub> CN.	98
Table 3.22	<sup>1</sup> H-NMR spectroscopic data for [ <b>3.6</b> ⊂ <b>TE-DB24C8</b> ] <sup>2+</sup> in CD <sub>3</sub> CN.	99



Table 4.1	Chemical shift data <b>[2.2][OTf]<sub>4</sub></b> , and [2]rotaxane, <b>[4.2cTE-DB24C8][OTf]<sub>4</sub></b> .	103
Table 4.2	Chemical shift data <b>TE-DB24C8</b> , and <b>[4.2cTE-DB24C8][OTf]<sub>4</sub></b> in CH <sub>3</sub> CN.	104
Table 4.3	A comparison of the <sup>1</sup> H NMR chemical shifts for dumbbell <b>[2.2][OTf]<sub>4</sub></b> , [2]rotaxane ligand <b>[4.2cTE-DB24C8][OTf]<sub>4</sub></b> and complex <b>[(Ru(terpy)<sub>2</sub>)(2.2)][OTf]<sub>8</sub></b> , <b>[(Ru(terpy)<sub>2</sub>)(4.2cTE-DB24C8)][OTf]<sub>8</sub></b> .	108
Table 4.4	The bite angle of <b>[(Ru(terpy)<sub>2</sub>)(4.2cTE-DB24C8)]<sup>8+</sup></b> and <b>[(Ru(terpy)<sub>2</sub>)(2.2cDB24C8)]<sup>8+</sup></b> .	109
Table 4.5	UV/Vis for complex <b>[(Ru(terpy)<sub>2</sub>)(4.2cTE-DB24C8)]<sup>8+</sup></b> and a few other selected ruthenium(II) complexes.	112
Table 4.6	<sup>1</sup> H NMR spectroscopic data for <b>[4.2cTE-DB24C8]<sup>4+</sup></b> in CD <sub>3</sub> CN.	118
Table 4.7	<sup>1</sup> H NMR spectroscopic data for <b>[(Ru(terpy)<sub>2</sub>)(4.2cTE-DB24C8)]<sup>8+</sup></b> in CD <sub>3</sub> CN.	119
Table 5.1	Comparison of the chemical shifts for <b>TB-DB24C8</b> , and wheel <b>TO-DB24C8</b> in CD <sub>2</sub> Cl <sub>2</sub> .	124
Table 5.2	Comparison of the chemical shifts of the dumbbell <b>[5.2][BF<sub>4</sub>]<sub>2</sub></b> , and [2]rotaxane, <b>[5.2cTO-DB24C8][BF<sub>4</sub>]<sub>2</sub></b> in CD <sub>3</sub> CN.	126
Table 5.3	Comparison of the chemical shifts of the wheel, <b>TO-DB24C8</b> and [2]rotaxane <b>[5.2cTO-DB24C8][BF<sub>4</sub>]<sub>2</sub></b> in CH <sub>2</sub> Cl <sub>2</sub> .	126
Table 5.4	Comparison of the chemical shifts of the <b>[5.2cTO-DB24C8][BF<sub>4</sub>]<sub>2</sub></b> and <b>[(Cd(MeCN)<sub>2</sub>(H<sub>2</sub>O))<sub>2</sub>(5.2cTO-DB24C8)][BF<sub>4</sub>]<sub>6</sub></b> in CH <sub>3</sub> CN.	127
Table 5.5	Comparison of the chemical shifts of the wheels <b>TB-DB24C8</b> , <b>T<sup>4</sup>P-DB24C8</b> , and <b>T<sup>3</sup>P-DB24C8</b> in CD <sub>2</sub> Cl <sub>2</sub> .	131
Table 5.6	Comparison of the chemical shifts of the dumbbell <b>[5.2][BF<sub>4</sub>]<sub>2</sub></b> , and [2]rotaxane <b>[5.2cT<sup>4</sup>P-DB24C8][BF<sub>4</sub>]<sub>2</sub></b> , and <b>[5.2cT<sup>3</sup>P-DB24C8][BF<sub>4</sub>]<sub>2</sub></b> in CD <sub>3</sub> CN.	132
Table 5.7	Comparison of the chemical shifts of the [2]rotaxanes <b>[5.2cT<sup>4</sup>P-DB24C8][BF<sub>4</sub>]<sub>2</sub></b> and <b>[5.2cT<sup>3</sup>P-DB24C8][BF<sub>4</sub>]<sub>2</sub></b> in CD <sub>3</sub> CN.	133
Table 5.8	<sup>1</sup> H NMR spectroscopic data for <b>TO-DB24C8</b> in CD <sub>2</sub> Cl <sub>2</sub> .	139

Table 5.9	$^{13}\text{C}$ NMR spectroscopic data for <b>TO-DB24C8</b> in $\text{CD}_2\text{Cl}_2$ .	140
Table 5.10	$^1\text{H}$ NMR spectroscopic data for <b>T<sup>4</sup>P-DB24C8</b> in $\text{CD}_2\text{Cl}_2$ .	141
Table 5.11	$^1\text{H}$ NMR spectroscopic data for <b>T<sup>4</sup>P-DB24C8</b> in $\text{CD}_3\text{CN}$ .	141
Table 5.12	$^{13}\text{C}$ NMR spectroscopic data for <b>T<sup>4</sup>P-DB24C8</b> in $\text{CD}_2\text{Cl}_2$ .	142
Table 5.13	$^1\text{H}$ NMR spectroscopic data for <b>T<sup>3</sup>P-DB24C8</b> in $\text{CD}_2\text{Cl}_2$ .	143
Table 5.14	$^1\text{H}$ NMR spectroscopic data for <b>T<sup>3</sup>P-DB24C8</b> in $\text{CD}_3\text{CN}$ .	143
Table 5.15	$^{13}\text{C}$ NMR spectroscopic data for <b>T<sup>3</sup>P-DB24C8</b> in $\text{CD}_2\text{Cl}_2$ .	144
Table 5.16	$^1\text{H}$ NMR spectroscopic data for <b>[5.2cTO-DB24C8][BF<sub>4</sub>]<sub>2</sub></b> in $\text{CD}_3\text{CN}$ .	145
Table 5.17	$^1\text{H}$ NMR spectroscopic data for <b>[5.2cTO-DB24C8][BF<sub>4</sub>]<sub>2</sub></b> in $\text{CD}_2\text{Cl}_2$ .	146
Table 5.18	$^1\text{H}$ NMR spectroscopic data for <b>[5.2cT<sup>4</sup>P-DB24C8][BF<sub>4</sub>]<sub>2</sub></b> in $\text{CD}_3\text{CN}$ .	147
Table 5.19	$^1\text{H}$ NMR spectroscopic data for <b>[5.2cT<sup>3</sup>P-DB24C8][BF<sub>4</sub>]<sub>2</sub></b> in $\text{CD}_3\text{CN}$ .	149
Table 5.20	$^1\text{H}$ NMR spectroscopic data for <b>[(Cd(MeCN)<sub>2</sub>(H<sub>2</sub>O)<sub>2</sub>(5.2cTO-DB24C8)]<sup>6+</sup></b> in $\text{CD}_3\text{CN}$ .	150
Table 6.1	Comparison of the chemical shifts of free ligand <b>MeCO<sub>2</sub>-BzBPMA</b> and metal complex <b>[Re(CO)<sub>3</sub>(MeCO<sub>2</sub>-BzBPMA)][OTf]</b> .	156
Table 6.2	The bond lengths (Å) and bond angles (°) of the complex <b>[Re(CO)<sub>3</sub>(MeCO<sub>2</sub>-BzBPMA)]<sup>+</sup></b> .	156
Table 6.3	Comparison of the chemical shifts of the axle of the dumbbell <b>[6.2][OTf]<sub>2</sub></b> , and [2]rotaxane, <b>[6.2cDB24C8][OTf]<sub>2</sub></b> .	159
Table 6.4	A comparison of the $^1\text{H}$ NMR chemical shifts for dumbbell <b>[6.2][OTf]<sub>2</sub></b> , [2]rotaxane ligand <b>[6.2cDB24C8][OTf]<sub>2</sub></b> and complex <b>[(Re((CO)<sub>3</sub>)<sub>2</sub>)(6.2)]<sup>4+</sup></b> , <b>[(Re((CO)<sub>3</sub>)<sub>2</sub>)(6.2cDB24C8)][OTf]<sub>4</sub></b> .	161
Table 6.5	Comparison of the chemical shifts for the [2]rotaxane <b>[6.2cDB24C8][OTf]<sub>2</sub></b> and complex <b>[(Ag)<sub>x</sub>(6.2cDB24C8)][OTf]<sub>x</sub></b> and <b>[(Cd)<sub>x</sub>(6.2cDB24C8)][OTf]<sub>x</sub></b> in $\text{CH}_3\text{CN}$ .	163

Table 6.6	$^1\text{H}$ NMR assignment for <b>[6.2][OTf]<sub>2</sub></b> , and <b>[6.2-<math>\text{T}^3\text{P-DB24C8}</math>][OTf]<sub>2</sub></b> in $\text{CD}_3\text{CN}$ .	165
Table 6.7	$^1\text{H}$ NMR assignment for <b><math>\text{T}^3\text{P-DB24C8}</math></b> and <b>[6.2-<math>\text{T}^3\text{P-DB24C8}</math>][OTf]<sub>2</sub></b> in $\text{CD}_3\text{CN}$ .	165
Table 6.8	$^1\text{H}$ NMR spectroscopic data for <b>BPMA</b> in $\text{CDCl}_3$ .	168
Table 6.9	$^{13}\text{C}$ -NMR spectroscopic data for <b>BPMA</b> in $\text{CDCl}_3$ .	168
Table 6.10	$^1\text{H}$ -NMR spectroscopic data for <b>MeCO<sub>2</sub>-BzBPMA</b> in $\text{CDCl}_3$ .	169
Table 6.11	$^1\text{H}$ -DMR spectroscopic data for <b>MeCO<sub>2</sub>-BzBPMA</b> in $\text{CD}_3\text{CN}$ .	170
Table 6.12	$^{13}\text{C}$ -NMR spectroscopic data for <b>MeCO<sub>2</sub>-BzBPMA</b> in $\text{CDCl}_3$ .	170
Table 6.13	$^1\text{H}$ -NMR spectroscopic data for <b>[Re(CO)<sub>3</sub>(MeCO<sub>2</sub>-BzBPMA)]<sup>+</sup></b> in $\text{CD}_3\text{CN}$ .	171
Table 6.14	$^1\text{H}$ -NMR spectroscopic data for <b>HCO<sub>2</sub>-BzBPMA</b> in $\text{CDCl}_3$ .	172
Table 6.15	$^1\text{H}$ -NMR spectroscopic data for <b>HCO<sub>2</sub>-BzBPMA</b> in $\text{CD}_3\text{CN}$ .	173
Table 6.16	$^{13}\text{C}$ -NMR spectroscopic data for <b>HCO<sub>2</sub>-BzBPMA</b> in $\text{CDCl}_3$ .	173
Table 6.17	$^1\text{H}$ -NMR spectroscopic data for <b>[6.2-DB24C8]<sup>2+</sup></b> in $\text{CD}_3\text{CN}$ .	175
Table 6.18	$^1\text{H}$ -NMR spectroscopic data for <b>[6.2]<sup>2+</sup></b> in $\text{CD}_3\text{CN}$ .	176
Table 6.19	$^1\text{H}$ -NMR spectroscopic data for <b>[(Re(CO<sub>3</sub>))<sub>2</sub>(6.2-DB24C8)]<sup>4+</sup></b> in $\text{CD}_3\text{CN}$ .	178
Table 6.20	$^1\text{H}$ -NMR spectroscopic data for <b>[(Re(CO<sub>3</sub>)<sub>2</sub>)(6.2)]<sup>4+</sup></b> in $\text{CD}_3\text{CN}$ .	179
Table 6.21	$^1\text{H}$ -NMR spectroscopic data for <b>[(Ag)<sub>x</sub>(6.2-DB24C8)]<sub>x</sub><sup>+</sup></b> in $\text{CD}_3\text{CN}$ .	181
Table 6.22	$^1\text{H}$ -NMR spectroscopic data for <b>[(Cd)<sub>x</sub>(6.2-DB24C8)]<sub>x</sub><sup>+</sup></b> in $\text{CD}_3\text{CN}$ .	182
Table 6.23	$^1\text{H}$ -NMR spectroscopic data for <b>[6.2-<math>\text{T}^3\text{P-DB24C8}</math>]<sup>2+</sup></b> in $\text{CD}_3\text{CN}$ .	184

## List of Abbreviations

Å	Angstrom
BF <sub>4</sub>	tetrafluoroborate
Br	bromide
Bu	butyl
BPP34C10	bis(para-phenylene)[34]crown-10
BPMA	Bis(2-pyridylmethyl)amine
δ	chemical shift
CHCl <sub>3</sub>	chloroform
CH <sub>2</sub> Cl <sub>2</sub>	dichloromethane
CP	coordination polymer
DB24C8	dibenzo-24-crown-8
DSDB24C8	disulfonated-dibenzo-24-crown-8
d	doublet
dd	doublets of doublets
ddd	doublet of doublets of doublets
d	days
°	degrees
°C	degrees Celsius
DCC	dicyclohexylcarbodiimide
ESI-MS	electrospray ionization mass spectroscopy
Et	ethyl
EtOH	ethanol

G	Gibbs free energy
g	grams
H	enthalpy
h	hours
Hz	hertz
J	Joules
K	degrees Kelvin
kJ	kilojoules
$K_a$	association constant
LC	ligand centered
M	moles per liter
m	multiplet
Me	methyl
MeCN	acetonitrile
MeNO <sub>2</sub>	nitromethane
MeOH	methanol
min	minute(s)
ml	millilitres
mol	mole
MHz	megahertz
m/e	mass per charge ratio
MLCT	metal to ligand charge transfer
MOF	metal organic framework

MORFs	metal organic rotaxane framework
<i>n</i>	normal chain
NMR	nuclear magnetic resonance
OTf	trifluoromethane sulphonate (triflate)
oxine	8-hydroxyquinoline
ppm	parts per million
PQT	paraquat
PCPs	porous coordination polymers
py	pyridine
3-py	3-pyridinemethanol
4-py	4-pyridinemethanol
q	quartet
R	gas constant
RT	room temperature
S	entropy
s	singlet
SBUs	secondary building units
T	temperature
t	triplet
<i>t, tert</i>	tertiary
terpy	2,2':6',2''-terpyridine
UV/Vis	Ultraviolet/visible spectroscopy
X-Ray	X-ray diffraction

## List of Abbreviations of Compounds

tolyterpy	4'- <i>p</i> -tolyl-2,2':6',2''-terpyridine
Br-tolyterpy	4'-(4-Bromobenzyl)-2,2':6',2''-terpyridine
TB-DB24C8	tetrakis(bromomethyl)-dibenzo-24-crown-8
TP-DB24C8	tetrakis(phenoxyethyl)-dibenzo-24-crown-8
TE-DB24C8	tetrakis(ethyl 4-methoxybenzoate)-dibenzo-24-crown-8
TO-DB24C8	tetrakis(8-methoxyquinoline)-dibenzo-24-crown-8
T <sup>3</sup> P-DB24C8	tetrakis(3-(methoxymethyl)pyridine)-dibenzo-24-crown-8
T <sup>4</sup> P-DB24C8	tetrakis(4-(methoxymethyl)pyridine)-dibenzo-24-crown-8
MeCO <sub>2</sub> BzBPMA	(( <i>p</i> -methylbenzoyl)benzyl)bis(2-pyridylmethyl)amine
HCO <sub>2</sub> -BzBPMA	N-( <i>p</i> -carboxy-benzyl) bis(2-pyridylmethyl)amine

# Chapter 1

## Background

### 1.1 Origins of Supramolecular Chemistry

Chemistry is a science of interactions, transformations and modeling. It has the power to create new molecules and new materials bearing novel properties. Ever since the synthesis of urea,<sup>1</sup> “molecular chemistry” has had the power of making and breaking covalent bonds. As time went on, it was shown that most biological molecules involve weak, non-covalent interactions that bind substrates to receptor proteins. The observations, study and utilization of these weak interactions have led to a new field of chemistry known as supramolecular chemistry, defined as “*chemistry beyond the molecule*”. Supramolecular chemistry relies on organized entities of higher complexity that result from the association of two or more chemical species held together by intermolecular forces.<sup>1</sup> This 1978 definition by Jean-Marie Lehn, was further elaborated, in 2002 to, “*Supramolecular chemistry aims at developing highly complex chemical systems from components interacting by non-covalent intermolecular forces.*”<sup>2</sup>

The field of supramolecular chemistry is different from molecular chemistry because it does not rely solely on covalent bonds. The molecules are instead held together by non-covalent interactions such as electrostatic forces, hydrogen bonds, and van der Waals forces. These interactions can generate new molecules known as supermolecules, with structures that depend on the non-covalent interactions between two or more species. These molecules that make up the new species must complement each other both in size and shape (geometry) and binding site (energy). When the two new molecules combine,



they give us the information needed to understand the weak interactions present in supermolecules.

The field of supramolecular chemistry has its origin in the 1960's with the development of macrocyclic chemistry from the groups of Curtis, Busch, Jager, and Pederson.<sup>2</sup> In 1967, Pederson<sup>3</sup> worked on new macrocyclic ligands known as “crown ethers” shown below in Figure 1.1.

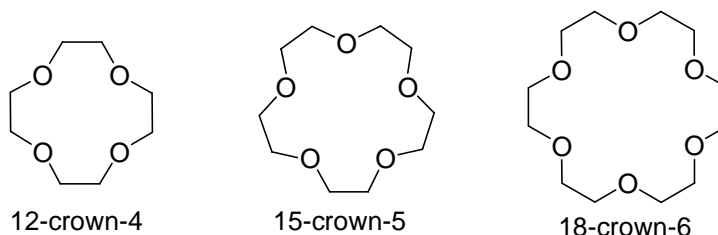


**Figure 1.1** Structures of crown ethers.

In the following years, Lehn developed bicyclic compounds similar to crown ethers called “cryptands”, shown in Figure 1.2. Both these cryptands and crown ethers have properties that allow them to bind to alkali metals, ammonium salts and anions. The properties that allow for the formation of complexes are: the size of the ring, the number of donor atoms, co-planarity of the donor atoms, the basicity of the donor atoms, steric hindrance and solvation of the ion.<sup>3</sup>

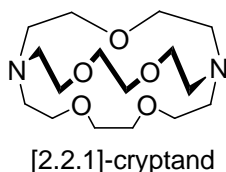


**Figure 1.2** Structure of a cryptand.

In 1973, Cram defined a new term to explain this phenomenon; he called it “host-guest complexation”.<sup>2</sup> Host-guest complexes are held together by non-covalent interactions. For their development in supramolecular chemistry of molecules with

specific structures and interactions, Cram, Lehn, and Pederson were rewarded with the Nobel Prize in chemistry in 1987.<sup>4</sup> Today, as a result of large collaborations between different researchers in physics, theoretical and computational modeling, crystallography, inorganic and solid state chemistry, synthetic organic chemistry, biochemistry and biology, a great deal of work is being done to expand and explain the relatively new area of supramolecular chemistry.

## 1.2 Interpenetrated and Interlocked Compounds

Since the beginning of supramolecular chemistry, much attention has focused on the formation of host and guest complexes. One such complex is the interpenetrated adduct called a pseudorotaxane, composed of two molecules threaded to each other, which can lead to interlocked compounds called rotaxanes and catenanes.

### 1.2.1 Pseudorotaxanes

Pseudorotaxanes are supramolecular complexes in which a cyclic wheel and a linear axle are interpenetrated but free to dissociate from each other as seen in Figure 1.3.<sup>5</sup>

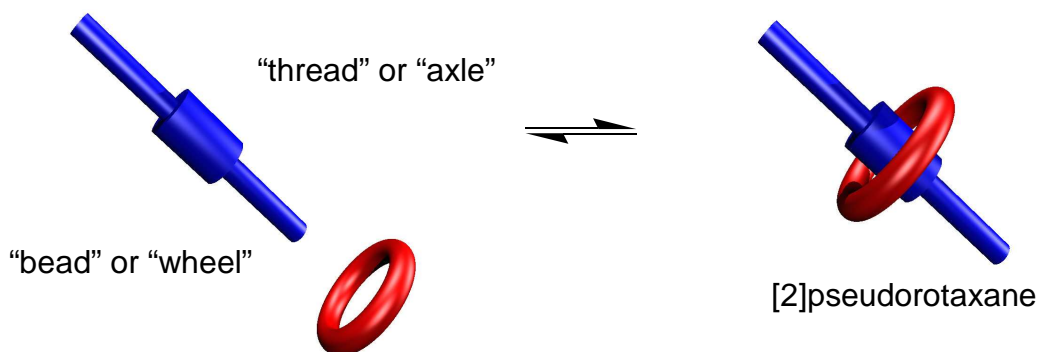


**Figure 1.3** Cartoon representation of [2]pseudorotaxane formation.

There are many different templates to construct pseudorotaxanes that rely on non-covalent interactions such as  $\pi$ - $\pi$  stacking (including C-H $\cdots$  $\pi$ ), hydrogen bonding, charge transfer complexes, and hydrophobic interactions.<sup>6,7</sup> The preformed [2]pseudorotaxane

comprised of a thiol-functionalized thread and  $\alpha$ -cyclodextrin which relies on the hydrophobic interaction was used to build a [2]catenane; Figure 1.4.<sup>8</sup>

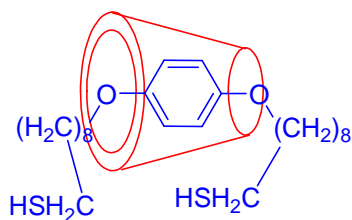


**Figure 1.4** The first interpenetrated molecular species.

Later on, molecules relying on  $\pi$ - $\pi$  stacking, and charge transfer interactions acted as templates for interpenetrated species between electron-rich  $\pi$  systems, and electron-deficient aromatic systems; Figure 1.5.<sup>9</sup>

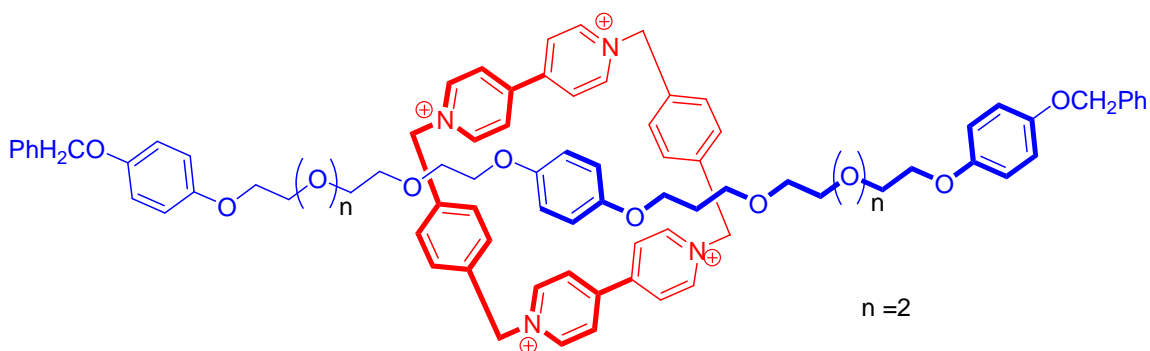


**Figure 1.5** A [2]pseudorotaxane that relies on electron rich and electron poor aromatics.

Hydrogen bonding templates were investigated as interpenetrated molecules were found to form between ammonium salts and large crown ethers. In particular, Stoddart showed dibenzo-24-crown-8 (**DB24C8**) and bis(paraphenylene)-34-crown-10 (**BPP34C10**) could form complexes with dialkylammonium ( $R_2NH_2^+$ ) ions that were [2]pseudorotaxanes.<sup>10</sup> Later on, the groups of Loeb<sup>11</sup>, Tiburcio<sup>12,13</sup> and Schmitzer<sup>14</sup> developed the axles 1,2-bis(pyridinium)ethane, bis(benzimidazolium), and methylenediimidazolium respectively which formed [2]pseudorotaxanes with crown ethers similar to the example shown in

Figure 1.6. Other templates involved the use of anions or halogen bonds to hold the [2]pseudorotaxane together. Figure 1.7 shows an example from Beer *et al.*<sup>15,16</sup>

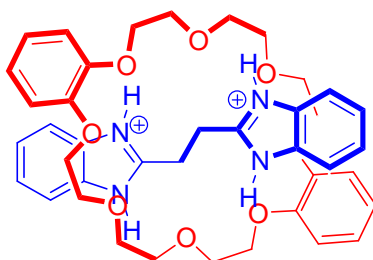


**Figure 1.6** A hydrogen bonding [2]pseudorotaxane.

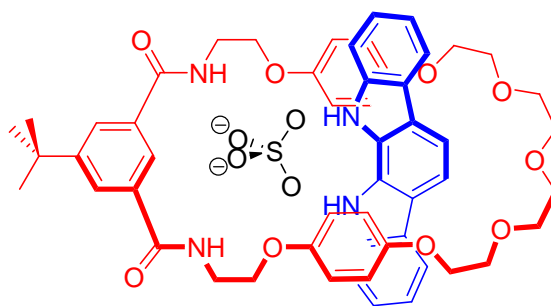


**Figure 1.7** An anion binding template.

Today, besides the use of crown ethers as wheels, research is focused on the development of other macrocyclic receptors as wheel components such as cyclodextrins, cucurbiturils, calix[n]arenes, and pillar[n]anes.<sup>17-20</sup> Sauvage was the first to use metal ions as templates, holding the different components together to form pseudorotaxanes, and then carrying out further reactions to form [n]rotaxanes (and [2]catenanes); Figure 1.8.<sup>21</sup> There has also been a focus on the use of metals as templates for [2]pseudorotaxanes formation. Wisner and co-workers have shown that *trans*-dichlorobis(pyridine)palladium(II) complexes undergo second-sphere interactions with a macrocyclic tetralactam; Figure 1.9.<sup>22</sup>

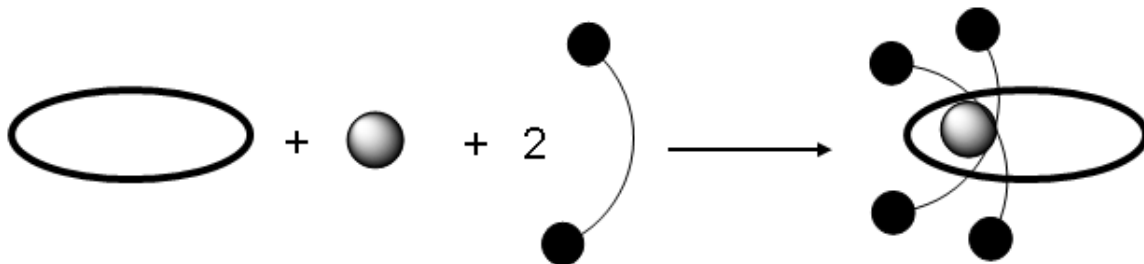


**Figure 1.8** Sauvage used metal ions as templates for [n]pseudorotaxane formation.

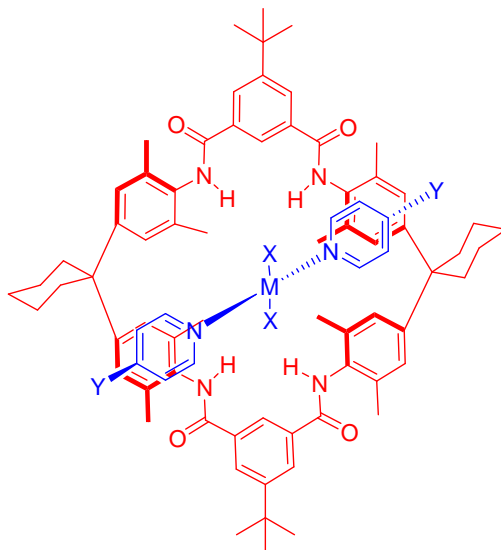


**Figure 1.9** Second-sphere interaction to form [2]pseudorotaxane.

### 1.2.2 Measuring Association Constant

While developing new templates for the formation of pseudorotaxanes, a question arises as to the strength of the interactions, which hold the wheel and the axle together. The higher the association constant, the more the product side of the equilibrium is favoured, *i.e.* formation of [2]pseudorotaxane. There are a number of methods that allow determination of the strength of the interaction: an example is the noticeable change of colour during a UV/Vis titration, while another is the observation of a significant chemical shift in  $^1\text{H}$  NMR spectroscopy. Two commonly used techniques –  $^1\text{H}$  NMR (single point determination, or titrations) and isothermal titration calorimetry (ITC) – will be discussed below:

## 1. $^1\text{H}$ NMR spectroscopy - Single point determination

At slow exchange on the NMR time scale, the bound and free components can be distinguished by their differences in chemical shifts. The association constant can be determined since the association is temperature dependent and both chemical shifts are known. The binding constant can be calculated simply from knowing the original host and guest concentrations and the abundance of each species at various temperatures as determined by integration. The association constant, enthalpic and entropic components can then be obtained from a van't Hoff plot ( $R\ln K$  vs  $T^{-1}$ ), which results in a straight line with a slope of  $-\Delta H$  and an intercept of  $\Delta S$ . There are cases where a van't Hoff plot is not a linear plot, as a result of the thermodynamic properties being temperature-invariant. Many factors contribute to this phenomenon including conformational, vibrational and hydrophobic interactions but the phenomena can be taken into account by introducing a heat capacity ( $\Delta C_p^\circ$ ) term.<sup>23-25</sup>

## 2. $^1\text{H}$ NMR spectroscopy - Titrations

When the component interactions are at fast exchange only an average signal is observed for both the wheel and axle resonances. The axle can be titrated with increasing amounts of wheel until saturation is reached and non-linear least-squares analysis results in the curvature of the van't Hoff plot becomes evident, utilized to extract the association constant using a non-linear refinement program. This requires starting concentrations of wheel from the observed protons shifts, and initial estimations of association constants, and complexed and uncomplexed chemical shifts of the probe proton.<sup>26</sup>

### 3. Isothermal Calorimetry

The thermodynamic parameters of the stoichiometry of the interaction ( $n$ ), the association constant ( $K_a$ ), the free energy ( $\Delta G_o$ ), enthalpy ( $\Delta H_o$ ), entropy ( $\Delta S_o$ ), and heat capacity of binding ( $\Delta C_p$ ) can be calculated by measuring the binding equilibrium directly from the heat evolved upon association of axle with the wheel. Upon titration of axle into a solution of the wheel, the heat released ( $H$ ) is measured over time. The addition of small volumes of axle until the heat diminishes results in a binding curve of heat release versus the mole ratio.<sup>27</sup>

#### 1.2.3 Rotaxanes

Rotaxanes are molecules that contain a linear component (the axle) encircled by one, or more, macrocyclic component (the wheel). In order to prevent the wheel from slipping off the axle, the linear component must be terminated at both ends by large blocking groups or stoppers, as seen in the cartoon representation of a rotaxane in Figure 1.10.

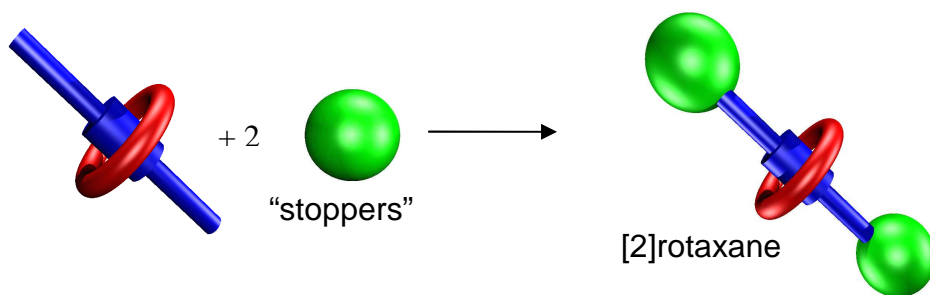


**Figure 1.10** Cartoon representation of [2]rotaxane.

#### 1.2.4 Early Attempts at the Synthesis of Interlocked Molecules

Interlocked supramolecular species can be traced back to when Harrison and Harrison made the first interlocked species with the help of a resin with a yield of 6%.<sup>28</sup> They used a "statistical" approach, when a molecular axle, functionalized on both ends, may enter into a macrocycle of adequate size, but the probability that cyclization occurring while

the linear axle is threaded through the macrocycle is very small. One can only expect poor yields in this kind of synthesis.<sup>29</sup> Later on, I. T. Harrison used a “statistical slipping” approach by heating a mixture of cyclic hydrocarbons over the end groups of the dumbbell-shaped 1,10-bis(triphenylmethoxy)-decane at 120°C; Figure 1.11.<sup>30</sup>

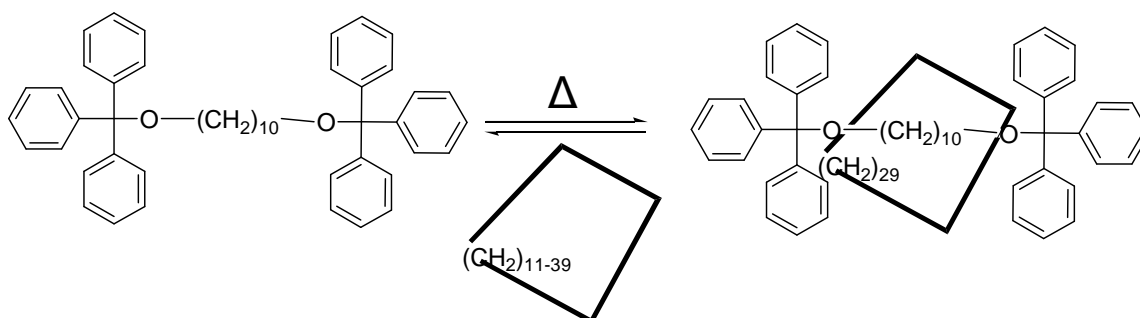


**Figure 1.11** Harrison’s “statistical slipping” methodology.<sup>30</sup>

The statistical method has disadvantages of using harsh conditions and producing low yields of the preferred product. An attempt to overcome these nuisances was developed by Schill with [2]catenanes, called “directed” synthesis. It involved making a pre-rotaxane composed of macrocyclic and acyclic components linked by covalent bonds. Subsequently, the linking bond is cleaved, leaving in place only mechanical bonds; Figure 1.12.<sup>31</sup> Unfortunately, this method proved to be challenging due to the multistep syntheses which are time-consuming and also of low yields. Other methods used to form rotaxanes were published by Stoddart in a review in 1995<sup>5</sup> with the advancement of supramolecular chemistry allowing for molecular recognition to improve on the yield of the [2]rotaxane formation.



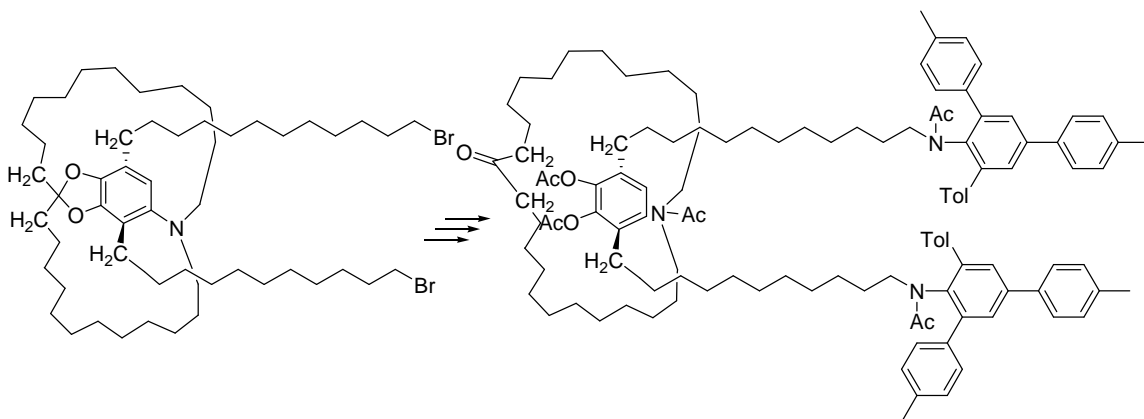
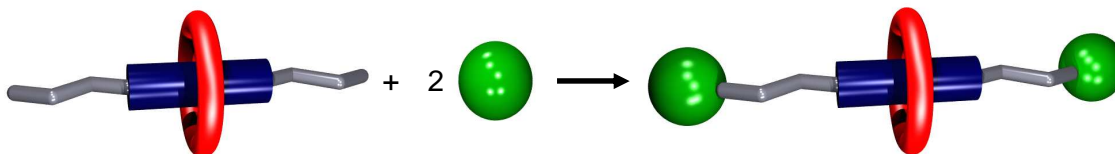


**Figure 1.12** “Directed” synthesis of a [2]rotaxane.<sup>31</sup>

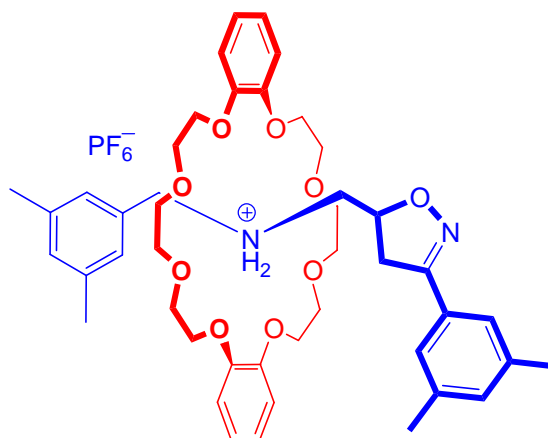
### 1.2.5 Synthesis of Rotaxane Using Molecular Recognition Templates

There exist a number of modern methods for rotaxane synthesis such as: capping, clipping and slippage. The capping method involves the formation of the equivalent [2]pseudorotaxane, to which bulky substituents or stoppers are added to the extremities of the axle after the equilibrium of the [2]pseudorotaxane has been achieved; Figure 1.13.

A number of synthetic methods have been made available for capping such as alkylation, ester (carbonate and acetal formation), oxidative coupling, cycloaddition, Wittig reactions, coordination chemistry, electronic blocking groups, and click chemistry.<sup>32-39</sup> Other elegant ways in which rotaxanes have been made include photoisomerization and boron-based, donor-acceptor chemistry.<sup>40,41</sup> Figure 1.14 shows an example of a click synthesis without the use of catalysts which uses a nitrile *N*-oxide as the stopper by reacting pseudorotaxanes possessing alkene, alkyne, or nitrile groups.<sup>39</sup>

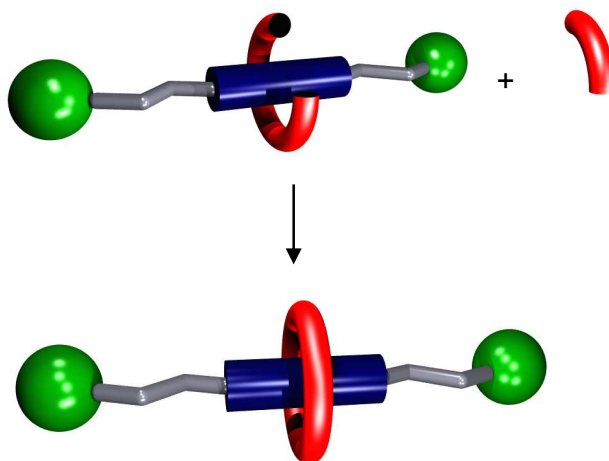


**Figure 1.13** Cartoon illustration of the treading/capping method.



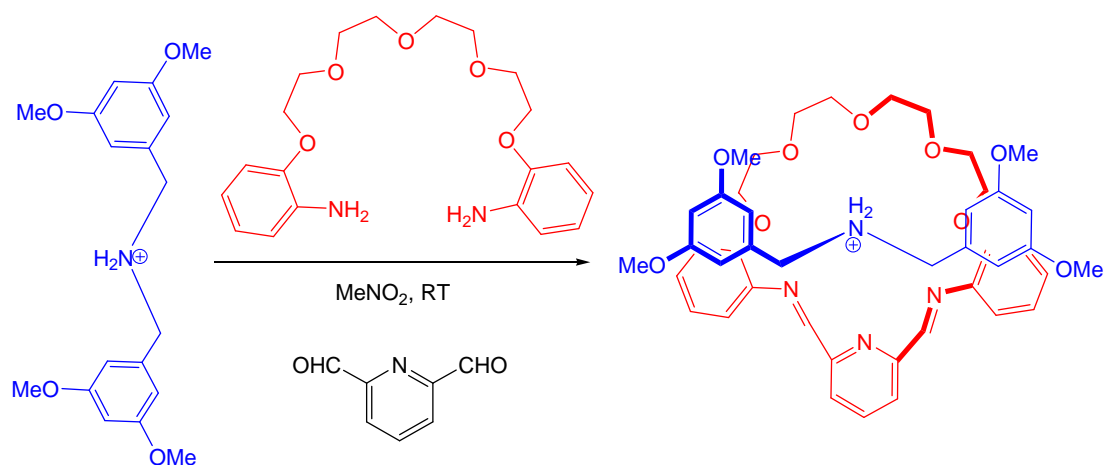
**Figure 1.14** Example of a [2]rotaxane formed by the threading/capping process.<sup>39</sup>

The clipping process relies on the macrocyclization of the subunits of a wheel-like component around the recognition site of a dumbbell-shaped component<sup>42</sup> followed by the clipping of another subunit to complete the cyclization; Figure 1.15.



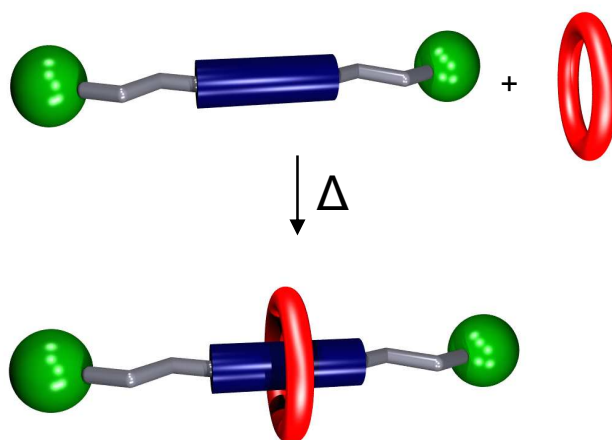
**Figure 1.15** Cartoon representation of clipping.

Stoddart used the clipping process to make [2]rotaxanes by formation of an imine bond from amine and carbonyl groups in the presence of a dibenzylammonium cation thread; Figure 1.16.



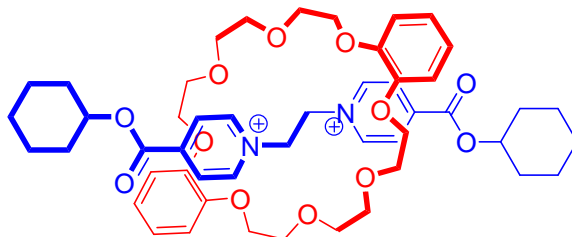
**Figure 1.16** Example of the clipping process in the formation [2]rotaxane.<sup>43</sup>

The final process called slippage requires a fine balance between the size of the bulky extremities on the axle and the macrocyclic wheel. Under proper thermodynamic conditions, the rotaxane may be slowly formed by the wheel slipping onto the axle, as the name suggests, and upon cooling the macrocyclic wheel becomes kinetically trapped causing the two components to be interlocked; Figure 1.17.



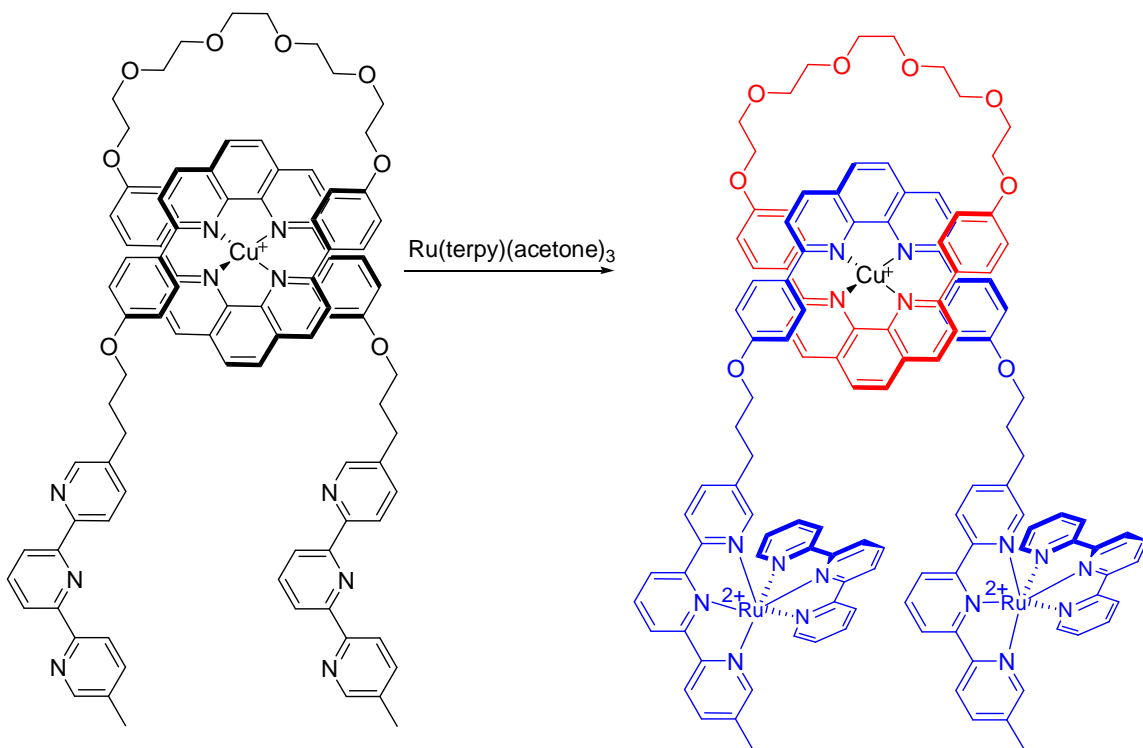
**Figure 1.17** Cartoon illustration of slippage of a [2]rotaxane.

Figure 1.18 shows a recent example of slippage rotaxane with a **DB24C8** wheel and a 1,2-bis(pyridinium)ethane type axle.<sup>44</sup>



**Figure 1.18** Example of a [2]rotaxane formed by slippage.<sup>44</sup>

Sauvage used Cu(I) to coordinate diphenylphenanthroline flanked by 2,2':6'2''-terpyridine groups and followed this by stoppering with Ru(terpy)Cl<sub>3</sub> to form a [2]rotaxane; Figure 1.19.<sup>45</sup>



**Figure 1.19** The use of transition metals for templation by Sauvage.

Metals have also been used for the catalytic, ring closing metathesis (RCM), the Huisgen–Meldal–Fokin copper(I)-catalysed terminal alkyne–azide cycloaddition; the CuAAC “click” reaction.<sup>46</sup> The newest methodology called “active template” involves transition metal ions acting as both the template for the threaded architecture and as the catalyst for the covalent bond forming reaction that captures the interlocked structure.

This removes the requirement for a recognition motif in the thread. Leigh has recently developed a [2]rotaxane using Ni(II) and a pyridine-2,6-bisoxazoline macrocycle ligand to and  $sp^3$ - $sp^3$  coupling of alkyl chains; Figure 1.20.<sup>47</sup>

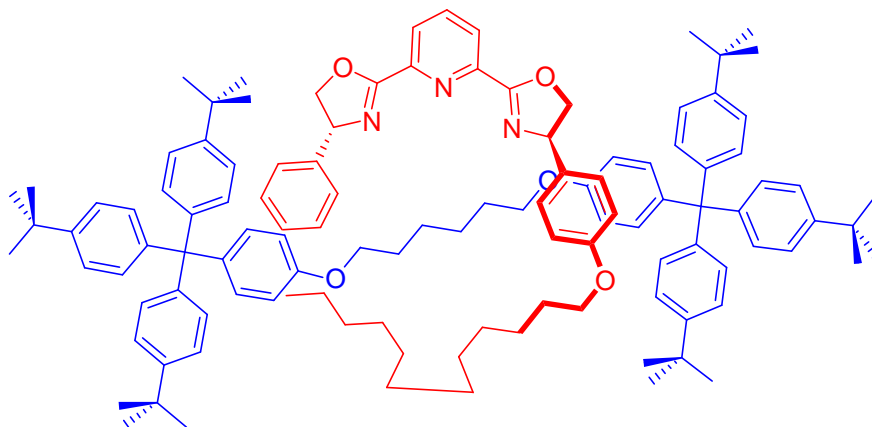


**Figure 1.20** A [2]rotaxane formed using Leigh's "active metal" template coupling of alkyl chains.<sup>47</sup>

Even though the synthesis of new interlocked molecules with metals allows for interesting rotaxane formation, the question arises whether one can use these moieties to form periodic crystalline frameworks via metal ligand interactions.

### 1.3 Polymeric Frameworks

Crystal engineering by Desiraju as "*the understanding of intermolecular interactions in the context of crystal packing and the utilization of such understanding in the design of new solids with desired physical and chemical properties*".<sup>2</sup> Over the years, chemists have begun to be able to control the non-covalent interactions that are used to form crystalline frameworks.

#### 1.3.1 Coordination Polymers

The term coordination polymer (CP) was first used in 1964 by J. C. Bailer to describe metal-ligand compounds that extend "infinitely" into one, two or three dimensions (1D, 2D or 3D) as illustrated in Figure 1.21.<sup>48</sup>

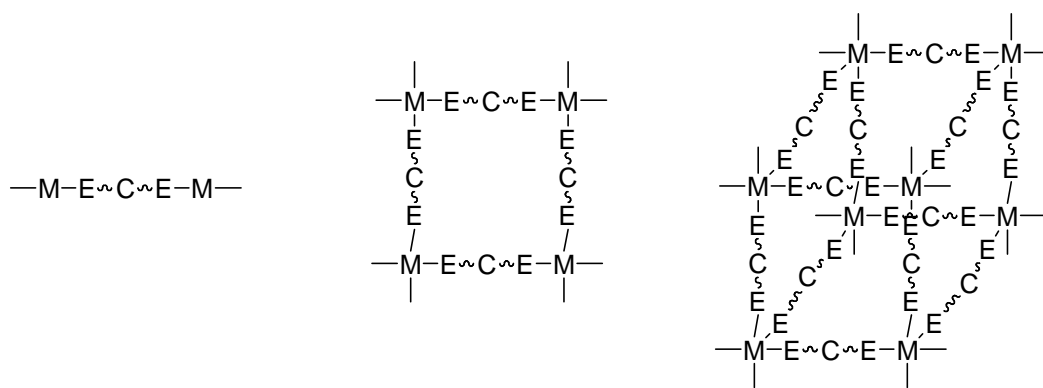


**Figure 1.21** Schematic representation of the networks that CPs can form, where E are donor atoms.

The construction of coordination polymers is usually carried out using polydentate ligands with rigid back bones and the donor atoms are usually nitrogen or oxygen. The mostly popular ligands are 4,4'-pyridine derivatives, pyrazine, or polycarboxylates.<sup>49</sup> The CPs are held together through coordination interactions and often combined with weaker forces such as hydrogen bonds,  $\pi$ - $\pi$  stacking or van der Waals interactions.<sup>50</sup>

The “node and spacer” approach developed by R. Robson has become a widely employed strategy for synthesizing coordination polymers with various dimensionalities and network topologies. It relies on the strength and directionality of the coordination bonds established between the metal ions and the ligands.<sup>51</sup> The type of network topology can be controlled by considering a numbers of factors such as geometry, charge, hard soft acids and bases (HSAB) behaviour of the metal, and shape, size, and HSAB behaviour of the ligands. One of the simplest of networks obtained is the diamond-like structure shown in Figure 1.22, where the diamondoid network in  $\text{Cu}[\text{C}(\text{C}_6\text{H}_5\text{CN})_4]\text{BF}_4$  is built around the tetrahedral Cu(I) centre and the central tetrahedral C-atom of the tetranitrile ligand. The spaces in the lattice are filled with solvent and  $\text{BF}_4$  anions. The crystal readily underwent anion exchange whilst retaining its crystal structure.<sup>52</sup>

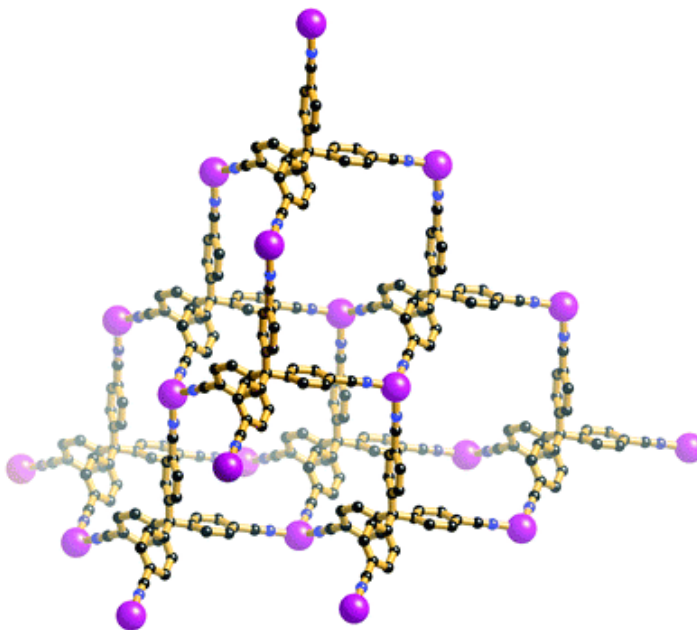


**Figure 1.22** Diamond-like network of  $\text{Cu}[\text{C}(\text{C}_6\text{H}_5\text{CN})_4]\text{BF}_4$ .<sup>52</sup>

Solid-state architectures are determined by several factors: 1) metal-to-ligand stoichiometry, 2) the stereochemical preference (coordination algorithm) of the assembling cations, 3) the use of ancillary ligands attached to the metal ions or the use of additional bridging ligands, 4) the intervention of noncovalent interactions (hydrogen bonds,  $\pi$ - $\pi$  stacking), 5) the role of the anions (coordinated, bridging, uncoordinated), and 6) the presence of organic guest molecules, which can act as templates.<sup>49</sup>

The solid-state architectures that are generated by the above interactions can lead to unusual properties in the polymers which are of great interest as potential candidates for new materials with applications such as fluorescence, magnetism, catalysis, nonlinear optics, gas absorption or as semiconductors.<sup>48,50</sup>

There are many molecular building blocks available to construct networks held together by weaker bonds like the ones seen here. Nowadays, another class of networks that gets a lot of attention uses robust metal clusters entirely formed by strong covalent bonds; the so-called metal organic frameworks (MOFs).

### 1.3.2 Metal Organic Framework

Over the years, a number of materials have been synthesized that contain a metal and an organic linker with varying terms of description such as coordination polymer, hybrid organic-inorganic, organic zeolite, and metal organic framework.

A metal organic framework can be defined as having 1) strong bonds providing robustness, 2) linking units that are available for modification by organic synthesis and 3) a geometrically well-defined structure.<sup>53</sup> One of the important parts in the construction of MOF is structure prediction. To aid in prediction, the concept of secondary building units (SBUs) is useful. These are most often multidentate linkers such as carboxylates, which have the ability to aggregate with metal anions into M-O-C clusters. These clusters are important in forming porous structures because 1) the M-O-C cores give a well-defined shape that is important in predicting the geometry of the overall topology, 2) the carboxylate ligands can be bi- or tridentate in order lead to extended frameworks, and 3) some clusters contain weak coordinating solvent molecules that can be removed to produce pores or replaced with other ligands.<sup>54</sup> The simplest example of a metal organic framework uses 1,4-benzenedicarboxylate. The resulting MOF-5 with the tetrahedral Zn(II) ions and formula  $[Zn_4O(BDC)_3]$  is a representative example of a cubic framework and is shown in Figure 1.23.<sup>54</sup>



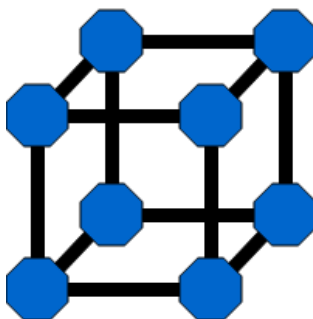


**Figure 1.23** A representation of the cubic arrangement of SBU and linkers in MOF-5 where blue blocks are M-O-C clusters and the black lines are the organic linkers.

With the large number of organic linkers available, numerous different topologies can be obtained. There are a number of ways to get single crystals from these frameworks such as slow evaporation of a solution of the precursors, layering of solutions, or slow diffusion of one component solution into another through a membrane or an immobilizing gel. For more robust frameworks, there is also the solvothermal technique available. These frameworks have found applications in hydrogen storage, carbon dioxide capture, gas separation, sensing, molecular recognition, nonlinear optics, luminescence, magnetic ordering, heterogeneous catalysis, and drug delivery.<sup>55</sup>

MOFs have also been made with mixed ligands by using pyridine linkers and carboxylate corners to develop more porous frameworks that give the system both stability and framework flexibility. These porous frameworks, called porous coordination polymers (PCPs), have the same properties as MOFs and have also been used in regulating polymerization.

PCPs usually involve a “pillaring” strategy as this allows for designing open metal-organic frameworks by using appropriate pillars to connect well-defined two-dimensional (2D) layers either in a one-pot reaction or in two separate steps. These 2D layered structures are based on common “paddlewheel” units.<sup>56</sup> With solvent molecules

occupying both ends of the binuclear centre, this type of charge-neutral 2D layer is an ideal candidate to pillar into a 3D open frameworks by using linear connectors that are usually nitrogen based linkers; Figure 1.24.

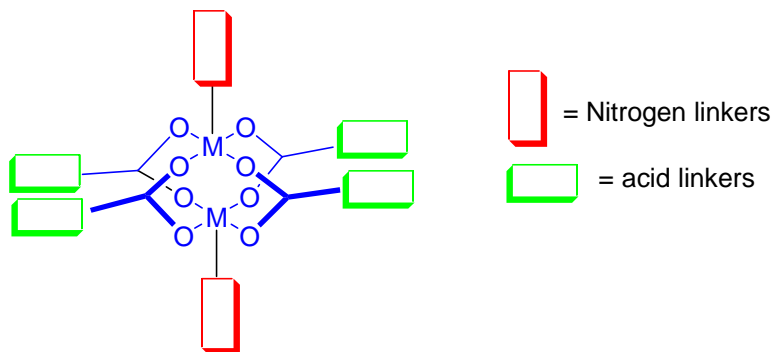


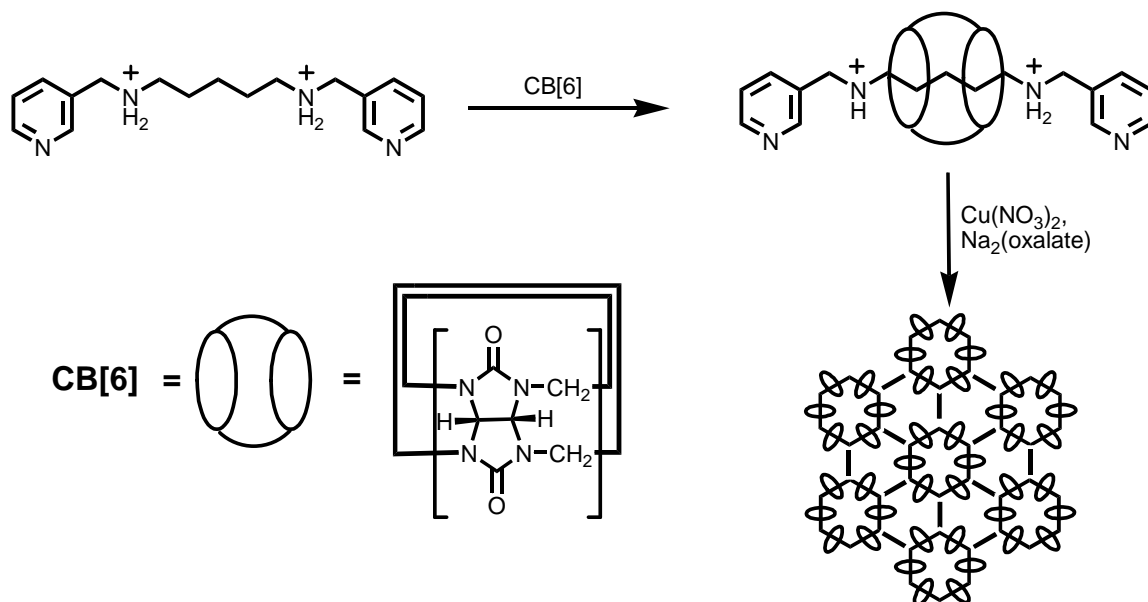
**Figure 1.24** Representation of a mixed linker system.

So... is there away to combine the interesting properties of interlocked molecules into such ordered frameworks producing materials that have readily addressable and controllable molecular components?

### 1.3.3 Metal Organic Rotaxane Framework (MORF)s

One such approach is to form metal-based polyrotaxanes, which involves taking an axle and a wheel that have suitable functional groups at both ends and coordinating them to metal centres thus forming coordination polymers or frameworks in 1-, 2- or 3D.

Kim *et al.* first demonstrated such structures by combining a cucurbituril (CB[6]) wheel with diaminoalkane axles containing pyridyl, cyano, or carboxylic acid functional groups to coordinate to metals.<sup>57</sup> They determined that the overall resulting topology can be controlled by the coordination number and geometry of the metal linker, as seen in Scheme 1.1.



**Scheme 1.1** Kim framework with diaminoalkanes, axle, and cucbituril(CB[6]) wheel.

Loeb *et al.* demonstrated that a 1,2-bis(pyridinium)ethane axle and a **DB24C8** wheel can form MORFs; Figure 1.25. However the nature of the framework does not simply depend on the metal but also on the solvent used in the formation of the MORFs. A linear 1D framework was obtained when a coordinating solvent, such as MeCN was used but a 2D grid network was obtained with non-coordinating such as MeNO<sub>2</sub>; Figure 1.26.<sup>58</sup>

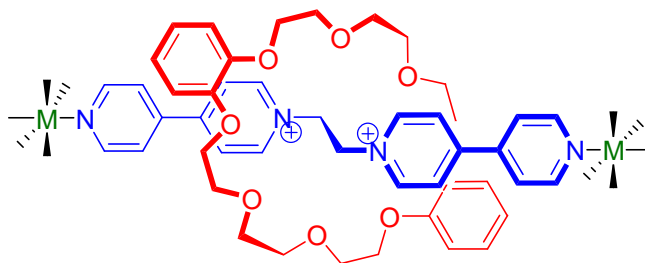


**Figure 1.25** A polyrotaxane.

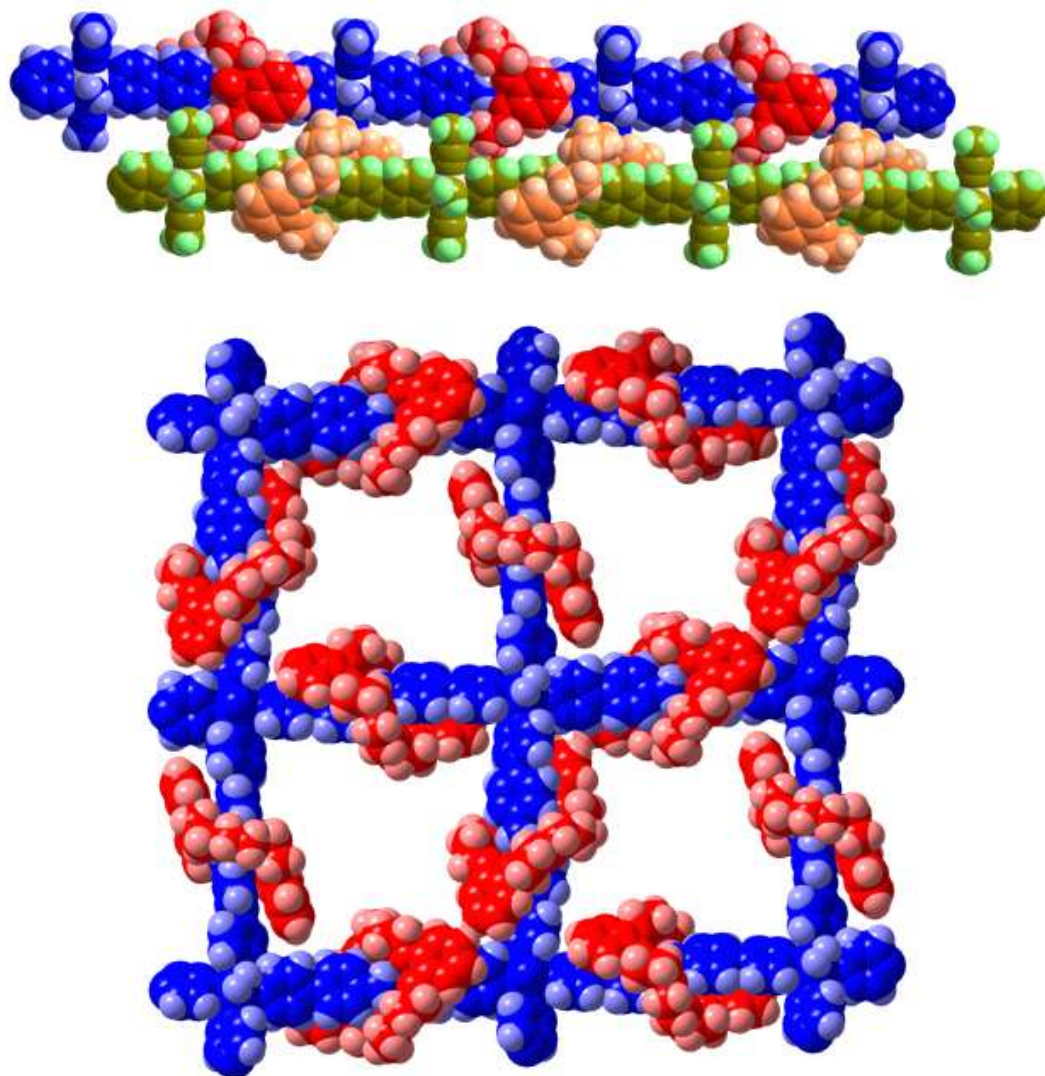


**Figure 1.26** (a) A 1D framework and (b) a 2D grid with 1,2-bis(4,4'-dipyridinium) ethane, thread and **DB24C8** wheel.

Regardless of the metal-to-ligand ratio, a 2D square net was the highest periodicity attainable with this dynamic ligand and d-block transition-metal ions. This is because the placement of six of these sterically demanding ligands around a single metal ion would be too crowded. To obtain a higher dimensional framework a longer axle was synthesized with N-oxide groups as seen in Figure 1.27.

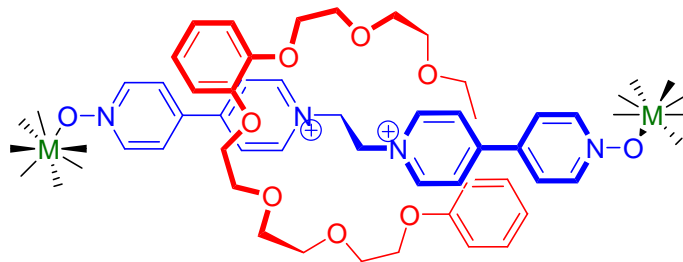


**Figure 1.27** N-oxide axles developed to form 3D networks.

Larger lanthanide ions, such as Sm(III), Eu(III), Gd(III), Tb(III) or Yb(III) prefer higher coordination numbers and can thus lead to 3D coordination polymers; Figure 1.28.<sup>58</sup> The cavities in the above framework are filled with solvents (MeCN) and counterions (OTf) and also another lattice due to interpenetration. Although these materials do meet the required stability for further study they are not porous but, it is reasoned that eventually we will be able to construct MORF materials that are crystalline solids that are physically and thermally robust and have sufficient porosity to allow the dynamic components to “function” in a well-defined “space”.<sup>59</sup>

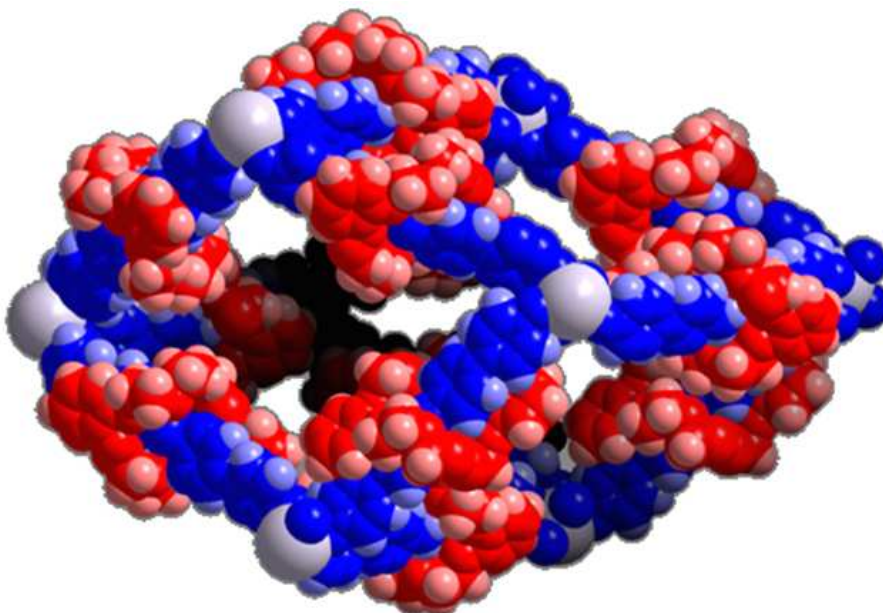


**Figure 1.28** 3-D Framework using a 1,2-bis(4,4'-dipyridinium-N-oxide)ethane axle and DB24C8 wheels.

Loeb's first approach to neutral frameworks was to eliminate counterions by using neutral [2]pseudorotaxane linkers containing the 1,2-bis(4,4'-dipyridinium)ethane dication and employing the *anti* isomer of disulfonated-dibenzo-24-crown (**DSDB24C8**) as the wheel (Figure 1.29).<sup>60</sup> The ligands can then be capped/linked with either the Cu(II) paddlewheel ( $\text{Cu}_2\text{BnO}_4$ ) or CuBr to form 1D MORFs as seen in Figure 1.30.<sup>60</sup>

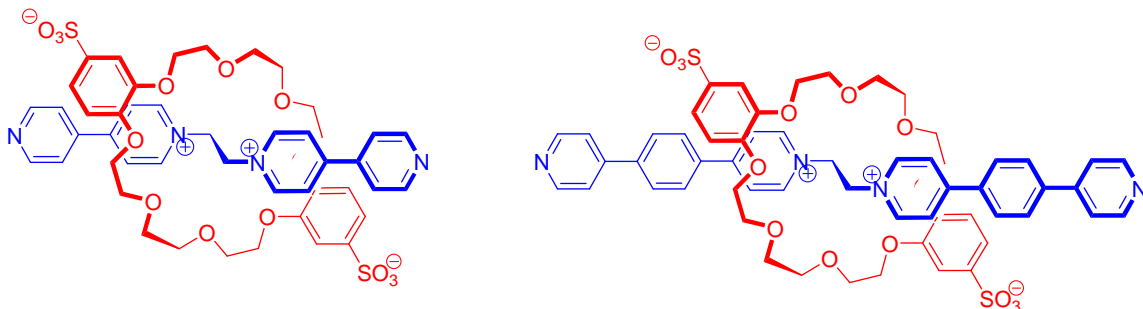


**Figure 1.29** Extended axle used for the neutral 1-D MORFs.

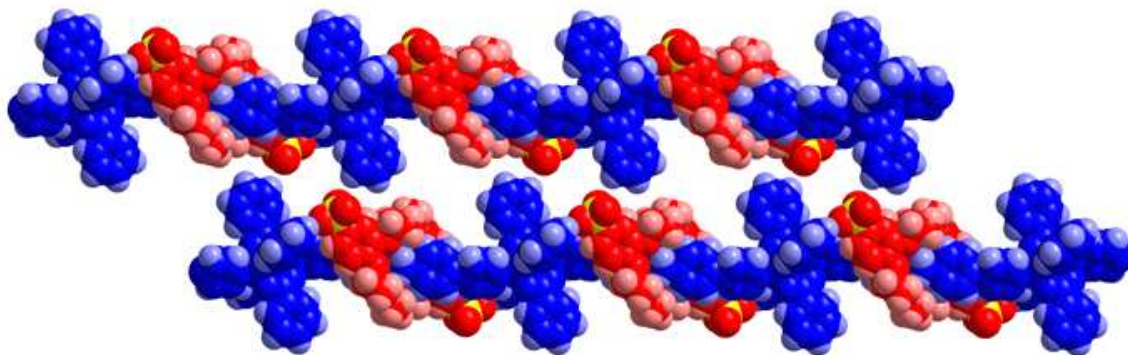


**Figure 1.30** 1-D Framework with 1,2-bis(4,4'-dipyridinium)ethane axle, **DSDB24C8** wheel and  $\text{Cu}_2\text{BnO}_4$  linker.<sup>60</sup>

Due to the limited number of neutral metal nodes available to create porous networks in this manner, attention was switched from neutral to anionic ligands. This was achieved by simply eliminating one of the positive charges of the axle. Combining this new axle with **DSDB24C8** resulted in a negatively charge [2]pseudorotaxane linker; Figure 1.31.<sup>60</sup>

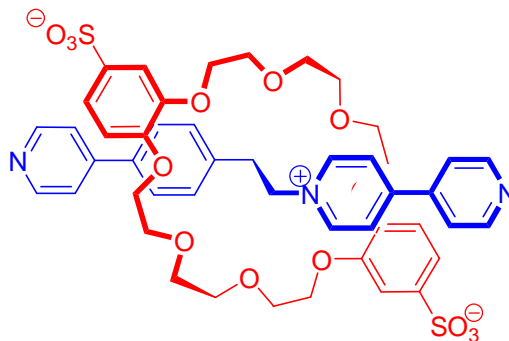


**Figure 1.31** A negatively charged [2]pseudorotaxane linker.

Reaction with one equivalent of  $\text{Zn}(\text{NO}_3)_2 \cdot 4\text{H}_2\text{O}$  in MeOH resulted in a 1D framework. By increasing the amount of metal used and using a mixture of 1:9 MeOH/MeNO<sub>2</sub> a 2D grid was formed, where each layer is stacked by water molecules through extensive hydrogen bonding.<sup>61</sup>

Besides using [2]pseudorotaxanes as linkers for the formation of MOFs, Stoddart and Yaghi developed macrocyclic polyethers which are themselves linkers containing carboxylate groups; Figure 1.32. These linkers can combine with  $\text{Zn}_4\text{O}(\text{CO}_2)_6$  clusters to form a MOF structure similar to MOF-5. These new MOFs are able to interact with paraquat as  $[\text{PQT}][\text{PF}_6]_2$  to form a [2]pseudorotaxanes inside the MOF as seen in Figure 1.32.<sup>62</sup> They later applied similar macrocyclic polyethers linkers to form 2D frameworks with [2]catenanes as shown in Figure 1.33.<sup>62</sup>



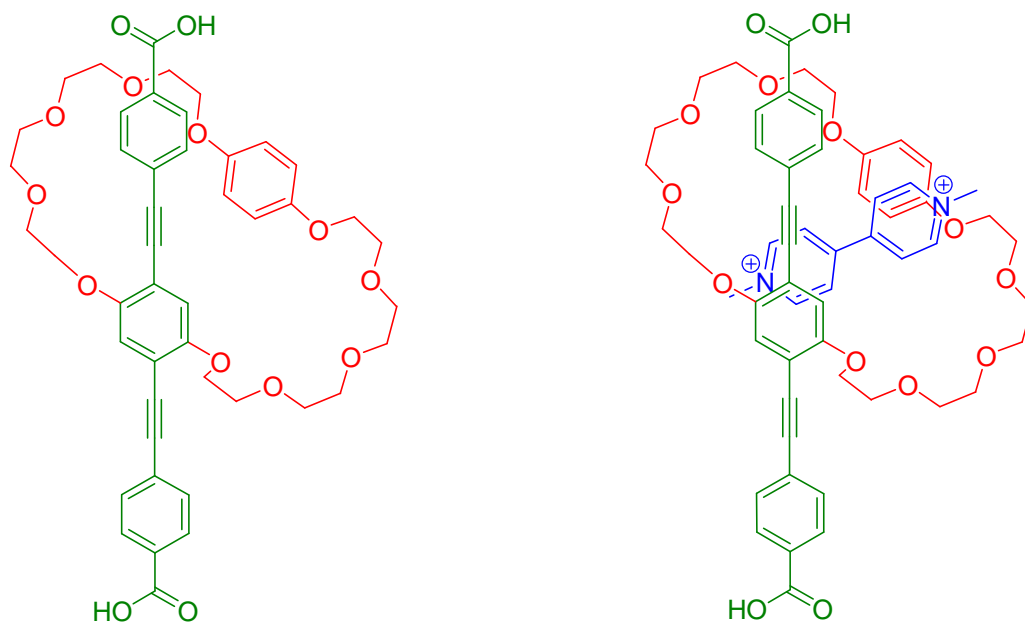


**Figure 1.32** Stoddart's macrocyclic polyether linkers that form a MOF-5 type structure use to “dock”  $\text{PQT}^{2+}$ .

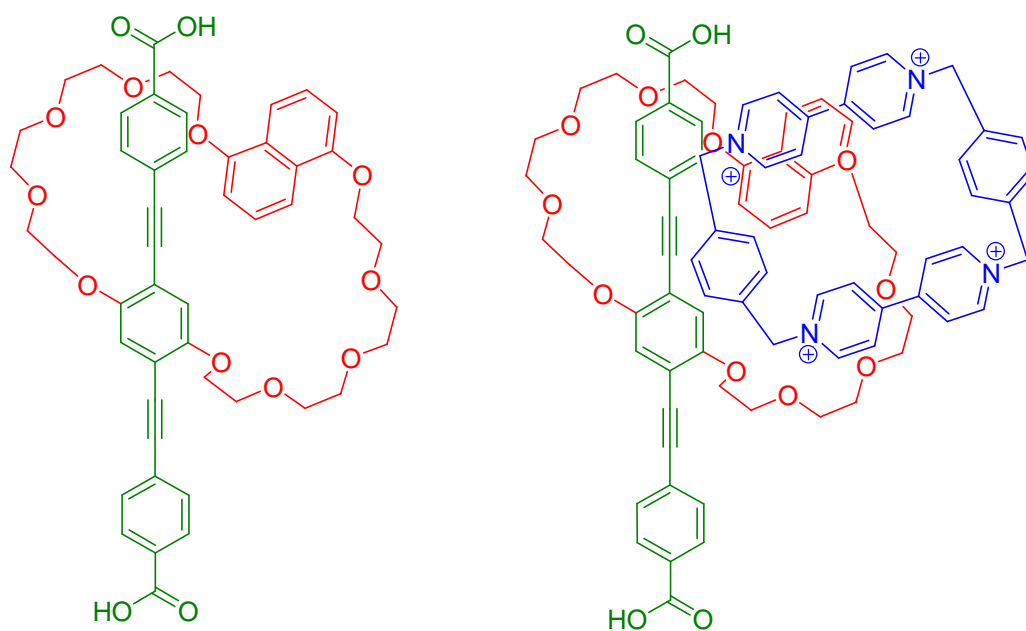


**Figure 1.33** Stoddart's macrocyclic polyether used to form a framework containing a [2]catenane.

Stoddard later developed a chiral MOFs containing  $\gamma$ -cyclodextrin that could potentially be used for chiral-recognition of substrate guests.<sup>63</sup>



Very recently an anionic 3D MORF, was developed by Sessler using flexible tetracationic imidazolium macrocycles and 2,6-naphthalene dicarboxylate dianions with Zn(II) cations (Figure 1.34).<sup>64</sup>

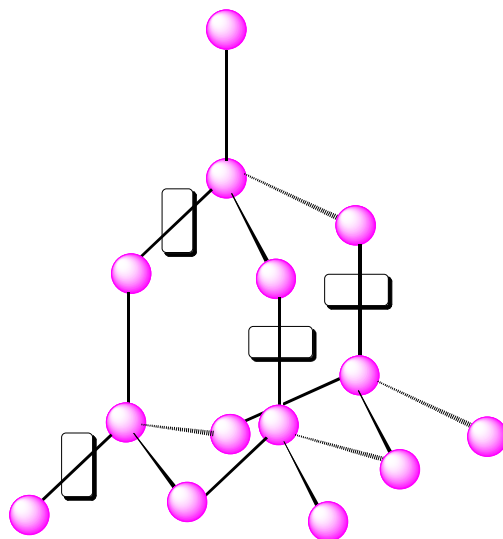


**Figure 1.34** Schematic representations of the binding mode of Sessler's MORF where the pink balls are the Zn(II) ions, black lines are the axes, and rectangles are the wheels.

#### 1.4 Scope of this Thesis

This thesis describes the incorporation of the 1,2-bis(pyridinium)ethane 24-crown-8 rotaxane motif into a variety of ligand-based architectures. This begins (in **Chapter 2**) by using the recognition elements of the axle to form a [2]rotaxane containing a terpyridine ligand that can act as stopper. The complexation with labile and inert metals is studied. The synthesis, characterization and solid-state of the metal based ligand [2]rotaxane are examined. The templating motif was then incorporated (in **Chapter 3**) into a series of tetrakis-substituted **DB24C8** wheels. Characterization and [2]pseudorotaxane formation studies were performed to investigate whether there would be any correlation between the appended groups of the macrocycle and the association constant with known axes. [2]Rotaxanes containing these new crown ethers were then synthesized and

characterized. The new crowns were incorporated (in **Chapter 4**) into metal based [2]rotaxane ligands and coordinated to an inert metal as well as used in the construction of MORFs. The study of the effect of the substituted crown ether on the MORF structure was investigated. Crown ethers with monodentate and chelating ligands on the macrocycle (in **Chapter 5**) were synthesized, characterized, and coordinated to metal ions. The resulting materials were studied in the solid-state. A new class of MORFs was discovered which links [2]rotaxane wheels rather than axles to propagate the structure. Finally, these chelating macrocycles were incorporated (in **Chapter 6**) into a [2]rotaxane based ligand with potential linking groups on *both* the axle and wheel. These multidentate, multi-topological ligands were synthesized and characterized.

#### References:

1. Lehn, J-M. *Supramolecular Chemistry: Concepts and Perspectives*; VCH: New York, 1995, pp 5.
2. a) Steed, J.W. *Encyclophedia of Supramolecular Chemistry*, **2004**, 1401, 329. b) Desiraju, G. R. *Crystal Engineering. The Design of Organic Solids*; Elsevier, 1989.
3. Pedersen, C. J. *J. Am. Chem. Soc.* **1967**, *89*, 7017.
4. Cram, D.J. *Angew. Chem. Int. Ed.* **1988**, *27*, 1009.
5. Amabilino, D. B.; Stoddart, J. F. *Chem. Rev.* **1995**, *95*, 2725.
6. Fyfe, M. C. T.; Stoddart, J. F. *Coord. Chem. Rev.* **1999**, *183*, 139.
7. Nepogodiev, S. A.; Stoddart, J. F. *Chem. Rev.* **1998**, *98*, 1959.
8. Lüttringhaus, A.; Creamer, F.; Prinzbach, H.; Henglein, F. M. *Liebigs Ann. Chem.* **1958**, *613*, 185.
9. Ashtron, P.R.; Douglas, P.; Spencer, N.; Stoddart, J. F. *Chem. Commun.* **1991**, 1677.

10. a) Glink, P. T.; Schiavo, C.; Stoddart, J. F.; Williams, D. J. *Chem. Commun.* **1996**, 1483. b) Allwood, B. L.; Spencer, N.; Shariari-Zavareh, H.; Stoddart, J. F.; Williams, D. J. *J. Chem. Soc. Chem. Commun.* **1987**, 1064.
11. a) Loeb, S. J.; Tiburcio, J.; Vella, S. J.; Wisner, J. A. *Org. Biomol. Chem.* **2006**, *4*, 660. b) Loeb, S. J.; Wisner, J. A. *Angew. Chem. Int. Ed.* **1998**, *37*, 2838.
12. Castillo, D.; Astudillo, P.; Mares, J.; Gonzalez, F. L.; Vela, A.; Tiburico, J. *Org. Biomol. Chem.* **2007**, *5*, 2252.
13. Li, L.; Clarkson G. L. *Org. Lett.* **2007**, *9*, 497.
14. Samsam, S.; Leclercq, L.; Schimitzer, A. R. *J. Phys. Chem. B* **2009**, *113*, 9493.
15. a) Vickers, M. S.; Beer, P. D. *Chem. Soc. Rev.* **2007**, *36*, 211. b) Chmielewski, M. J.; Zhao, L.; Brown, A.; Curiel, D.; Sambrook, M. R.; Thompson, A. L.; Santos, S. M.; Felix, V.; Davis, J. J.; Beer, P. D. *Chem. Commun.* **2008**, 3154.
16. Serpell, C. J.; Kilah, N. L.; Costa, P. J.; Felix, V.; Beer, P. D. *Angew. Chem. Int. Ed.* **2010**, *49*, 5322.
17. Harada, A.; Takanishima, Y.; Yamaguchi, H. *Chem. Soc. Rev.* **2009**, *38*, 875.
18. Lagona, J.; Mukhopadhyay, P.; Chakrabarti, S.; Isaacs, L. *Angew. Chem. Int. Ed.* **2005**, *44*, 4844.
19. a) Gattuso, G.; Notti, A.; Parisi, M. F.; Pisagatti, I.; Amato, M. E.; Pappalardo, A.; Pappalardo, S. *Chem. Eur. J.* **2010**, *16*, 2381; b) Semeraro, M.; Arduini, A.; Baroncini, M.; Battelli, R.; Credi, A.; Venturi, M.; Pochini, A.; Secchi, A.; Silvi, S. *Chem. Eur. J.* **2010**, *16*, 3467.
20. Li, C.; Zhao, L.; Ding, X.; Chen, C.; Zhang, S.; Zhang, Q.; Yu, Y.; Jia, X. *Chem. Commun.* **2010**, *46*, 9016.
21. Prikhod'ko, A.; I. Sauvage, J-P. *J. Am. Chem. Soc.* **2009**, *131*, 6794.
22. Blight, B. A.; Wisner, J. A.; Jennings, M. C. *Inorg. Chem.* **2009**, *48*, 1929.
23. Adrian, J. C.; Wilcox, C.S. *J. Am. Chem. Soc.* **1991**, *113*, 678.
24. Stauffer, D. A.; Barrans, R. E.; Dougherty, D. *J. Org. Chem.* **1990**, *55*, 2762.
25. Ashton, P. R.; Chrystal, E. J. T.; Glink, P. T.; Menzer, S.; Schiavo, C.; Spencer, N.; Stoddart, J. F.; Tasker, P. A.; White, A. J. P.; Williams, D. J. *Chem. Eur. J.* **1996**, *2*, 709.

26. Hynes, M. J. *Dalton Trans.*, **1993**, 311.
27. Piecre, M.; Raman, C. S.; Nall, B. T. *Methods*, **1999**, *19*, 213.
28. Harrison, I. T.; Harrison, S. *J. Am. Chem. Soc.* **1967**, *89*, 5723.
29. Dietrich-Buchecker, C.; Sauvage, J. P. *Chem. Rev.* **1987**, 795.
30. Harrison, I. T. *J. Chem. Soc., Chem. Commun.* **1972**, 231.
31. Schill, G. *Catenanes, Rotaxanes and Knots*, Academic Press: CA, 1971. b) Schill, G.; Zollenkopf, H. *Liebigs Ann. Chem.* **1969**, *721*, 53.
32. a) Georges, N.; Loeb, S. J.; Tiburcio, J.; Wisner, J. A. *Org. Biomol. Chem.* **2004**, *2*, 2751. b) Loeb, S. J.; Wisner, J. A. *Chem. Commun.* **1998**, 2757. c) Loeb, S. J.; Wisner, J. A. *Chem. Commun.* **2000**, 845. d) Loeb, S. J.; Wisner, J. A. *Chem. Commun.* **2000**, 1939. e) Hubbard, A. L.; Davidson, G. J.E.; Patel, R. H.; Wisner, J. A.; Loeb, S. J. *Chem. Commun.* **2004**, 138.
33. Takata, T. *J. Org. Chem.* **2006**, *71*, 5093.
34. Giguère, J. B.; Thibeault, D.; Cronier, F.; Marois, J. S.; Auger, M.; Morin, J. S. *Tetrahedron Lett.* **2009**, *50*, 5497.
35. Chiu, S.-H.; Rowan, S. J.; Cantrill, S. J.; Ridvan, L.; Ashton, P. R.; Garrell, R. L.; Stoddart, J. F. *Tetrahedron* **2002**, *58*, 807.
36. Loeb, S. J. *Chem. Soc. Rev.* **2007**, *36*, 226.
37. Mahan, E. J.; Dennis, J. A. *Org. Lett.* **2006**, *8*, 5085.
38. Coutrot, F.; Busseron, E. *Chem. Eur. J.* **2008**, *14*, 4784.
39. Mastsumura, T.; Ishiwari, F.; Kovama, Y.; Takata, T. *Org. Lett.* **2010**, *12*, 3828.
40. Tokunaga, Y.; Koichiro, A.; Nobuharu, H.; Shou, Y.; Kenji, H.; Youji, S.; Suzuka, K. *J. Org. Chem.* **2009**, *74*, 2374.
41. Christinat, N.; Scopelliti, R.; Severin, K. *Chem. Commun.* **2008**, 3660.
42. a) Meyer, C. D.; Joiner, S. C.; Stoddart, J. F. *Chem. Soc. Rev.* **2007**, *36*, 1705. b) Belowich, E. M.; Valente, C.; Stoddart, J. F. *Angew. Chem. Int. Ed.* **2010**, *49*, 7208. c) Yin, J.; Dasgupta, S.; Wu, J. *Org. Lett.* **2010**, *12*, 1712. d) Haussman, P. C.; Stoddart, J. F. *Chem. Rev.* **2009**, *9*, 136.

43. Stoddart, J. F.; Williams, D. J.; White, A. J. P.; Oliva, A. I.; Glink, P. T. *Angew. Chem. Int. Ed.* **2001**, *40*, 1870.
44. Bolla, M. A.; Tiburcio, J.; Loeb, S. J. *Tetrahedron*, **2008**, *64*, 8423.
45. Dietrich-Buchecker, C. O.; Sauvage, J. P. *J. Am. Chem. Soc.* **1984**, *106*, 3043.
46. Crowley, J. D.; Goldup, S. M.; Lee, A.; Leigh, D. A., McBurney, R. T. *Chem. Soc. Rev.* **2009**, *38*, 1530.
47. Goldup, S. M.; Leigh, D. A.; McBurney, R. T.; McGonigal, P. R.; Plant, A. *Chem. Sci.*, **2010**, *1*, 383.
48. a) Janiak, C. *Dalton Trans.*, **2003**, 2781. b) J. C. Bailar, Jr. *Preparative Inorganic Reactions*, W. L. Jolly, Interscience, New York, **1964**, pp. 1.
49. Gheorghe, R.; Cucos, P.; Andruh, M.; Costes, J. P.; Donnadiou, B.; Shova, S. *Chem. Eur. J.* **2006**, *12*, 187.
50. Fromm, K. M.; Robin, A. Y. *Coord. Chem. Rev.* **2006**, *250*, 2127.
51. Aziz, A. S. *Abd-El Macromolecules Containing Metal and Metal-Like Elements Vol. 9*; Wiley: New Jersey 2009, pp 451.
52. Robin, R. *Dalton Trans.* **2008**, 5113.
53. Rowsell, J. L. C.; Yaghi, O. M. *Microporous and Mesoporous Materials* **2004**, *73*, 3.
54. Eddaoudi, M.; Moler, D. B.; Li, H.; Chen, B.; Reineke, T. M.; O'Keeffe, M.; Yaghi, O. M. *Acc. Chem. Res.* **2001**, *34*, 319.
55. a) Murray, L. J.; Dinca, M.; Long, J. R. *Chem. Soc. Rev.* **2009**, *38*, 1294. b) Li, J. R.; Kuppel, R. J.; Zhou, H. C. *Chem. Soc. Rev.* **2009**, *38*, 1477. c) Duren, T.; Bae, Y.-S.; Snurr, R. *Chem. Soc. Rev.* **2009**, *38*, 1237. Ma, L.; Abney, C.; Lin, W. *Chem. Soc. Rev.* **2009**, *38*, 1249. d) Guo, Z.; Cao, R.; Wang, X.; Li, H.; Yuan, W.; Wang, G.; Wu, H.; Li, J. *J. Am. Chem. Soc.* **2009**, *131*, 6894. e) Allendorf, M. D.; Bauer, C. A.; Bhakta, R. K.; Houk, R. J. T., *Chem. Soc. Rev.* **2009**, *38*, 1330. f) Kurmoo, M.; *Chem. Soc. Rev.* **2009**, *38*, 1353. g) Banerjee, S.; Adarsh, N. N.; Dastidar, R. *Eur J. Org. Chem.* **2010**, 3770. h) Horcajada, P.; Serre, C.; Maurin, G.; Ramsahye, N. A.; Balas, F.; Vallet-Rege, M.; Taulelle, T.; Sebban, M.; Ferey, G. *J. Am. Chem. Soc.* **2008**, *130*, 6774.
56. a) Chun, H.; Dybtsev, D. N.; Kim, H.; Kim, K. *Chem. Eur. J.* **2005**, *11*, 3521. b) Chun, H.; Dybtsev, D. N.; Kim, K. *Angew. Chem. Int. Ed.* **2004**, *43*, 5033. c)

- Bourne, S. A.; Lu, J.; Mondal, A. ; Moulton, B. ; Zaworotko, M. J. *Angew. Chem. Int. Ed.* **2001**, *40*, 2111
57. Kim, K. *Chem. Soc. Rev.* **2002**, *31*, 96
58. a) Davidson, G. J. E.; Loeb, S. J. *Angew. Chem. Int. Ed.* **2003**, *42*, 74. b) Hoffart, D. J.; Loeb, S. J. *Angew. Chem. Int. Ed.* **2005**, *44*, 901. c) Loeb, S. J. *Organic Nanostructure*; Wiley: Weinheim 2003, pp 33. d) Loeb, S. J. *Chem. Commun.* **2005**, 1511.
59. Hoffart, D. J.; Loeb, S. J. *Supramol. Chem.* **2007**, *19*, 89.
60. Knight, L. K.; Vukotic, V. N.; Viljoen, E.; Caputo, C. B.; Loeb, S. L. *Chem. Commun.* **2009**, 5585.
61. Vukotic, V. N.; Loeb, S. L. *Chem. Eur. J.* **2010**, *16*, 13630.
62. a) Li, Q.; Zhang, W.; Miljanic, O. S.; Sue, C-H.; Zhao, Y-L.; Liu, L.; Knobler, C. B.; Stoddart, J. F.; Yaghi, O. M. *Science*, **2009**, *325*, 855. b) Li, Q.; Zhang, W.; Miljanic, O. S.; Knobler, C. B.; Stoddart, J. F.; Yaghi, O. M. *Chem. Commun.* **2010**, *46*, 380. c) Valente, C.; Choi, E.; Belowich, M. E.; Doonan, C. J.; Li, Q.; Gasa, T. B.; Botros, Y. V.; Yaghi, O. M.; Stoddart, J. F. *Chem. Commun.* **2010**, *46*, 4911. d) Li, Q.; Sue, C-H.; Basu, S.; Shveyed, A. K.; Zhang, W.; Barin, G.; Fang, L.; Sarjeant, A. A.; Stoddart, S. J.; Yaghi, O. M. *Angew. Chem. Int. Ed.* **2010**, *49*, 6751. e) Zhao, Y. L.; Liu, L.; Zhang, W.; Sue, C-H.; Li, Q.; Miljanic, O. S.; Yaghi, O. M.; Stoddart, J. F. *Chem. Eur. J.*, **2009**, *15*, 133356. f) Deng, H.; Olson, M. A.; Stoddart, J. F.; Yaghi, O. M. *Nature Chemistry*, **2010**, *2*, 439.
63. Smaldone, R. A.; Forgan, R. S.; Furukawa, H.; Gassensmith, J. J.; Slawin, A., M. Z.; Yaghi, O. M.; Stoddart, J. F. *Angew. Chem. Int. Ed.* **2010**, *49*, 8630.
64. Gong, H.-Y.; Rambo, B. M.; Cho, W.; Lynch, V. M.; Oh, M.; Sessler, J. L. *Chem. Commun.* **2011**, *47*, 5973.

# Chapter 2

## A [2]Rotaxane Ligand with Terminal Terpyridine Groups

### 2.1. Introduction

Combining the properties of transition metals (electronic, magnetic, and catalytic) with the dynamic properties of interlocked molecules has the potential to create chemical systems that can lead to new applications.<sup>1</sup> A number of such systems have been developed where the transition metal acts as 1) a templating ion to help interpenetration,<sup>2</sup> 2) a reporter group to sense the binding of a guest,<sup>3</sup> 3) an additive that elicits molecular motion,<sup>4</sup> or 4) a building block to create coordination polymers (MOFs).<sup>5</sup> However, the synthesis of interlocked ligands and their transition metal complexes is still a major problem to overcome. The conversion of [2]pseudorotaxane into [2]rotaxane with metal coordination has been demonstrated in the literature where a metal complexes to the [2]pseudorotaxane.<sup>5-8</sup> For **[2.1-DB24C8]<sup>2+</sup>** (see Figure 2.1), the external pyridine groups have been shown to form metal coordination with a cationic palladium complex and an anionic metal fragment such as  $MBr_3^-$  ( $M = Co, Mn$ ), as shown in Figure 2.2.<sup>9,10</sup> In addition, Branda and Goldberg used porphyrins with either Ru(II) or Zn(II) to act as stoppers as seen in Figure 2.3<sup>11,12</sup> while Sanders has reported that porphyrin can be attached to nanoparticles to form a metal based [2]rotaxane.<sup>13</sup>

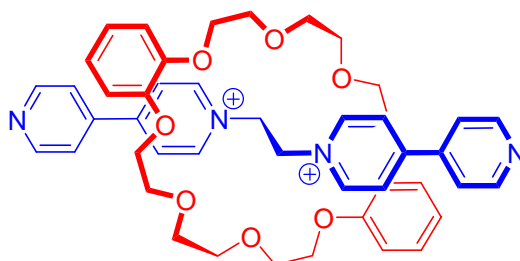


**Figure 2.1** Rotaxane ligand **[2.1-DB24C8]<sup>2+</sup>**.

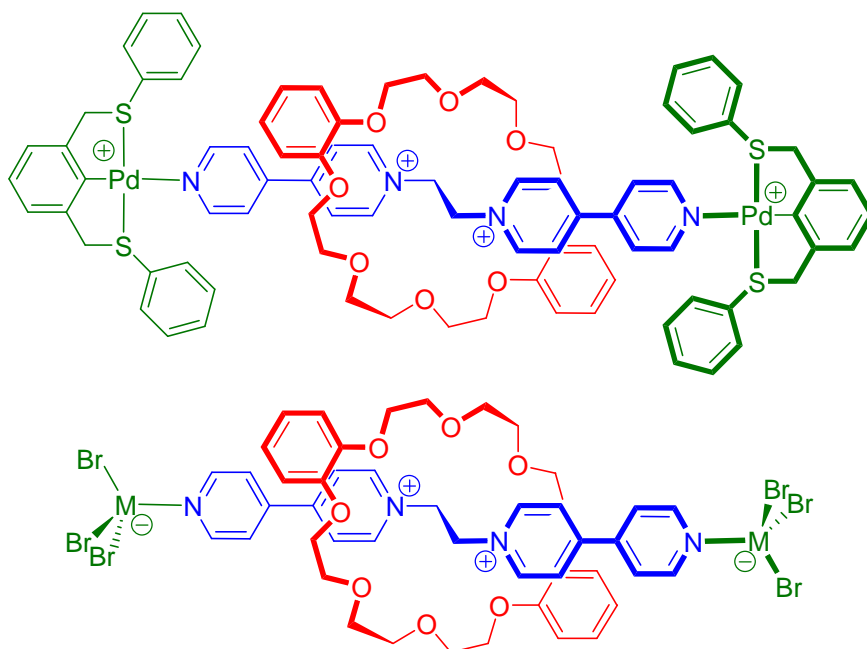


**Figure 2.2** Rotaxane formation via metal coordination.

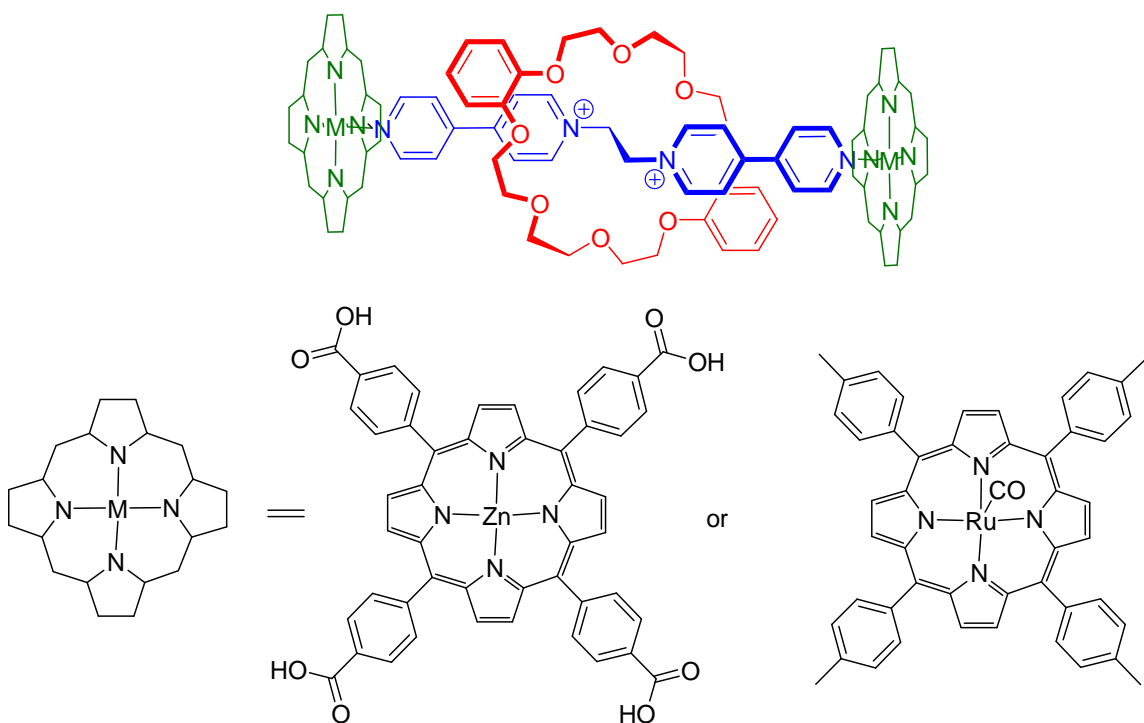


**Figure 2.3** Rotaxane formation via porphyrin coordination.

The problem with the self-assembly process for metal incorporation is that conditions for formation of the metal-ligand bonds must be compatible with the weak non-covalent



bonds that hold the [2]pseudorotaxane together. One way to overcome that problem is to change monodentate to polydentate ligands. Previously in the Loeb group, an axle containing 2,2':6',2''-terpyridine was employed as a blocking group, at one end of the axle, but, there still needed to be a stopper added at the other end; Figure 2.4. This ligand was shown to be capable of binding to Fe(II) and Ru(II) centres.<sup>14,15</sup>

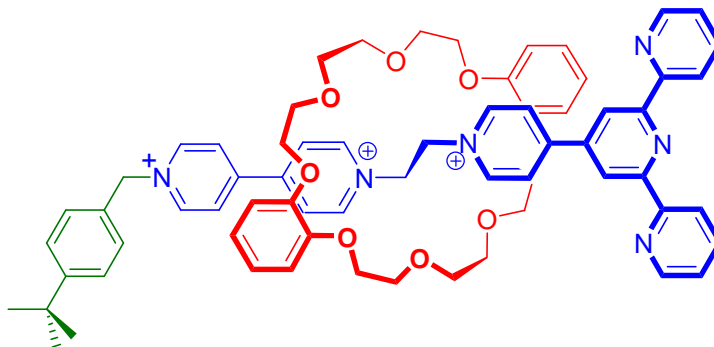


**Figure 2.4** 2,2':6',2''-Terpyridine group ligand utilized as stopper for a [2]rotaxane.

In a similar fashion, Leigh has incorporated the polydentate ligand bis(2-pyridylmethyl)amine (**BPMA**) to form molecular shuttles; Figure 2.5,<sup>16</sup> but this was made by the clipping method which is not possible with the bis-pyridinium axle.

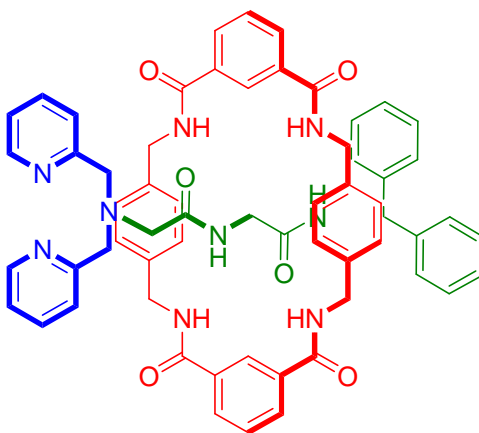
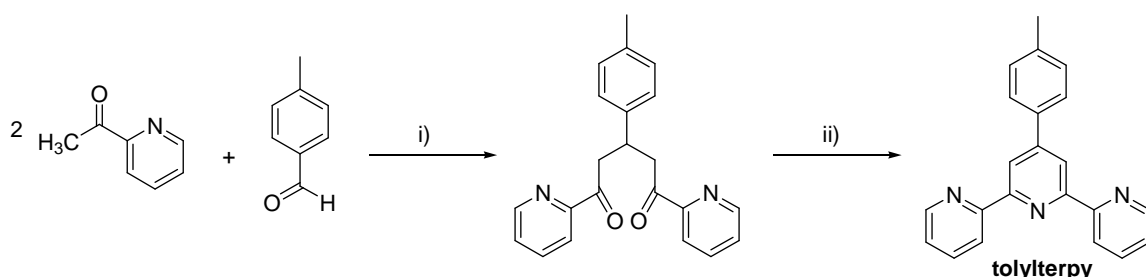


**Figure 2.5** Bis(2-pyridylmethyl)amine utilized as a stopper for a [2]rotaxane.

## 2.2. Results and Discussion

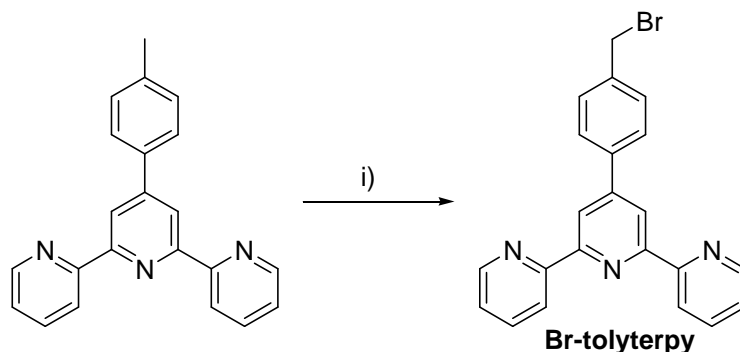
### 2.2.1 Terpyridine based ligands

The ligand 4'-*p*-tolyl-2,2':6',2''-terpyridine (**tolylterpy**) was chosen as the source of the terpy unit which will act as the stopper for [2]rotaxanes. The synthesis of **tolylterpy** proceeded smoothly via the condensation of 2-acetylpyridine with 4-tolualdehyde, in the presence of base, forming the 1,5-diketone. Subsequent ring closure of the 1,5-diketone, *in situ* with ammonium acetate (NH<sub>4</sub>OAc) produced the desired compound, **tolylterpy**, as previously reported (Scheme 2.1).<sup>17</sup>



**Scheme 2.1** i) 1:1 MeOH/H<sub>2</sub>O, NaOH, ii) excess NH<sub>4</sub>OAc, reflux.

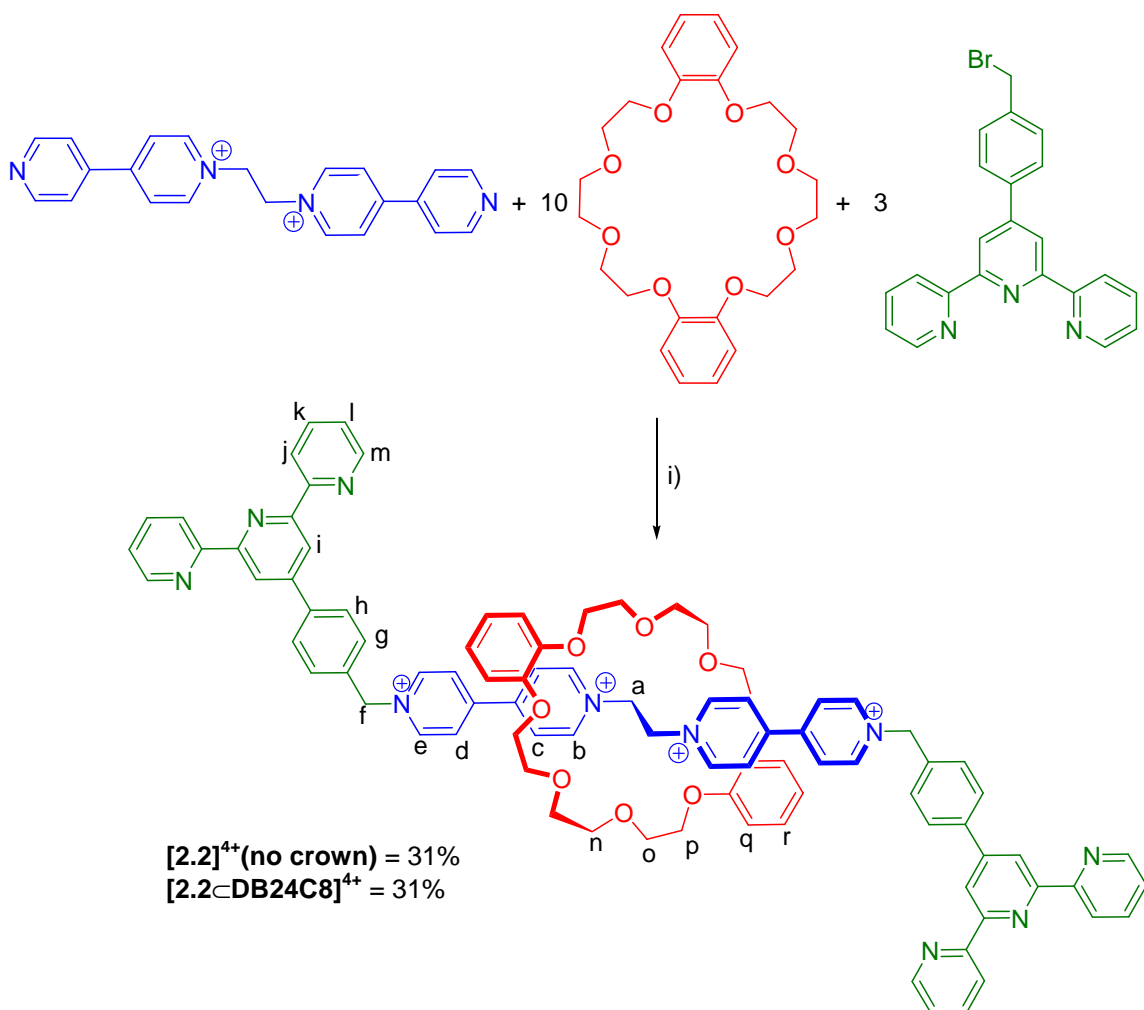
Bromination of **tolylterpy** occurred thermally through a radical process with *N*-bromosuccinimide in the presence benzoyl peroxide to produce the desired compound, **Br-tolylterpy**, as previously reported (Scheme 2.2).<sup>17</sup>



**Scheme 2.2** i) NBS, BzO<sub>2</sub>, CCl<sub>4</sub>, reflux.

*N*-alkylation of the 4-pyridyl group of the pseudorotaxane formed between bis-1,2-(4,4'-dipyridinium)ethane and **DB24C8** was accomplished by stirring in MeNO<sub>2</sub> at room

temperature for 7 days to produce compound **[2.1-DB24C8]**<sup>4+</sup> in relatively low yield, but high purity, as mixtures of dibromide and ditriflate salts. Treatment of **[2.1-DB24C8]**<sup>4+</sup> in a two-phase nitromethane/sodium triflate (MeNO<sub>2</sub>/NaOTf<sub>(aq)</sub>) mixture at room temperature resulted in a red solid; as shown in Scheme 2.3.



**Scheme 2.3** i) **[2.1][OTf]<sub>2</sub>**, **DB24C8**, **Br-tolyterpy** in MeNO<sub>2</sub>/NaOTf(aq) at RT for 168 h.

The <sup>1</sup>H NMR spectrum of compound **[2.2][OTf]<sub>4</sub>** and **[2.2-DB24C8][OTf]<sub>4</sub>** in CD<sub>3</sub>CN are shown in Figure 2.6 and some of the major peaks are summarized in Table 2.1. The spectra show evidence supporting the various supramolecular interactions in this rotaxane such as hydrogen bonding and π-π stacking.

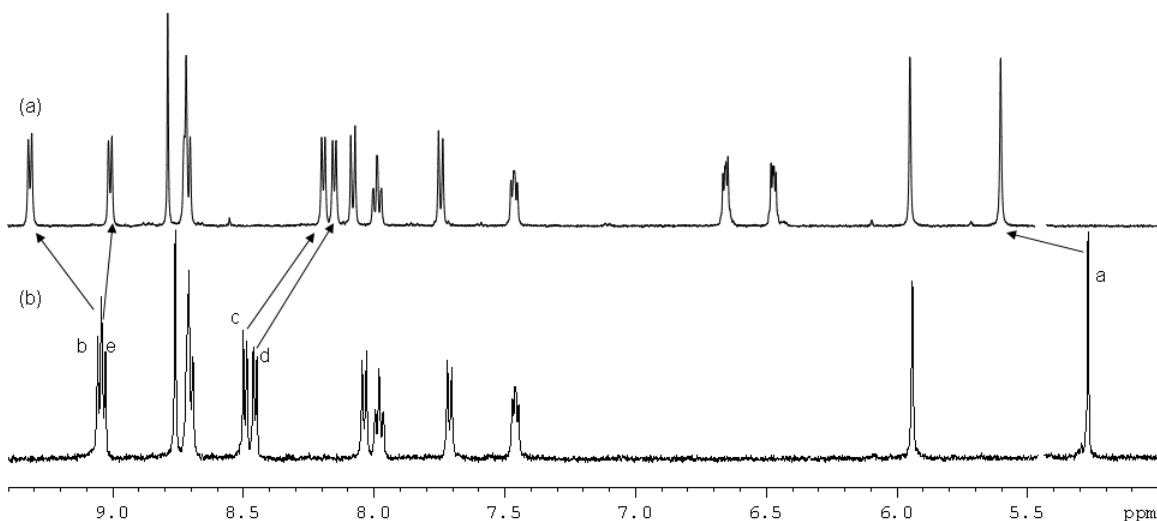


**Figure 2.6** Comparison of the  $^1\text{H}$  NMR shifts of (a)  $[\mathbf{2.2-DB24C8}][\text{OTf}]_4$ , and (b)  $[\mathbf{2.2}][\text{OTf}]_4$  in  $\text{CD}_3\text{CN}$  at 500 MHz.

**Table 2.1** Comparison of the chemical shifts of the dumbbell  $[\mathbf{2.2}][\text{OTf}]_4$ , and  $[\mathbf{2}]\text{rotaxane}$ ,  $[\mathbf{2.2-DB24C8}][\text{OTf}]_4$ .

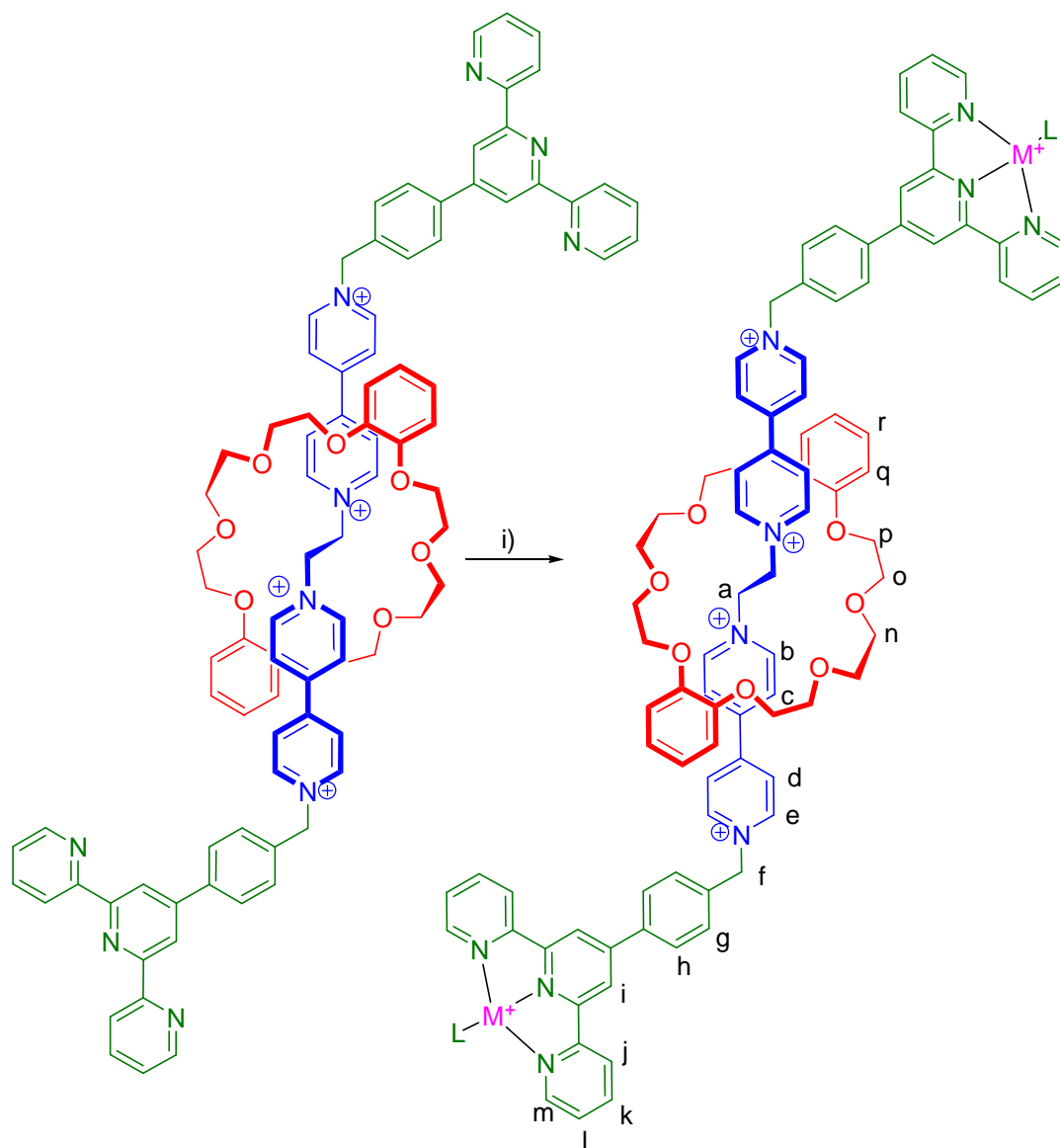
Protons	$[\mathbf{2.2}]^{4+}$	$[\mathbf{2.2-DB24C8}]^{4+}$
<i>a</i>	5.27	5.60 (0.33)
<i>b</i>	9.04	9.31 (0.27)
<i>c</i>	8.49	8.19 (-0.30)
<i>d</i>	8.46	8.15 (-0.31)
<i>e</i>	9.04	9.01 (-0.03)

Hydrogen bonding between the ethylene (**a**) and  $\alpha$ -pyridinium (**b**) protons of the axle with the polyether oxygen atoms of the macrocycle is evidenced by a downfield shift of the signals for **a** and **b** of 0.33 and 0.27 ppm respectively. The  $^1\text{H}$  NMR spectrum also reveals the presence of two separate resonances for protons **q** and **r** at 6.66 and 6.48 ppm, compared to 6.93 ppm for free **DB24C8**, which are indicative of  $\pi$ -stacking between pairs of electron-poor pyridinium and electron-rich crown aromatic rings. The electrospray ionization mass spectroscopy (ESI-MS) result of ligand  $[\mathbf{2.2-DB24C8}][\text{OTf}]_4$  also confirmed the interlocked nature of the complex, with just the loss of two counter ions resulting in observation of the parent molecule as  $\{[\mathbf{2.2-DB24C8}][\text{OTf}]_2\}^{2+}$  at 865.2775 m/e.

### 2.2.2 Labile metal complexes

To investigate the coordination ability of this unique rotaxane ligand, silver(I), palladium(II), and zinc(II) complexes were prepared. These metals are known from literature to adopt square planer or distorted octahedral environments depending on the metal with any open coordination sites occupied by solvent molecules.<sup>18-23</sup> Scheme 2.4, shows generally how the monomer would look in solution when two equivalents of [Ag][OTf], [Pd(MeCN)<sub>4</sub>][BF<sub>4</sub>]<sub>2</sub>, or [Zn(H<sub>2</sub>O)<sub>6</sub>][OTf]<sub>2</sub> in MeCN were added to [2.2-DB24C8][OTf]<sub>4</sub>.

The <sup>1</sup>H NMR spectrum of the Ag(I) complex was recorded in CD<sub>3</sub>CN and the numbering scheme can be seen in Scheme 2.4. The spectrum for the Ag(I) complex revealed upfield shifts of the protons **m-j**. Proton **m** in complex [(Ag(MeCN))<sub>2</sub>(2.2-DB24C8)]<sup>6+</sup> shifts from 8.70 ppm for the uncomplexed [2]rotaxane to 8.48 ppm when coordinated to the Ag(I) centre. The <sup>1</sup>H NMR spectrum of the Pd(II) complex was recorded in CD<sub>3</sub>NO<sub>2</sub>. The spectrum for the Pd(II) complex also showed upfield shifts of the protons **m-j**. Proton **m** in complex [(Pd(MeCN))<sub>2</sub>(2.2-DB24C8)]<sup>8+</sup> shifts from 8.77 ppm for the uncomplexed [2]rotaxane to 8.65 ppm when coordinated to the palladium (II) centre. The <sup>1</sup>H NMR spectrum of resulting Zn(II) complex showed only broadened resonances for [2.2-DB24C8]<sup>4+</sup> presumably due to rapid metal ligand exchange.



**Scheme 2.4** i) 2 equivalents of  $\text{Ag}(\text{OTf})$  or  $\text{Pd}(\text{MeCN})_4[\text{BF}_4]_2$  or  $\text{Zn}(\text{H}_2\text{O})_6[\text{OTf}]_2$  in MeCN for 24 h at RT.

The ESI-MS of labile metal species show a loss of one of the metals from the complex.  $[(\text{Ag}(\text{MeCN}))_2(\mathbf{2.2\text{-}DB24C8})][\text{OTf}]_4$  shows how labile Ag(I) is with the loss of AgOTf and MeCN to give the mass of 697.8  $m/e$  with formula of  $\{[(\text{Ag}(\text{MeCN}))(\mathbf{2.2\text{-}DB24C8})][\text{OTf}]_5\}^+$ . The Pd(II) complex becomes  $\{[\text{Pd}(\text{H}_2\text{O})(\mathbf{2.2\text{-}DB24C8})][\text{OTf}+\text{BF}_4]\}^{4+}$  with a mass of 448.6074  $m/e$ . The Zn(II) complex just shows the parent molecule of  $[(\mathbf{2.2\text{-}DB24C8})]^{4+}$

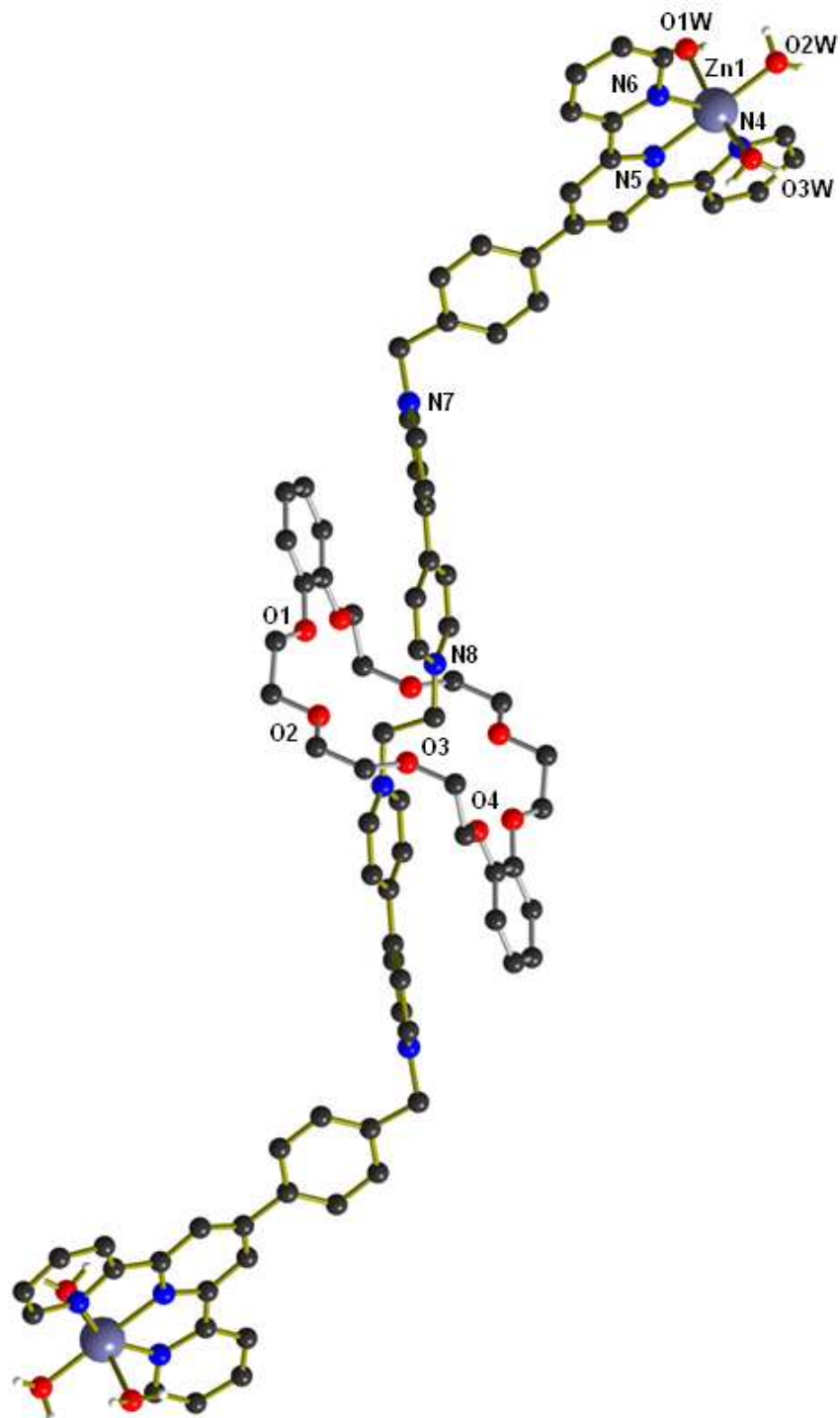


**Figure 2.7** A ball-stick representation of the cationic portion of the X-ray crystal structure of  $[(\text{Zn}(\text{H}_2\text{O})_3)_2(\text{2.2-DB24C8})]^{8+}$ . The complex occupies a crystallographic centre of symmetry. All hydrogen atoms, except those on the coordinated water molecules, all anions and all solvent molecules have been omitted for clarity. (Zn = blue-gray, O = red, N = blue, C = black, H = white; wheel bonds = silver, axle bonds = gold).

Single crystals of the Zn(II) complexes were grown by slow diffusion of isopropyl ether into a solution of MeNO<sub>2</sub> producing orange crystals. Two different cations were present in the structure [(Zn(H<sub>2</sub>O)<sub>3</sub>)<sub>2</sub>(**2.2-DB24C8**)]<sup>8+</sup> and [(Zn(H<sub>2</sub>O)(BF<sub>4</sub>))<sub>2</sub>(**2.2-DB24C8**)]<sup>6+</sup>. Only the former isomer is shown in Figure 2.7; the other simply has a BF<sub>4</sub> anion coordinated to the Zn(II) in place of a water molecule.

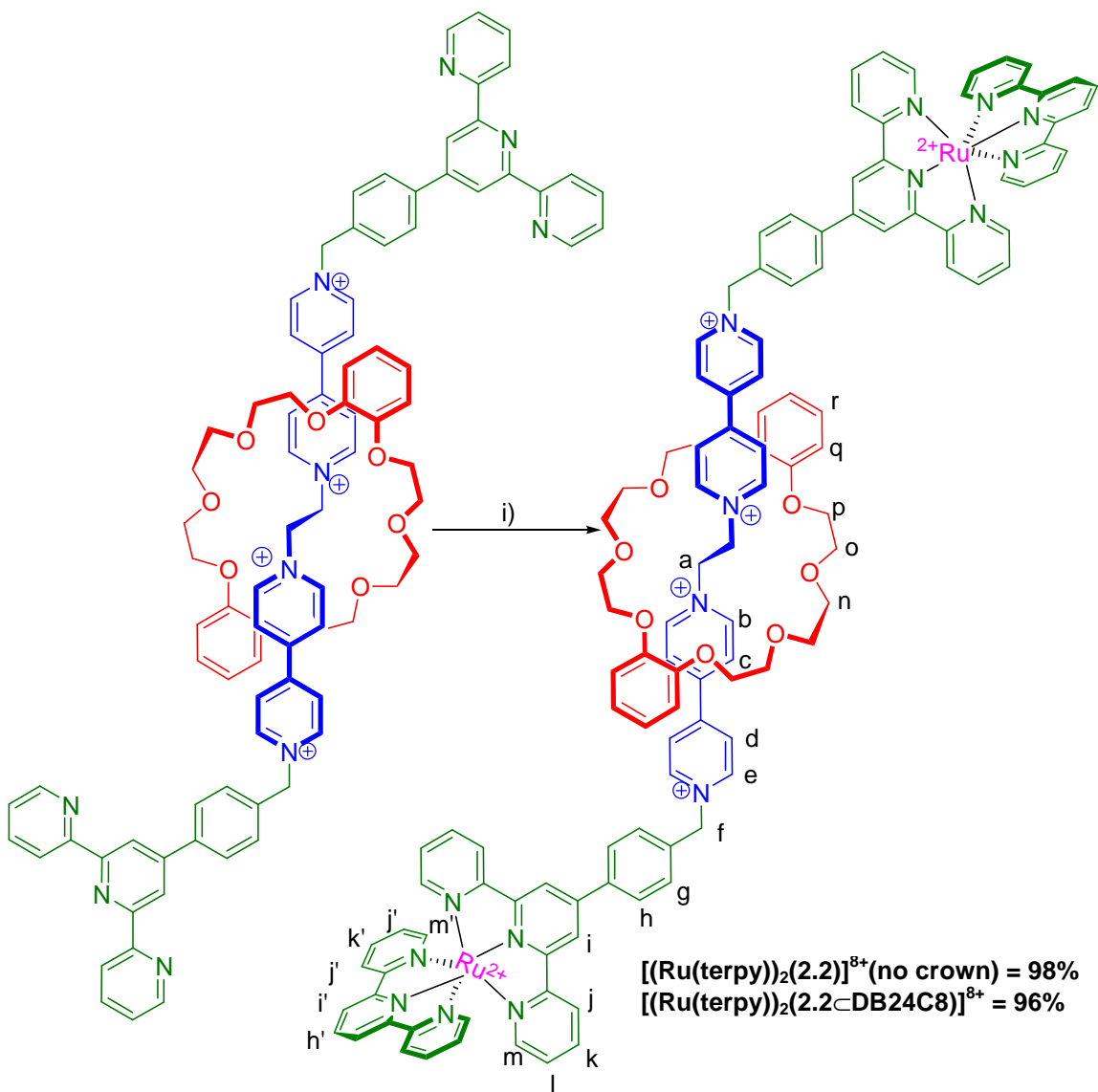
As seen with other [2]rotaxanes made using the axle [**2.1**]<sup>2+</sup>, the [2]rotaxane adopts an *anti* conformation of the central NCH<sub>2</sub>CH<sub>2</sub>N moiety while the **DB24C8** wheel exhibits a typical S-shaped conformation. Coordination to Zn(II) changes the terpyridine stopper from a *transoid* arrangement in the free ligand to a *cisoid* arrangement. The [(Zn(H<sub>2</sub>O)<sub>3</sub>)<sub>2</sub>(**2.2-DB24C8**)]<sup>8+</sup> complex has a distorted octahedral environment, Zn-N bond distances range from 2.06(1) Å for Zn(1)-N(6) to 2.14(1) Å for Zn(1)-N(4). The other three coordination sites are filled with water molecules, with Zn-O bond distances ranging from 2.05(2) Å for Zn(1)-O(1) to 2.11(2) Å for Zn(1)-O(2). The Zn(II) metal to metal distance is 37.1 Å. The complex [(Zn(H<sub>2</sub>O)(BF<sub>4</sub>))<sub>2</sub>(**2.2-DB24C8**)]<sup>6+</sup> adopts a trigonal bipyramidal geometry with one water molecule, and one BF<sub>4</sub> anion. The Zn-N bond distances range from 2.02(9) Å for Zn(1)-N(2) to 2.14(9) Å for Zn(1)-N(1), the Zn-O bond is 2.01(1) Å, and the Zn-F bond distance is 1.97(1) Å. The Zn(II) metal to metal distance is 34.0 Å. All of the Zn-N bonding parameters are similar to other mono terpyridine structures reported in literature.<sup>22,23</sup>

### 2.2.3 Inert metal complex

The reaction of [2]rotaxane ligand [**2.2-DB24C8**][OTf]<sub>4</sub> with Ru(terpy)Cl<sub>3</sub> resulted in the formation of a Ru(II) complex. As outlined in Scheme 2.5, the synthesis was carried out in a 1:1 EtOH/H<sub>2</sub>O mixture and the reaction mixture was refluxed for 1 day. As was



shown previously in the Loeb group, these conditions are sufficient for the reduction of the metal centre and showed no decomposition of the [2]rotaxane. The dark red complex could be easily isolated and purified by recrystallization from acetonitrile and diethyl ether.



**Scheme 2.5** i)  $Ru(terpy)Cl_3$ , 1:1 EtOH/H<sub>2</sub>O, reflux, 24h.

The <sup>1</sup>H NMR spectrum of the ruthenium complex was recorded in CD<sub>3</sub>CN as the triflate salt. The numbering scheme can be seen in Scheme 2.5. The spectrum for the Ru(II) complex revealed upfield shifts of the protons **m-j** and **m'-j'** attributed to the

electronic effects of the ruthenium(II) centre, confirming the formation of the complex. The spectrum also reveals a nice pattern whereby chemically equivalent peaks from the two different terpy groups, **m** and **m'** or **l** and **l'** were different enough that they could be resolved as seen in Figure 2.8 for complex  $[(\text{Ru}(\text{terpy}))_2(\mathbf{2.2\text{-}DB24C8})][\text{OTf}]_4$ .

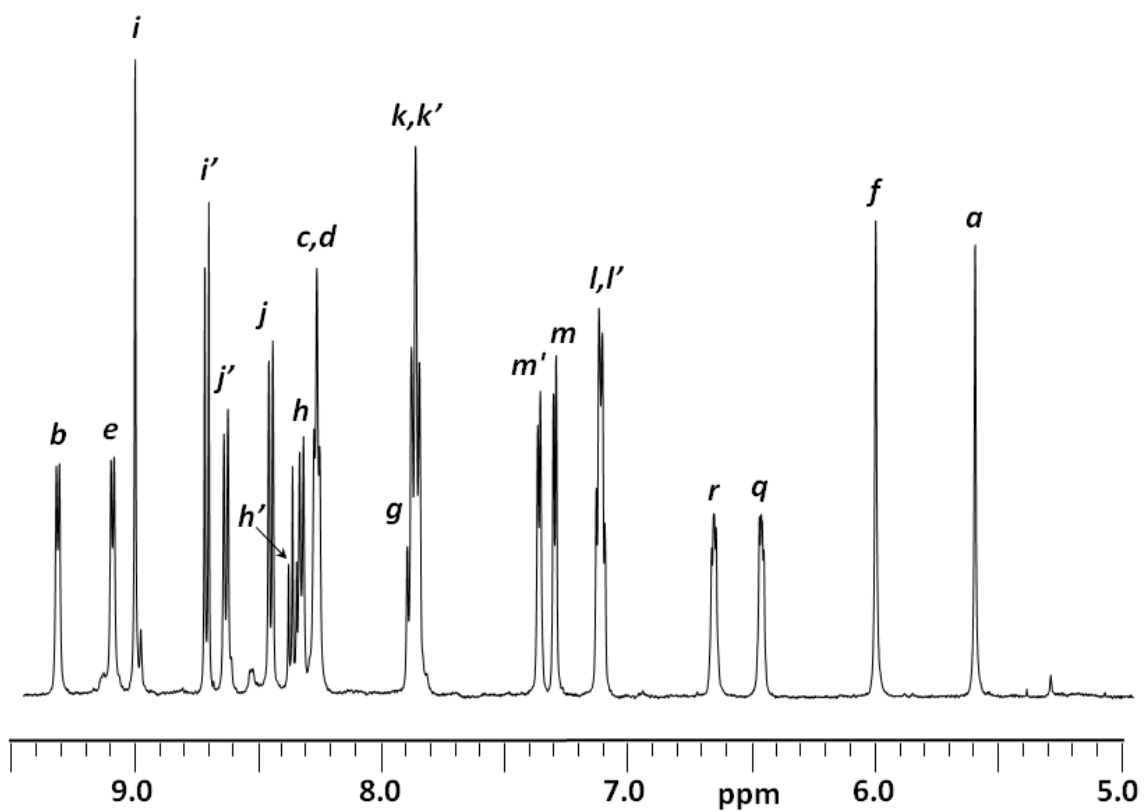


**Figure 2.8**  $^1\text{H}$  NMR spectrum of  $[(\text{Ru}(\text{terpy}))_2(\mathbf{2.2\text{-}DB24C8})][\text{OTf}]_4$  at 500MHz

In order to determine which set of peaks belonged to which terpyridine unit, conventional 2D NMR techniques ( $^1\text{H} - ^1\text{H}$  COSY) were employed.

**Table 2.2** A comparison of the  $^1\text{H}$  NMR chemical shifts for dumbbell **[2.2][OTf]<sub>4</sub>**, [2]rotaxane ligand **[2.2-DB24C8][OTf]<sub>4</sub>** and complexes **[(Ru(terpy)<sub>2</sub>)(2.2)][OTf]<sub>8</sub>**, **[(Ru(terpy)<sub>2</sub>)(2.2-DB24C8)][OTf]<sub>8</sub>**.

proton	<b>[2.2]<sup>4+</sup></b>	<b>[2.2-DB24C8]<sup>4+</sup></b>	<b>[(Ru(terpy)<sub>2</sub>)(2.2)]<sup>8+</sup></b>	<b>[(Ru(terpy)<sub>2</sub>)(2.2-DB24C8)]<sup>8+</sup></b>
<i>a</i>	5.27	5.60 (+0.33)	5.34 (+0.07)	5.64 (+0.04)
<i>b</i>	9.04	9.31 (+0.27)	9.19 (+0.15)	9.36 (+0.05)
<i>c</i>	8.49	8.19 (-0.30)	8.58 (+0.09)	8.31 (+0.12)
<i>d</i>	8.46	8.15 (-0.31)	8.58 (+0.12)	8.31 (+0.16)
<i>e</i>	9.04	9.01 (-0.03)	9.14 (+0.10)	9.14 (+0.13)
<i>f</i>	5.94	5.95 (0.01)	6.04 (+0.10)	6.05 (+0.10)
<i>g</i>	7.71	7.47 (-0.24)	7.88 (+0.17)	7.94 (+0.47)
<i>h</i>	8.04	7.75 (-0.39)	8.34 (+0.30)	8.37 (+0.62)
<i>i</i>	8.76	8.79 (+0.03)	9.03 (+0.27)	9.05 (+0.26)
<i>j</i>	8.70	8.72 (0.02)	8.50 (-0.20)	8.50 (-0.22)
<i>k</i>	7.98	7.99 (0.01)	7.92 (-0.06)	7.91 (-0.08)
<i>l</i>	7.46	8.08 (+0.61)	7.16 (-0.30)	7.16 (-0.92)
<i>m</i>	8.70	8.72 (0.02)	7.41 (-1.29)	7.41 (-1.31)

Proton **m**, in complex **[(Ru(terpy)<sub>2</sub>)(2.2-DB24C8)]<sup>8+</sup>**, shifts from 8.72 ppm for the uncomplexed rotaxane to 7.41 ppm ( $\Delta\delta = -1.31$ ). Proton **i** is also shifted downfield from 8.79 ppm to 9.05 ppm ( $\Delta\delta = +0.26$ ) in the complex when coordinated to a Ru(II) centre. The difference in chemical shifts between the [2]rotaxane and the corresponding Ru(II) complex are summarized in Table 2.2. An informative peak that appears for the compound is **h'**. This proton appears as a triplet at approximately 8.41 ppm with coupling constant of roughly 8 Hz. This proton, which lies on the mirror plane of the complex, integrates to half of most of the others, as expected, and again confirms the formation of the desired ruthenium(II) complex.

The ESI-MS of complex **[(Ru(terpy)<sub>2</sub>)(2.2-DB24C8)][OTf]<sub>8</sub>** also confirmed their interlocked nature as the **{[(Ru(terpy)<sub>2</sub>)(2.2-DB24C8)][OTf]<sub>5</sub>}<sup>3+</sup>** ion at 949.2072 *m/e* was observed.

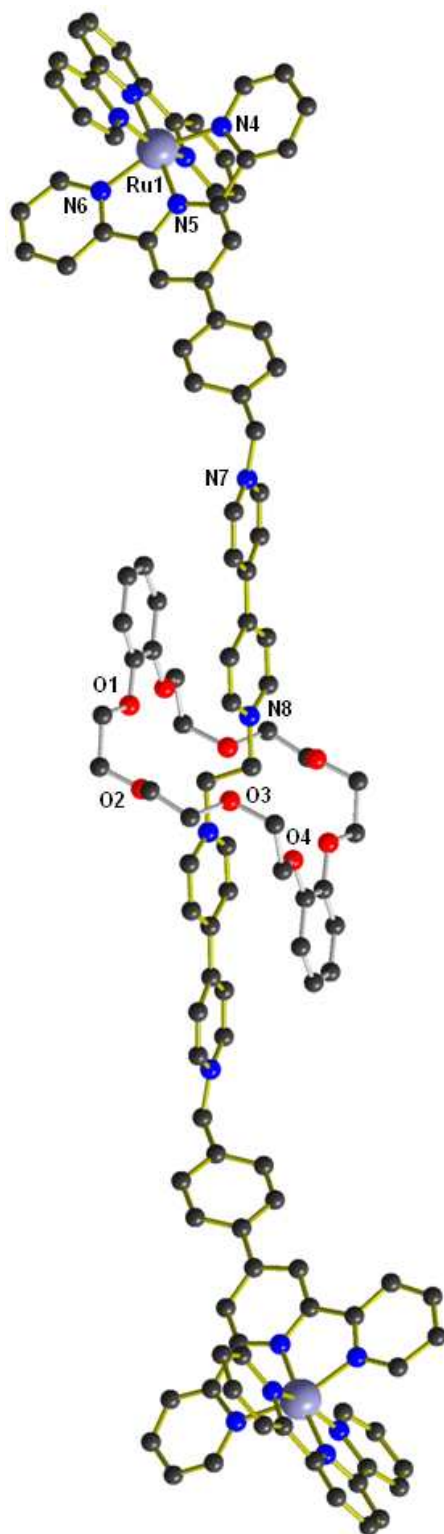


**Figure 2.9** Ball-and-stick representation of the cationic portion of the X-ray crystal structure of  $[(\text{Ru}(\text{terpy}))_2(2.2\text{CDB}24\text{C}8)]^{8+}$ . The complex occupies a crystallographic centre of symmetry. All anions and all solvent molecules have been omitted for clarity. (Ru = blue-gray, O = red, N = blue, C = black, H = white; wheel bonds = silver, axle bonds = gold).

Single crystals of  $[(\text{Ru}(\text{terpy}))_2(\mathbf{2.2-DB24C8})][\text{OTf}]_8$  suitable for X-ray diffraction were grown by the diffusion of isopropyl ether into a solution of  $\text{MeNO}_2$  containing the complex; Figure 2.9 shows a ball-and-stick representation of the cationic portion of  $[(\text{Ru}(\text{terpy}))_2(\mathbf{2.2-DB24C8})]^{8+}$ . As was observed previously for the Zn(II) complex, the dumbbells adopts a zig-zag shaped conformation that is essentially linear throughout the interlocked component but bent at the benzylic units linking the terpyridine and pyridinium groups. Coordination to the Ru(II) changes the terpyridine stopper from a *transoid* arrangement in the free ligand to a *cisoid* arrangement. The ruthenium(II) metal to metal distance is 36.6 Å. The ruthenium(II) metal centre sits in a distorted octahedral environment as a result of the terpyridine bite angle.<sup>24</sup> The bite angle can be measured from the terminal nitrogen of the ligand to the central nitrogen of the other ligand and has a range between 75-80°. Table 2.3 summarizes the bite angle for complex  $[(\text{Ru}(\text{terpy}))_2(\mathbf{2.2-DB24C8})]^{8+}$ , which compare to  $[\text{Ru}(\text{terpy})_2]^{2+}$  and other Ru(II) complexes. The ruthenium-nitrogen bond distances range from the 1.95(5) Å for Ru(1)-N(3) to 2.07(4) Å for Ru(1)-N(6).

**Table 2.3** The bite angle of complex  $[(\text{Ru}(\text{terpy}))_2(\mathbf{2.2-DB24C8})]^{8+}$  as compared to other  $[\text{Ru}(\text{terpy})_2]^{2+}$  complexes.

Atoms	$\text{Ru}(\text{terpy})_2$ Angle (°) <sup>25</sup>	$\text{Ru}(\text{biphterpy})(\text{terpy})$ Angle (°) <sup>26</sup>	$(\text{Ru}(\text{terpy}))_2(\mathbf{2.2-DB24C8})$ Angle (°)
N(1)-Ru-N(2)	78.3(4)	79.5(4)	79.7(2)
N(2)-Ru-N(3)	79.3(4)	78.6(3)	78.8(3)
N(1)-Ru-N(3)	177.5(4)	158.1(3)	158.4(3)
N(4)-Ru-N(5)	-	78.8(3)	79.0(3)
N(5)-Ru-N(6)	-	79.2(3)	80.6(3)
N(4)-Ru-N(6)	-	158.0(3)	159.5(3)

The UV/Vis absorption spectra of ruthenium(II) complexes containing heterocyclic ligands show characteristic absorption bands arising from how the metal

interacts with the ligand, or how the ligand interacts with the metal. The bands in the UV region can be assigned to a ligand centered (LC)  $\pi \rightarrow \pi^*$  transitions. The intense and broad band in the visible region that gives the complex an intense red look is caused by a spin allowed  $d \rightarrow \pi$  metal to ligand charge transfer (MLCT).<sup>27</sup> The MLCT are caused by the  $\pi^*_L$  and  $\sigma^*_M$  orbitals on the metal being the HOMO and the  $\pi^*$  orbital being the LUMO; Figure 2.10.<sup>28</sup>

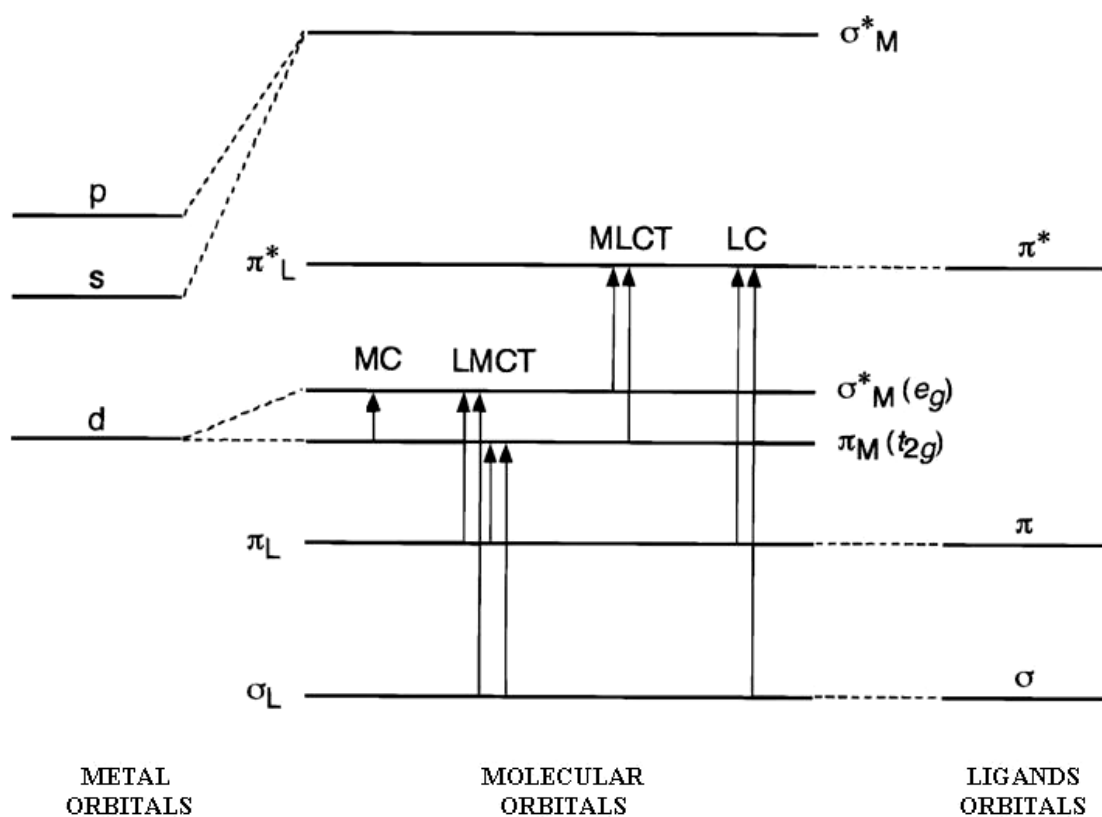


**Figure 2.10** Schematic energy level diagram of an octahedral metal complex showing possible transitions.<sup>28</sup>

The UV/Vis spectra of compounds  $[(Ru(terpy))_2(\mathbf{2.2})]^{8+}$  and  $[(Ru(terpy))_2(\mathbf{2.2-DB24C8})]^{8+}$  are dominated by the high energy  $\pi-\pi^*$  LC bands at 271 nm and 303 nm respectively. The MLCT band for the complex was found at 485 nm, which is red shifted from that of the parent compound  $[Ru(terpy)_2]^{2+}$ . The red shift is

caused by the electron-donating tolyl group, the MLCT excited state energy decreases as a consequence of the larger destabilization of the metal-centered  $\pi_{(t2g)}$  orbital compared with the ligand-centered  $\pi^*$  orbital.<sup>33</sup> The extinction coefficients ( $\epsilon$ ) for both were found to be  $11,900 \text{ L mol}^{-1} \text{ cm}^{-1}$ . Figure 2.11 shows the UV/vis spectra of both  $[(\text{Ru}(\text{terpy}))_2(\mathbf{2.2})]^{8+}$  and  $[(\text{Ru}(\text{terpy}))_2(\mathbf{2.2-DB24C8})]^{8+}$  for comparison. Table 2.4 summarizes the UV/Vis data for  $[\text{Ru}(\text{terpy})_2(\mathbf{2.2})]^{8+}$ ,  $[\text{Ru}(\text{terpy})_2(\mathbf{2.2-DB24C8})]^{8+}$  and other related  $[\text{Ru}(\text{terpy})_2]^{2+}$  based complexes.

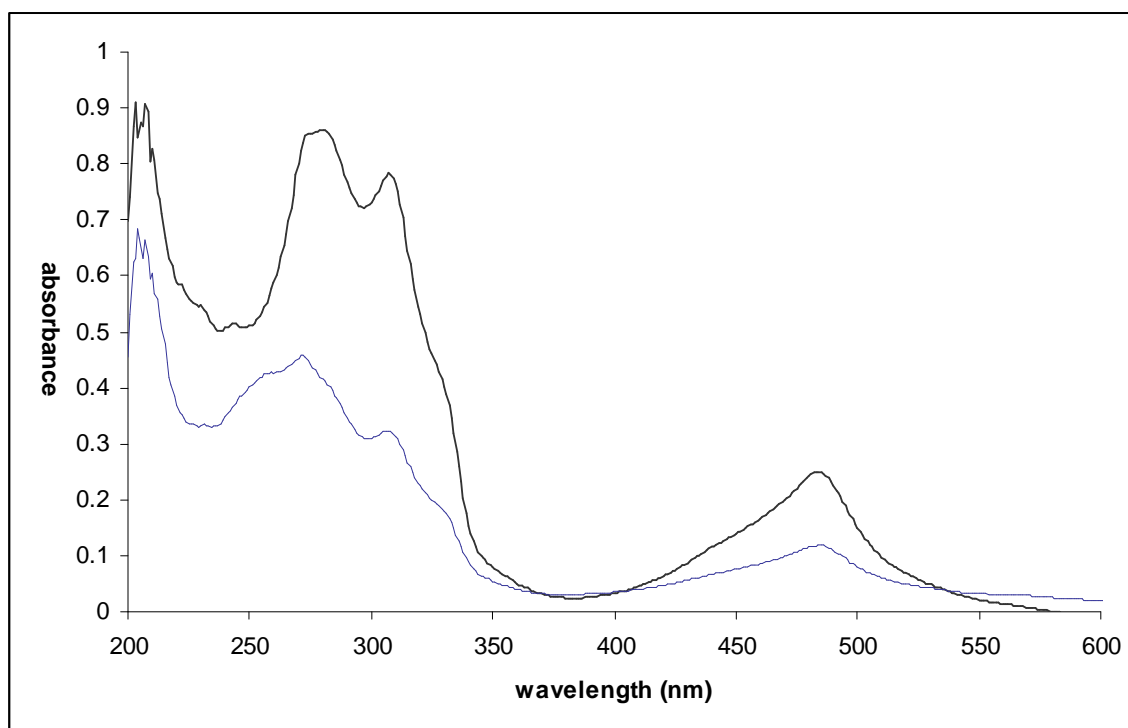


**Figure 2.11** UV/Vis spectra of complex  $[\text{Ru}(\text{terpy})_2(\mathbf{2.2})]^{8+}$  (—) and  $[\text{Ru}(\text{terpy})_2(\mathbf{2.2-DB24C8})]^{8+}$  (—) at concentration of  $1.0 \times 10^{-5} \text{ M}$  in  $\text{CH}_3\text{CN}$ .

**Table 2.4** UV/Vis data for complex  $[\text{Ru}(\text{terpy})_2(\mathbf{2.2})]^{8+}$ ,  $[\text{Ru}(\text{terpy})_2(\mathbf{2.2-DB24C8})]^{8+}$  and a few other selected ruthenium(II) complexes.

<b>Ru complex</b> <sup>(a)</sup>	<b>MLCT <math>\lambda_{\text{max}}</math> (nm)</b>	<b><math>\epsilon</math> (L mol<sup>-1</sup> cm<sup>-1</sup>)</b>	<b>ref#</b>
Ru(bipy) <sub>3</sub>	452	13 000	29
Ru(terpy) <sub>2</sub>	475	17 600	30
Ru(tolyterpy) <sub>2</sub>	490	28 000	31
Ru(terpy)(tolyterpy)	483	19 300	31
Ru(biptpy)(tpy)	484	17 000	26
$[(\text{Ru}(\text{terpy}))_2(\mathbf{2.2})]^{8+}$	485	25 000	35
$[(\text{Ru}(\text{terpy}))_2(\mathbf{2.2-DB24C8})]^{8+}$	485	11 900	35
Ru(terpy)(tolyterpy-DAP)	482	20 300	32

<sup>(a)</sup> Counter ion of PF<sub>6</sub><sup>-</sup>

### 2.3. Conclusion

The idea of creating an interlocked molecule with a chelating group as a stopper that can be used to form binuclear species has been presented. The robust nature of the [2]rotaxane was confirmed by <sup>1</sup>H NMR spectroscopy, which showed that the interlocked components have not dissociated from each other. Complexes of the labile metals silver(I), palladium(II), and zinc(II) were synthesized and characterized. The solid state structure of the binuclear Zn(II) with co-ligands showed that the ligand has the potential of self-assembly into 1-periodic terpy-based coordination polymer. A binuclear complex of the inert metal ruthenium(II) was synthesized and characterized. The solid state structure of the mixed ligand complex of the Ru(II), clearly demonstrates the utility of the “rotaxane as ligand” approach for providing a way to form robust complexes that require harsh reactions conditions.



## 2.4 Experimental

### 2.4.1 General Methods

4-Tolualdehyde, 2-acetylpyridine, N-bromosuccinimide, 2,2':6',2''-terpyridine,  $\text{RuCl}_3 \cdot x\text{H}_2\text{O}$ , and DB24C8 were purchased from Aldrich and used as received.  $[\text{RuCl}_3(\text{tpy})]$ ,<sup>34</sup> and 1,2-bis(4,4'-bipyridinium)ethane triflate  $[\mathbf{2.1}][\text{OTf}]_2$ <sup>36</sup> was synthesized using literature methods. Solvents were dried using an Innovative Technology Solvent Purification Systems.  $^1\text{H}$  NMR spectra were obtained on a Bruker Avance 500 instrument operating at 500 MHz. Deuterated solvents were purchased from Cambridge Isotope Laboratories Inc. and used as received. High-resolution mass spectra were recorded in 50/50 MeCN/ $\text{H}_2\text{O}$  on a Micromass LCT Electrospray TOF mass spectrometer. UV/Vis absorption spectra were run on a Cary 50 series spectrometer. The absorption spectra were recorded in acetonitrile ( $\text{BDH}^\circledR$ ) at concentrations of  $1.0 \times 10^{-5}$  M for complexes  $[\text{Ru}(\text{terpy})_2(\mathbf{2.2})]^{8+}$  and  $[\text{Ru}(\text{terpy})_2(\mathbf{2.2} \subset \mathbf{DB24C8})]^{8+}$ .

#### Synthesis 4-tolylterpyridine

4-Tolualdehyde (12.6 g, 12.4 mL, 0.105 mol) was dissolved in methanol (40 mL) and cooled to  $0^\circ\text{C}$ . To this was added 2-acetylpyridine (25.4 g, 23.5 mL, 0.209 mol) dissolved in methanol (20 mL) and 40% aqueous solution NaOH (30 mL). The mixture was stirred at  $-10^\circ\text{C}$  for an hour then allowed to warm to room temperature and stirred overnight.  $\text{NH}_4\text{CH}_3\text{CO}_2$  (40.0 g, 0.516 g) was added to the reaction mixture which was then refluxed for 24 h. The reaction was cooled to room temperature and then the methanol was evaporated. The product was extracted with  $\text{CHCl}_3$ , and then the  $\text{CHCl}_3$  was dried with  $\text{MgSO}_4$ , filtered, and evaporated. The residue was recrystallized from  $\text{CH}_3\text{CN}$  to yield 4-tolylterpyridine as an off-white powder. Yield: 11 g (31%).

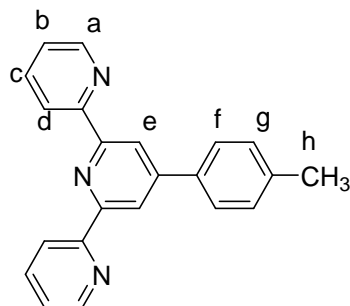


**Table 2.5**  $^1\text{H}$  NMR spectroscopic data in  $\text{CD}_3\text{CN}$

Proton	$\delta$ (ppm)	Multiplicity	# protons	J (Hz)
<i>a</i>	8.73	d	2	$^3J_{ab} = 5.8$
<i>b</i>	7.44	ddd	2	$^3J_{ba} = 5.8, ^3J_{bc} = 7.5, ^4J_{bd} = 0.8$
<i>c</i>	7.96	ddd	2	$^3J_{cb} = 7.5, ^3J_{cd} = 7.8, ^4J_{ca} = 1.7$
<i>d</i>	8.68	d	2	$^3J_{dc} = 7.8$
<i>e</i>	8.73	s	2	-
<i>f</i>	7.81	d	2	$^3J_{fg} = 8.1$
<i>g</i>	7.40	d	2	$^3J_{gf} = 8.1$
<i>h</i>	2.43	s	3	-

### Synthesis **Bromo-4-tolyterpyridine**

4'-(4-Tolyl)-2,2',6',2''-terpyridine (2.0011 g, 0.0062 mol) was dissolved in  $\text{CCl}_4$  (40 mL). To this solution was added N-bromosuccinimide (1.10 g, 0.0062 mol) and benzoyl peroxide (0.54 g, 0.0022 mol) and the reaction solution refluxed overnight and cooled to room temperature. The reaction was filtered to remove succinimide and then the  $\text{CCl}_4$  organic layer was washed with  $\text{NaHCO}_3(\text{aq})$  (3 x 50 mL) then  $\text{H}_2\text{O}$  (2 x 50 mL), dried with  $\text{MgSO}_4$ , filtered and then evaporated. The residue was recrystallized from 2:1 EtOH/Acetone mixture to give an off-white powder. Yield: 0.872 g (31%).

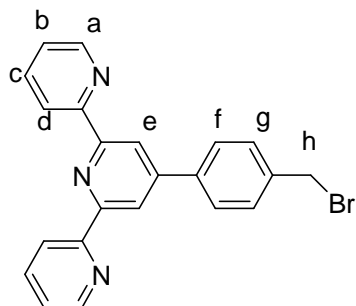


**Table 2.6**  $^1\text{H}$  NMR spectroscopic data in  $\text{CD}_3\text{CN}$

Proton	$\delta$ (ppm)	Multiplicity	# protons	J (Hz)
<i>a</i>	8.73	d	2	$^3J_{ab} = 6.0$
<i>b</i>	7.45	ddd	2	$^3J_{ba} = 6.0, ^3J_{bc} = 7.4, ^3J_{bd} = 1.6$
<i>c</i>	7.97	ddd	2	$^3J_{cb} = 7.4, ^3J_{cd} = 7.8, ^4J_{ca} = 1.6$
<i>d</i>	8.69	d	2	$^3J_{dc} = 7.8$
<i>e</i>	8.75	s	2	-
<i>f</i>	7.90	d	2	$^3J_{fg} = 8.2$
<i>g</i>	7.63	d	2	$^3J_{gf} = 8.2$
<i>h</i>	4.69	s	2	-

#### Synthesis [2.2][OTf]<sub>4</sub>

[2.1][OTf]<sub>2</sub> (0.100 g, 0.157 mmol) was dissolved in  $\text{MeNO}_2$  (10 mL) and bromo-4-tolyterpyridine (0.189 g, 0.470 mmol) added and the mixture allowed to heat at 60 °C for 3 days. The organic layer was removed and the orange solid dissolved in a two layer solution of  $\text{MeNO}_2$  and  $\text{NaOTf}_{(aq)}$  and stirred overnight. The colourless layer was separated, dried with anhydrous  $\text{MgSO}_4$ , filtered and the solvent removed by evaporation. The residue was stirred in  $\text{CHCl}_3$ . The resulting white solid was dissolved in  $\text{CH}_3\text{CN}$ , and *iso*-propyl ether allowed to slowly diffused into the solution producing an off-white solid, yield 0.100 g (31%).

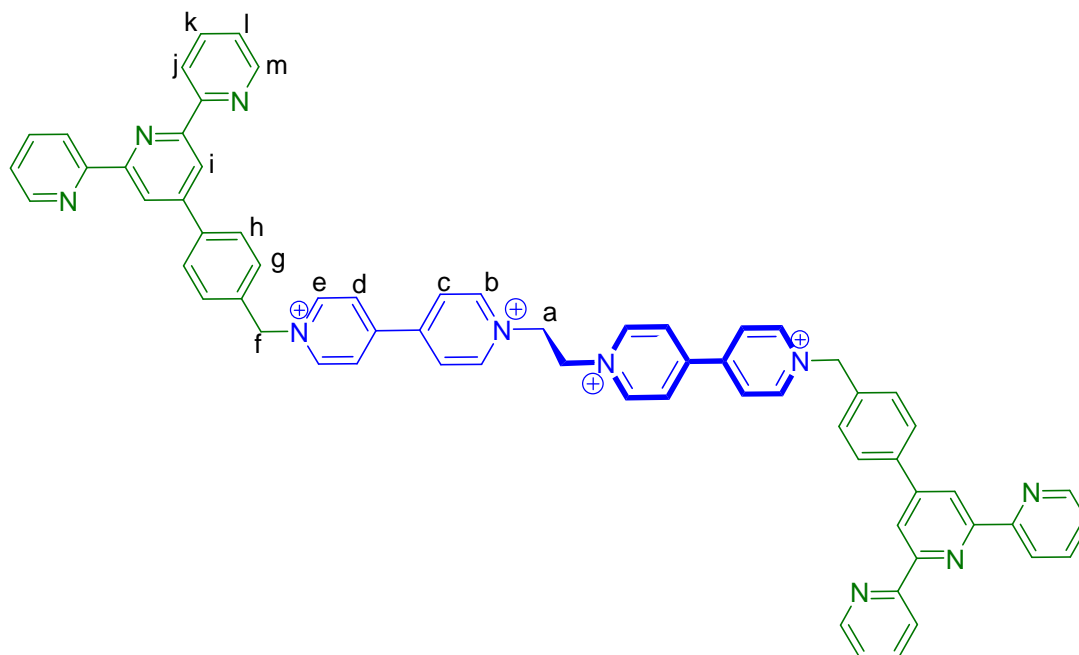


**Table 2.7**  $^1\text{H}$  NMR spectroscopic data for [2.2][OTf] $_4$  in  $\text{CD}_3\text{CN}$

Proton	$\delta$ (ppm)	Multiplicity	# protons	J (Hz)
<i>a</i>	5.27	s	4	-
<i>b</i>	9.04	m	4	-
<i>c</i>	8.49	d	4	$^3J_{cb} = 6.8$
<i>d</i>	8.46	d	4	$^3J_{de} = 6.8$
<i>e</i>	9.04	m	4	-
<i>f</i>	5.94	s	4	-
<i>g</i>	7.71	d	4	$^3J_{gh} = 8.0$
<i>h</i>	8.04	d	4	$^3J_{hg} = 8.2$
<i>i</i>	8.76	s	4	-
<i>j</i>	8.70	m	4	-
<i>k</i>	7.98	t	4	$^3J_{kl} = 7.5, ^3J_{kj} = 7.7$
<i>l</i>	7.46	t	4	$^3J_{lm} = 5.6, ^3J_{lk} = 6.9$
<i>m</i>	8.70	m	4	-

Synthesis [2.2-DB24C8][OTf]<sub>4</sub>

**DB24C8** (0.702 g, 157 μmol) and **[2.1][OTf]<sub>2</sub>** (0.100 g, 0.157 μmol) were dissolved in MeNO<sub>2</sub> (10 mL) and stirred overnight. Bromo-4-tolyterpyridine (0.189 g, 0.470 μmol) was dissolved in MeNO<sub>2</sub>, and the mixture was stirred for 7 days. The organic layer was removed, and the orange solid dissolved in a two layer solution of MeNO<sub>2</sub> and NaOTf<sub>(aq)</sub> stirred overnight. The organic layer was separated, dried with MgSO<sub>4</sub> and evaporated. The residue was stirred in toluene. The orange solid was dissolved in CH<sub>3</sub>CN; isopropyl ether was slowly diffused in to give an orange solid. Yield: 0.100 g (31%). **ESI-MS**: *m/z* [2.2-DB24C8]<sup>2+</sup> calc. 865.2752, found 865.2775.

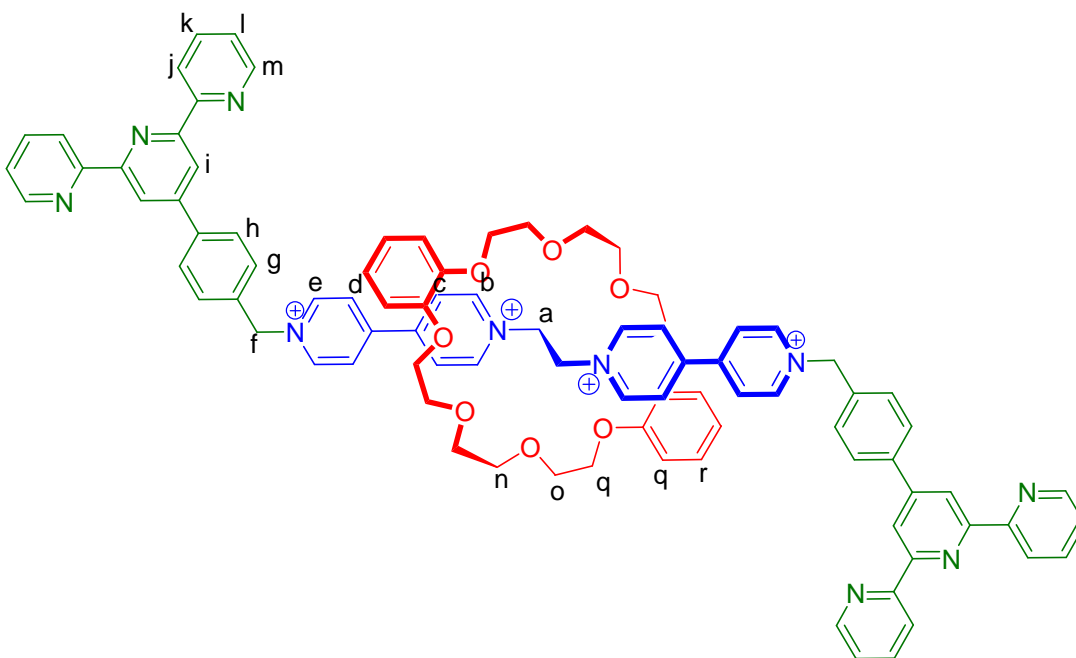


**Table 2.8**  $^1\text{H}$  NMR spectroscopic data for [2.2-**DB24C8**][OTf]<sub>4</sub> in CD<sub>3</sub>CN

Proton	$\delta$ (ppm)	Multiplicity	# protons	J (Hz)
<i>a</i>	5.60	s	4	-
<i>b</i>	9.31	d	4	$^3J_{bc} = 6.6$
<i>c</i>	8.19	d	4	$^3J_{cb} = 6.6$
<i>d</i>	8.15	d	4	$^3J_{de} = 6.6$
<i>e</i>	9.01	d	4	$^3J_{ed} = 6.6$
<i>f</i>	5.95	s	4	-
<i>g</i>	8.08	d	4	$^3J_{gh} = 8.2$
<i>h</i>	7.73	d	4	$^3J_{hg} = 8.1$
<i>i</i>	8.79	s	4	-
<i>j</i>	8.71	m	4	-
<i>k</i>	7.99	t	4	$^3J_{kl} = 6.8, ^3J_{kj} = 8.7$
<i>l</i>	7.47	t	4	$^3J_{lm} = 5.3, ^3J_{lk} = 5.3$
<i>m</i>	8.71	m	4	-
<i>q</i>	6.66	m	4	-
<i>r</i>	6.48	m	4	-
<i>n-p</i>	4.04-4.00	m	24	-

**Table 2.9**  $^1\text{H}$  NMR spectroscopic data for [2.2-**DB24C8**][OTf]<sub>4</sub> in CD<sub>3</sub>NO<sub>2</sub>

Proton	$\delta$ (ppm)	Multiplicity	# protons	J (Hz)
<i>a</i>	5.90	s	4	-
<i>b</i>	9.60	d	4	$^3J_{bc} = 5.1$
<i>c</i>	8.36	d	4	$^3J_{cb} = 5.4$
<i>d</i>	8.32	d	4	$^3J_{de} = 4.8$
<i>e</i>	9.18	d	4	$^3J_{ed} = 5.5$
<i>f</i>	6.12	s	4	-
<i>g</i>	7.52	m	4	-
<i>h</i>	7.84	d	4	$^3J_{hg} = 7.4$
<i>i</i>	8.84	s	4	-
<i>j</i>	8.77	m	4	-
<i>k</i>	8.05	m	4	-
<i>l</i>	8.18	d	4	$^3J_{lk} = 7.3$
<i>m</i>	8.77	m	4	-
<i>q</i>	6.61	m	4	-
<i>r</i>	6.76	m	4	-
<i>n-p</i>	4.13-4.04	m	24	-

### Synthesis [(Ru(terpy))<sub>2</sub>(**2.2-DB24C8**)](OTf)<sub>8</sub>

To a solution of [**2.2-DB24C8**](OTf)<sub>4</sub> (0.030 g, 0.0148 mmol) dissolved in 1:1 EtOH/H<sub>2</sub>O solution was added solid (terpy)RuCl<sub>3</sub> (0.013 g, 0.0246 mmol) and the mixture was brought to reflux for 24 h to give a deep red solution. The reaction mixture was cooled to room temperature and filtered through a Celite pad and washed with EtOH until the eluent was colourless. The filtrate was then reduced to half the volume and the addition of NaOTf produced a red precipitate. The red solid in CH<sub>3</sub>CN, isopropyl ether was slowly diffused in to give a red solid in quantitative yield. Yield: 0.047 g (98%).

**ESI-MS:** *m/z* [(Ru(terpy))<sub>2</sub>(**2.2-DB24C8**) + 5 OTf]<sup>3+</sup> calc. 949.2006, found 949.2072.

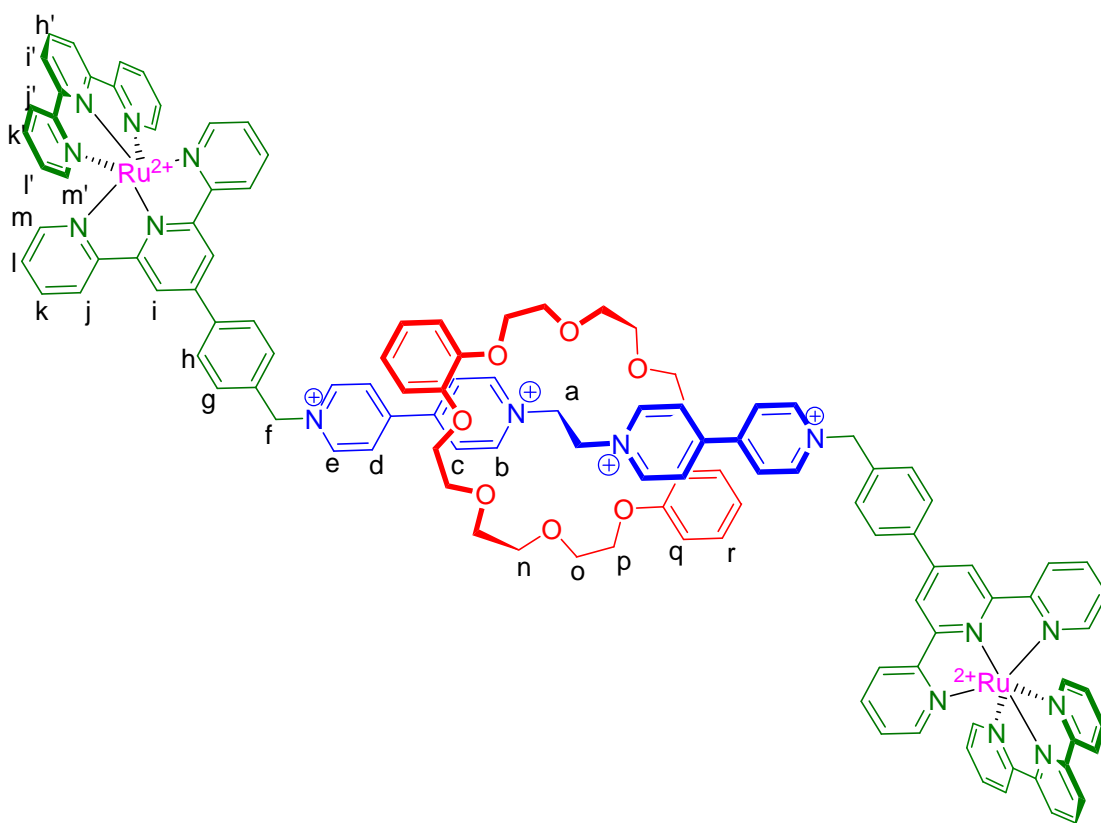


**Table 2.10**  $^1\text{H}$  NMR spectroscopic data for  $[(\text{Ru}(\text{terpy}))_2(\mathbf{2.2}\text{-DB24C8})][\text{OTf}]_8$  in  $\text{CD}_3\text{CN}$

Proton	$\delta$ (ppm)	Multiplicity	# protons	J (Hz)
<i>a</i>	5.64	s	4	-
<i>b</i>	9.36	d	4	$^3J_{bc} = 6.1$
<i>c</i>	8.31	m	4	-
<i>d</i>	8.31	m	4	-
<i>e</i>	9.14	d	4	$^3J_{ed} = 6.2$
<i>f</i>	6.04	s	4	-
<i>g</i>	7.94	m	4	-
<i>h</i>	8.37	d	4	$^3J_{hg} = 8.0$
<i>i</i>	9.05	s	4	-
<i>j</i>	8.50	d	4	$^3J_{jk} = 8.1$
<i>k</i>	7.91	m	4	-
<i>l</i>	7.16	m	4	-
<i>m</i>	7.41	d	4	$^3J_{ml} = 5.2$
<i>q</i>	6.70	m	4	-
<i>r</i>	5.10	m	4	-
<i>n-p</i>	4.07-4.03	m	24	-
<i>m'</i>	7.35	d	4	$^3J_{m'l'} = 5.3$
<i>l'</i>	7.16	m	4	-
<i>k'</i>	7.91	m	4	-
<i>j'</i>	8.68	d	4	$^3J_{j'k'} = 8.0$
<i>i'</i>	8.76	d	4	$^3J_{i'h'} = 8.1$
<i>h'</i>	8.41	t	2	$^3J_{h'i'} = 8.1$

#### Synthesis $[(\text{Ru}(\text{terpy}))_2(\mathbf{2.2})][\text{OTf}]_8$

To a solution of  $[\mathbf{2.2}][\text{OTf}]_4$  (0.030 g, 0.0148 mmol) dissolved in 1:1 EtOH/H<sub>2</sub>O solution was added solid  $\text{RuCl}_3(\text{terpy})$  (0.013 g, 0.0246 mmol) and the mixture was brought to reflux for 24 h to give a deep red solution. The reaction mixture was cooled to room temperature, filtered through a Celite pad and then washed with EtOH until the eluent was colourless. The filtrate was then reduced to half the original volume and NaOTf added which produced a red precipitate. The red solid was dissolved in  $\text{CH}_3\text{CN}$  and *iso*-propyl ether slowly diffused to give a red solid. Yield: 0.046 g (96%).



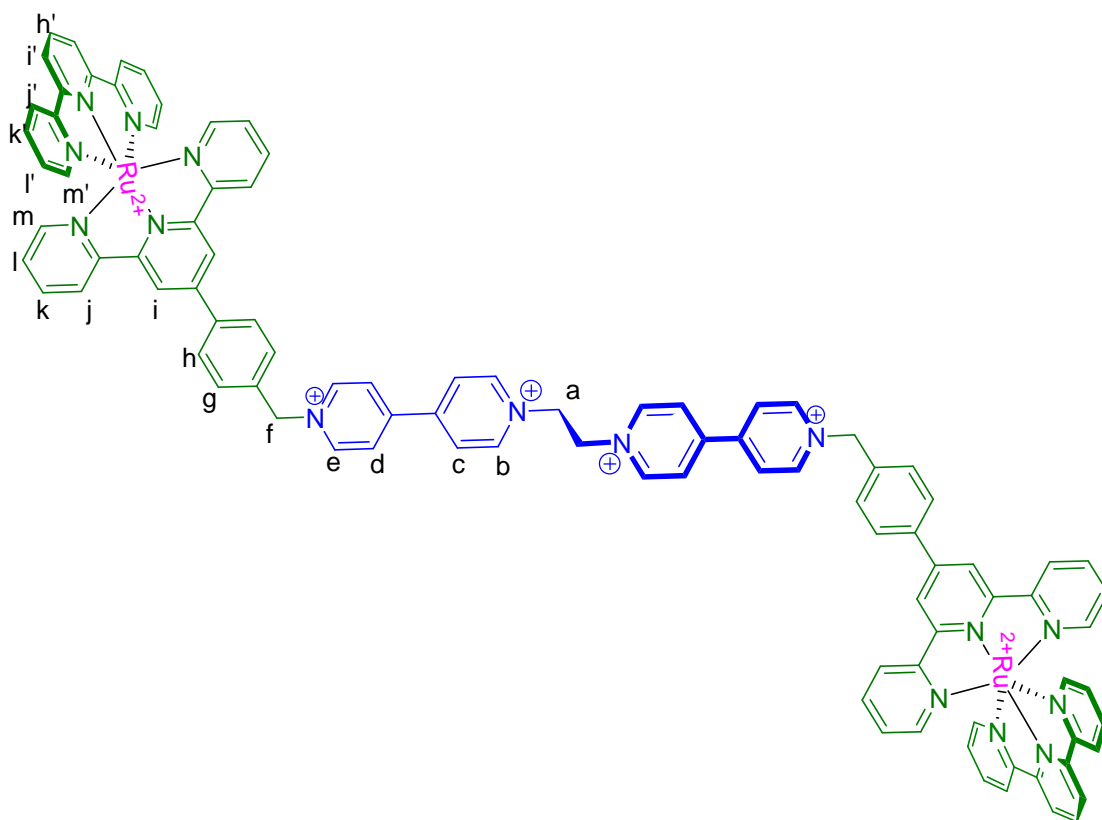


**Table 2-11**  $^1\text{H}$  NMR spectroscopic data for  $[(\text{Ru}(\text{terpy}))_2(\mathbf{2.2})][\text{OTf}]_8$  in  $\text{CD}_3\text{CN}$ .

Proton	$\delta$ (ppm)	Multiplicity	# protons	J (Hz)
<i>a</i>	5.34	s	4	-
<i>b</i>	9.19	d	4	$^3J_{bc} = 6.9$
<i>c</i>	8.58	d	4	$^3J_{cb} = 6.6$
<i>d</i>	8.58	d	4	$^3J_{de} = 6.6$
<i>e</i>	9.14	d	4	$^3J_{ed} = 6.9$
<i>f</i>	6.04	s	4	-
<i>g</i>	7.88	d	4	$^3J_{gh} = 8.3$
<i>h</i>	8.34	d	4	$^3J_{hg} = 8.3$
<i>i</i>	9.03	s	4	-
<i>j</i>	8.50	d	4	$^3J_{jk} = 8.0$
<i>k</i>	7.92	dd	4	$^3J_{kj} = 8.0$
<i>l</i>	7.16	m	4	-
<i>m</i>	7.41	d	4	$^3J_{ml} = 5.1$
<i>m'</i>	7.35	d	4	$^3J_{m'l'} = 5.5$
<i>l'</i>	7.16	m	4	-
<i>k'</i>	7.92	dd	4	$^3J_{k'l'} = 8.1$
<i>j'</i>	8.67	d	4	$^3J_{j'k'} = 8.1$
<i>i'</i>	8.76	d	4	$^3J_{i'h'} = 8.2$
<i>h'</i>	8.42	t	2	$^3J_{h'l'} = 8.2$

Synthesis [(Ag(MeCN))<sub>2</sub>(**2.2-DB24C8**)](OTf)<sub>6</sub>

To a solution of [**2.2-DB24C8**](OTf)<sub>4</sub> (0.030 g, 0.0148 mmol) was dissolved in 1mL of CH<sub>3</sub>CN was added to AgOTf (9 mg, 0.0350 mmol) and the mixture was stirred at room temperature overnight. Isopropyl ether was slowly diffuse to give an orange solid in quantitative yield. **ESI-MS**: *m/z* [Ag<sub>2</sub>(**2.2-DB24C8**) + 3 OTf ]<sup>3+</sup> calc. 697.7707, found 698.4532.

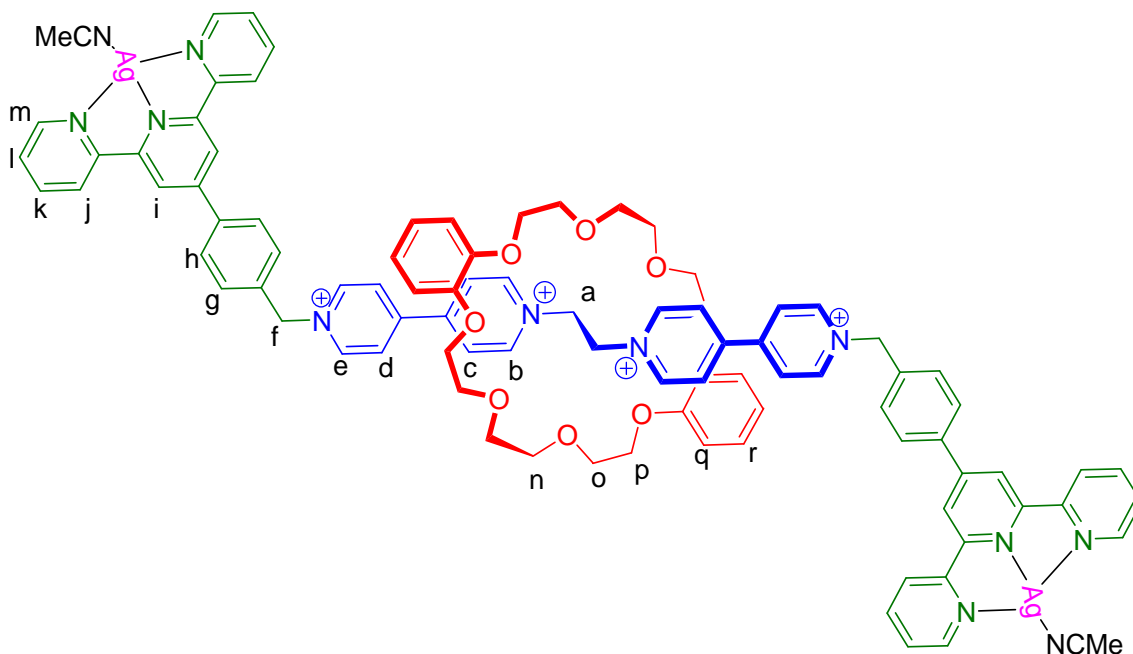


**Table 2.12**  $^1\text{H}$  NMR spectroscopic data for  $[(\text{Ag}(\text{MeCN}))_2(\mathbf{2.2\text{-}DB24C8})][\text{OTf}]_6$  in  $\text{CD}_3\text{CN}$

Proton	$\delta$ (ppm)	Multiplicity	# protons	J (Hz)
<i>a</i>	5.61	s	4	-
<i>b</i>	9.34	d	4	$^3J_{bc} = 6.0$
<i>c</i>	8.26	d	4	$^3J_{cb} = 7.0$
<i>d</i>	8.23	d	4	$^3J_{de} = 6.9$
<i>e</i>	9.06	d	4	$^3J_{ed} = 6.2$
<i>f</i>	5.97	s	4	-
<i>g</i>	8.14	m	4	-
<i>h</i>	7.77	d	4	$^3J_{hg} = 8.0$
<i>i</i>	8.59	s	4	-
<i>j</i>	8.49	d	4	$^3J_{jk} = 7.5$
<i>k</i>	8.07	ddd	4	$^4J_{km} = 1.7, ^3J_{kl} = 6.0, ^3J_{kj} = 6.1$
<i>l</i>	7.59	dd	4	$^3J_{lm} = 5.8, ^3J_{lk} = 6.6$
<i>m</i>	8.72	d	4	$^3J_{ml} = 5.0$
<i>q</i>	6.67	m	4	-
<i>r</i>	6.48	m	4	-
<i>n-p</i>	4.06 – 4.01	m	24	-

Synthesis  $[(\text{Pd}(\text{MeCN}))_2(\mathbf{2.2\text{-}DB24C8})][\text{OTf}]_8$

To a solution of  $[\mathbf{2.2\text{-}DB24C8}][\text{OTf}]_4$  (0.030 g, 0.0148 mmol) was dissolved in 1mL of  $\text{CH}_3\text{CN}$  was added to  $\text{Pd}(\text{MeCN})_4[\text{BF}_4]_2$  (14 mg, 0.0315 mmol) and the mixture was stirred at room temperature overnight. Isopropyl ether was slowly diffuse to give an orange solid in quantitative yield. **ESI-MS:**  $m/z$   $[\text{Pd}_2(\mathbf{2.2\text{-}DB24C8})+\text{H}_2\text{O}+\text{OTf}+\text{BF}_4]^{4+}$  calc. 448.1286, found 448.6074.

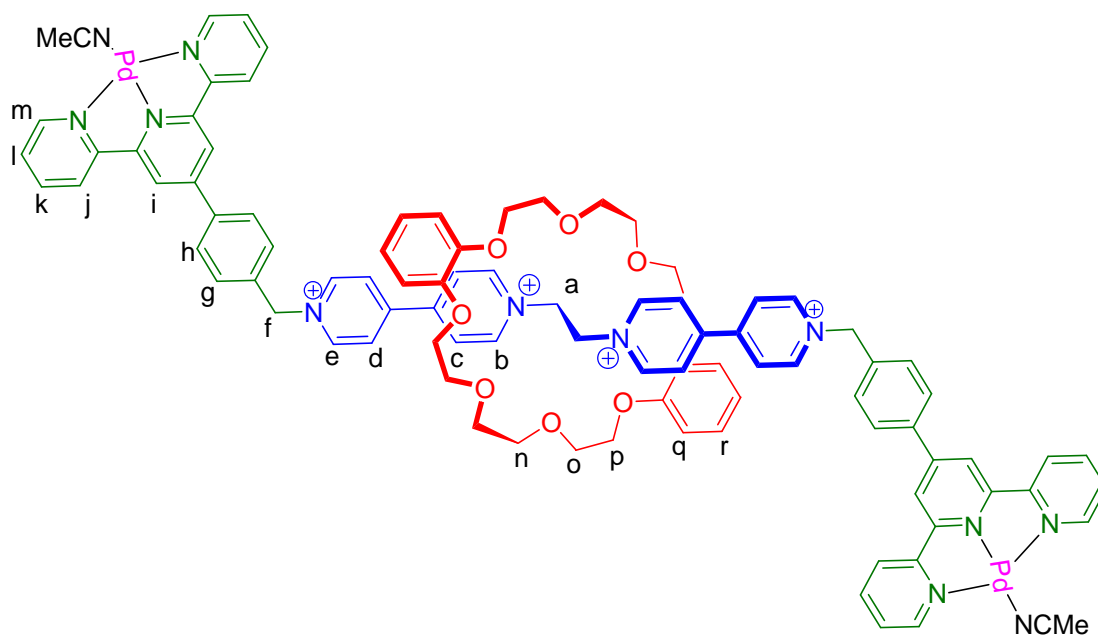


**Table 2.13**  $^1\text{H}$  NMR spectroscopic data for  $[(\text{Pd}(\text{MeCN}))_2(2.2\text{-DB24C8})][\text{OTf}]_8$  in  $\text{CD}_3\text{NO}_2$

Proton	$\delta$ (ppm)	Multiplicity	# protons	J (Hz)
<i>a</i>	5.90	s	4	-
<i>b</i>	9.60	d	4	$^3J_{bc} = 5.1$
<i>c</i>	8.36	d	4	$^3J_{cb} = 5.4$
<i>d</i>	8.33	d	4	$^3J_{de} = 5.9$
<i>e</i>	9.17	d	4	$^3J_{ed} = 5.1$
<i>f</i>	6.14	s	4	-
<i>g</i>	8.22	d	4	$^3J_{gh} = 7.8$
<i>h</i>	7.90	d	4	$^3J_{hg} = 7.3$
<i>i</i>	8.65	m	4	-
<i>j</i>	8.65	m	4	-
<i>k</i>	8.54	m	4	-
<i>l</i>	7.95	m	4	-
<i>m</i>	8.65	m	4	-
<i>q</i>	6.78	m	4	-
<i>r</i>	6.61	m	4	-
<i>n-p</i>	4.11-4.14	m	24	-

### Synthesis [(Zn(H<sub>2</sub>O))<sub>3</sub>(**2.2-DB24C8**)](OTf)<sub>8</sub>

To a solution of [**2.2-DB24C8**](OTf)<sub>4</sub> (0.030g, 0.0148mmol) dissolved in 1mL of CH<sub>3</sub>CN was added to Zn(OTf)<sub>2</sub> (11mg, 0.0311mmol) and the mixture was stirred at room temperature overnight. Isopropyl ether was slowly diffused to give an orange solid in quantitative yield.

### References:

1. Suzuki, Y.; Taria, T.; Osakada, K.; Horie, M. *Dalton Trans.* **2008**, 4823.
2. Crowley, J. D.; Goldup, S. M.; Lee, A.; Leigh, D. A.; McBurney, R. T. *Chem. Soc. Rev.* **2009**, 38, 1530.
3. Chmielewski, M. J.; Davis, J. J.; Beer, P. D. *Org. Biomol. Chem.* **2009**, 7, 415.
4. Collin, J.-P.; Durola, F.; Lux, J.; Sauvage, J.-P. *New J. Chem.*, **2010**, 34, 34.
5. Loeb, S. J. *Chem. Commun.* **2009**, 5585.
6. Ogino, H. *J. Am. Chem. Soc.* **1981**, 103, 1303.
7. Wylie, R. S.; Macartney, D. H. *J. Am. Chem. Soc.* **1992**, 114, 3136.
8. Cardenas, D. J.; Sauvage, J.-P. *Chem. Commun.* **1996**, 1915.
9. Loeb, S. J.; Wisner, J. A. *Chem. Commun.* **1998**, 2757.
10. Davidson, G. J. E.; Loeb, S. J.; Parekn, N. A.; Wisner, J. A. *Dalton Trans.* **2001**, 3135.
11. Chickak, K.; Walsh, M. C.; Branda, N. R. *Chem. Commun.* **2000**, 847.
12. Diskin-Posner, Y.; Patra, G. K.; Goldberg, I. *Eur. J. Inorg. Chem.* **2001**, 2515.
13. Mullen, K. E.; Johnstone, K. D.; Nath, D.; Bampos, N.; Sanders, J. K. M.; Gunter, M. J. *Org. Biomol. Chem.* **2009**, 7, 293.
14. Davidson, G. J. E.; Loeb, S. J. *Dalton Trans.* **2003**, 4319.
15. Davidson, G. J. E.; Loeb, S. J.; Passaniti, P.; Silvi, S.; Credi, A. *Chem. Eur. J.* **2006**, 12, 3233.

16. Marlin, D. S.; Carbrera, D. G.; Leigh, D. A.; Slawin, A. M. Z. *Angew. Chem. Int. Ed.* **2006**, *45*, 77.
17. Collins, J.-P.; Guillerez, S.; Sauvage, J. P.; Barigelletti, F.; De Cola, L.; Flamigni, L.; Balzan, V. *Inorg. Chem.* **1991**, *30*, 4230.
18. Hou, L.; Li, D.; Yin, Y-G; Wu, T.; Ng, S. W. *Acta Cryst. Sect. C* **2004**, *E24*, m1106.
19. Hou, L.; Li, D. *Inorg. Chem. Commun.*, **2006**, *8*, 128.
20. Mei, G.Q.; Huang, K. L. *Acta Cryst. Sect. E* **2007**, *E63*, m2029.
21. Sommer, R. D.; Rheingold, A. L.; Goshe, A. J.; Bosnich, B. *J. Am. Chem. Soc.* **2001**, *123*, 3940.
22. Hou, L.; Li, D.; Ng, S. H. *Acta Cryst. Sect. E* **2004**, *E60*, m1734.
23. Ma, Z.; Cao, Y.; Li, Q.; Pombeiro, A. J. L. *J. Inorg. Biochem.* **2010**, *104*, 704.
24. Constable, E. C. *Chem. Soc. Rev.*, **2007**, *36*, 246.
25. Pyo, S.; Perez-Cordero, E.; Bott, S. G.; Echegoyen, L. *Inorg. Chem.* **1999**, *38*, 3337.
26. Alcock, N. A.; Barker, P. R.; Hailder, J. M.; Hannon, M. J.; Painting, C. L.; Pikramenou, Z.; Plummer, E. A.; Rissanen, K.; Saarenketo, P. *Dalton Trans.* **2000**, 1447.
27. Sauvage, J.-P.; Collin, J.-P.; Chambron, J.-C.; Gullerez, S.; Coudret, C. *Chem. Rev.*, **1994**, *94*, 993
28. Balzani, V.; Juris, A.; Venturi, M.; Campagna, S.; Serroni, S. *Chem. Rev.*, **1996**, *96*, 759.
29. Juris, A.; Balzani, V.; Belser, P.; von Zelewsky, A. *Helv. Chim. Acta.* **1981**, *64*, 7, 2175.
30. Constable, E. C.; Thompsom, A. M. W. C.; Tocher, D. A.; Danials, A. M. *New J. Chem.*, **1992**, *16*, 855.
31. Hofmeirer, H.; Andres, P. R.; Hoogenboom, R.; Herdtwerk, E.; Schubert, U. S. *Aust. J. Chem.*, **2004**, *57*, 419.

32. Ashton, P. R.; Ballardini, R.; Balzani, V.; Constable, E. C.; Credi, A; Kocian, O.; Langford, S. J.; Preece, J. A.; Prodi, L.; Schofield, E. R.; Spencer, N.; Stoddart, J. F.; Wenger, S., *Chem. Eur. J.* **1998**, *4*, 2413.
33. Maestri, M.; Armaroli, N.; Balzani, V.; Constable, E. C.; Thomson, A. M. W. C. *Inorg. Chem.* **1995**, *34*, 2759
34. Sullivan, B. P.; Calvert, J. M.; Meyer, T. L. *Inorg. Chem.* **1980**, *19*, 1404.
35. Mercer, D. J.; Loeb, S. J. *Dalton Trans.* **2011**, *40*, 6385.
36. Loeb, S. J.; Tiburcio, J.; Vella, S. J.; Wisner, J. A. *Org. Biomol. Chem.* **2006**, *4*, 660.

# Chapter 3

## The Effect of Crown Ether Substitution on the 1,2-Bis(pyridinium)ethane $\subset$ 24-Crown-8 Templating Motif

### 3.1 Introduction

There are a number of strategies for the preparation of interlocked molecules, the most common way involves utilizing non-covalent interactions between a linear axle and a cyclic wheel to form an interpenetrated adduct, a [2]pseudorotaxane, followed by conversion to a permanently interlocked [2]rotaxane by capping with bulky end groups. There are a number of linear axles available such as dibenzylammonium ions, N-benzylanilinium cations, and 1,2-bis(pyridinium)ethanes cations. The electronic properties of these axles can be tuned by adding different functional groups or changing their positions.<sup>1,2</sup> A question that has not been addressed to the same extent, is can the association between the axle and wheel be effected in a similar fashion by varying the steric and electronic nature of the wheel?

It seems, however, that the preparation of derivatives of **DB24C8** can be challenging with reported long reactions times and low yields and only a few examples have been studied to evaluate their effect on pseudorotaxane formation. Gibson reported a version of **DB24C8** containing two ester groups that gave a lower association constant with dibenzylammonium axle,  $[(\text{Bn})_2\text{NH}_2\subset\text{DEDB24C8}]^+$ ; see Figure 3.1.<sup>3</sup> It was concluded that the two electron withdrawing groups reduce the electron density of the oxygen atoms in the crown ether ring both inductively and through resonance therefore weakening the hydrogen bonding with the acidic protons on the axle.



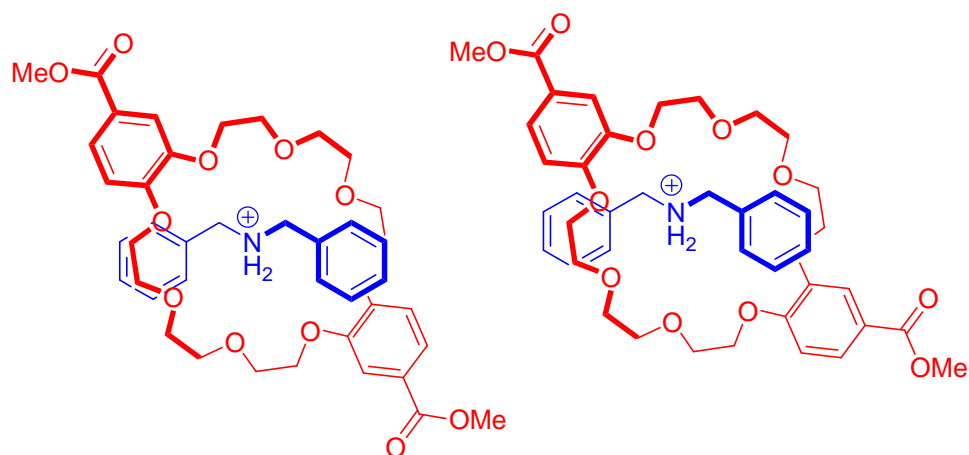


**Figure 3.1** [2]Pseudorotaxane with  $[(\text{Bn})_2\text{NH}_2\text{CDEDB24C8}]^+$ .

Another study with 1,2-bis(pyridinium)ethanes axes by Liu, looked at both electron donating groups and electron withdrawing groups attached to **DB24C8**; see Figure 3.2.<sup>4</sup> It was concluded, similar to Gibson's study, that electron donating groups enhanced the binding ability, whereas electron withdrawing groups reduced binding ability. One significant difference between the two studies was that Gibson pointed out that different association constants could be obtained if the ester groups were *syn* or *anti* to each other, with the more symmetric crown having the higher  $K_a$ , while Liu, and took no efforts to separate the positional isomers.

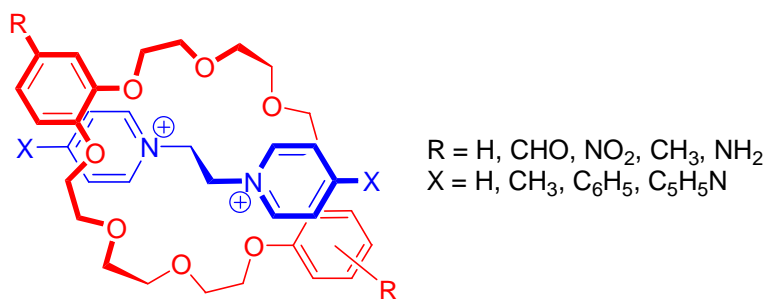


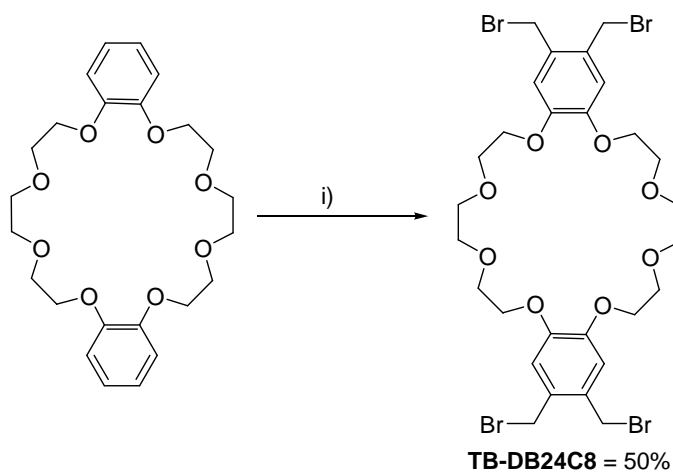
**Figure 3.2** Structural formula of the [2]pseudorotaxane studied by Liu.<sup>4</sup>

In this chapter, we look at the effects on pseudorotaxane formation of using **DB24C8** with four aryl ether groups and various 1,2-bis(pyridinium)ethanes derivatives. We will also report the preparation of *two* classes of [2]rotaxanes using these new crown ethers.

## 3.2 Results and Discussion

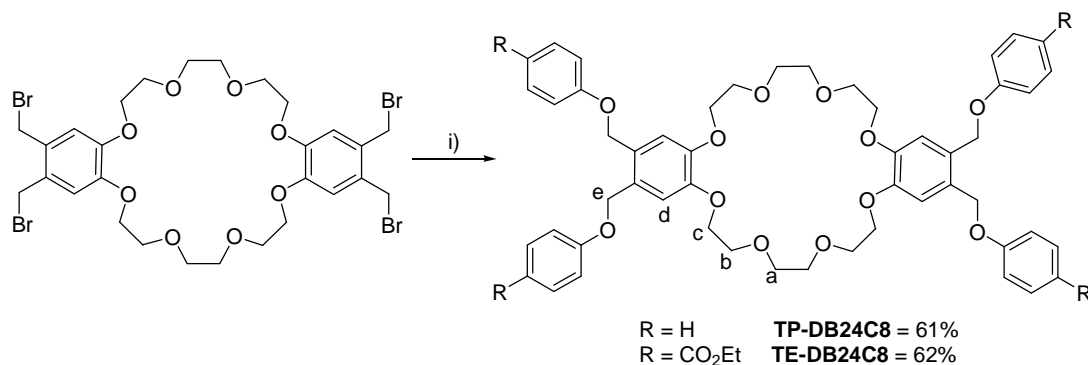
### 3.2.1 Synthesis of tetrakis-substituted crown ethers

Tetrakis(bromomethyl)dibenzo-24-crown-8 was synthesized using a modified version of the procedure reported by Nishimura involving a double Friedel-Crafts alkylation of both the **DB24C8** aromatic rings followed by bromination *in-stiu* to give **TB-DB24C8** as a white solid; Scheme 3.1.<sup>5</sup> The <sup>1</sup>H NMR spectrum of **TB-DB24C8** in CD<sub>2</sub>Cl<sub>2</sub> reveals the presence of one aromatic peak at 6.85 ppm and the benzylic protons at 4.62 ppm. The main core remains virtually unchanged.



**Scheme 3.1:** i) (CH<sub>2</sub>O)<sub>n</sub>, CHCl<sub>3</sub>/CH<sub>3</sub>COOH, HBr, 60°C 48h.

In order to gain insight into the effect that these relatively bulky substituted groups have on [2]pseudorotaxane formation, different phenols groups were appended to **DB24C8**. The new crown ethers were prepared using a Williamson ether synthesis conditions with K<sub>2</sub>CO<sub>3</sub> as the base (Scheme 3.2) and precipitation from MeCN. The desired compound was isolated as off white solids in about 60 % yield.



**Scheme 3.2 i)** **TB-DB24C8**, PhOH or 4-EtO<sub>2</sub>CPhOH, K<sub>2</sub>CO<sub>3</sub>, MeCN, N<sub>2</sub>, Δ 120h.

The <sup>1</sup>H NMR spectrum of compounds **TP-DB24C8** and **TE-DB24C8** show the main core remains unchanged, relative to the starting material **TB-DB24C8**. The major differences arise from the aromatic (**d**) and the benzylic (**e**) protons. In both **TP-DB24C8** and **TE-DB24C8** these resonances are shifted downfield due to the change from Br to phenolic oxygen; Table 3.1. The ESI-MS verifies that four substituent groups have been added to the crown ether. In each, the crown ethers interact strongly with sodium ions present; [**TP-DB24C8** + Na]<sup>+</sup> and [**TE-DB24C8** + Na]<sup>+</sup> at 895.3658 and 1183.4524 *m/e*, respectively.

**Table 3.1** Comparison of the chemical shifts of the wheels **TB-DB24C8**, **TP-DB24C8**, and **TE-DB24C8** in CD<sub>2</sub>Cl<sub>2</sub>.

Proton	<b>TB-DB24C8</b>	<b>TP-DB24C8</b>	<b>TE-DB24C8</b>
<i>a</i>	3.37	3.54 (0.17)	3.74 (0.37)
<i>b</i>	3.85	3.77 (-0.08)	3.90 (0.05)
<i>c</i>	4.12	4.01 (-0.11)	4.17 (0.05)
<i>d</i>	6.86	7.03 (0.17)	7.01 (0.15)
<i>e</i>	4.62	5.05 (0.43)	5.10 (0.48)

Single crystals of **TP-DB24C8** were grown by slow diffusion of hexanes into a saturated solution containing **TP-DB24C8** in CHCl<sub>3</sub>. The new crown ether crystallizes with two molecules in a triclinic unit cell in space group P-1. The molecule takes on an S-shaped conformation similar to other **DB24C8** derived crown ethers, the appended ring

of the phenyl groups are pointing away from the opening of the macrocyclic cavity; Figure 3.3. The plane of the catechol rings extends to C11 and C16 ( $C17-C10-O2-C11 = -169.47^\circ(4)$  and  $C10-C17-O5-C16 = 178.07^\circ(4)$ ). The adjacent carbon atoms in the polyether chain are included in the plane as well ( $C10-O2-C11-C12 = 168.87^\circ(4)$  and  $C17-O5-C16-C15 = 176.81^\circ(4)$ ).

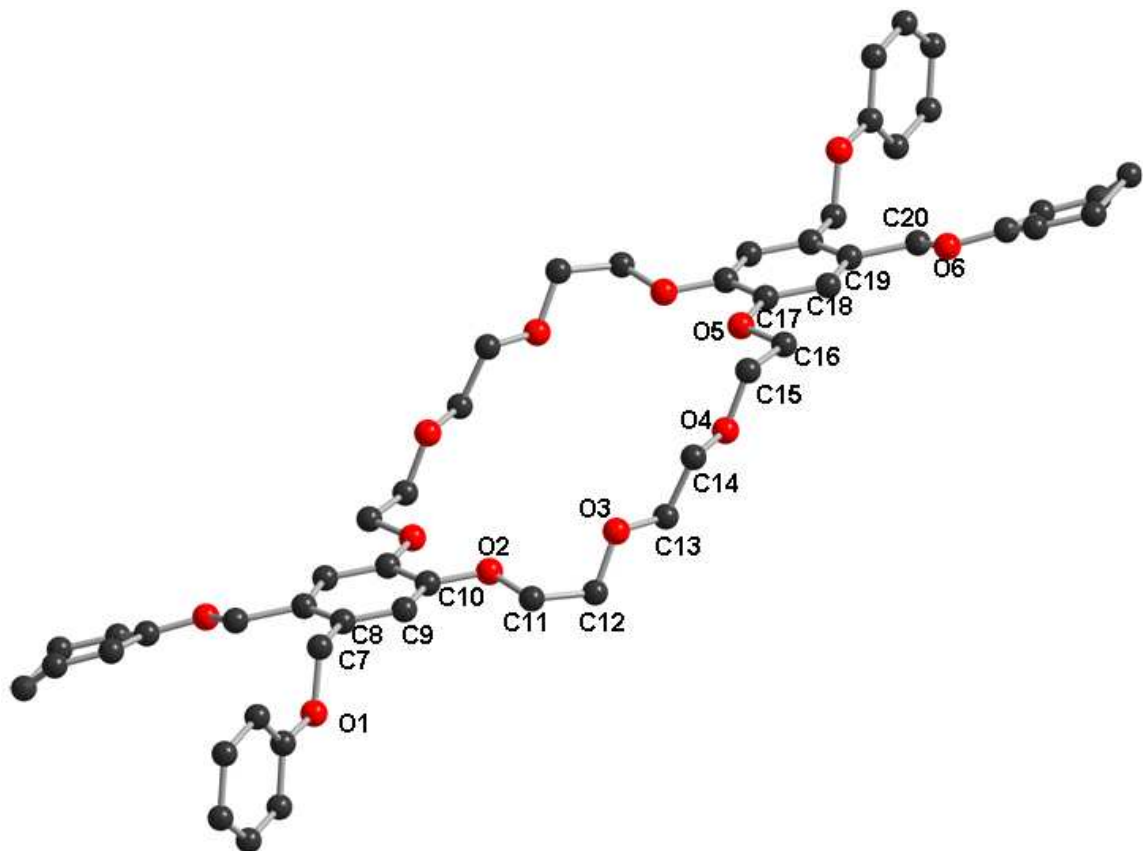
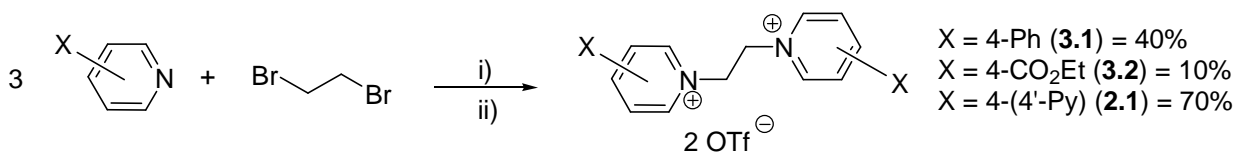
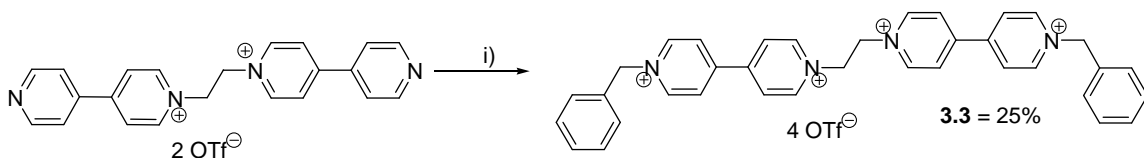


**Figure 3.3** Crystal structure of **TP-DB24C8**. (O = red, C = black, wheel bonds = silver).

The axles used for the [2]pseudorotaxane study were synthesized by a Menshutkin reaction with substituted pyridines and 1,2-dibromoethane; Scheme 3.3. The benzyl axle was synthesized by quaternization of the nitrogens of the 4-4'-pyridyl thread; Scheme 3.4.<sup>2a</sup>



**Scheme 3.3** i) MeCN,  $\Delta$  72 h ii) NaOTf<sub>(aq)</sub>.



**Scheme 3.4** i) benzyl bromide in MeNO<sub>2</sub>, NaOTf<sub>(aq)</sub>, for 72 h.

Due to the low solubility of the two tetrakis-substituted crown ethers in polar solvents such as MeCN, the crown ethers were individually dissolved with heat, and cooled to room temperature before being combined with the threads. The position of resonances from the individual components relative to their threaded counterparts allowed facile identification of the non-covalent interactions occurring between the two components and suggests that threading of the axle through the wheel gives rise to a [2]pseudorotaxane geometry. These chemical shift changes are summarized in Table 3.2 for [2]pseudorotaxanes.

**Table 3.2** <sup>1</sup>H NMR chemical shifts for the axles and [2]pseudorotaxanes undergoing slow exchange.

Compound	CH <sub>2</sub> N	H-ortho-N <sup>+</sup>	H-meta-N <sup>+</sup>
[ <b>3.1</b> ] <sup>2+</sup>	5.13	8.68	8.34
[ <b>3.1</b> ⊂TP-DB24C8] <sup>2+</sup>	5.48	9.02	7.54
[ <b>3.1</b> ⊂TE-DB24C8] <sup>2+</sup>	5.44	9.03	7.90
[ <b>3.2</b> ] <sup>2+</sup>	5.24	8.96	8.52
[ <b>3.2</b> ⊂TP-DB24C8] <sup>2+</sup>	5.56	9.21	8.17
[ <b>3.2</b> ⊂TE-DB24C8] <sup>2+</sup>	5.55	9.24	8.16
[ <b>2.1</b> ] <sup>2+</sup>	5.16	8.89	8.40
[ <b>2.1</b> ⊂TP-DB24C8] <sup>2+</sup>	5.54	9.18	8.04
[ <b>2.1</b> ⊂TE-DB24C8] <sup>2+</sup>	5.55	9.17	8.05
[ <b>3.3</b> ] <sup>2+</sup>	5.27	9.04	8.42
[ <b>3.3</b> ⊂TP-DB24C8] <sup>2+</sup>	5.63	9.33	8.22
[ <b>3.3</b> ⊂TP-DB24C8] <sup>2+</sup>	5.66	9.36	8.25

With observation of both the free and complexed components via slow exchange, the  $^1\text{H}$  NMR spectra were used to measure the association constants ( $K_a$ ) using the single point determination analysis. A complete set of thermodynamic parameters ( $\Delta H^\circ$ , and  $\Delta S^\circ$ ) could be extracted utilizing a standard van't Hoff analysis as follows.

Starting from equation 1.1.

$$\Delta G^\circ = -RT \ln K \quad (1.1)$$

and solving for the natural log, equation 1.2 can be obtained.

$$\ln K = \frac{-\Delta G^\circ}{RT} \quad (1.2)$$

Since for a change in temperature, the Gibbs free energy can be expressed in terms of enthalpy ( $\Delta H$ ), and entropy ( $\Delta S$ ), as in equation 1.3.

$$\Delta G = \Delta H - T\Delta S \quad (1.3)$$

Substitution of equation 1.3 into 1.2 gives the linear expression of the van't Hoff relationship, equation 1.4.

$$\begin{aligned} \ln K &= -\left(\frac{\Delta H - T\Delta S}{RT}\right) \\ \ln K &= -\frac{\Delta H}{RT} + \frac{\Delta S}{R} \\ R \ln K &= -\frac{\Delta H}{T} + \Delta S \\ R \ln K &= -\Delta H \frac{1}{T} + \Delta S \end{aligned} \quad (1.4)$$

The [2]pseudorotaxane adducts formed between **TP-DB24C8** or **TE-DB24C8** and **3.1-3.3** and **2.1** were subjected to variable temperature  $^1\text{H}$  NMR spectroscopy (VTNMR) experiments. The association constants of the new crown ethers with the selected threads

are reported in Table 3.3 along with previously measured parameters for **DB24C8** as a comparison.

**Table 3.3**  $K_a$  ( $M^{-1}$ ) and  $\Delta G$  ( $kJ\ mol^{-1}$ ) values for the [2]pseudorotaxane formed between **TP-DB24C8**, **TE-DB24C8** and **3.1-3.3** and **2.1** at 298K.

Axle	DB24C8	TP-DB24C8	TE-DB24C8
[3.1] <sup>2+</sup>	400 (-14.8)	1260 (-17.7)	880 (-16.8)
[3.2] <sup>2+</sup>	1940 (-18.8)	570 (-15.7)	390 (-14.8)
[2.1] <sup>2+</sup>	930 (-16.9)	1620 (-18.3)	1190 (-17.7)
[3.3] <sup>4+</sup>	1000 (-17.1)	820 (-16.6)	430 (-15.1)

With respect to the association constants for [2]pseudorotaxanes derived from standard 1,2-bis(pyridinium)ethane axles and these new substituted crown ethers, it is clear that deviations from values found for **DB24C8** must be a result of either electronic or steric effects. One would predict that, the association constant would increase due to the presence of four weakly inductive alkyl groups which make the crown aromatic rings more electron rich. This would increase the strength of the non-covalent interactions compared to **DB24C8**; Table 3.3. Therefore, the lower  $K_a$  values observed in Table 3.3 must be the result of steric effects playing a major role and off-setting these electronic effects. In general,  $\Delta H^\circ$  values are significantly negative indicating strong interactions and a true molecular recognition process.<sup>2</sup> Interestingly, both  $\Delta H^\circ$  and  $\Delta S^\circ$  (see Table 3.4.) are significantly more favourable than with **DB24C8**.<sup>2</sup> Both these trends can be attributed to the more efficient  $\pi$ -stacking contributions between axles and the crown.

**Table 3.4** Complete listing of  $\Delta H^\circ$  ( $kJmol^{-1}$ ) and  $\Delta S^\circ$  ( $Jmol^{-1}K^{-1}$ ) values for [2]pseudorotaxanes in  $CD_3CN$ .

Axle	DB24C8	TP-DB24C8	TE-DB24C8
[3.1] <sup>2+</sup>	-60.8 (-147.2)	-53.2 (-34.9)	-71.6 (-54.1)
[3.2] <sup>2+</sup>	-44.3 (-98.8)	-58.9 (-41.2)	-52.2 (-45.4)
[2.1] <sup>2+</sup>	-48.4 (-99.4)	-58.5 (-42.8)	-34.2 (-19.5)
[3.3] <sup>4+</sup>	-57.7 (-136.7)	-53.7 (-37.0)	-63.1 (-48.1)

Single crystals of **[3.2-TP-DB24C8][OTf]<sub>2</sub>** were grown by the slow diffusion of isopropyl ether into a MeCN solution of the [2]pseudorotaxane mixture. Figure 3.5 shows a ball-and-stick representation of the cation **[3.2-TP-DB24C8]<sup>2+</sup>**. The crown ether takes up an S-shaped conformation comparable to the free crown itself. The axle takes on an *anti* conformation as observed previously.<sup>2a</sup> As expected, the cationic axle interpenetrates the central cavity of the wheel allowing the electron-rich aromatic portion of the wheel to  $\pi$ -stack with the electron-deficient axle. The structure is held together by a combination of N<sup>+</sup>...O ion dipole interactions, C-H...O hydrogen bonding and  $\pi$ -stacking. For the N<sup>+</sup>...O ion dipole interaction, there are close contacts between the quaternarized dipyridinium nitrogen atoms and the oxygen ethers at N1...O8 = 3.61, N1...O5 = 3.54, N1...O7 = 3.95, N1...O6 3.82 Å. The C-H...O hydrogen bonds between the methylene components of the thread and alternating oxygen atoms of the crown are summarized in Table 3.5 and the ~3.5 Å distance between aromatic rings of the axle and wheel is evidence of the  $\pi$ -stacking. In addition to these interactions which are known for all [2]pseudorotaxanes involving **DB24C8**, there is a close approach of an axle ester group of the quaternized N-atom of the axle to the crown ether at a distance of ~3.25 Å and a C-H... $\pi$  interaction with a phenyl groups on the crown with a distance ~3.01 Å; Figure 3.4.

**Table 3.5:** Hydrogen bonds parameter in the crystal structure of [2]pseudorotaxane **[3.2-TP-DB24C8][OTf]<sub>2</sub>**.

Hydrogen bonded atoms	Distance (Å)	C-H...O Angle (°)
C9-O5	3.55	149
C9-O7	3.50	163
C6-O6	3.49	155
C7-O6	3.10	129

Single crystals of **[3.3-TE-DB24C8][OTf]<sub>4</sub>** were also grown by the slow diffusion of isopropyl ether into a MeCN solution of [2]pseudorotaxane. Figure 3.6 shows a ball-and-



stick representation of the cation  $[3.3\text{-TE-DB24C8}]^{4+}$ . As expected, the two components are held together by the same non-covalent interaction as the previous structure. The  $\text{N}^+\cdots\text{O}$  ion dipole interactions are  $\text{N2}\cdots\text{O4} = 3.39$ ,  $\text{N2}\cdots\text{O12} = 3.60$ ,  $\text{N2}\cdots\text{O4} = 3.39$ ,  $\text{N2}\cdots\text{O12} = 3.60$  Å. The hydrogen bonds to the methylene components of the axle are with alternating oxygen's on the crown ether as summarized in Table 3.6.

**Table 3.6:** Hydrogen bonds parameter in the crystal structure of [2]rotaxane  $[3.3\text{-TE-DB24C8}][\text{OTf}]_4$ .

Hydrogen bonded atoms	Distance (Å)	C-H $\cdots$ O Angle (°)
C14-O4	3.30	142
C14-O12	3.32	121
C15-O5	3.23	153
C13-O13	3.38	140

The [2]pseudorotaxane  $[3.3\text{-TE-DB24C8}]^{4+}$  also shows evidence of  $\pi$ -stacking between the aromatic ring of the axle with the catechol ring on the crown ether. There is also a C-H $\cdots$  $\pi$  interaction from the benzoate group to the benzyl group of a distance of 3.53 Å; Figure 3.4.

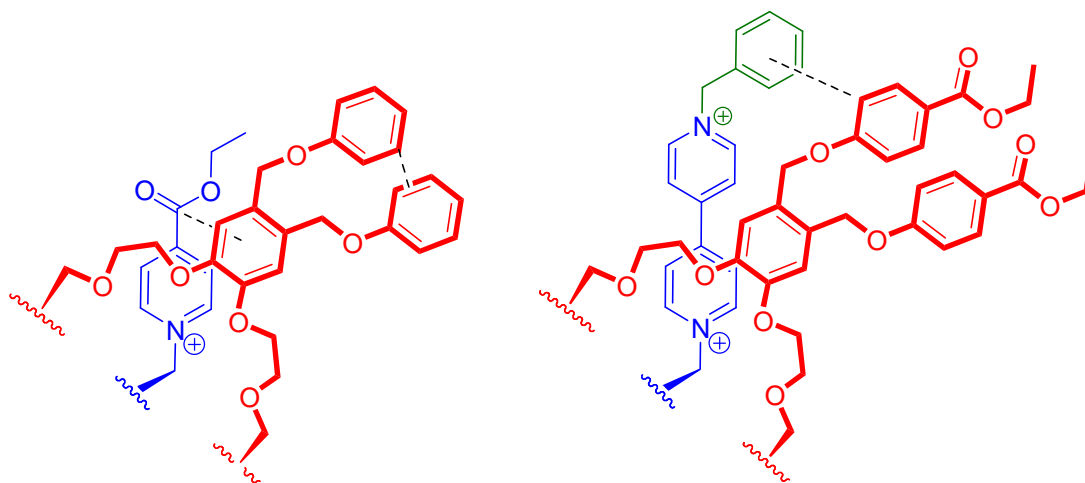


**Figure 3.4** Cartoon representation of the new addition interactions observed in the crystal of [2]rotaxane. The black dash lines indicate new secondary interactions.

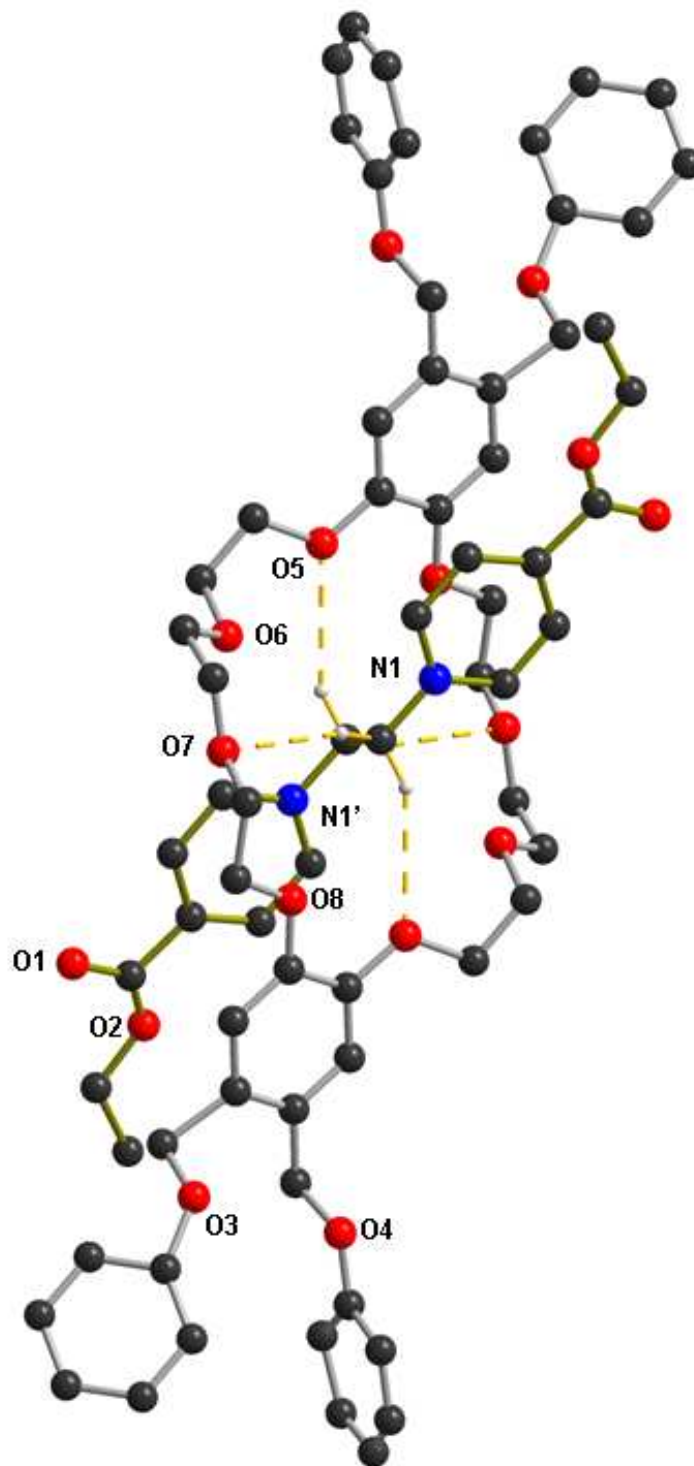


**Figure 3.5** A ball-stick representation of the cationic portion of the X-ray crystal structure of  $[3.2\text{cTP-DB24C8}]^{2+}$ . The complex occupies a crystallographic centre of symmetry. All hydrogen atoms, all anions, and all solvent molecules have been omitted for clarity. (O = red, N = blue, C = black; wheel bonds = silver, axle bonds = gold).

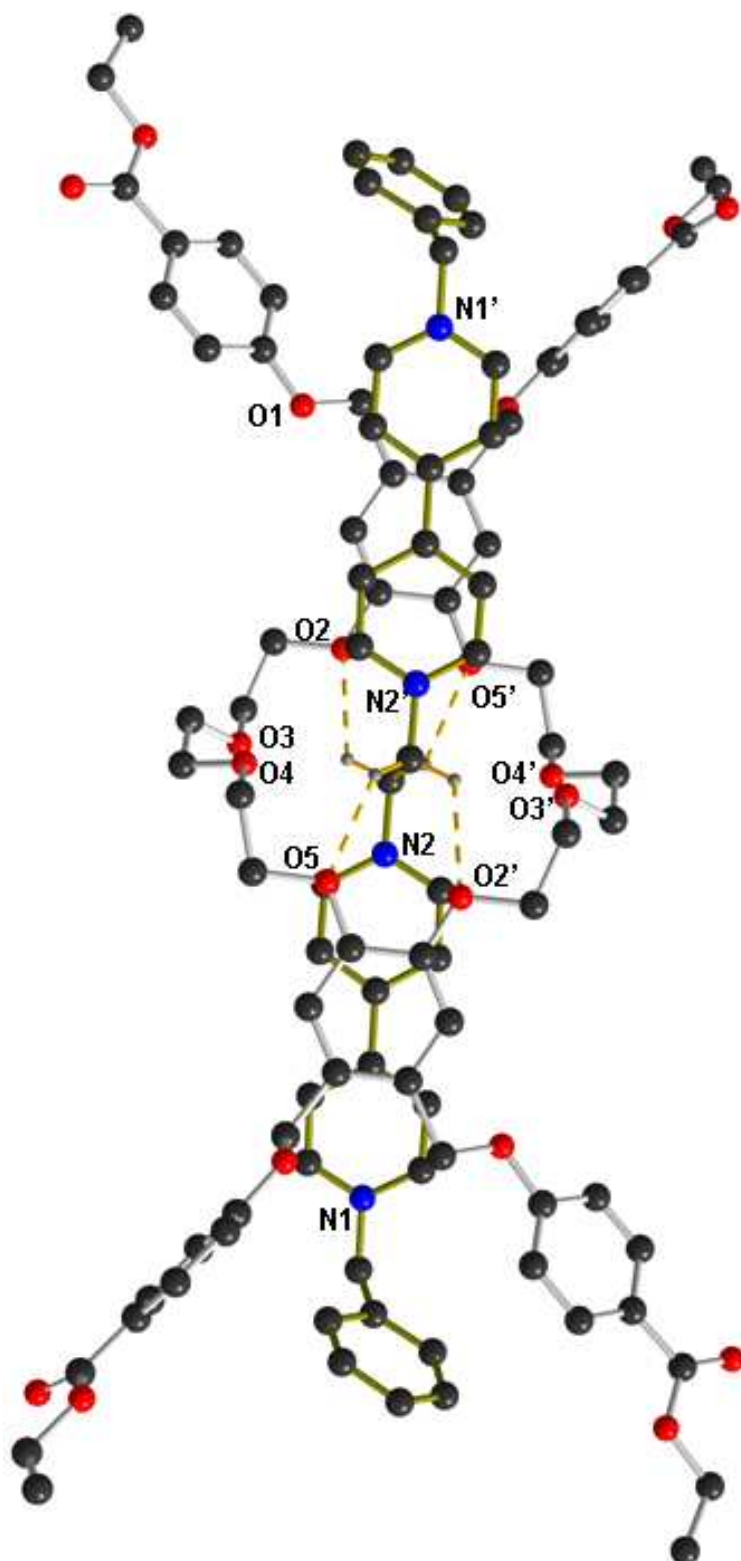
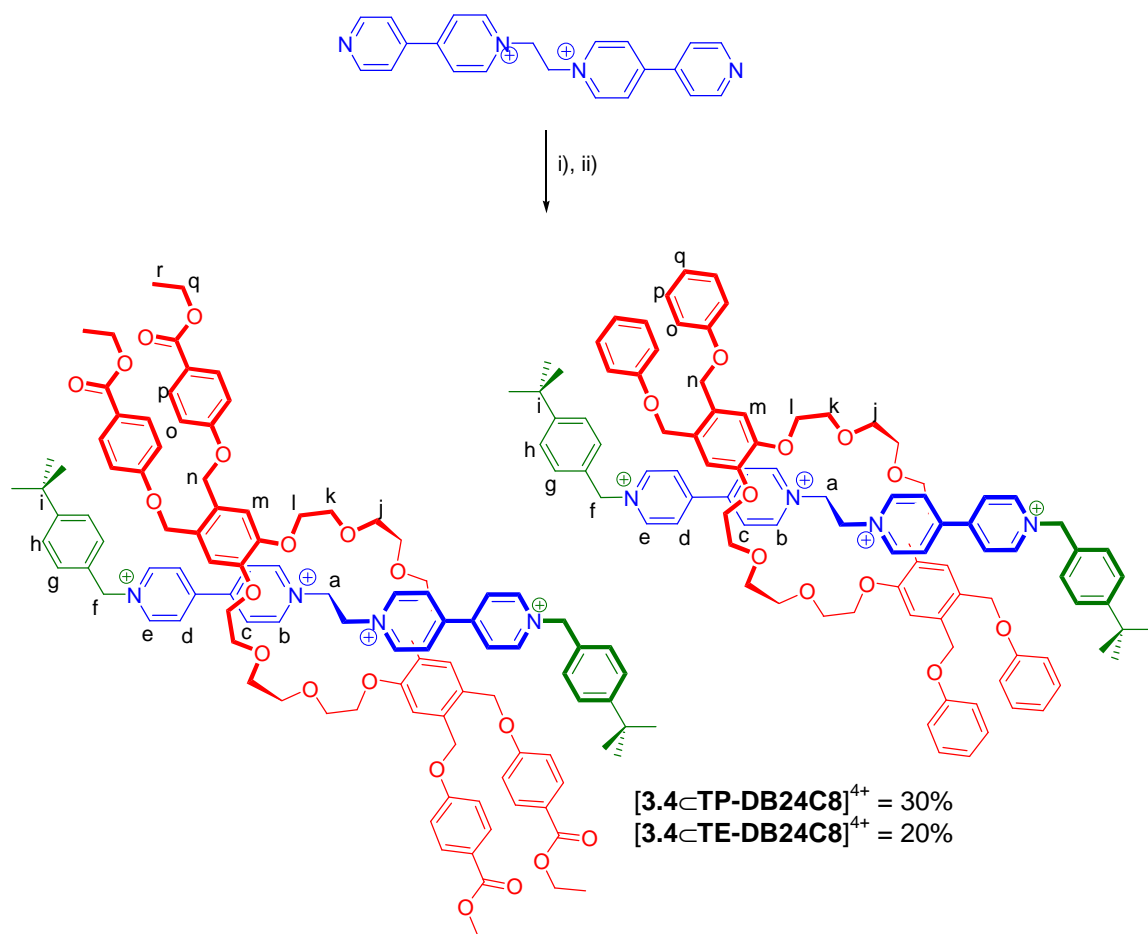


**Figure 3.6** A ball-stick representation of the cationic portion of the X-ray crystal structure of  $[3.3\text{-TE-DB24C8}]^{4+}$ . The complex occupies a crystallographic centre of symmetry. All hydrogen atoms, all anions, and all solvent molecules have been omitted for clarity. (O = red, N = blue, C = black; wheel bonds = silver, axle bonds = gold).

### 3.2.2 Synthesis of the [2]rotaxanes via alkylation

*N*-Alkylation of the 4-pyridyl group of the [2]pseudorotaxane formed between [2.1][OTf]<sub>2</sub> and TP-DB24C8, or TE-DB24C8 was accomplished by stirring in MeCN with 4-*t*-butylbenzyl bromide at room temperature for 4 days to produce compounds [3.4cTP-DB24C8]<sup>4+</sup>, or [3.4cTE-DB24C8]<sup>4+</sup> in relatively low yield, but high purity, as mixtures of dibromide and ditriflate salts. Treatment of [3.4cTP-DB24C8]<sup>4+</sup>, or [3.4cTE-DB24C8]<sup>4+</sup> in a two-phase nitromethane/sodium triflate (MeNO<sub>2</sub>/NaOTf<sub>(aq)</sub>) mixture at room temperature resulted in a red solid, as shown in Scheme 3.5.



**Scheme 3.5** i) [2.1][OTf]<sub>2</sub>, TP-DB24C8 or TE-DB24C8, 4-*t*-butylbenzyl bromide, CH<sub>3</sub>CN, RT 96 h ii) MeNO<sub>2</sub>/NaOTf<sub>(aq)</sub> at RT for 24 h.

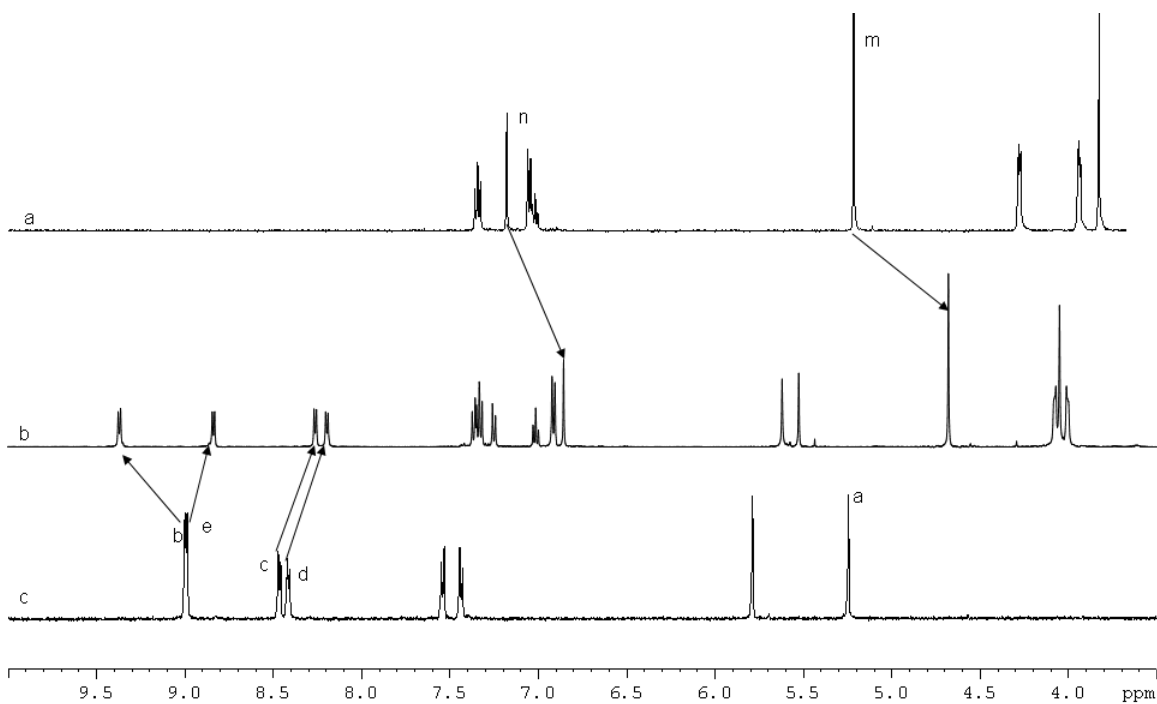


**Figure 3.7** Comparison of the  $^1\text{H}$  NMR shifts of (a) **TP-DB24C8** (b)  $[\mathbf{3.4}][\text{OTf}]_4$ , and (c)  $[\mathbf{3.4-TP-DB24C8}][\text{OTf}]_4$  in  $\text{CD}_3\text{CN}$  at 500 MHz.

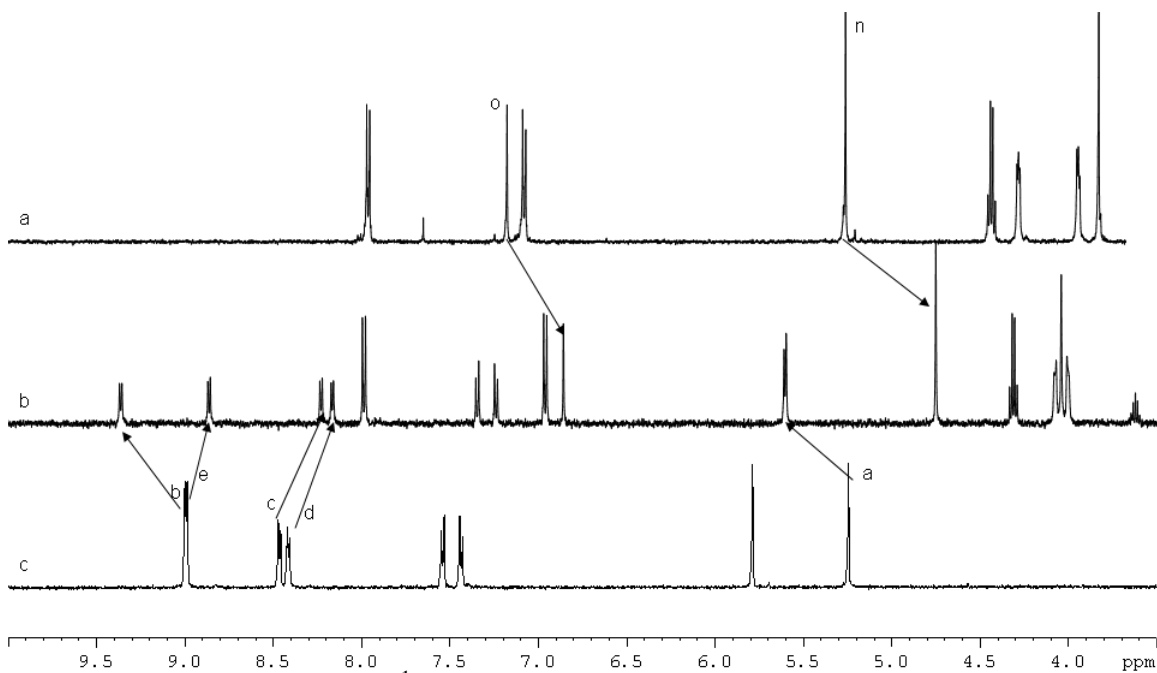


**Figure 3.8** Comparison of the  $^1\text{H}$  NMR shifts of (a) **TE-DB24C8** (b)  $[\mathbf{3.4}][\text{OTf}]_4$ , and (c)  $[\mathbf{3.4-TE-DB24C8}][\text{OTf}]_4$  in  $\text{CD}_3\text{CN}$  at 500 MHz.

The  $^1\text{H}$  NMR spectra of compound  $[\mathbf{3.4-TP-DB24C8}][\text{OTf}]_4$  and  $[\mathbf{3.4-(TE-DB24C8)}][\text{OTf}]_4$  in  $\text{CD}_3\text{CN}$  are shown in Figure 3.7 and 3.8, and some of the major peaks

are summarized in Table 3.7. Evidence supporting the various supramolecular interactions such as hydrogen bonding and  $\pi$ - $\pi$  stacking are apparent. Hydrogen bonding between the ethylene (**a**) and  $\alpha$ -pyridinium (**b**) protons of the thread and the polyether oxygen atoms of the wheel are demonstrated by a downfield shift of the signals for **a** at 5.53 ppm for compound  $[3.4\text{-TP-DB24C8}]^{4+}$  and 5.61 ppm for compound  $[3.4\text{-TE-DB24C8}]^{4+}$ . The  $\alpha$ -pyridinium (**b**) proton signal is at 9.36 ppm for both compound  $[3.4\text{-TP-DB24C8}]^{4+}$  and  $[3.4\text{-TE-DB24C8}]^{4+}$ .

**Table 3.7**  $^1\text{H}$  NMR assignments for  $[3.4][\text{OTf}]_4$ ,  $[3.4\text{-TP-DB24C8}][\text{OTf}]_4$ , and  $[3.4\text{-TE-DB24C8}][\text{OTf}]_4$  in  $\text{CH}_3\text{CN}$ .

Proton	$[3.4]^{4+}$	$[3.4\text{-TP-DB24C8}]^{4+}$	$[3.4\text{-TE-DB24C8}]^{4+}$
<i>a</i>	5.26	5.61 (0.35)	5.53 (0.27)
<i>b</i>	8.99	9.36 (0.37)	9.36 (0.37)
<i>c</i>	8.47	8.23 (-0.24)	8.25 (-0.22)
<i>d</i>	8.42	8.16 (-0.26)	8.19 (-0.23)
<i>e</i>	8.99	8.86 (-0.13)	8.83 (-0.16)

**Table 3.8** Comparison of the chemical shifts of the [2]rotaxanes  $[3.4\text{-TP-DB24C8}][\text{OTf}]_4$  and  $[3.4\text{-TE-DB24C8}][\text{OTf}]_4$  in  $\text{CD}_3\text{CN}$ .

Proton	TP-DB24C8	$[3.4\text{-TP-DB24C8}]^{4+}$	TE-DB24C8	$[3.4\text{-TE-DB24C8}]^{4+}$
<i>j</i>	3.66	4.05 (0.39)	3.65	4.05 (0.40)
<i>k</i>	3.78	4.05 (0.27)	3.77	4.05 (0.28)
<i>l</i>	4.14	4.05 (-0.09)	4.12	4.05 (-0.07)
<i>m</i>	7.10	6.86 (-0.24)	7.10	6.86 (-0.24)
<i>n</i>	5.09	4.67 (-0.42)	5.14	4.76 (-0.42)

The  $^1\text{H}$  NMR spectrum also shows changes for the wheel as is summarized in Table 3.8. The differences arise from the single aromatic proton on the catechol ring (**m**), and the benzylic protons (**n**). As mentioned, the free crown ether, **TP-DB24C8**, shows a singlet at 7.10 ppm for **m** but for the [2]rotaxane  $[3.4\text{-TP-DB24C8}]^{4+}$  this singlet shifts upfield to 6.86 ppm ( $\Delta\delta = 0.24$  ppm). Also the benzylic protons for the free crown ether show a singlet at 5.09 ppm but this singlet shifts upfield to 4.67 ppm ( $\Delta\delta = 0.42$  ppm). Similarly, for crown ether **TE-DB24C8**, the singlet appears at 7.10 ppm for **m** but for the

[2]rotaxane  $[3.4\text{-TE-DB24C8}]^{4+}$  this singlet shifts upfield to 6.86 ppm ( $\Delta\delta = 0.24$  ppm). Also the benzylic protons for the free crown ether, show a singlet at 5.14 ppm but for the [2]rotaxane this singlet shifts upfield to 4.76 ppm ( $\Delta\delta = 0.38$  ppm). The ESI-MS confirmed the interlocked nature of the complex, with just the loss of three counter ions  $\{[3.4\text{-TP-DB24C8}][\text{OTf}]\}^{3+}$ , and  $\{[3.4\text{-TE-DB24C8}][\text{OTf}]\}^{3+}$  at 551.9100 *m/e* and 647.9409 *m/e* respectively.

Single crystals were grown by the slow diffusion of isopropyl ether into a MeCN solution containing  $[3.4\text{-TP-DB24C8}][\text{OTf}]_4$ . The red crystals appeared as small blocks over a few days. Figure 3.10 shows a ball-and-stick representation of the cationic portion of  $[3.4\text{-TP-DB24C8}]^{4+}$ . The structure reveals typical features for the **DB24C8** portion adopting an S-conformation while the  $\text{NCH}_2\text{CH}_2\text{N}$  unit exhibits an *anti* conformation.  $[3.4\text{-TP-DB24C8}]^{4+}$  is stoppered at both ends by a *t*-butyl benzyl group. As expected, the cationic axle interpenetrates the central cavity of the wheel allowing the electron-rich aromatic portion of the wheel to  $\pi$ -stack with electron-deficient axle. The structure also reveals a high degree of C-H $\cdots$ O hydrogen bonding between the components. The four protons *ortho*- to N3- as well the four central protons attached to ethylene bridge form eight hydrogen bonds with the oxygens of the wheel with C-O distances ranging from 3.42 - 3.64 Å. Examination of the appended phenolic ether groups of the crown shows there is T-shaped  $\pi$ -interaction of the phenolic ether group of O1 with the benzylic protons off the stopper, as seen in Figure 3.9a.

Single crystals were grown by the slow diffusion of isopropyl ether into a MeCN solution containing  $[3.4\text{-TE-DB24C8}][\text{OTf}]_4$ . Figure 3.11 shows a ball-and-stick representation of the cationic portion of  $[3.4\text{-TE-DB24C8}]^{4+}$ . The structure reveals

typical features of the **DB24C8** portion which adopts a typical S-conformation while the  $\text{NCH}_2\text{CH}_2\text{N}$  unit exhibits an *anti* conformation.  $[\mathbf{3.4}\text{-TE-DB24C8}]^{4+}$  is stoppered at both ends by a *t*-butyl benzyl group. As expected, the cationic axle interpenetrates the central cavity of the wheel allowing the electron-rich aromatic portion of the wheel to  $\pi$ -stack with electron-deficient axle. The structure also reveals a high degree of C-H...O hydrogen bonding between the components. The four proton *ortho*- to N3- as well the four central protons attached to ethylene bridge form eight hydrogen bonds with the oxygen's of the wheel with C-O distances ranging from 3.63 to 3.73 Å. Examination of the appended benzoate groups of the crown shows that one of the aromatic rings is involved in  $\pi$ -stacking with the aromatic ring of a 4-*t*-butyl benzyl stopper at a distance of approximately 3.5 Å; Figure 3.9b

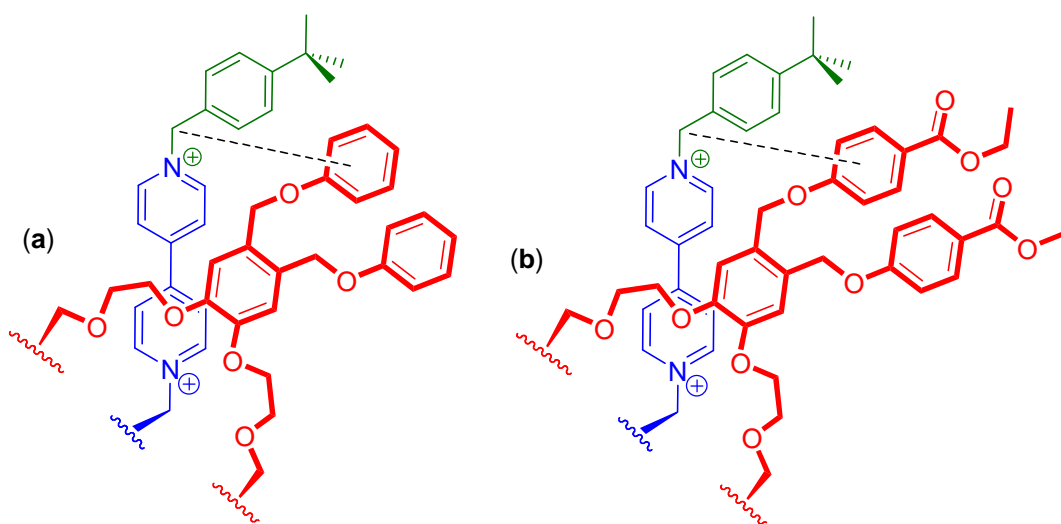


**Figure 3.9** Cartoon representation of the new additional interactions observed in the crystal structure of [2]rotaxanes. The black dash lines indicate new secondary interactions.



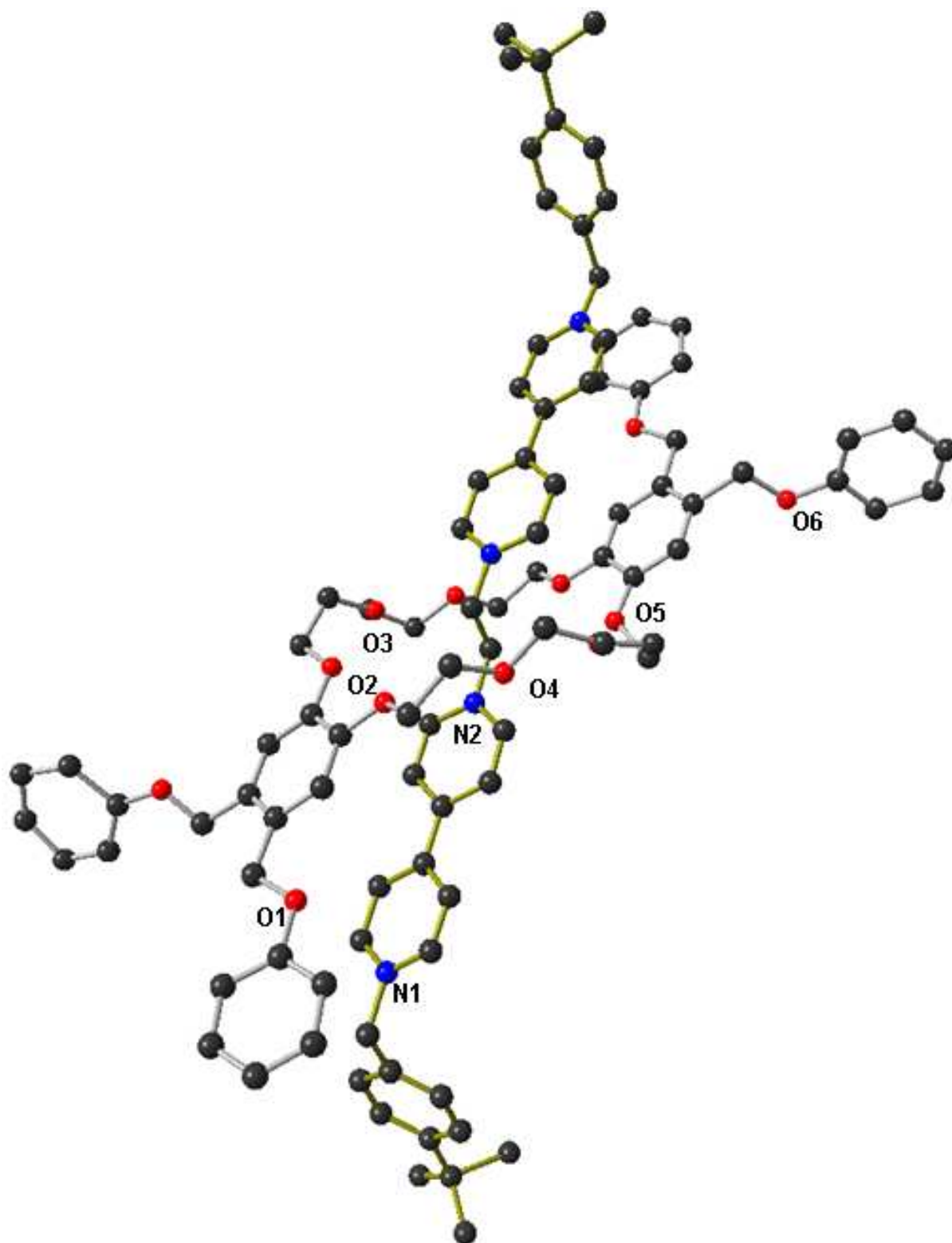


**Figure 3.10** A ball-stick representation of the cationic portion of the X-ray crystal structure of  $[3.4\text{-TP-DB24C8}]^{4+}$ . The complex occupies a crystallographic centre of symmetry. All hydrogen atoms, all anions, and all solvent molecules have been omitted for clarity. (O = red, N = blue, C = black; wheel bonds = silver, axle bonds = gold).

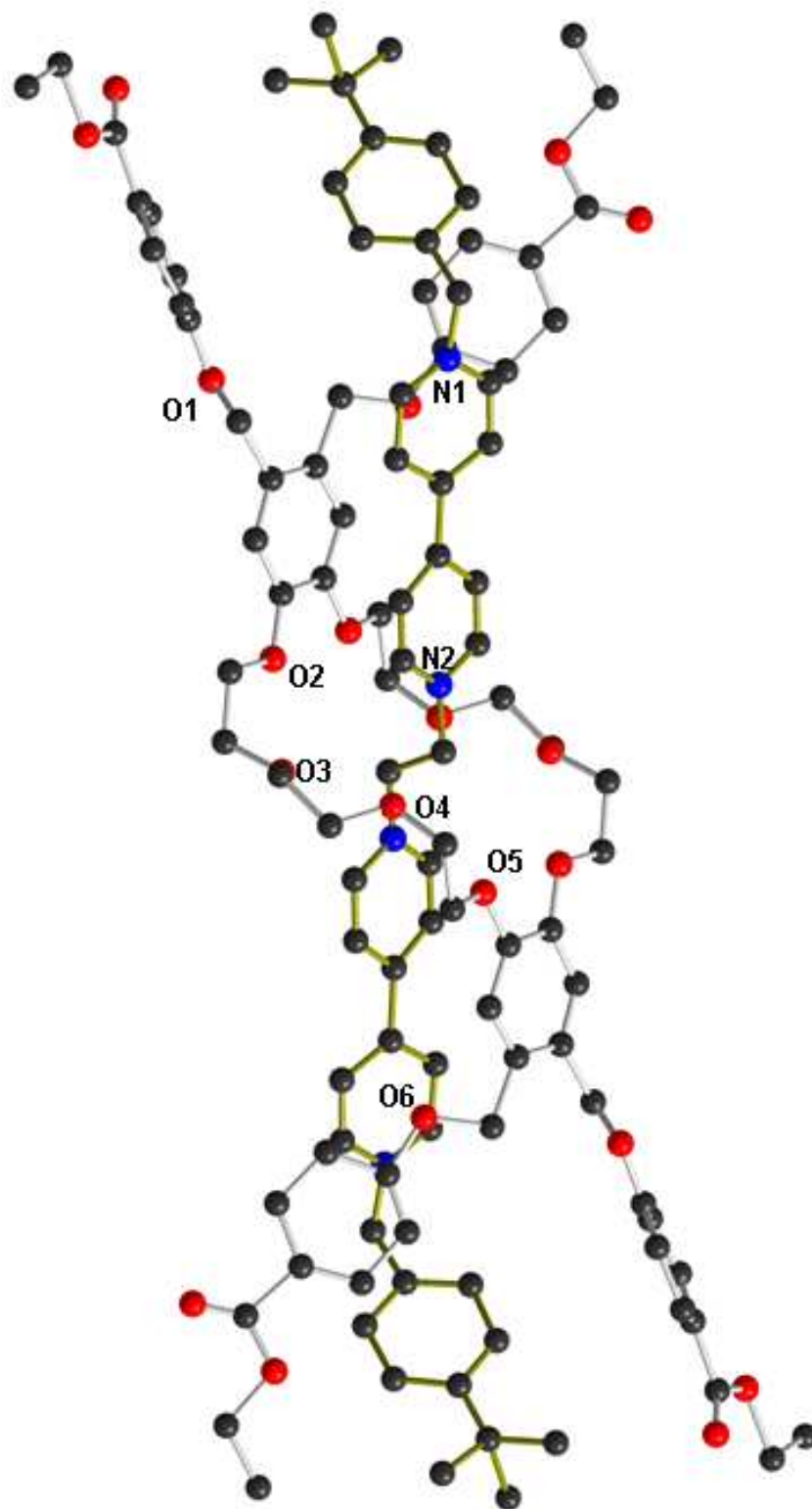
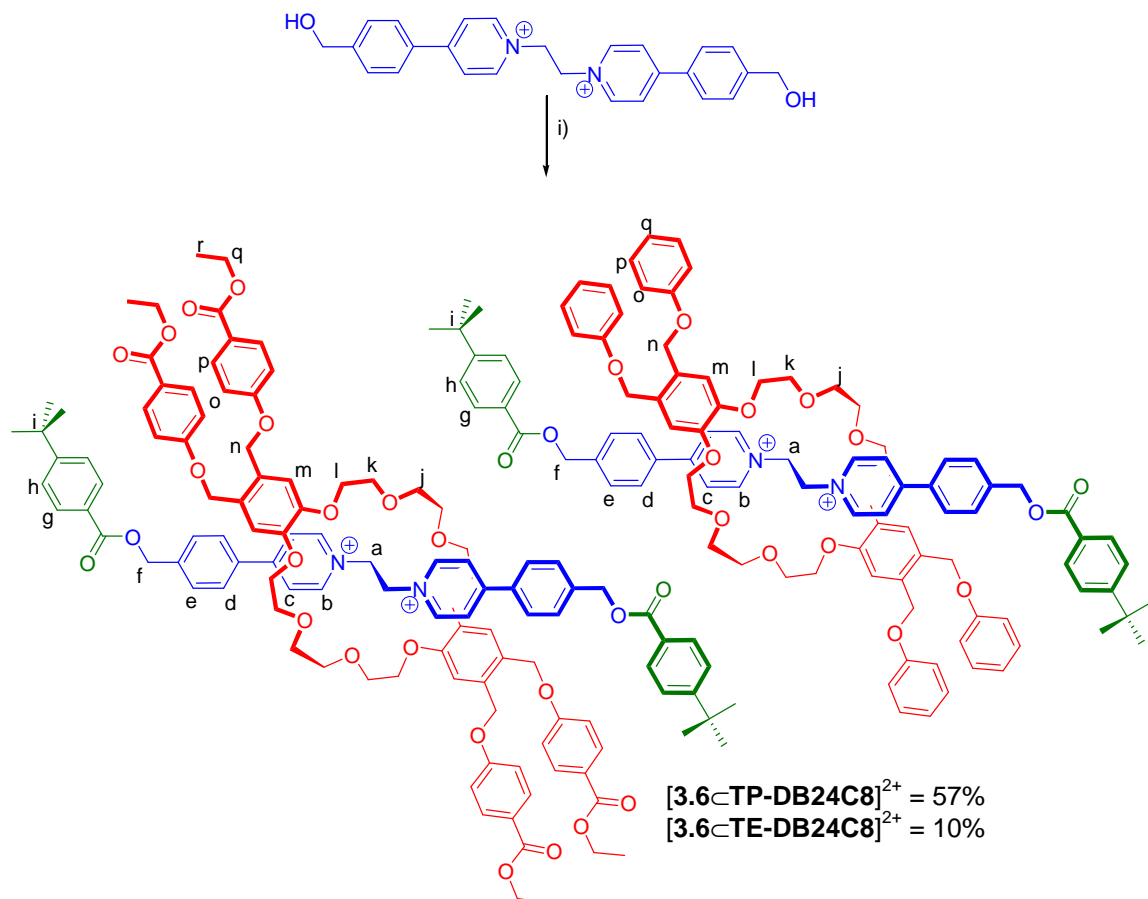


**Figure 3.11** A ball-stick representation of the cationic portion of the X-ray crystal structure of  $[3.4\text{TE-DB24C8}]^{4+}$ . The complex occupies a crystallographic centre of symmetry. All hydrogen atoms, all anions, and all solvent molecules have been omitted for clarity. (O = red, N = blue, C = black; wheel bonds = silver, axle bonds = gold).

### 3.2.3 Synthesis of [2]rotaxanes through acylation

[2]Rotaxanes were synthesized through esterification of the [2]pseudorotaxane formed between 1,2-bis(4-pyridine-4-phenylmethanol)ethane **[3.5]**[BF<sub>4</sub>]<sub>2</sub> with **TP-DB24C8**, or **TE-DB24C8** stirring in MeCN/CH<sub>2</sub>Cl<sub>2</sub> at room temperature for 3 days.



**Scheme 3.6** i) **[3.5]**[BF<sub>4</sub>]<sub>2</sub>, **TP-DB24C8** or **TE-DB24C8**, 4-*tert*-butylbenzoic anhydride, <sup>n</sup>Bu<sub>3</sub>P (cat.), MeCN/CH<sub>2</sub>Cl<sub>2</sub> for 72 h.

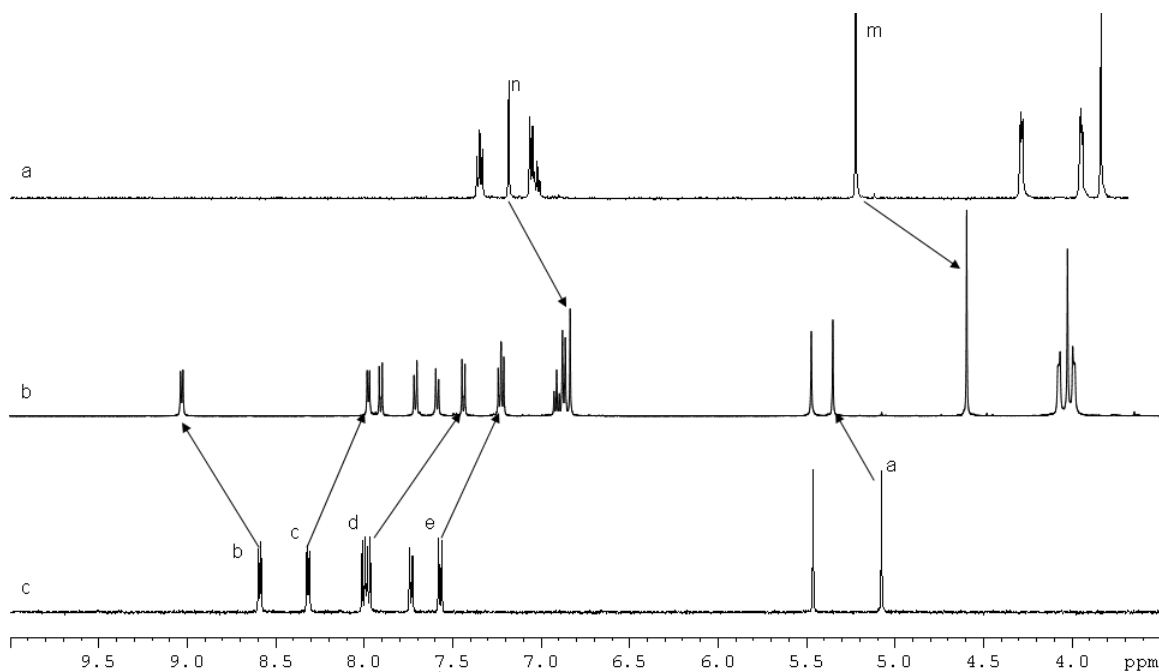


**Figure 3.12** Comparison of the  $^1\text{H}$  NMR shifts of (a) **TP-DB24C8** (b)  $[\mathbf{3.6}][\text{BF}_4]_2$ , and (c)  $[\mathbf{3.6}\subset\text{TP-DB24C8}][\text{BF}_4]_2$  in  $\text{CD}_3\text{CN}$  at 500 MHz.

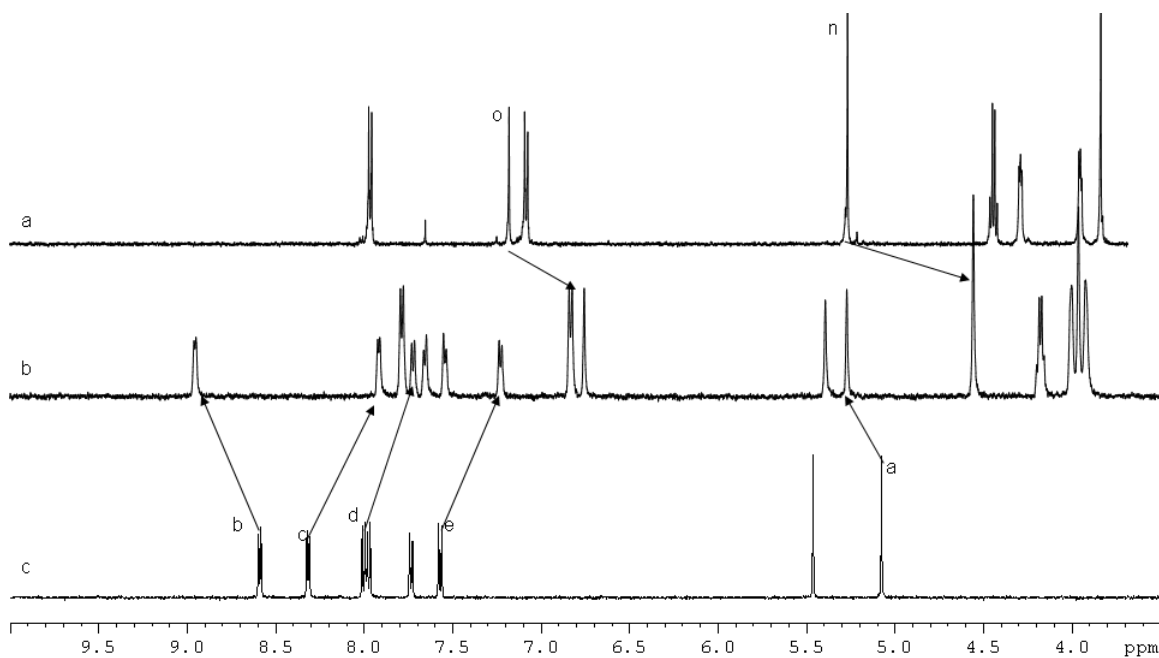


**Figure 3.13** Comparison of the  $^1\text{H}$  NMR shifts of (a) **TE-DB24C8** (b)  $[\mathbf{3.6}][\text{BF}_4]_2$ , and (c)  $[\mathbf{3.6}\subset\text{TE-DB24C8}][\text{BF}_4]_2$  in  $\text{CD}_3\text{CN}$  at 500 MHz.

For the  $^1\text{H}$  NMR spectra of compounds  $[\mathbf{3.6}\subset\text{TP-DB24C8}][\text{BF}_4]_2$  and  $[\mathbf{3.6}\subset\text{TE-DB24C8}][\text{BF}_4]_2$  in  $\text{CD}_3\text{CN}$  (see Scheme 3.6, and Figure 3.12, 3.13), some of the major

peaks are summarized in Table 3.9. Evidence supporting the various supramolecular interactions such as hydrogen bonding and  $\pi$ - $\pi$  stacking are apparent. Hydrogen bonding between the ethylene (**a**) and  $\alpha$ -pyridinium (**b**) protons of the thread with the polyether oxygen atoms of the wheel are demonstrated by the downfield shift of these signals; (**a**) protons to 5.48 ppm for both and (**b**) protons to 9.03 and 9.04 ppm for **[3.6 $\subset$ TP-DB24C8]<sup>2+</sup>** and **[3.6 $\subset$ TE-DB24C8]<sup>2+</sup>** respectively.

**Table 3.9** <sup>1</sup>H NMR assignments for **[3.6][BF<sub>4</sub>]<sub>2</sub>**, **[3.6 $\subset$ TP-DB24C8][BF<sub>4</sub>]<sub>2</sub>**, and **[3.6 $\subset$ TE-DB24C8][BF<sub>4</sub>]<sub>2</sub>** in CH<sub>3</sub>CN.

Protons	<b>[3.6]<sup>2+</sup></b>	<b>[3.6<math>\subset</math>TP-DB24C8]<sup>2+</sup></b>	<b>[3.6<math>\subset</math>TE-DB24C8]<sup>2+</sup></b>
<i>a</i>	5.10	5.48 (0.38)	5.48 (0.38)
<i>b</i>	8.65	9.03 (0.38)	9.04 (0.39)
<i>c</i>	8.30	7.98 (-0.32)	8.00 (-0.30)
<i>d</i>	7.96	7.59 (-0.37)	7.63 (-0.33)
<i>e</i>	7.54	7.44 (-0.10)	7.31 (-0.23)

The <sup>1</sup>H NMR spectra also show changes in the wheel, which are summarized in Table 3.10. The differences arise from the single aromatic proton on the parent **DB24C8** unit (**m**), and the benzylic protons (**n**). As mentioned, the free crown ether, **TP-DB24C8**, shows a singlet at 7.10 ppm for **m** but for the [2]rotaxane **[3.6 $\subset$ TP-DB24C8]<sup>2+</sup>** this singlet shifts upfield to 6.87 ppm ( $\Delta\delta = 0.23$  ppm). Also the benzylic protons for the free crown ether, shows a singlet at 5.09 ppm but this singlet shifts upfield to 4.63 ppm ( $\Delta\delta = 0.46$  ppm). Similarly the crown ether, **TE-DB24C8** the singlet at 7.10 ppm for **m** but for the [2]rotaxane **[3.6 $\subset$ TE-DB24C8]<sup>2+</sup>** but this singlet shifts upfield to 6.84 ppm ( $\Delta\delta = 0.26$  ppm). Also the benzylic proton for the free crown ether show a singlet at 5.14 ppm but for the [2]rotaxane this singlet shifts upfield to 4.65 ppm ( $\Delta\delta = 0.49$  ppm). The ESI-MS confirmed the interlocked nature of the complex, with just the loss of two counter

ions,  $[3.6\text{-TP-DB24C8}]^{2+}$  and  $[3.6\text{-TE-DB24C8}]^{2+}$  at 795.3798 *m/e* and 939.4182 *m/e*, respectively.

**Table 3.10** Comparison of the chemical shifts of the [2]rotaxanes  $[3.6\text{-TP-DB24C8}][\text{BF}_4]_2$  and  $[3.6\text{-TE-DB24C8}][\text{BF}_4]_2$  in  $\text{CD}_3\text{CN}$ .

Proton	TP-DB24C8	$[3.6\text{-TP-DB24C8}]^{2+}$	TE-DB24C8	$[3.6\text{-TE-DB24C8}]^{2+}$
<i>j</i>	3.66	4.02 (0.36)	3.65	4.05 (0.40)
<i>k</i>	3.78	4.02 (0.24)	3.77	4.05 (0.28)
<i>l</i>	4.14	4.02 (-0.12)	4.12	4.05 (-0.07)
<i>m</i>	7.10	6.87 (-0.23)	7.10	6.84 (-0.26)
<i>n</i>	5.09	4.63 (-0.46)	5.14	4.65 (-0.49)

### 3.3 Conclusion

The combination of linear 1,2-bis-(pyridinium)ethane axles with symmetric substituted crown ethers is a versatile templating motif for the formation of [2]pseudorotaxanes, both in solution and solid state. It was shown that the strength of the non-covalent interactions can be controlled by varying the nature of the substituent on the wheel. In general, with electron donating groups on wheel the association increases relative to **DB24C8**. However, we have also shown that the besides electronic effects, sterics can affect the strength of these non-covalent interactions if the axles are elaborated with large stoppers. The bulky groups of the wheel can interfere with the benzyl group of the axle therefore lowering the association. The 1,2-bis(pyridinium)ethane–24-crown-8 templating motif is a versatile recognition entity for the formation of [2]rotaxanes with these substituted crown ethers adding additional non-covalent interactions to the motif.

### 3.4 Experimental

#### 3.4.1 General Methods

**DB24C8**, paraformaldehyde, phenol, 4-hydroxybenzoate, 4-*t*-butylbenzyl bromide, 47% HBr, and nitromethane were obtained from Aldrich and used as received. Acetic acid was obtained from ACP chemicals, and chloroform obtained from VWR; both were used as received. Solvents were dried using an Innovative Technology Solvent Purification System. 4-*t*-Butylbenzoic anhydride, 1,2-bis(4-phenyl-1-pyridyl)ethane[OTf]<sub>2</sub> [**3.1**][OTf]<sub>2</sub>,<sup>2a</sup> (1,2-bis(4-ethylester-1-pyridyl)ethane[OTf]<sub>2</sub> [**3.2**][OTf]<sub>2</sub>,<sup>2a</sup> 1,2-bis(4,4'-dipyridyl)ethane[OTf]<sub>2</sub> [**2.1**][OTf]<sub>2</sub>,<sup>2a</sup> and 1,2-bis(4'-benzyl-4-4'-dipyridyl)ethane[OTf]<sub>4</sub> [**3.3**][OTf]<sub>4</sub>,<sup>2a</sup> 1,2-bis(4'-*t*-butyl-benzyl-4-4'-dipyridyl)ethane[OTf]<sub>4</sub> [**3.4**][OTf]<sub>4</sub>,<sup>2a</sup> 1,2-bis(4-pyridine-4ylphenylmethanol)ethane[BF<sub>4</sub>]<sub>2</sub> [**3.5**][BF<sub>4</sub>]<sub>2</sub><sup>6</sup> and 1,2-bis(4-*t*-butylbenzoate)benzyl-pyridinium))ethane tetrafluoroborate [**3.6**][BF<sub>4</sub>]<sub>2</sub><sup>6</sup> were synthesized using literature methods. Thin layer chromatography (TLC) was performed on Merck Silica gel F<sub>254</sub> plates and viewed under UV light. Column chromatography was performed using Silicycle Ultra Pure Silica Gel (230 – 400 mesh). <sup>1</sup>H NMR spectra were obtained on a Bruker Avance 500 instrument operating at 500 MHz. Deuterated solvents were purchased from Cambridge Isotope Laboratories Inc. and used as received. High-resolution mass spectra were recorded in 50/50 MeCN/H<sub>2</sub>O on a Micromass LCT Electrospray TOF mass spectrometer.

Synthesis **TB-DB24C8**

**DB24C8** (2.00 g, 4.45 mmol) and paraformaldehyde (3.17 g, 20 mmol) were added to 1:1 mixture CHCl<sub>3</sub>/AcOH (20 mL) and heated to 60 °C before a solution 47% HBr (4 mL) in AcOH (5 mL) was added. The reaction was heated at 60 °C for 2 days during which time a white solid forms. The reaction was poured over ice, and washed with CHCl<sub>3</sub> (2 x 20 mL). The solvent was evaporated and recrystallized twice from CHCl<sub>3</sub>. Yield 1.62 g (50%). MP: 202-205°C.

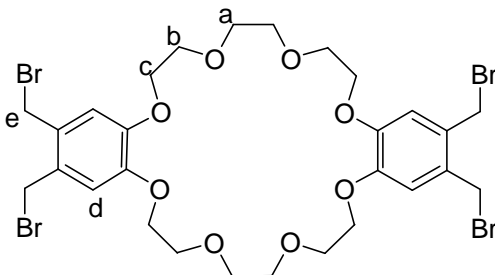


**Table 3.11** <sup>1</sup>H-NMR spectroscopic data for **TB-DB24C8** in CDCl<sub>3</sub>

Proton	δ (ppm)	Multiplicity	# protons	J (Hz)
<i>a</i>	3.79	m	8	-
<i>b</i>	3.90	m	8	-
<i>c</i>	4.15	m	8	-
<i>d</i>	6.83	s	4	-
<i>e</i>	4.59	s	8	-

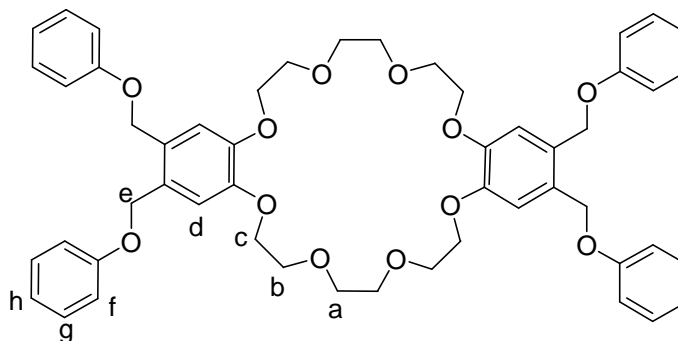
**Table 3.12** <sup>1</sup>H-NMR spectroscopic data for **TB-DB24C8** in CD<sub>2</sub>Cl<sub>2</sub>

Proton	δ (ppm)	Multiplicity	# protons	J (Hz)
<i>a</i>	3.37	m	8	-
<i>b</i>	3.85	m	8	-
<i>c</i>	4.12	m	8	-
<i>d</i>	6.86	s	4	-
<i>e</i>	4.62	s	8	-



### Synthesis **TP-DB24C8**

To a solution of **TB-DB24C8** (1.00 g, 1.22 mmol) and phenol (0.459 g, 4.88 mmol) in degassed MeCN was added  $K_2CO_3$  (1.01 g, 7.32 mmol) and the mixture was stirred under reflux for 5 days. The solvent was then evaporated and the residue was partitioned between  $CH_2Cl_2$  and water. The organic layer was washed with water (2 x 50 mL), dried ( $MgSO_4$ ), and concentrated to give **TP-DB24C8** as an off-white solid which was recrystallized from MeCN. Yield 0.806 g (76%). MP: 135-136°C. **ESI-MS**:  $m/z$  [**TP-DB24C8** +  $Na$ ] $^+$  calc. 895.3669, found 895.3658.

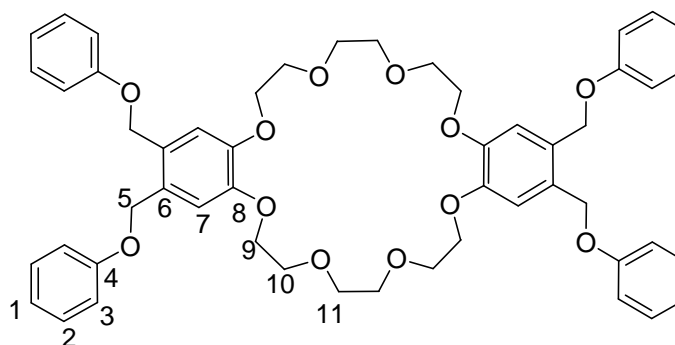


**Table 3.13**  $^1H$ -NMR spectroscopic data for **TP-DB24C8** in  $CD_2Cl_2$

Proton	$\delta$ (ppm)	Multiplicity	# protons	J (Hz)
<i>a</i>	3.75	m	8	-
<i>b</i>	3.85	m	8	-
<i>c</i>	4.14	m	8	-
<i>d</i>	7.04	s	4	-
<i>e</i>	5.06	s	8	-
<i>f,h</i>	6.95	m	12	-
<i>g</i>	7.27	t	8	$J_{g,f} = 7.6, J_{g,h} = 8.2$

**Table 3.14**  $^1\text{H-NMR}$  spectroscopic data for **TP-DB24C8** in  $\text{CD}_3\text{CN}$ 

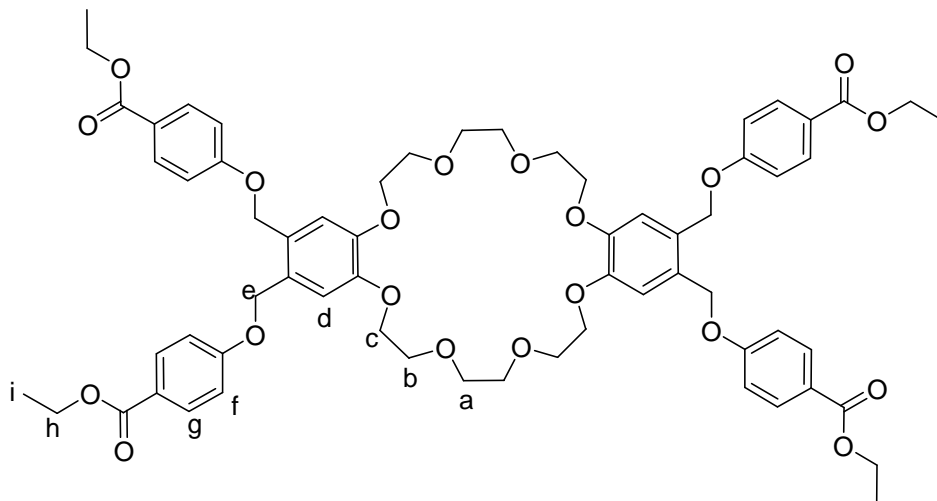
Proton	$\delta$ (ppm)	Multiplicity	# protons	J (Hz)
<i>a</i>	3.66	m	8	-
<i>b</i>	3.78	m	8	-
<i>c</i>	4.13	m	8	-
<i>d</i>	7.10	s	4	-
<i>e</i>	5.09	s	8	-
<i>f,h</i>	6.92	m	12	-
<i>g</i>	7.27	t	8	$J_{g,f} = 7.6, J_{g,h} = 8.2$

**Table 3.15**  $^{13}\text{C-NMR}$  spectroscopic data for **TP-DB24C8** in  $\text{CD}_2\text{Cl}_2$ 

Carbon	$\delta$ (ppm)
<i>1</i>	121.3
<i>2</i>	128.7
<i>3</i>	115.6
<i>4</i>	159.0
<i>5</i>	67.8
<i>6</i>	129.8
<i>7</i>	115.6
<i>8</i>	149.0
<i>9</i>	69.8
<i>10</i>	70.1
<i>11</i>	71.5

### Synthesis **TE-DB24C8**

The same procedure as for the preparation of **TB-DB24C8** (1.00 g, 1.22 mmol) was used with ethyl 4-hydroxybenzoate (0.810 g, 4.88 mmol) instead of phenol. Yield 0.877g, (62%). MP: 120-123°C. **ESI-MS:**  $m/z$  [**TE-DB24C8** + Na]<sup>+</sup> calc. 1183.4515, found 1183.4524.

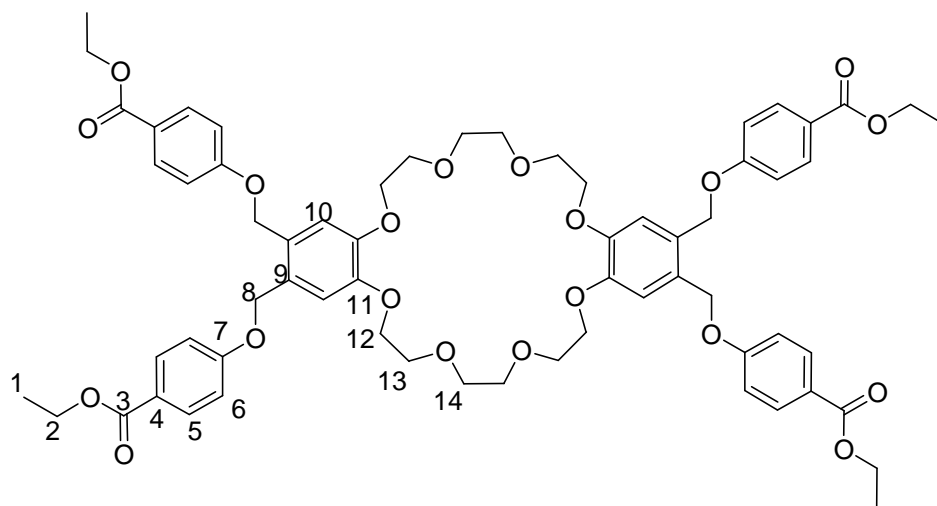


**Table 3.16** <sup>1</sup>H-NMR spectroscopic data for **TE-DB24C8** in CD<sub>2</sub>Cl<sub>2</sub>

Proton	$\delta$ (ppm)	Multiplicity	# protons	J (Hz)
<i>a</i>	3.79	m	8	-
<i>b</i>	3.90	m	8	-
<i>c</i>	4.17	m	8	-
<i>d</i>	7.01	s	4	-
<i>e</i>	5.10	s	8	-
<i>f</i>	6.95	d	8	$J_{f,g} = 8.5$
<i>g</i>	7.98	d	8	$J_{g,f} = 8.4$
<i>h</i>	4.35	q	8	$J_{h,i} = 7.0$
<i>i</i>	1.39	t	12	$J_{i,h} = 7.0$

**Table 3.17**  $^1\text{H-NMR}$  spectroscopic data for **TE-DB24C8** in  $\text{CD}_3\text{CN}$ 

Proton	$\delta(\text{ppm})$	Multiplicity	# protons	J (Hz)
<i>a</i>	3.65	m	8	-
<i>b</i>	3.77	m	8	-
<i>c</i>	4.12	m	8	-
<i>d</i>	7.10	s	4	-
<i>e</i>	5.14	s	8	-
<i>f</i>	7.03	d	8	$J_{f,g} = 8.5$
<i>g</i>	7.90	d	8	$J_{g,f} = 8.4$
<i>h</i>	4.28	q	8	$J_{h,i} = 7.0$
<i>i</i>	1.32	t	12	$J_{i,h} = 7.0$

**Table 3.18**  $^{13}\text{C-NMR}$  spectroscopic data for **TE-DB24C8** in  $\text{CD}_2\text{Cl}_2$ 

Carbon	$\delta$ (ppm)
<i>1</i>	14.7
<i>2</i>	61.2
<i>3</i>	166.6
<i>4</i>	124.0
<i>5</i>	128.3
<i>6</i>	116.1
<i>7</i>	162.8
<i>8</i>	68.4
<i>9</i>	132.0
<i>10</i>	114.9
<i>11</i>	145.0
<i>12</i>	70.0
<i>13</i>	70.3
<i>14</i>	71.6

Synthesis [3.4-TP-DB24C8][OTf]<sub>4</sub>

**TP-DB24C8** (0.140 g, 0.160 mmol) and **[2.1][OTf]<sub>2</sub>** (0.050 g, 0.078 mmol) were dissolved in CH<sub>3</sub>CN (10 mL) and stirred overnight. 4-*t*-Butylbenzyl bromide (0.150 g, 0.660 mmol) was added, and the mixture stirred for 4 days. The organic layer was removed, CH<sub>2</sub>Cl<sub>2</sub> (25 mL) was added to the residue and the mixture was stirred for 30 min. The solid that remained was filtered and the CH<sub>2</sub>Cl<sub>2</sub> was removed. The resulting orange solid was added to a mixture of MeNO<sub>2</sub> and NaOTf(aq) stirred overnight. The organic layer was separated, dried (MgSO<sub>4</sub>) and then evaporated to give an orange residue which was stirred in toluene. The remaining orange solid was dissolved in CH<sub>3</sub>CN and isopropyl ether was slowly diffused to give an orange solid. Yield 0.030 g, 30 %. **ESI-MS:  $m/z$  [3.4-TP-DB24C8 + OTf]<sup>3+</sup> calc. 551.9104, found 551.9100.**

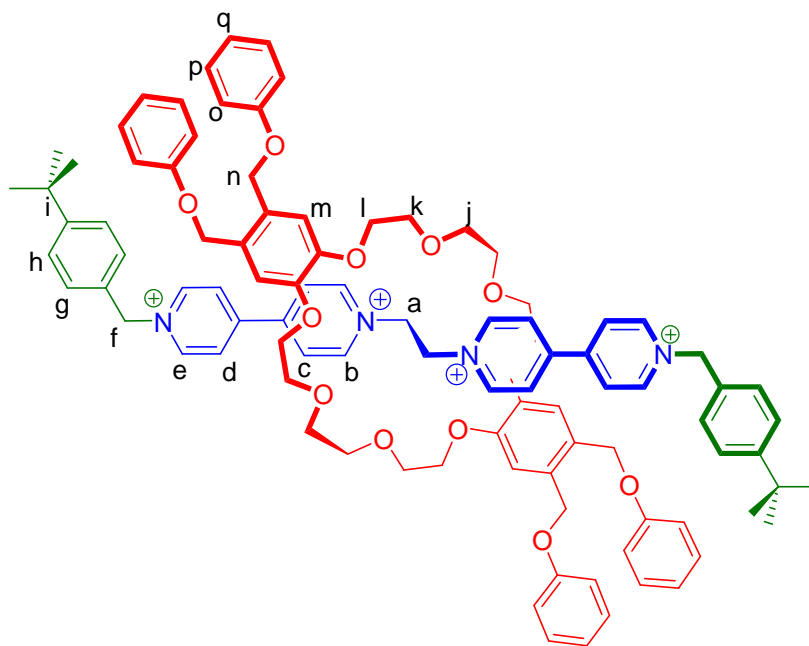


**Table 3.19**  $^1\text{H-NMR}$  spectroscopic data for  $[\mathbf{3.4-TP-DB24C8}]^{4+}$  in  $\text{CD}_3\text{CN}$ 

Proton	$\delta$ (ppm)	Multiplicity	# protons	J (Hz)
<i>a</i>	5.53	s	4	-
<i>b</i>	9.36	d	4	$J_{b,c} = 6.6$
<i>c</i>	8.25	d	4	$J_{c,b} = 6.6$
<i>d</i>	8.19	d	4	$J_{d,e} = 6.6$
<i>e</i>	8.83	d	4	$J_{e,d} = 7.0$
<i>f</i>	5.62	s	4	-
<i>g</i>	7.02	d	4	$J_{g,h} = 7.3$
<i>h</i>	7.24	d	4	$J_{h,g} = 8.3$
<i>i</i>	1.22	s	18	-
<i>q,p</i>	7.32-7.36	dd	12	$J_{k,l} = 8.0, J_{k,j} = 6.9$
<i>o</i>	6.91	d	8	$J_{l,k} = 8.0$
<i>n</i>	4.67	s	8	-
<i>m</i>	6.86	s	4	-
<i>l,k,j</i>	4.08-4.02	m	24	-

Synthesis  $[\mathbf{3.4-TE-DB24C8}][\text{OTf}]_4$ 

**TE-DB24C8** (0.185 g, 0.159 mmol) and **[2.1]** $[\text{OTf}]_2$  (0.050 g, 0.078 mmol) were dissolved in  $\text{CH}_3\text{CN}$  (10 mL) and stirred overnight. 4-*t*-Butylbenzyl bromide (0.150 g, 0.660 mmol) was added, and the mixture was stirred for 4 days. The organic layer was removed,  $\text{CH}_2\text{Cl}_2$  (25 mL) was added to the residue and the mixture stirred for 30 min. The solid that remained was filtered and the  $\text{CH}_2\text{Cl}_2$  was removed. The orange solid was dissolved in a mixture of  $\text{MeNO}_2$  and  $\text{NaOTf}(\text{aq})$  and then stirred overnight. The organic layer was separated, dried ( $\text{MgSO}_4$ ) and evaporated. The residue was then stirred in toluene. The remaining orange solid was dissolved in  $\text{CH}_3\text{CN}$  and isopropyl ether slowly diffused to give an orange solid. Yield 0.037 g, 20 %. **ESI-MS:**  $m/z$   $[\mathbf{3.4-TE-DB24C8} + \text{OTf}]^{3+}$  calc. 647.9385, found 647.9409.

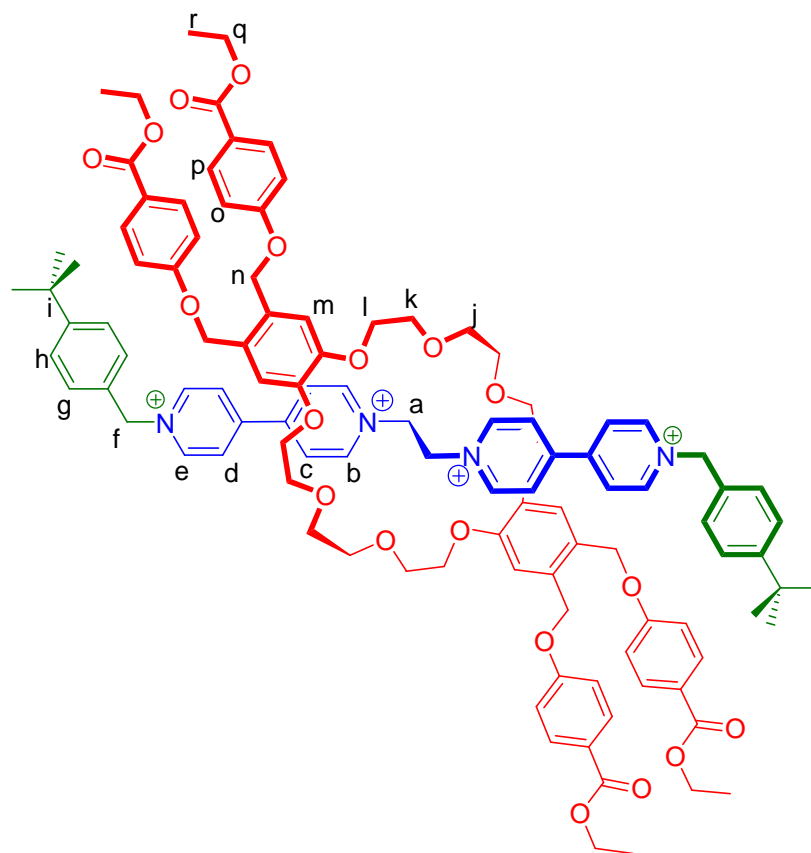


**Table 3.20**  $^1\text{H-NMR}$  spectroscopic data for  $[\mathbf{3.4-TE-DB24C8}]^{4+}$  in  $\text{CD}_3\text{CN}$

Proton	$\delta$ (ppm)	Multiplicity	# protons	J (Hz)
<i>a</i>	5.61	s	4	-
<i>b</i>	9.36	d	4	$J_{b,c} = 6.8$
<i>c</i>	8.23	d	4	$J_{c,b} = 6.8$
<i>d</i>	8.16	d	4	$J_{d,e} = 6.6$
<i>e</i>	8.86	d	4	$J_{e,d} = 6.9$
<i>f</i>	5.62	s	4	-
<i>g</i>	7.24	d	8	$J_{g,h} = 8.3$
<i>h</i>	7.34	d	8	$J_{h,g} = 8.3$
<i>i</i>	1.22	s	18	-
<i>r</i>	1.35	t	8	$J_{i,k} = 7.1$
<i>q</i>	4.33	q	8	$J_{k,i} = 7.1$
<i>p</i>	7.98	d	8	$J_{l,m} = 8.8$
<i>o</i>	6.96	d	8	$J_{m,l} = 8.8$
<i>n</i>	4.76	s	8	-
<i>m</i>	6.86	s	4	-
<i>j,k,l</i>	4.02-4.08	m	24	-

Synthesis [3.6-TP-DB24C8][BF<sub>4</sub>]<sub>2</sub>

[3.5][BF<sub>4</sub>]<sub>2</sub> (0.060 g, 0.105 mmol) was combined with TP-DB24C8 (0.183 g, 0.210 mmol) and 4-*t*-butylbenzoic anhydride (0.142 g, 0.63 mmol) in acetonitrile/CH<sub>2</sub>Cl<sub>2</sub> (10 mL). <sup>n</sup>Bu<sub>3</sub>P (5 mol %) was added as a catalyst and the mixture was allowed to stir for 72 h at room temperature. The solvent was removed under pressure and the product was stirred in anhydrous ethanol for 30 min. Column chromatography was performed using MeOH/CH<sub>2</sub>Cl<sub>2</sub> (3:2) and the solvent removed. The product was dissolved in acetonitrile and isopropyl ether was allowed to diffuse into the solution. The final product was white solid. Yield 0.107 g, 57 %. **ESI-MS:** *m/z* [3.6-TP-DB24C8]<sup>2+</sup> calc. 795.3766, found 795.3798.

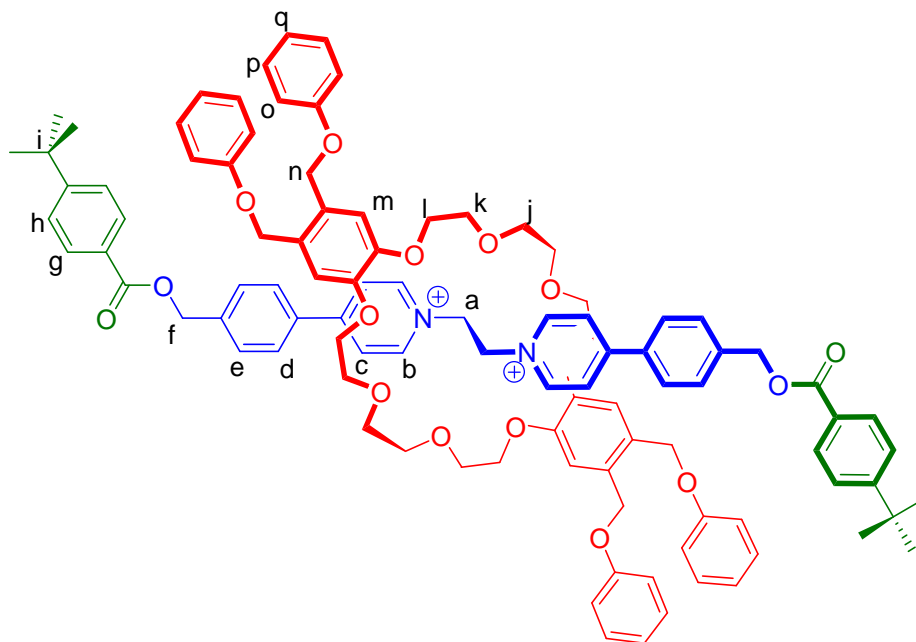




**Table 3.21**  $^1\text{H-NMR}$  spectroscopic data for  $[\mathbf{3.6-TP-DB24C8}]^{2+}$  in  $\text{CD}_3\text{CN}$ 

Proton	$\delta$ (ppm)	Multiplicity	# protons	J (Hz)
<i>a</i>	5.48	s	4	-
<i>b</i>	9.03	d	4	$J_{b,c} = 6.9$
<i>c</i>	7.98	d	4	$J_{c,b} = 6.9$
<i>d</i>	7.59	d	4	$J_{d,e} = 8.3$
<i>e</i>	7.44	d	4	$J_{e,d} = 8.6$
<i>f</i>	5.36	s	4	-
<i>g</i>	7.91	d	4	$J_{g,h} = 8.6$
<i>h</i>	7.71	d	4	$J_{h,g} = 8.4$
<i>i</i>	1.31	s	18	-
<i>q</i>	6.92	dd	4	$J_{i,k} = 7.4$
<i>p</i>	7.23	dd	8	$J_{k,l} = 7.5, J_{k,j} = 7.4$
<i>o</i>	6.90	d	8	$J_{l,k} = 7.9$
<i>n</i>	4.63	s	8	-
<i>m</i>	6.87	s	4	-
<i>l,k,j</i>	4.03-4.11	m	24	-

Synthesis  $[\mathbf{3.6-TE-DB24C8}][\text{BF}_4]_2$ 

$[\mathbf{3.5}][\text{BF}_4]_2$  (0.060 g, 0.105 mmol) was combined with **TE-DB24C8** (0.242 g, 0.210 mmol) and 4-*t*-butylbenzoic anhydride (0.142 g, 0.63 mmol) in acetonitrile/ $\text{CH}_2\text{Cl}_2$  (10 mL).  $^n\text{Bu}_3\text{P}$  (5 mol %) was added as a catalyst and the mixture was allowed to stir for 72 h at room temperature. The solvent was removed under pressure and the product was stirred in anhydrous ethanol for 30 min. Column chromatography was performed with  $\text{MeOH}/\text{CH}_2\text{Cl}_2$  (3:2) and the solvent removed. The product was dissolved in acetonitrile and isopropyl ether was allowed to diffuse into the solution. The resultant product was white solid. Yield 0.015 g, 10 %. **ESI-MS:**  $m/z$   $[\mathbf{3.6-TE-DB24C8}]^{2+}$  calc. 939.4188, found 939.4182.

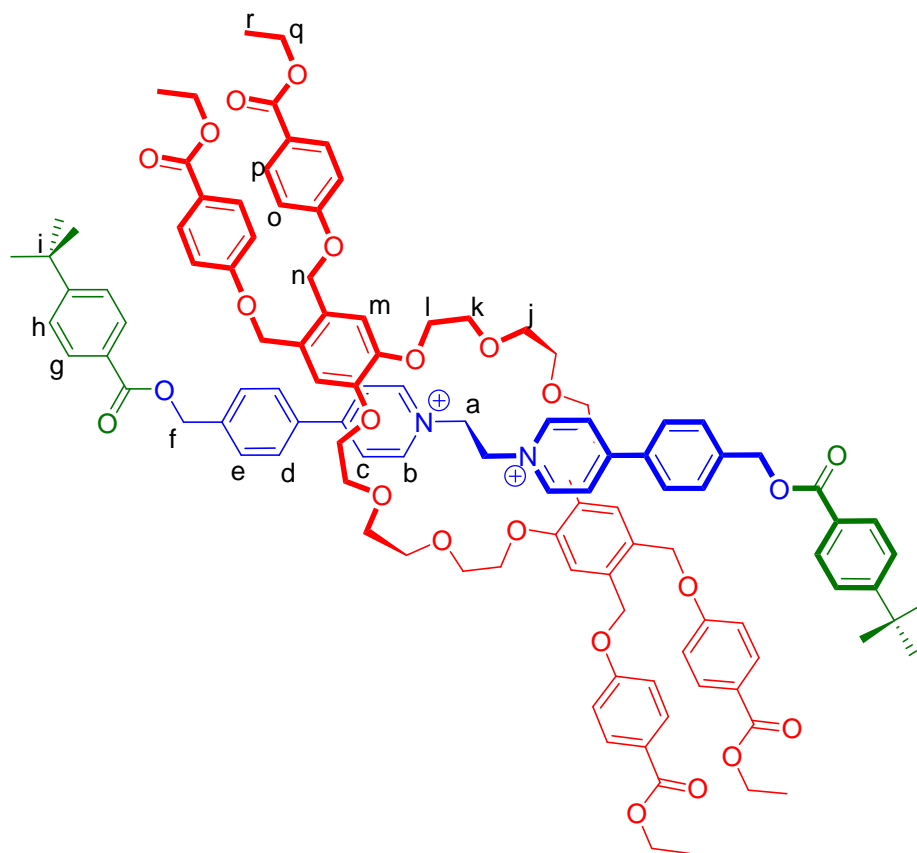


**Table 3.22**  $^1\text{H-NMR}$  spectroscopic data for  $[\mathbf{3.6-TE-DB24C8}]^{2+}$  in  $\text{CD}_3\text{CN}$

Proton	$\delta$ (ppm)	Multiplicity	# protons	J (Hz)
<i>a</i>	5.48	s	4	-
<i>b</i>	9.04	d	4	$J_{b,c} = 5.4$
<i>c</i>	8.00	d	4	$J_{c,b} = 5.6$
<i>d</i>	7.63	d	4	$J_{d,e} = 7.7$
<i>e</i>	7.74	d	4	$J_{e,d} = 7.5$
<i>f</i>	5.36	s	4	-
<i>g</i>	7.31	d	4	$J_{g,h} = 7.9$
<i>h</i>	7.81	d	4	$J_{h,g} = 7.9$
<i>i</i>	1.26	s	18	-
<i>r</i>	1.32	t	12	$J_{j,k} = 7.1$
<i>q</i>	4.27	q	8	$J_{k,j} = 7.1$
<i>p</i>	7.87	d	8	$J_{l,m} = 8.5$
<i>o</i>	6.91	d	8	$J_{l,m} = 8.5$
<i>n</i>	4.65	s	8	-
<i>m</i>	6.84	s	4	-
<i>l,k,j</i>	4.01 – 4.09	m	24	-

## Reference:

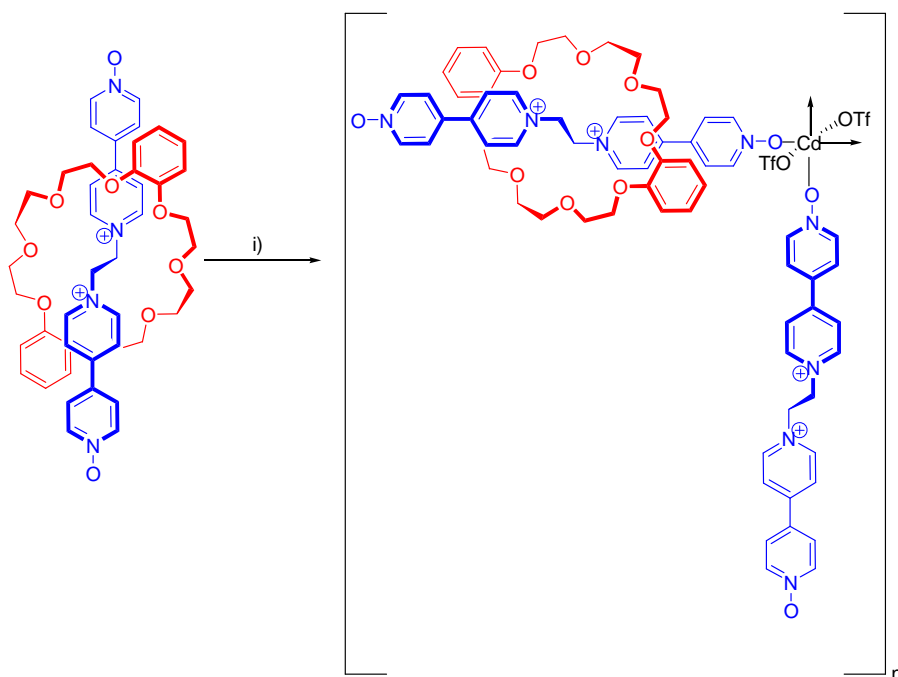
1. a) Ashton, P. R.; Chrystal, E. J. T.; Glink, P. T.; Menzer, S.; Schiavo, C.; Spence, N.; Stoddart, J. F.; Tasker, P. A.; White, A. J. P.; Williams, D. J. *Chem. Eur. J.* **1996**, *2*, 709. b) Ashton, P. R.; Fyfe, M. C. T.; Hickingbottom, S. K.; Stoddart, J. F.; White, A. J. P.; Williams, D. J. *J. Chem. Soc., Perkin Trans. 2* **1998**, 2117.
2. a) Loeb, S. J.; Tiburcio, J.; Vella, S. J.; Wisner, J. A. *Org. Biomol. Chem.* **2006**, *4*, 660. b) Loeb, S. J.; Tiburcio, J.; Vella, S. J. *Org. Lett.* **2005**, *7*, 4923.
3. Gibson, H. W.; Wang, H.; Bonrad, K.; Jones, J. W.; Slebodnick, C.; Zackharov, L. N.; Rheingold, A. L.; Habenicht, B.; Lobue, P.; Ratliff, A. E. *Org. Biomol. Chem.* **2005**, *2*, 2114.
4. Liu, Y.; Li, C. J.; Zhang, H. Y.; Wang, L. H.; Li, X. Y. *Eur. J. Org. Chem.* **2007**, 4510.
5. Nakamura, Y.; Asami, A.; Ogawa, T.; Inokuma, S.; Nishimura, J. *J. Am. Chem. Soc.* **2002**, *124*, 4329.
6. a) Mercer, D. J. W.; Vella, S. J.; Guertin, L.; Sudan, N. D.; Tiburico, J.; Vukotic, N.; Wisner, J. A.; Loeb, S. J. *Eur. J. Org. Chem.* **2011**, *9*, 1763.

# Chapter 4

## Effects of Crown Ether Substituents on [2]Rotaxane ligands, Complexes and Metal-Organic Frameworks

### 4.1 Introduction

Incorporating transition metals into interlocked molecules has created a number of interesting systems such as coordination polymers (CPs), metal organic frameworks (MOFs)<sup>1</sup> and interlocked molecules with stoppers as ligands.<sup>2</sup> Since the rotaxane linker can be modified by changing the crown ether wheel but retaining the bridging axle unit, this may be a useful methodology for changing the resulting properties of the polymer, framework or complex. Recently, Loeb changed the length of the axle by converting pyridine linkers to pyridine N-oxides, allowing the formation of 3D MORFs with lanthanide ions.<sup>3</sup> Using transition metals with this extended axle gave an interesting 2D-square grid framework with two pseudorotaxane ligands, and two axles (Scheme 4.1).

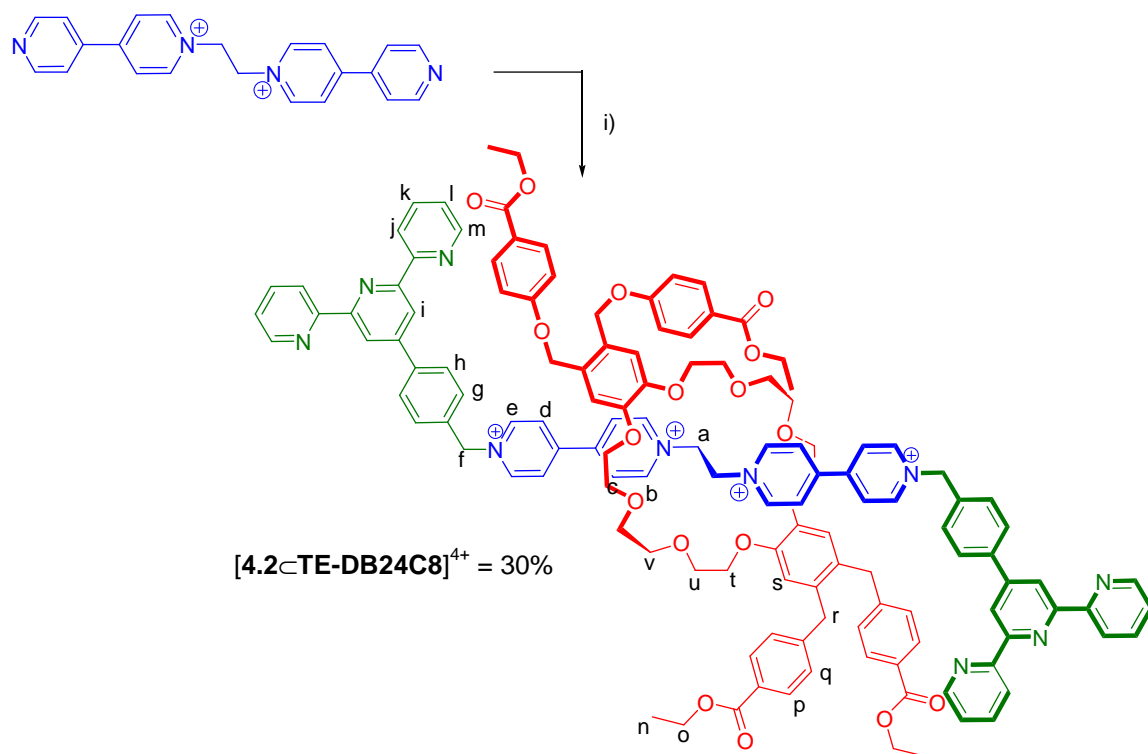


**Scheme 4.1** i) Cd(OTf)<sub>2</sub> in MeNO<sub>2</sub>.

## 4.2 Results and Discussion

### 4.2.1 Synthesis of tolyterpy [2]Rotaxane

As in Chapter 2, the ligand **tolylterpy** was chosen as the source of the terpyridine unit to be introduced as the stopper for a [2]rotaxane ligand. N-alkylation of the [2]pseudorotaxane formed between  $[2.1]^{2+}$  and **TE-DB24C8**, was accomplished by stirring in MeNO<sub>2</sub> at room temperature for 7 days to produce  $[4.2\subset(\text{TE-DB24C8})]^{4+}$  in relatively low yield, but high purity, as mixtures of bromide and triflate salts. Treatment of  $[4.2\subset(\text{TE-DB24C8})]^{4+}$  in a two-phase MeNO<sub>2</sub>/NaOTf<sub>(aq)</sub> mixture at room temperature resulted in a red solid; Scheme 4.2.



**Scheme 4.2** i)  $[4.1\subset(\text{TE-DB24C8})]^{2+}$ , **Br-tolylterpy** in MeNO<sub>2</sub>/NaOTf<sub>(aq)</sub> at RT for 168 h.

The <sup>1</sup>H NMR spectrum of  $[4.2][\text{OTf}]_4$ ,  $[4.2\subset(\text{TE-DB24C8})][\text{OTf}]_4$  and **TE-DB24C8** in CD<sub>3</sub>CN are shown in Figure 4.1 and some of the major peaks are summarized in

Tables 4.1 and 4.2. The rotaxane shows evidence supporting the various supramolecular interactions such as hydrogen bonding and  $\pi$ - $\pi$  stacking. Hydrogen bonding between the ethylene (**a**) and  $\alpha$ -pyridinium (**b**) protons of the axle with the polyether oxygen atoms of the macrocycle is evidenced by a downfield shift of the signals for **a** and **b** with a  $\Delta\delta$  of 0.35 and 0.32 ppm respectively. The benzylic protons (**f**) from the stopper are shifted  $\Delta\delta$  0.17 ppm. The  $^1\text{H}$  NMR spectrum reveals the presence of benzylic protons (**r**), and a singlet for the aromatic protons (**s**) which are shifted upfield by  $\Delta\delta$  0.50 and 0.25 ppm respectively due to  $\pi$ -stacking.

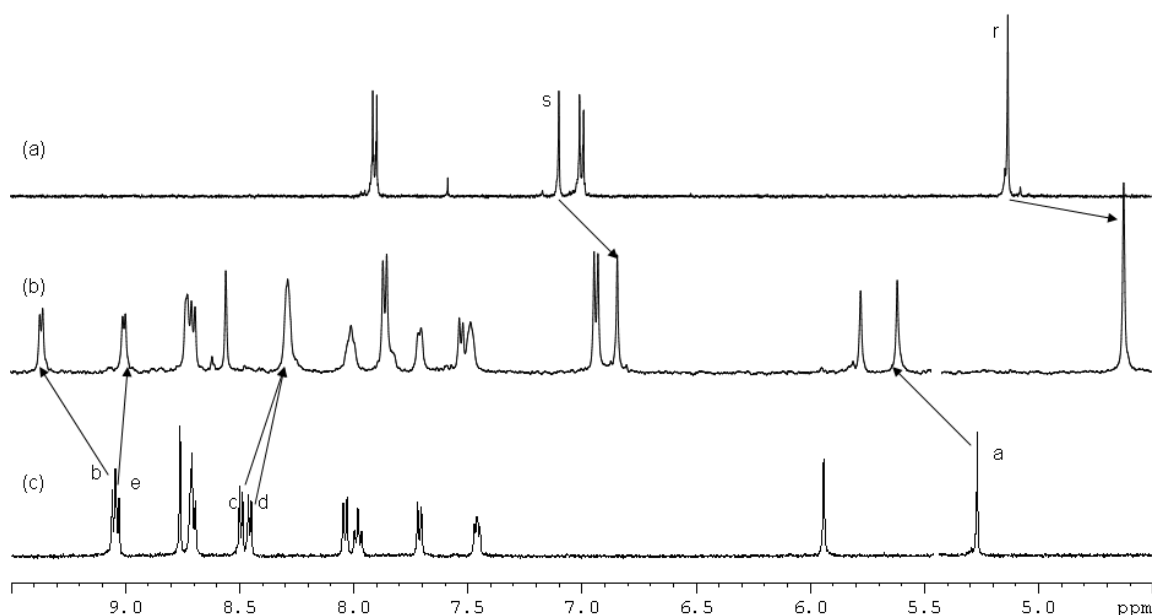


**Figure 4.1** Comparison of the  $^1\text{H}$  NMR spectra of **TE-DB24C8**, **[4.2-TE-DB24C8][OTf]<sub>4</sub>**, and **[2.2][OTf]<sub>4</sub>**, and in  $\text{CD}_3\text{CN}$  at 500 MHz.

**Table 4.1** Chemical shift data **[2.2][OTf]<sub>4</sub>**, and [2]rotaxane, **[4.2-TE-DB24C8][OTf]<sub>4</sub>**.

Protons	<b>2.2<sup>4+</sup></b>	<b>[4.2-TE-DB24C8]<sup>4+</sup></b>
<i>a</i>	5.27	5.62 (0.35)
<i>b</i>	9.04	9.36 (0.32)
<i>c</i>	8.49	8.27 (-0.22)
<i>d</i>	8.46	8.27 (-0.18)
<i>e</i>	9.04	8.98 (-0.06)

**Table 4.2** Chemical shift data **TE-DB24C8**, and **[4.2C(TE-DB24C8)][OTf]<sub>4</sub>** in CH<sub>3</sub>CN.

Protons	TE-DB24C8	[4.2C(TE-DB24C8)] <sup>4+</sup>
<i>s</i>	7.10	6.84 (0.26)
<i>r</i>	5.14	4.64 (0.50)
<i>q</i>	6.95	6.94 (0.01)
<i>p</i>	7.98	7.88 (0.10)
<i>o</i>	4.35	4.14 (0.21)
<i>n</i>	1.39	1.21 (0.18)

The ESI-MS of {[4.2C(TE-DB24C8)][OTf]}<sup>2+</sup> shows a peak at 1221.4041 *m/e*, which demonstrates the [2]rotaxane containing the substituent crown ether present.

Single crystals of [4.2C(TE-DB24C8)][OTf]<sub>4</sub> were grown by the slow diffusion of isopropyl ether into a MeNO<sub>2</sub> solution. The orange crystals appeared as blocks in a few days. The tetra-substituted crown ether shows the typical features of the parent **DB24C8** adopting an *S*-conformation; Figure 4.3. The appended ethyl 4-hydroxybenzoate groups point towards the stoppers, while the cationic NCH<sub>2</sub>CH<sub>2</sub>N unit exhibits an *anti* conformation typically exhibited by other [2]rotaxanes built with this 1,2-bis(pyridinium)ethane core. [4.2C(TE-DB24C8)]<sup>4+</sup> is stopped at both ends with a **tolylterpy** group. The structure also reveals a high degree of C-H...O hydrogen-bonding between the components. The four  $\alpha$ -pyridinium protons as well as the four protons attached to the ethylene bridge form eight hydrogen-bonds with the oxygen atoms of the wheel with C-H...O distances ranging from 3.25(8) – 3.34(8) Å. The terpyridine group is essentially planar with the nitrogen atoms in the expected *transoid* arrangement.<sup>4</sup> In addition to the hydrogen-bonding and  $\pi$ -stacking between the thread and the wheel, there is  $\pi$ -stacking between the tolyl group of the terpyridine and one of the appended ethyl 4-hydroxybenzoate groups at ~3.4 Å; Figure 4.2. This interaction is reflected in a 0.17 ppm upfield shift of proton **f**.

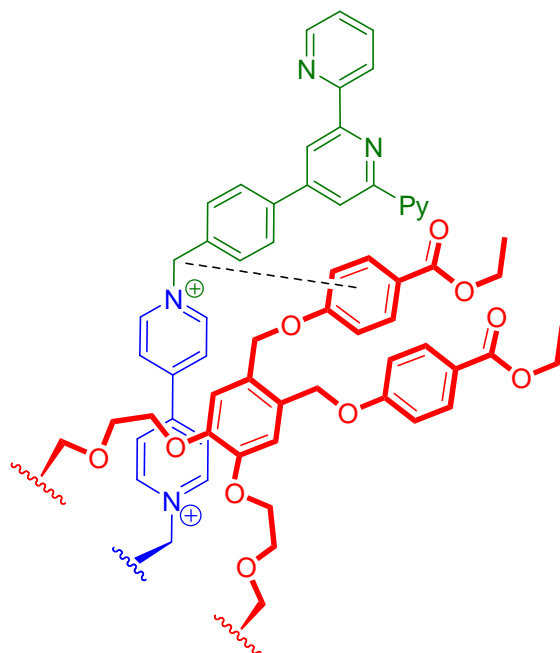


**Figure 4.2** Additional interaction observed in the crystal of  $[4.2\text{-TE-DB24C8}]^{4+}$ . The black dash line indicates a new secondary interaction.



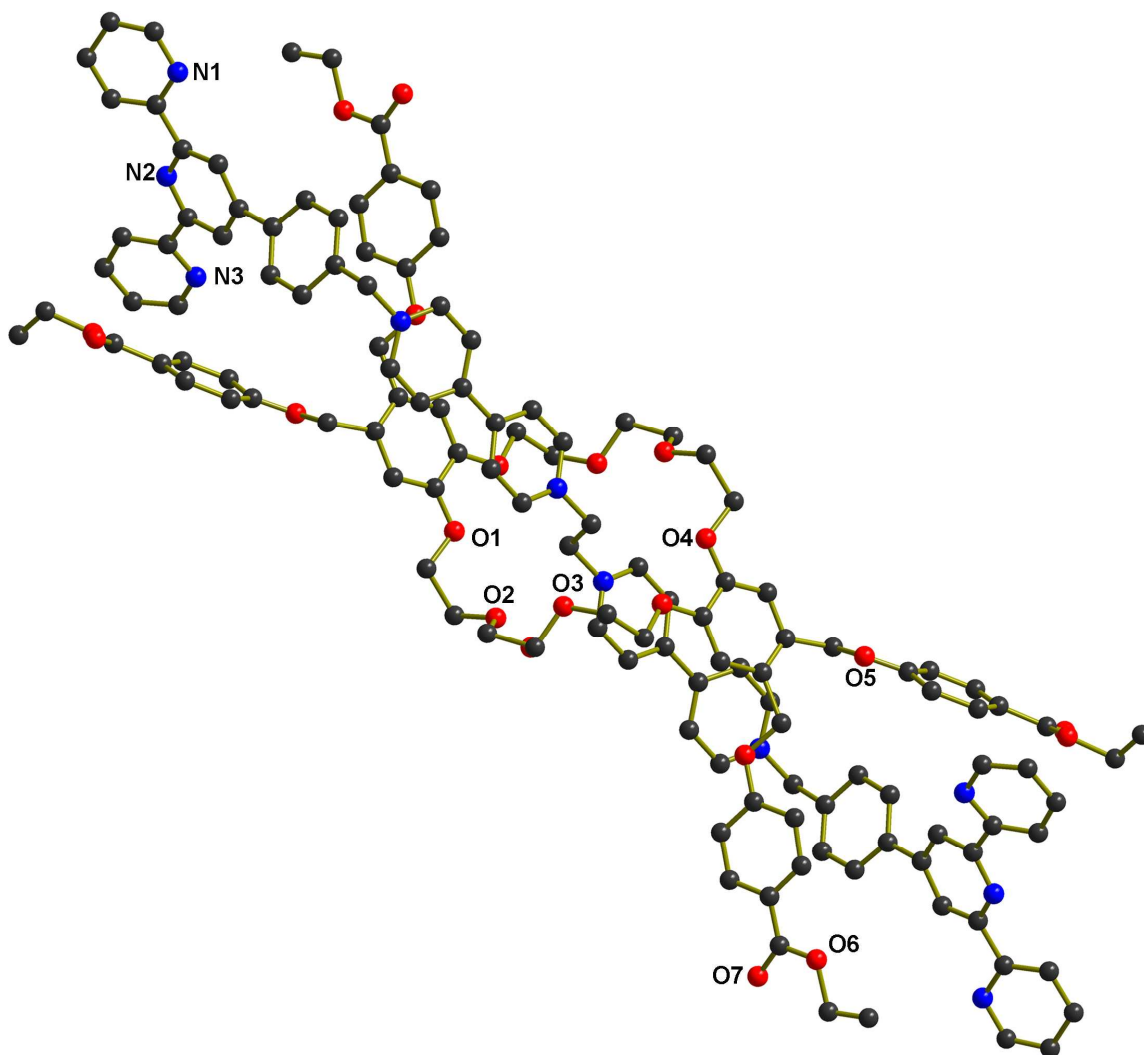
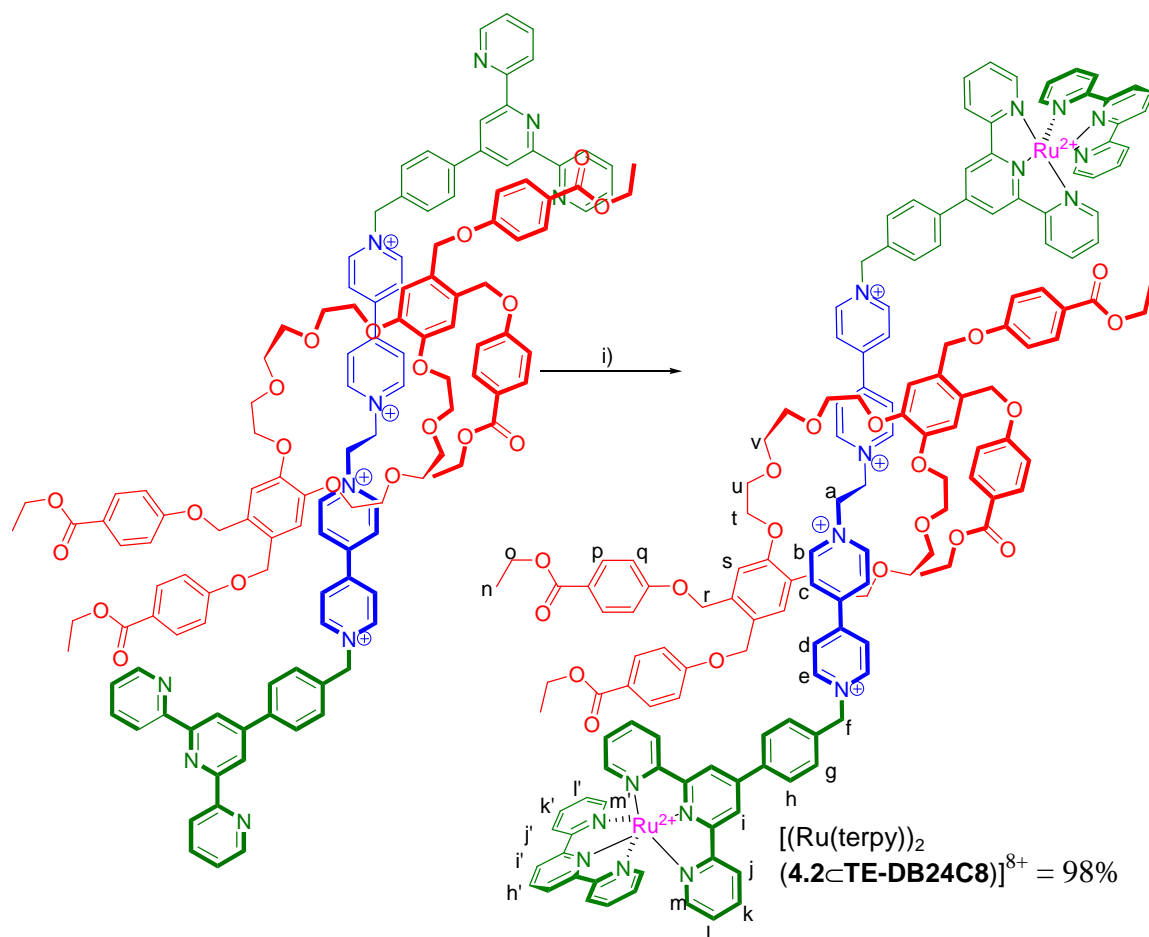


**Figure 4.3** Ball-and-stick representation of the cationic portion of the X-ray crystal structure of  $[4.2\text{-TE-DB24C8}]^{4+}$ . The complex occupies a crystallographic centre of symmetry. All anions and all solvent molecules have been omitted for clarity. (Ru = blue-gray, O = red, N = blue, C = black; wheel bonds = silver, axle bonds = gold).

The reaction of  $[4.2\text{-TE-DB24C8}][\text{OTf}]_4$  with  $\text{Ru}(\text{terpy})\text{Cl}_3$  is outlined in Scheme 4.3. The synthesis was carried out in a 1:1 EtOH/H<sub>2</sub>O mixture and the reaction mixture was refluxed for 1 day. The dark red complex could be easily isolated and purified by recrystallization from acetonitrile and diethyl ether.



**Scheme 4.3** i) Ru (terpy)Cl<sub>3</sub>, 1:1 EtOH/H<sub>2</sub>O, reflux, 24 h.

The <sup>1</sup>H NMR spectrum of the ruthenium complex was recorded in CD<sub>3</sub>CN as the triflate salt. The numbering scheme can be seen in Scheme 4.3. The spectrum revealed an upfield shift of the protons **m-j** and **m'-j'** attributed to the electronic effects of the ruthenium(II) centre, confirming the formation of the complex. The spectrum also showed a nice pattern whereby chemically equivalent peaks from the two different terpy groups, that belong **m** and **m'** or **l** and **l'** were resolved enough that they could be clearly distinguished from each other; Figure 4.4. In order to determine which set of peaks belonged to which terpyridine unit, conventional 2D NMR techniques (<sup>1</sup>H – <sup>1</sup>H COSY) were employed.

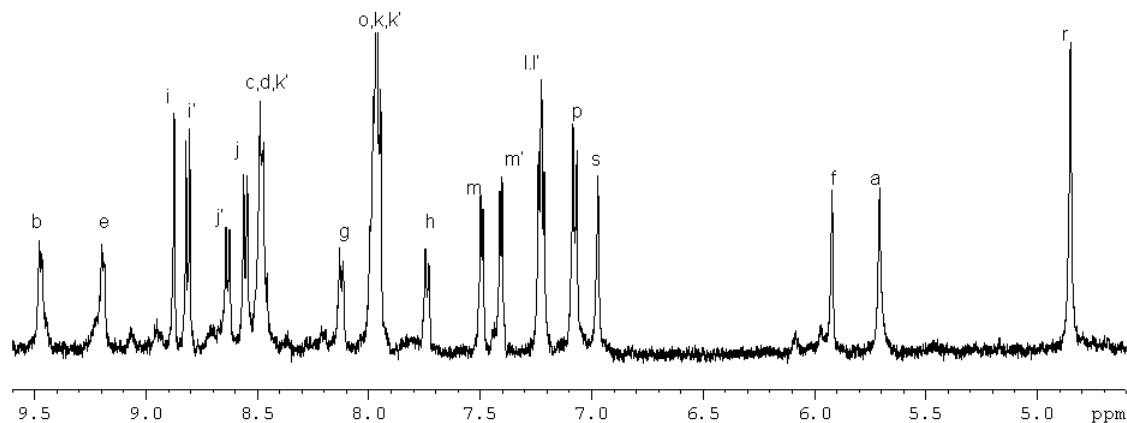


**Figure 4.4**  $^1\text{H}$  NMR spectrum of  $[\text{Ru}(\text{terpy})_2(4.2\text{-TE-DB24C8})][\text{OTf}]_8$  at 500MHz.

**Table 4.3** A comparison of the  $^1\text{H}$  NMR chemical shifts for dumbbell  $[\mathbf{2.2}][\text{OTf}]_4$ ,  $[\mathbf{2}]$ rotaxane ligand  $[\mathbf{4.2-TE-DB24C8}][\text{OTf}]_4$  and complex  $[(\text{Ru}(\text{terpy})_2)(\mathbf{2.2})][\text{OTf}]_8$ ,  $[(\text{Ru}(\text{terpy})_2)(\mathbf{4.2-TE-DB24C8})][\text{OTf}]_8$ .

proton	$[\mathbf{2.2}]^{4+}$	$[\mathbf{4.2-TE-DB24C8}]^{4+}$	$[(\text{Ru}(\text{terpy})_2)(\mathbf{2.2})]^{8+}$	$[(\text{Ru}(\text{terpy})_2)(\mathbf{4.2-TE-DB24C8})]^{8+}$
<i>a</i>	5.27	5.62 (0.35)	5.34 (0.07)	5.67 (0.05)
<i>b</i>	9.04	9.36 (0.32)	9.19 (0.15)	9.43 (0.07)
<i>c</i>	8.49	8.27 (-0.22)	8.58 (0.09)	8.42 (0.15)
<i>d</i>	8.46	8.27 (-0.19)	8.58 (0.12)	8.42 (0.15)
<i>e</i>	9.04	8.98 (-0.85)	9.14 (0.10)	9.11 (0.13)
<i>f</i>	5.94	5.77 (-0.17)	6.04 (0.10)	5.87 (0.10)
<i>g</i>	7.71	7.71 (0.00)	7.88 (0.17)	8.09 (0.38)
<i>h</i>	8.04	7.52 (-0.52)	8.34 (0.30)	7.69 (0.17)
<i>i</i>	8.76	8.57 (-0.19)	9.03 (0.27)	8.83 (0.26)
<i>j</i>	8.70	8.73 (0.03)	8.50 (-0.20)	8.51 (-0.22)
<i>k</i>	7.98	7.99 (0.01)	7.92 (-0.06)	7.92 (-0.06)
<i>l</i>	7.46	7.47 (0.01)	7.16 (-0.30)	7.19 (-0.28)
<i>m</i>	8.70	8.70 (0.00)	7.41 (-1.29)	7.45 (-1.25)

Proton **m**, in complex  $[(\text{Ru}(\text{terpy})_2)(\mathbf{4.2-TE-DB24C8})]^{8+}$ , shifts from 8.70 ppm for the uncomplexed rotaxane to 7.45 ppm ( $\Delta\delta = -1.25$ ). The differences in chemical shifts between the  $[\mathbf{2}]$ rotaxane and the corresponding Ru(II) complex are summarized in Table 4.3. The ESI-MS also confirmed their interlocked nature with the loss of four counter ions and observation of  $\{[(\text{Ru}(\text{terpy})_2)(\mathbf{4.2-TE-DB24C8})][\text{OTf}]_4\}^{4+}$  at 852.6795 *m/e*.

Single crystals of  $[(\text{Ru}(\text{terpy}))_2(\mathbf{4.2}\text{-TE-DB24C8})][\text{OTf}]_8$  suitable for X-ray diffraction were grown by the diffusion of isopropyl ether into a solution of MeCN containing the complex. Figure 4.5 shows a ball-and-stick representation of the cationic portion of  $[(\text{Ru}(\text{terpy}))_2(\mathbf{4.2}\text{-TE-DB24C8})]^{8+}$ . The Ru(II) changes the terpyridine stopper from *transoid* arrangement in the free complex to a *cisoid* arrangement. The Ru(II)...Ru(II) distance is 34.4 Å. There is evidence of a T-shaped C-H  $\pi$ -interaction occurring between the tolyl- group of the terpyridine and one of the appended ethyl 4-hydroxybenzoate groups  $\sim 2.8$  Å. Table 4.4 summarizes the bite angle for complex  $[(\text{Ru}(\text{terpy}))_2(\mathbf{4.2}\text{-TE-DB24C8})]^{8+}$  which are in good agreement with  $[(\text{Ru}(\text{terpy}))_2(\mathbf{4.2}\text{-DB24C8})]^{8+}$ . The ruthenium-nitrogen bond distances range from 1.90(4) for Ru(1)-N(3) to 2.11(4) Å for Ru(1)-N(6).

**Table 4.4** The bite angle for  $[(\text{Ru}(\text{terpy}))_2(\mathbf{4.2}\text{-TE-DB24C8})]^{8+}$  and  $[(\text{Ru}(\text{terpy}))_2(\mathbf{2.2}\text{-DB24C8})]^{8+}$ .

Atoms	$[(\text{Ru}(\text{terpy}))_2(\mathbf{2.2}\text{-DB24C8})]^{8+}$ Angle (°)	$[(\text{Ru}(\text{terpy}))_2(\mathbf{4.2}\text{-TE-DB24C8})]^{8+}$ Angle (°)
N(1)-Ru-N(2)	79.7(24)	76.1(19)
N(2)-Ru-N(3)	78.8(25)	80.4(17)
N(1)-Ru-N(3)	158.4(26)	156.6(20)
N(4)-Ru-N(5)	79.0(28)	76.1(14)
N(5)-Ru-N(6)	80.6(28)	77.5(14)
N(4)-Ru-N(6)	159.6(34)	153.1(13)

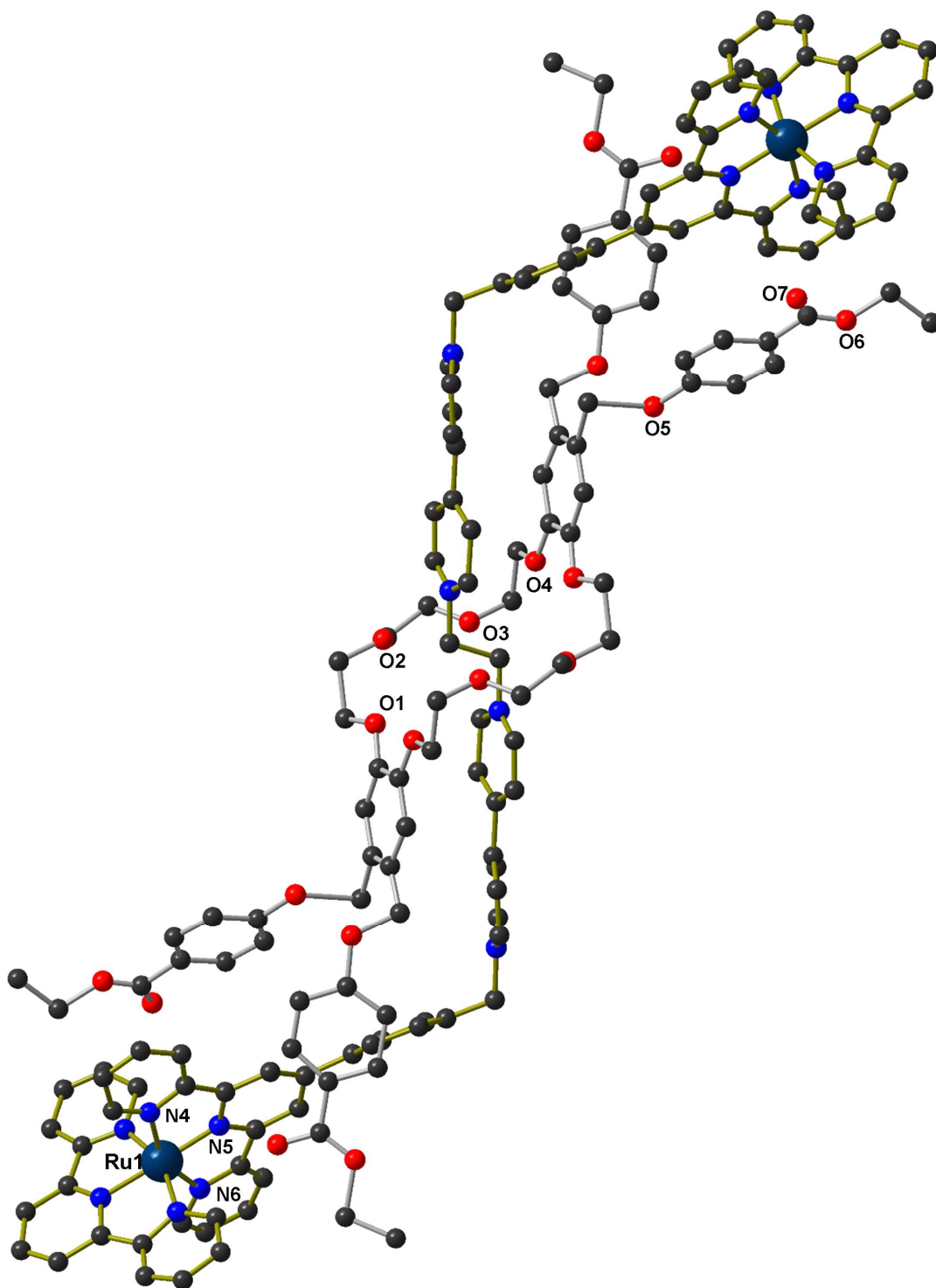


**Figure 4.5** Ball-and-stick representation of the cationic portion of the X-ray crystal structure of  $[(\text{Ru}(\text{terpy}))_2(4.2\text{-TE-DB24C8})]^{8+}$ . (Ru = blue-gray, O = red, N = blue, C = black; wheel bonds = silver, axle bonds = gold).

The UV/Vis spectrum of  $[\text{Ru}(\text{terpy})_2(\mathbf{4.2}\text{-TE-DB24C8})]^{8+}$  is dominated by the high energy  $\pi\text{-}\pi^*$  ligand centered bands at 270 nm and 306 nm respectively but also shows an MLCT band at 485 nm, which is red-shifted from that of the parent compound  $[\text{Ru}(\text{terpy})_2]^{2+}$ . The red shift is caused by the  $\pi^*$  orbital being stable by the cationic nature of the thread. The extinction coefficient ( $\epsilon$ ) for  $[(\text{Ru}(\text{terpy}))_2(\mathbf{4.2}\text{-TE-DB24C8})]^{8+}$  was found to be  $48,510 \text{ L mol}^{-1} \text{ cm}^{-1}$ ; Figure 4.6. Table 4.5 compares the UV/Vis data for  $[(\text{Ru}(\text{terpy}))_2(\mathbf{4.2}\text{-TE-DB24C8})]^{8+}$  to other related  $[\text{Ru}(\text{terpy})_2]^{2+}$  based complexes.

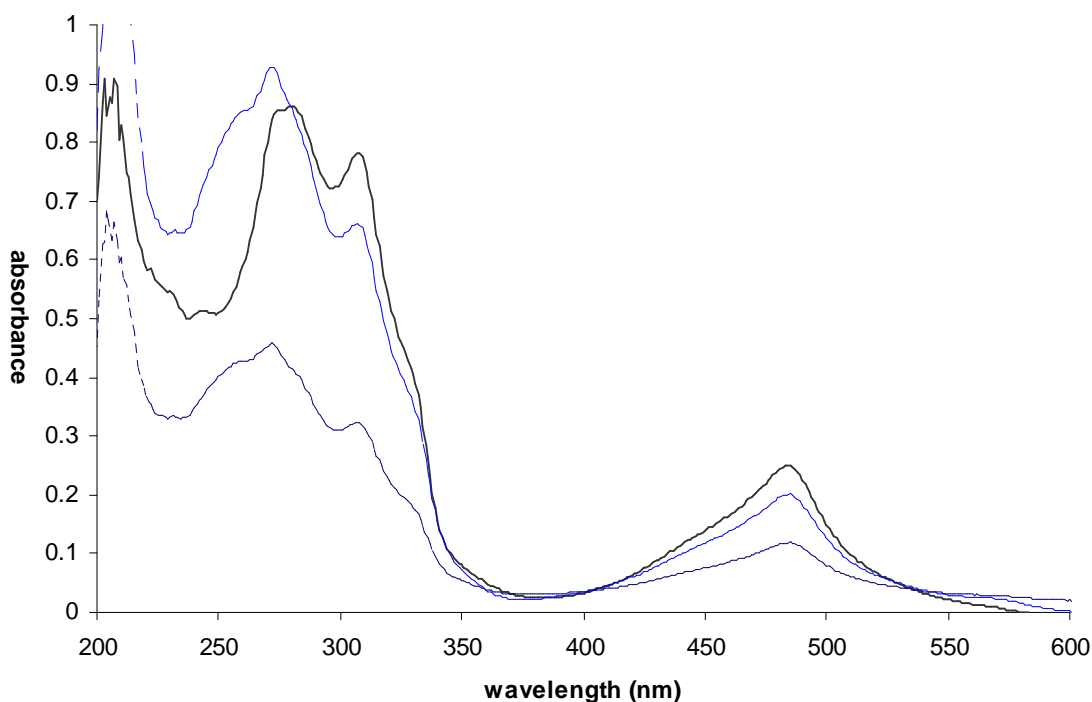


**Figure 4.6** UV/Vis spectra of complex  $[(\text{Ru}(\text{terpy}))_2(\mathbf{2.2})]^{8+}$  (---) and  $[(\text{Ru}(\text{terpy}))_2(\mathbf{2.2}\text{-DB24C8})]^{8+}$  (— —) and  $[(\text{Ru}(\text{terpy}))_2(\mathbf{4.2}\text{-TE-DB24C8})]^{8+}$  (—) at concentration of  $1.0 \times 10^{-5} \text{ M}$  in  $\text{CH}_3\text{CN}$ .

**Table 4.5** UV/Vis spectra for  $[(\text{Ru}(\text{terpy}))_2(\mathbf{4.2cTE-DB24C8})]^{8+}$  and a few other selected ruthenium(II) complexes.

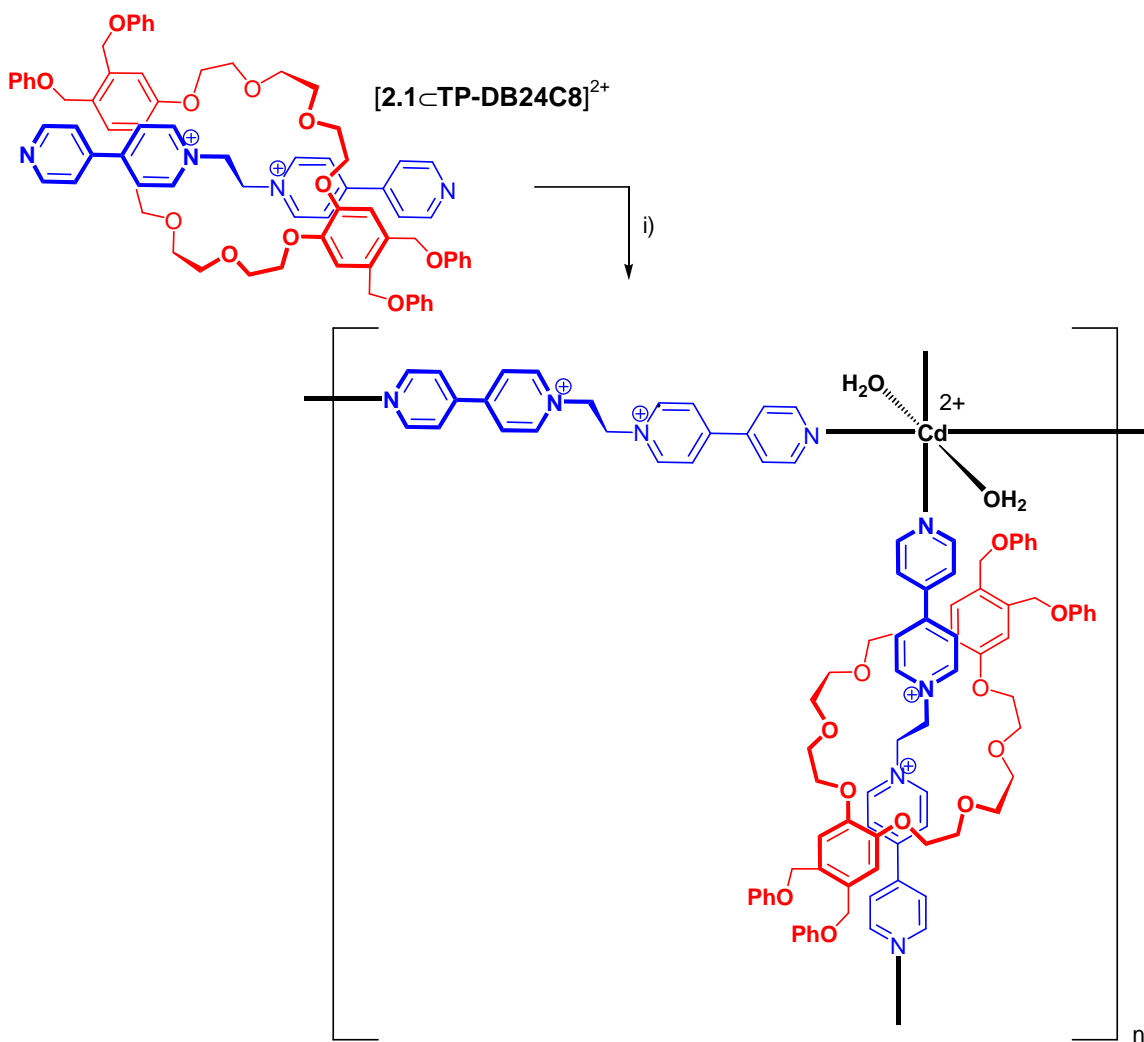
<b>Ru complex<sup>(a)</sup></b>	<b>MLCT <math>\lambda_{\text{max}}</math> (nm)</b>	<b><math>\epsilon</math> (L mol<sup>-1</sup> cm<sup>-1</sup>)</b>	<b>ref#</b>
Ru(terpy) <sub>2</sub>	475	17 600	5
Ru(tolyterpy) <sub>2</sub>	490	28 000	6
Ru(terpy)(tolyterpy)	483	19 300	6
$[(\text{Ru}(\text{terpy}))_2(\mathbf{2.2})]^{8+}$	485	25 000	2
$[(\text{Ru}(\text{terpy}))_2(\mathbf{2.2cDB24C8})]^{8+}$	485	11 900	2
$[(\text{Ru}(\text{terpy}))_2(\mathbf{4.2cTE-DB24C8})]^{8+}$	485	20 200	

<sup>(a)</sup> Counter ion of PF<sub>6</sub><sup>-</sup>

Comparing the bottom three Ru(II) complexes in the table, the addition of crown ether wheels has no effect on the MLCT band. This is presumably because the metal is too far away from the cationic center of the rotaxane to have an appreciable effect.

#### 4.2.2 Synthesis of a 2-D polyrotaxane

It has previously been shown that 1-, 2- and 3-dimensional metal organic frameworks could be constructed using a 1,2-bis(4,4'-dipyridinium)ethane axle and **DB24C8**.<sup>7</sup> The question arises, what would be the effect if one molecular component of the supramolecular structure was to change; in this case the wheel component with a substituted crown ether? We were successful in creating a 2-dimensional framework by reacting one **[2.1][BF<sub>4</sub>]<sub>2</sub>** with two equivalents of **TP-DB24C8** and half an equivalent of **[Cd(H<sub>2</sub>O)<sub>6</sub>][BF<sub>4</sub>]<sub>2</sub>** in MeNO<sub>2</sub>.



**Scheme 4.4 i)** MeNO<sub>2</sub>, excess TP-DB24C8.

X-ray quality crystals of  $[(\text{Cd}(\text{H}_2\text{O})_2)(2.1)(4.3\subset\text{TP-DB24C8})]^{8+}$  were grown by diffusion of isopropyl ether into the reaction mixture. The yellow-orange blocks crystallized in the monoclinic space group Pc. Figure 4.7 shows the use of Cd(II) ions in a non-coordinating solvent such as MeNO<sub>2</sub> results in an octahedral coordination geometry comprised of two [2]pseudorotaxane ligands, and two “naked” axes in a square planar arrangement, and two water molecules in the axial positions. The sides of the square net are defined by Cd⋯Cd distance of 22.2 Å.



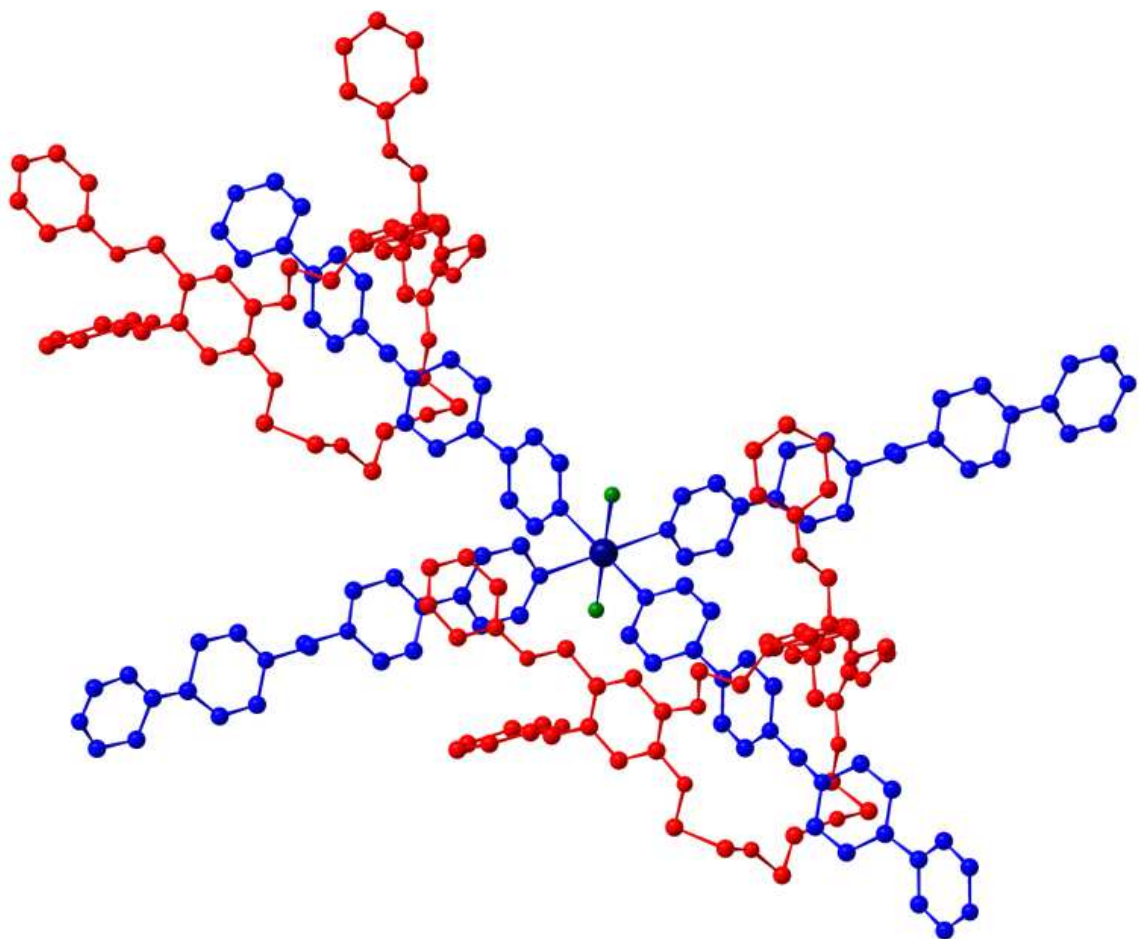


**Figure 4.7** Ball and stick representation of the coordination sphere of the metal centre in  $[(\text{Cd}(\text{H}_2\text{O}))_2(\mathbf{2.1})(\mathbf{4.3}\text{-TP-DB24C8})]^{8+}$ . (Key: dark blue = Cd(II), blue =  $\mathbf{2.1}^{2+}$ , red = crown, green = water).

The structure is very similar to the 2D MORF  $\{[(\text{Cd}(\text{H}_2\text{O})(\text{BF}_4)(\mathbf{2.1}\text{-DB24C8})_2]^{8+}\}_x$  but is probably best described as a 1D polyrotaxane in which the individual polyrotaxane units have the crown ether in a C-conformation and these polyrotaxane strands are bridged by an ancillary linker; in this case the “naked” axle; Figure 4.8. The C-conformation of the crown ether enshrouds the “naked” axle with several edge-to-face and T-shaped C-H $\cdots\pi$  interactions between the phenolic ether appendages of the crown ether and the  $\alpha$ -pyridyl group of the “naked” axle.

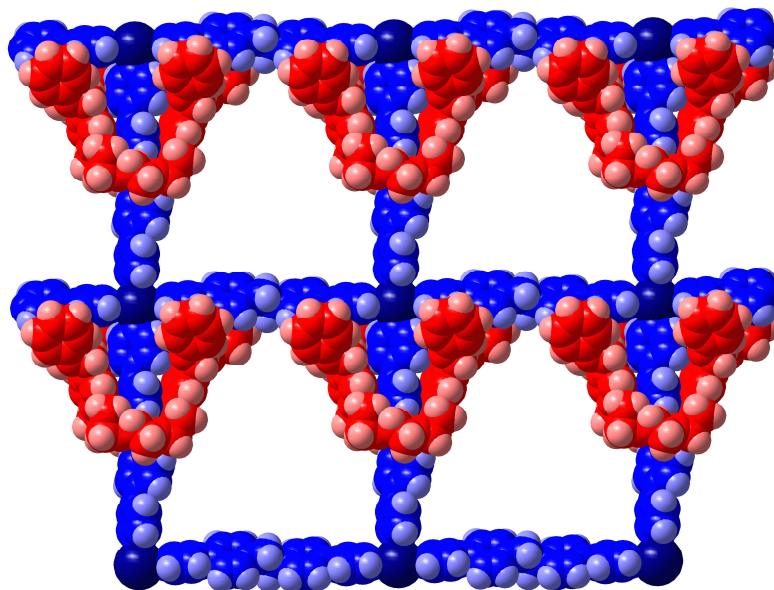


**Figure 4.8** A space-filling model showing four square-grids of  $[(\text{Cd}(\text{H}_2\text{O})_2(2.1)(4.3\text{-TP-DB24C8}))]^{8+}$ .  $\text{MeNO}_2$  solvent molecules and anions are omitted for clarity.

Figure 4.9 compares the previously reported 2-D MORF structure containing **DB24C8** in the S-conformation with this new one containing **TP-DB24C8** in the C-conformation.

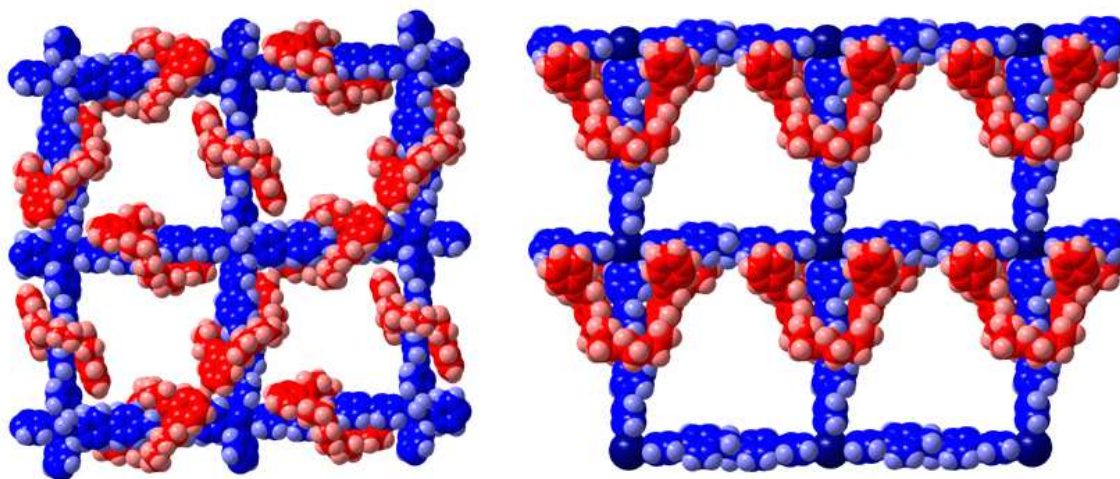


**Figure 4.9** Comparing MORFs with **DB24C8** (left) and **TP-DB24C8** (right).

The reasons for the change in network topology upon changing from a simple wheel such as **DB24C8** to a substituted version such as **TP-DB24C8** are presumably steric in nature.

The adoption of a C-conformation for **TP-DB24C8** likely minimizes the interactions

between phenyl groups of adjacent crown ethers while still allowing the phenyl groups to undergo favourable interactions with the pyridyl groups from the “naked” axles.

### 4.3 Conclusion

Pseudorotaxane and rotaxane ligands were prepared with **DB24C8** derivatives having four fairly large substituents on the aromatic rings. The ability of these new interlocked ligands to form transition metal complexes and metal organic frameworks was studied and compared to similar systems already known with **DB24C8**. The robust nature of the [2]rotaxane was confirmed by  $^1\text{H}$  NMR spectroscopy and a binuclear complex of  $[\text{Ru}(\text{terpy})]^{2+}$  was synthesized and characterized. The solid state structure of the mixed ligand complex demonstrated that addition of a substituted wheel yields additional non-covalent interactions between components. The use of similar tetra-substituted crown ether in the formation of MORFs yielded a 2D square network but with only one rotaxane.

### 4.4 Experimental

#### 4.4.1 General Methods

2,2':6',2''-Terpyridine,  $\text{RuCl}_3 \cdot x\text{H}_2\text{O}$ , and cadmium(II) tetrafluoroborate were obtained from Sigma-Aldrich and used as received.  $[\text{RuCl}_3(\text{tpy})]$ ,<sup>7</sup> and 1,2-bis(4,4'-bipyridinium)ethane triflate<sup>8</sup> [**2.1**][OTf]<sub>2</sub> was synthesized using literature methods. Solvents were dried using an Innovative Technologies Solvent Purification System.  $^1\text{H}$  NMR spectra were obtained on a Bruker Avance 500 instrument operating at 500 MHz. Deuterated solvents were purchased from Cambridge Isotope Laboratories Inc. and used as received. High-resolution mass spectra were recorded in 50/50 MeCN/H<sub>2</sub>O on a Micromass LCT Electrospray ToF mass spectrometer. UV/Vis absorption spectra were

recorded on a Cary 50 series spectrometer. The absorption spectra were recorded in acetonitrile (BDH<sup>®</sup>) at concentrations of  $1.0 \times 10^{-5}$  M for complexes  $[(\text{Ru}(\text{terpy}))_2(\mathbf{4.2}\text{-TP-DB24C8})]^{8+}$ . Single crystal X-ray diffraction experiments were run on a Bruker APEX diffractometer with CCD detector.

#### Synthesis $[\mathbf{4.2}\text{-TE-DB24C8}][\text{OTf}]_4$

**TE-DB24C8** (0.185 g, 0.159 mmol) and **[2.1]** $[\text{OTf}]_2$  (0.050 g, 0.078 mmol) were dissolved in  $\text{MeNO}_2$  (10 mL) and stirred overnight. Bromo-4-tolyterpyridine (0.189 g, 0.147 mmol) was dissolved in  $\text{CH}_2\text{Cl}_2$ , and the mixture was stirred for 7 days. The organic layer was removed, and the orange solid stirred between  $\text{MeNO}_2$  and  $\text{NaOTf}(\text{aq})$  stirred overnight. The organic layer was separated, dried ( $\text{MgSO}_4$ ) and evaporated. The residue was stirred in toluene. The orange solid was dissolved in  $\text{CH}_3\text{CN}$ , isopropyl ether was slowly diffused to give an orange solid. Yield: 0.065g (30%). **ESI-MS:**  $m/z$   $[\mathbf{4.2}\text{-TE-DB24C8}]^{2+}$  calc. 1221.4011, found 1221.4041.

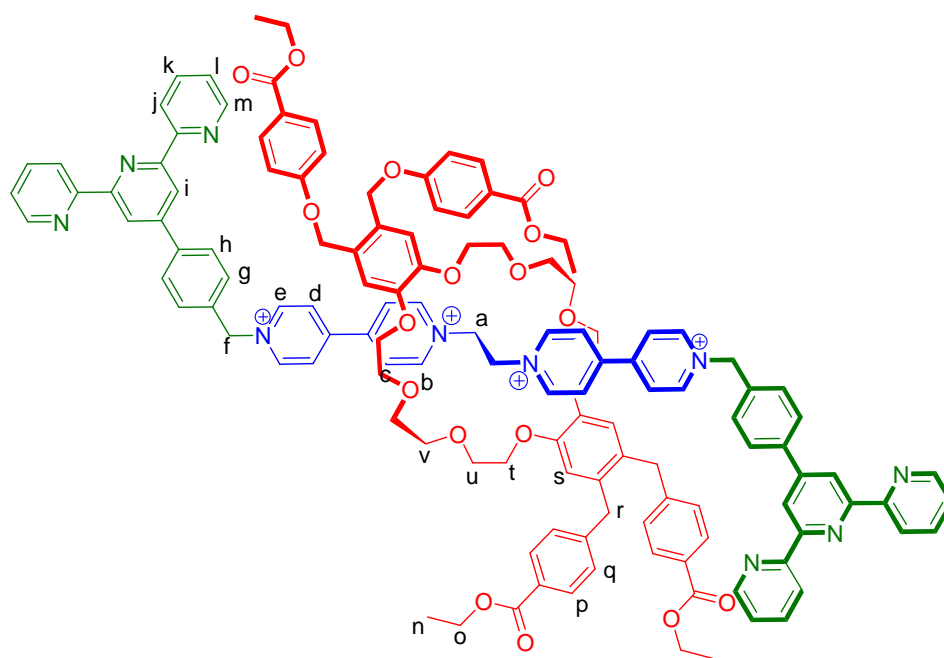


**Table 4.6**  $^1\text{H}$  NMR spectroscopic data for  $[\mathbf{4.2cTE-DB24C8}]^{4+}$  in  $\text{CD}_3\text{CN}$ 

Proton	$\delta$ (ppm)	Multiplicity	# protons	J (Hz)
<i>a</i>	5.62	s	4	-
<i>b</i>	9.36	d	4	$^3J_{bc} = 6.8$
<i>c</i>	8.27	m	4	-
<i>d</i>	8.27	m	4	-
<i>e</i>	8.98	d	4	$^3J_{ed} = 6.7$
<i>f</i>	5.77	s	4	-
<i>g</i>	7.71	d	4	$^3J_{gh} = 8.2$
<i>h</i>	7.52	d	4	$^3J_{hg} = 8.1$
<i>i</i>	8.57	s	4	-
<i>j</i>	8.73	d	4	$^3J_{jk} = 4.5$
<i>k</i>	7.99	t	4	$^3J_{kl} = 7.8, ^3J_{jk} = 7.6$
<i>l</i>	7.47	t	4	$^3J_{lm} = 5.7, ^3J_{lk} = 4.9$
<i>m</i>	8.70	d	4	$^3J_{lm} = 7.9$
<i>n</i>	4.14	q	12	$^3J_{no} = 7.1, ^3J_{on} = 7.2$
<i>o</i>	1.21	t	8	$^3J_{on} = 7.0, ^3J_{no} = 7.0$
<i>p</i>	7.88	d	8	$^3J_{pq} = 8.8$
<i>q</i>	6.94	d	8	$^3J_{qp} = 8.9$
<i>r</i>	4.64	s	8	-
<i>s</i>	6.84	s	4	-
<i>t, u, v</i>	4.02 – 4.07	m	24	-

**Synthesis  $[(\text{Ru}(\text{terpy}))_2(\mathbf{4.2cTE-DB24C8})][\text{OTf}]_8$** 

To a solution of  $[\mathbf{4.2cTE-DB24C8}][\text{OTf}]_4$  (0.030 g, 0.0109 mmol) dissolved in 1:1 EtOH/H<sub>2</sub>O solution was added solid (terpy)RuCl<sub>3</sub> (0.010 g, 0.020 mmol) and the mixture was brought to reflux for 24 h to give a deep red solution. The reaction mixture was cooled to room temperature, filtered through a Celite pad and washed with EtOH until the eluent was colorless. The filtrate was then reduced to half the volume and the addition of NaOTf produced a red precipitate. To the red solid in CH<sub>3</sub>CN, isopropyl ether was

slowly diffused to give a red solid in quantitative yield. **ESI-MS:**  $m/z$

$[(\text{Ru}(\text{terpy}))_2(\mathbf{4.2}\text{-TE-DB24C8})]^{4+}$  calc. 852.67613, found 852.6795.

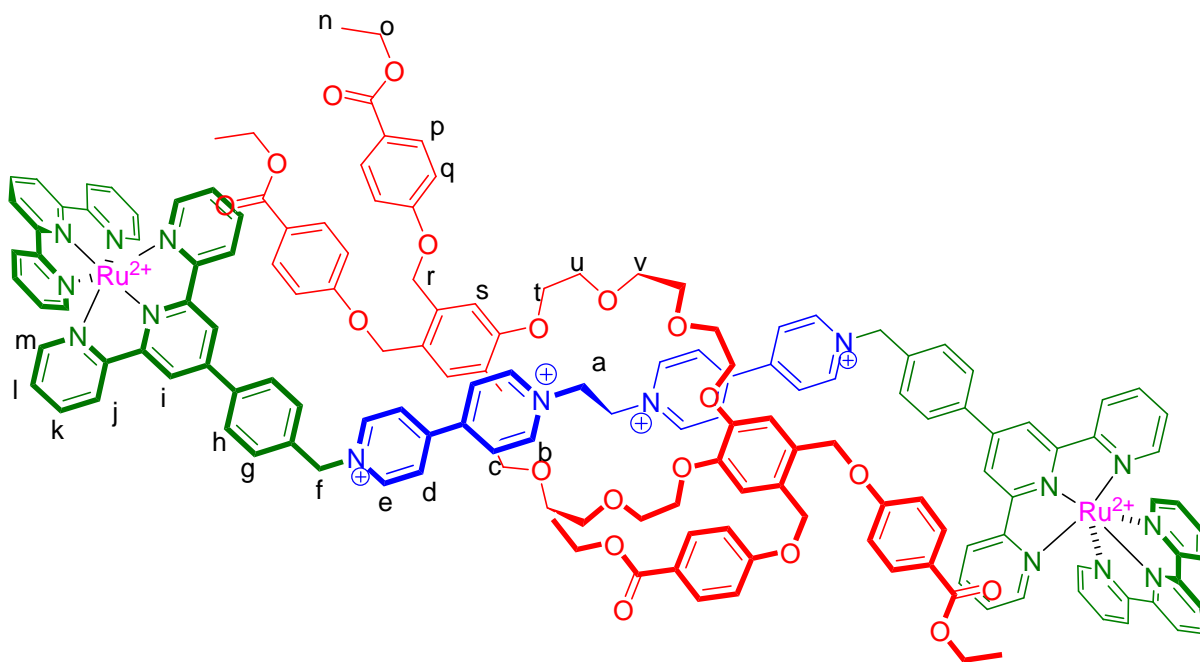


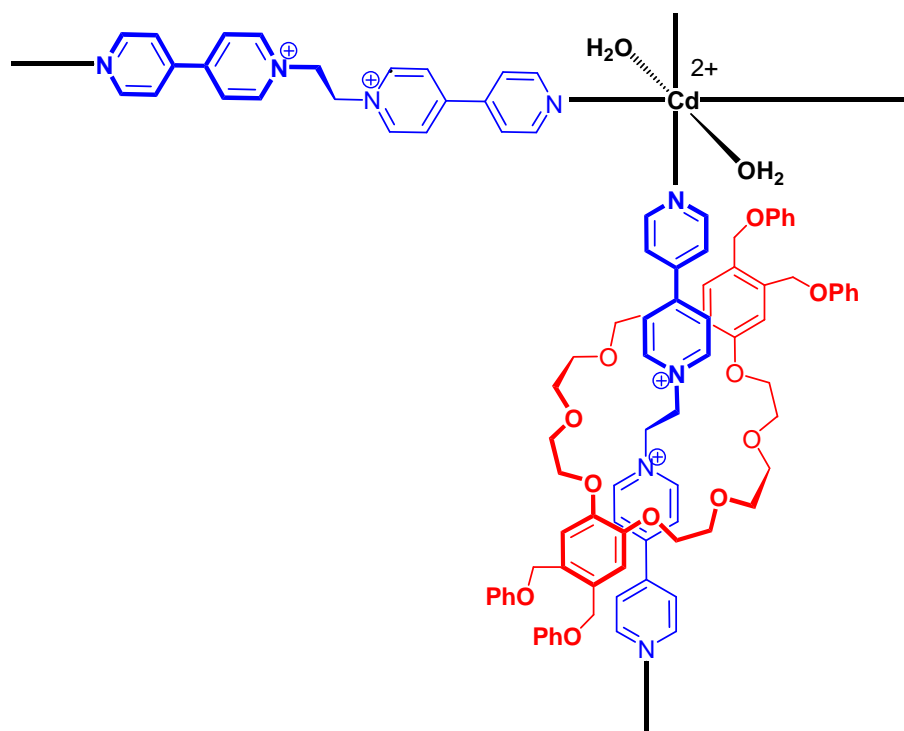
**Table 4.7**  $^1\text{H}$  NMR spectroscopic data for  $[(\text{Ru}(\text{terpy}))_2(\mathbf{4.2}\text{-TE-DB24C8})]^{8+}$  in  $\text{CD}_3\text{CN}$

Proton	$\delta$ (ppm)	Multiplicity	# protons	J (Hz)
<i>a</i>	5.67	s	4	-
<i>b</i>	9.43	d	4	$^3J_{bc} = 6.4$
<i>c</i>	8.42	m	4	-
<i>d</i>	8.42	m	4	-
<i>e</i>	9.11	d	4	$^3J_{ed} = 6.4$
<i>f</i>	5.87	s	4	-
<i>g</i>	8.09	d	4	$^3J_{gh} = 8.0$
<i>h</i>	7.69	d	4	$^3J_{hg} = 8.0$
<i>i</i>	8.83	s	4	-
<i>j</i>	8.51	d	4	$^3J_{jk} = 8.1$
<i>k</i>	7.92	m	4	-
<i>l</i>	7.19	dd	4	$^3J_{lm} = 6.4, ^3J_{lk} = 6.3$
<i>m</i>	7.45	d	4	$^3J_{ml} = 5.2$
<i>n</i>	4.06-4.13	m	12	-
<i>o</i>	1.21	t	8	$^3J_{on} = 7.0, ^3J_{no} = 7.0$
<i>p</i>	7.92	m	8	-
<i>q</i>	7.03	d	8	$^3J_{qp} = 8.7$

<i>r</i>	4.81	<i>s</i>	8	-
<i>s</i>	6.92	<i>s</i>	4	-
<i>t, u, v</i>	4.06-4.13	<i>m</i>	24	-
<i>m'</i>	7.37	<i>d</i>	4	$^3J_{m'l'} = 5.3$
<i>l'</i>	7.19	<i>dd</i>	4	$^3J_{lm} = 6.4, ^3J_{lk} = 6.3$
<i>k'</i>	7.92	<i>m</i>	4	-
<i>j'</i>	8.59	<i>d</i>	4	$^3J_{j'r} = 8.0$
<i>i'</i>	8.77	<i>d</i>	4	$^3J_{i'r} = 8.2$
<i>h'</i>	8.42	<i>m</i>	2	-

### Synthesis [(Cd(H<sub>2</sub>O))<sub>2</sub>(**2.1**)(**4.3c-TP-DB24C8**)] [BF<sub>4</sub>]<sub>8</sub>

To a solution of 1,2-bis(4,4'-dipyridinium)ethane, [**2.1**][BF<sub>4</sub>]<sub>2</sub>, (13 mg, 0.025 mmol) in MeNO<sub>2</sub> (1mL) was added 2 equivalents of **TP-DB24C8** (42 mg, 0.048 mmol). The resulting solution was stirred at room temperature for 1hr, at which time [Cd(H<sub>2</sub>O)<sub>6</sub>][BF<sub>4</sub>]<sub>2</sub> (5 mg, 13 mmol) dissolved in 0.5 mL of MeNO<sub>2</sub>/MeOH was added. Slow diffusion of isopropyl ether into the MeNO<sub>2</sub> produced yellow crystals.



## Reference:

1. Loeb, S. J. *Chem. Commun.* **2005**, 1511.
2. Mercer, D. J.; Loeb, S. J. *Dalton Trans.* **2011**, 40, 6385.
3. Hoffart, D. J.; Loeb, S. J. *Supramol. Chem.* **2007**, *19*, 89
4. Constable, E. C. *Chem. Soc. Rev.*, **2007**, *36*, 246.
5. Constable, E. C.; Thompsen, A. M. W. C.; Tocher, D. A.; Daniels, A. M. *New J. Chem.*, **1992**, *16*, 855.
6. Hofmeier, H.; Andres, P. R.; Hoogenboom, R.; Herdtwerk, E.; Schubert, U. S. *Aust. J. Chem.*, **2004**, *57*, 419.
7. Davidson, G. J. E.; Loeb, S. J. *Angew. Chem. Int. Ed.* **2003**, *42*, 74.
8. Sullivan, B. P.; Calvert, J. M.; Meyer, T. L. *Inorg. Chem.* **1980**, *19*, 1404.
9. Loeb, S. J.; Tiburcio, J.; Vella, S. J.; Wisner, J. A. *Org. Biomol. Chem.* **2006**, *4*, 660.



# Chapter 5

## Linking [2]Rotaxane Wheels to Create a New Type of Metal-Organic Rotaxane Framework

### 5.1 Introduction

The use of rotaxanes as ligands in the construction of coordination polymers (CPs) is a unique methodology for the creation of new materials; a sub-class of metal-organic frameworks (MOFs) known as metal organic rotaxane frameworks (MORFs).<sup>1</sup> To date, MORFs have been constructed by utilizing the axle  $[2.1\text{-DB24C8}]^{2+}$  as an organic linker to connect metal nodes with the wheel not participating in any type of interaction with the metal centres (see Figure 5.1).

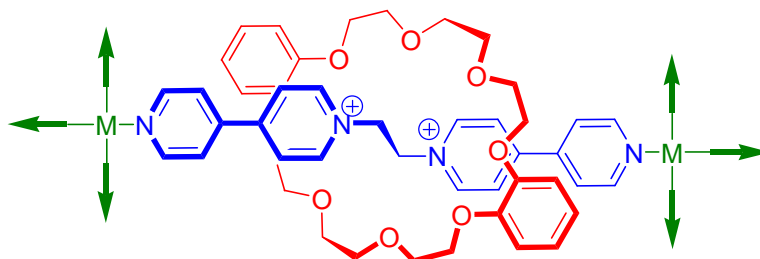


**Figure 5.1** An example of the axle used in the construction of MORFs.

A number of crown ether compounds possessing chelating groups have been synthesized such as those containing terpyridine<sup>2</sup>, pyridine diacid<sup>3</sup>, bipyridine<sup>4</sup> or 1,10-phenanthroline units.<sup>5</sup> Stang has reported crown ether derivatives that contain either acceptors or donor groups designed to form different metal-ligand architectures when coordinated to Pt(II) corners, while the crown ether wheel was available to form [2]pseudorotaxanes with an ammonium axle.<sup>6</sup>

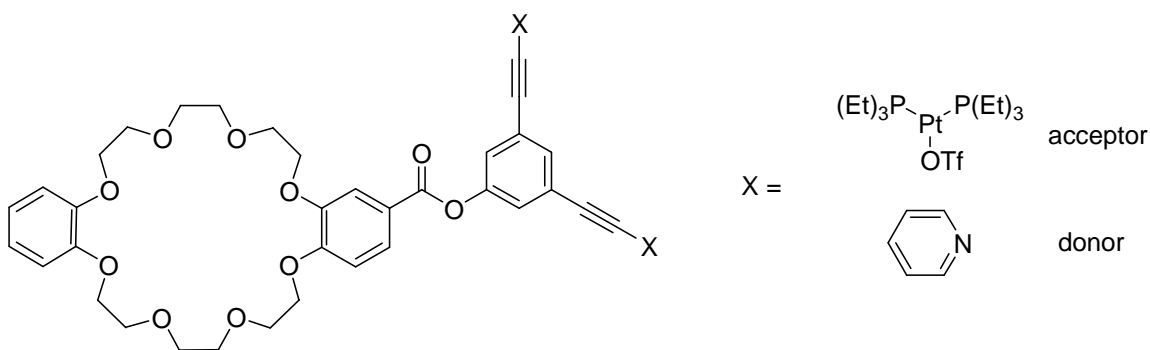


**Figure 5.2** Stang's acceptor and donor crown ethers.<sup>6</sup>

Can a new strategy for MORFs be developed that inverts the function of the axle and the wheel, making the wheel act as the linker while the axle does not participate in metal coordination?

## 5.2 Results and Discussion

### 5.2.1 Chelating [2]rotaxane

For a simple and convenient chelating group, we turned to a ligand developed by Steel *et al.* containing 8-hydroxyquinoline (oxine) as the donor group. As can be seen in Figure 5.3<sup>7</sup>, the backbone of the ligand is similar to the aromatic group of **DB24C8**.

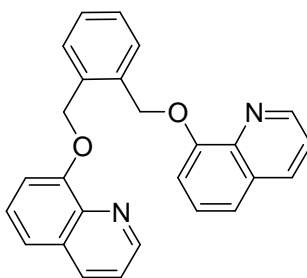
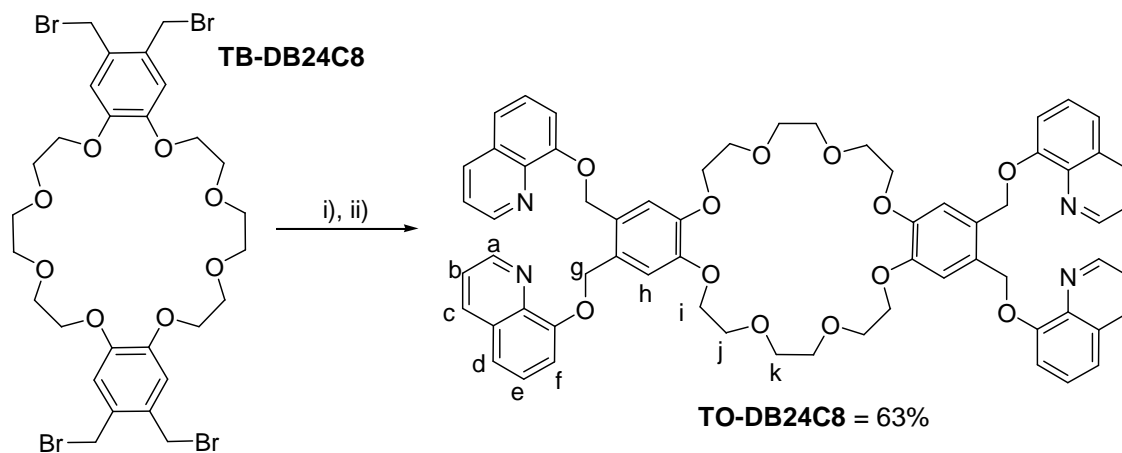


**Figure 5.3** Steel's oxine type chelating ligand.<sup>7</sup>

The chelating crown ether containing the oxine groups was prepared by a Williamson ether synthesis from **TB-DB24C8**, and oxine (Scheme 5.1). The product precipitated from MeCN, the desired compound was isolated, generating a red solid in moderate yield.



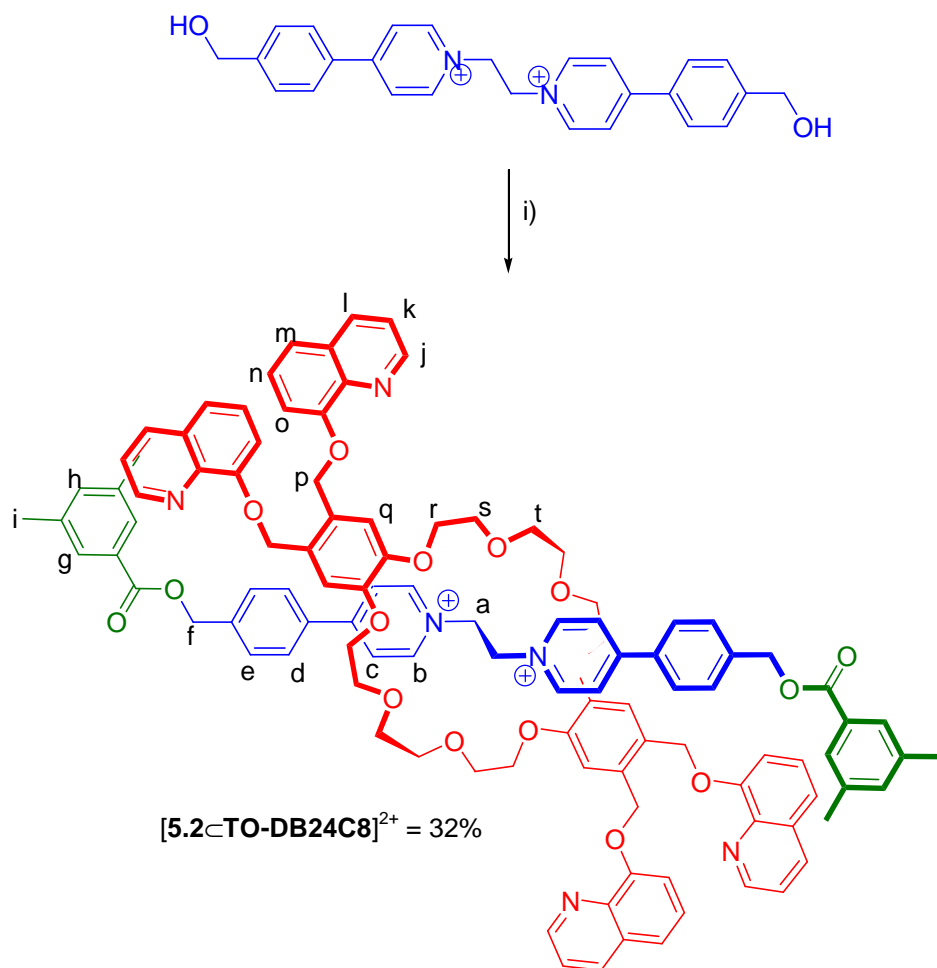
**Scheme 5.1** i) NaH, oxine, THF, stirred 2 h ii) **TB-DB24C8**,  $\Delta$  36 h.

The  $^1\text{H}$  NMR spectrum of **TO-DB24C8** shows the main core remains unchanged relative to the starting material **TB-DB24C8**. The main differences arise from the aromatic (**h**) and the benzylic protons (**g**). For **TO-DB24C8**, these protons are shifted downfield compared to the starting material due to the weaker electron-donating effect of the phenolic oxygen. Some of the major peaks are summarized in Table 5.1. The ESI-MS shows that four oxine groups are now present on the crown ether.

**Table 5.1** Comparison of the chemical shifts for **TB-DB24C8**, and wheel **TO-DB24C8** in  $\text{CD}_2\text{Cl}_2$ .

Protons	<b>TB-DB24C8</b>	<b>TO-DB24C8</b>
<i>j</i>	3.37	3.79 (0.42)
<i>k</i>	3.85	3.83 (-0.02)
<i>i</i>	4.12	4.29 (0.17)
<i>g</i>	6.86	7.17 (0.31)
<i>h</i>	4.62	5.50 (0.88)

The chelating [2]rotaxane,  $[\mathbf{5.2} \subset \mathbf{TO-DB24C8}]^{2+}$  was synthesized in moderate yield through esterification of the [2]pseudorotaxane formed between  $[\mathbf{3.5}][\text{BF}_4]_2$  and **TO-DB24C8** by stirring in MeCN/ $\text{CH}_2\text{Cl}_2$  at room temperature for 3 days; see Scheme 5.2.



**Scheme 5.2** i) 3 eq.  $[3.5]^{2+}$ , 1 eq. **TO-DB24C8**, 9 eq. 3,5-dimethylbenzoic anhydride,  $t\text{Bu}_3\text{P}$  (cat.), MeCN/ $\text{CH}_2\text{Cl}_2$  for 72 h.

Some of the major peaks from the  $^1\text{H}$  NMR spectrum of  $[5.2c\text{TO-DB24C8}][\text{BF}_4]_2$  in  $\text{CD}_3\text{CN}$ , are summarized in Table 5.2. The [2]rotaxane shows evidence supporting the various supramolecular interactions such as hydrogen-bonding and  $\pi$ - $\pi$  stacking. Hydrogen bonding between the ethylene (**a**) and  $\alpha$ -pyridinium (**b**) protons of the axle with the polyether oxygen atoms of the wheel is evidenced by a downfield shifts of the signals for **a** and **b** of 0.67 and 0.37 ppm respectively.

**Table 5.2** Comparison of the chemical shifts of the dumbbell [5.2][BF<sub>4</sub>]<sub>2</sub>, and [2]rotaxane, [5.2cTO-DB24C8][BF<sub>4</sub>]<sub>2</sub> in CD<sub>3</sub>CN.

Protons	[5.2] <sup>2+</sup>	[5.2cTO-DB24C8] <sup>2+</sup>
<i>a</i>	5.11	5.78 (0.67)
<i>b</i>	8.66	9.03 (0.37)
<i>c</i>	8.33	8.20 (-0.13)
<i>d</i>	7.98	7.46 (-0.52)
<i>e</i>	7.73	7.46 (-0.27)
<i>f</i>	5.46	5.32 (-0.14)

The <sup>1</sup>H NMR spectrum also shows changes in the wheel, which are summarized in Table 5.3. The differences arise from the single aromatic proton on the parent **DB24C8** unit, (**q**), and the benzylic protons (**p**). As mentioned, the free crown ether, **TO-DB24C8**, shows a singlet at 7.18 ppm for **q** but the singlet shifts upfield to 7.03 ppm ( $\Delta\delta = 0.15$  ppm) for [5.2cTO-DB24C8][BF<sub>4</sub>]<sub>2</sub>. Furthermore, the benzylic protons for the free crown ether shows a singlet at 5.50 ppm but the singlet shifts upfield to 5.01 ppm ( $\Delta\delta = 0.49$  ppm) for the [2]rotaxane. The ESI-MS also confirmed the interlocked nature of the complex, with just the loss of two counter ions resulting in observation of the molecular ion [5.2cTO-DB24C8]<sup>2+</sup> at 869.3685 *m/e*.

**Table 5.3** Comparison of the chemical shifts of the wheel, **TO-DB24C8** and [2]rotaxane [5.2cTO-DB24C8][BF<sub>4</sub>]<sub>2</sub> in CD<sub>2</sub>Cl<sub>2</sub>.

Protons	TO-DB24C8	[5.2cTO-DB24C8] <sup>2+</sup>
<i>j</i>	8.85	8.71 (-0.14)
<i>k</i>	7.41	7.43 (0.02)
<i>l</i>	8.10	8.13 (0.03)
<i>m</i>	7.36	7.43 (0.07)
<i>n</i>	7.36	7.85 (0.49)
<i>o</i>	7.14	7.17 (0.03)
<i>p</i>	5.50	5.01 (-0.49)
<i>q</i>	7.18	7.03 (-0.15)

A metal complex was prepared by stirring [Cd(H<sub>2</sub>O)<sub>6</sub>][BF<sub>4</sub>]<sub>2</sub> with [5.2cTO-DB24C8][BF<sub>4</sub>]<sub>2</sub> in CH<sub>3</sub>CN overnight to give a brown solid. The <sup>1</sup>H NMR spectrum of the product showed evidence of coordination to Cd(II) revealed by upfield shifts of the

protons **j-o**. Protons **j**, in  $[(\text{Cd}(\text{MeCN})_2(\text{H}_2\text{O}))_2(\mathbf{5.2}\text{-}\mathbf{TO}\text{-}\mathbf{DB24C8})]^{6+}$  shifted upfield from 8.81 ppm as observed in the uncomplexed compound to 9.13 ppm ( $\Delta\delta = 0.32$  ppm), when coordinated to the Cd(II) centre. Table 5.4 compares the crown protons of the uncomplexed oxine rotaxane ligand to the Cd(II) complex. The ESI-MS of this labile metal species showed loss of both Cd(II) ions resulting in observation of only cations of the parent ligand  $[\mathbf{5.2}\text{-}\mathbf{TO}\text{-}\mathbf{DB24C8}]^{2+}$ .

**Table 5.4** Comparison of the chemical shifts of the  $[\mathbf{5.2}\text{-}\mathbf{TO}\text{-}\mathbf{DB24C8}][\text{BF}_4]_2$  and  $[(\text{Cd}(\text{MeCN})_2(\text{H}_2\text{O}))_2(\mathbf{5.2}\text{-}\mathbf{TO}\text{-}\mathbf{DB24C8})][\text{BF}_4]_6$  in  $\text{CD}_3\text{CN}$ .

Proton	$[\mathbf{5.2}\text{-}\mathbf{TO}\text{-}\mathbf{DB24C8}]^{2+}$	$[(\text{Cd}(\text{MeCN})_2(\text{H}_2\text{O}))_2(\mathbf{5.2}\text{-}\mathbf{TO}\text{-}\mathbf{DB24C8})]^{6+}$
<i>j</i>	8.81	9.13 (0.32)
<i>k</i>	7.37	7.67 (0.30)
<i>l</i>	8.03	7.88 (-0.15)
<i>m</i>	7.40	7.73 (0.33)
<i>n</i>	6.67	7.88 (1.48)
<i>o</i>	7.11	7.00 (-0.11)
<i>p</i>	4.88	4.97 (0.09)
<i>q</i>	6.97	6.93 (-0.04)
<i>r, s, t</i>	4.09 - 4.00	4.17-4.05 (0.07)

Single crystals of the Cd(II) complexes were obtained by slow diffusion of isopropyl ether into a solution of  $\text{CH}_3\text{CN}$  containing the complex. Figure 5.4 shows a ball-and-stick representation of the cationic portion of  $[(\text{Cd}(\text{MeCN})_2(\text{H}_2\text{O}))_2(\mathbf{5.2}\text{-}\mathbf{TO}\text{-}\mathbf{DB24C8})]^{6+}$ . As seen with other [2]rotaxanes made using the axle  $[\mathbf{3.5}]^{2+}$ , the [2]rotaxane adopts an *anti* conformation of the central  $\text{NCH}_2\text{CH}_2\text{N}$  moiety while the wheel **TO-DB24C8** exhibits a typical S-shaped conformation, with 3,5-dimethylphenyl groups as the stopper.

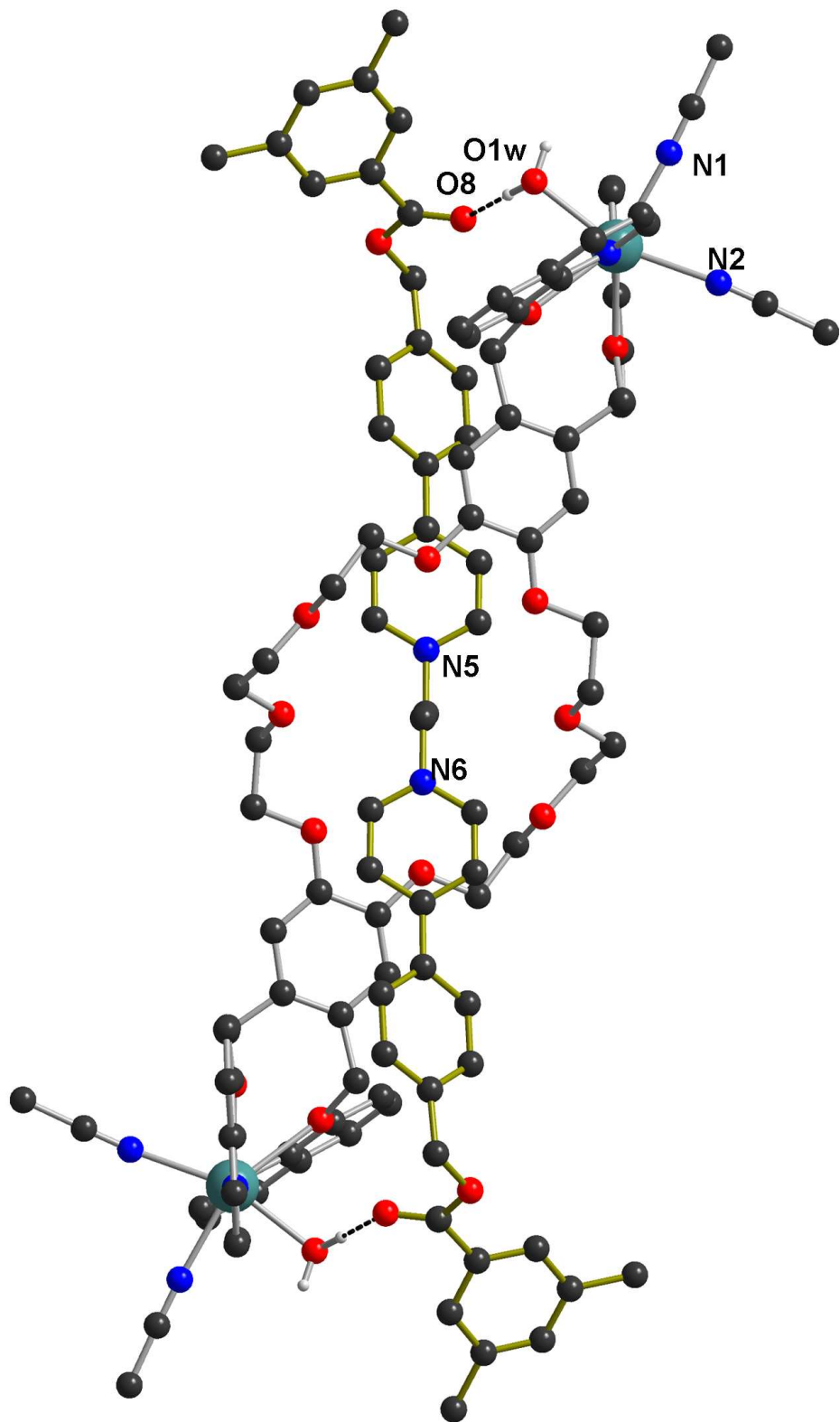


**Figure 5.4** Ball-and stick presentation of  $[(\text{Cd}(\text{MeCN})_2(\text{H}_2\text{O})_2)(5.2\text{c-TO-DB24C8})]^{6+}$ , with H-atoms and anions omitted for clarity. (Colour key: Cd = teal, O = red, N = blue, C = dark gray, axle = gold bonds, wheel = silver bonds).

To emphasize how the metal coordinates, the axle is removed in Figure 5.5.

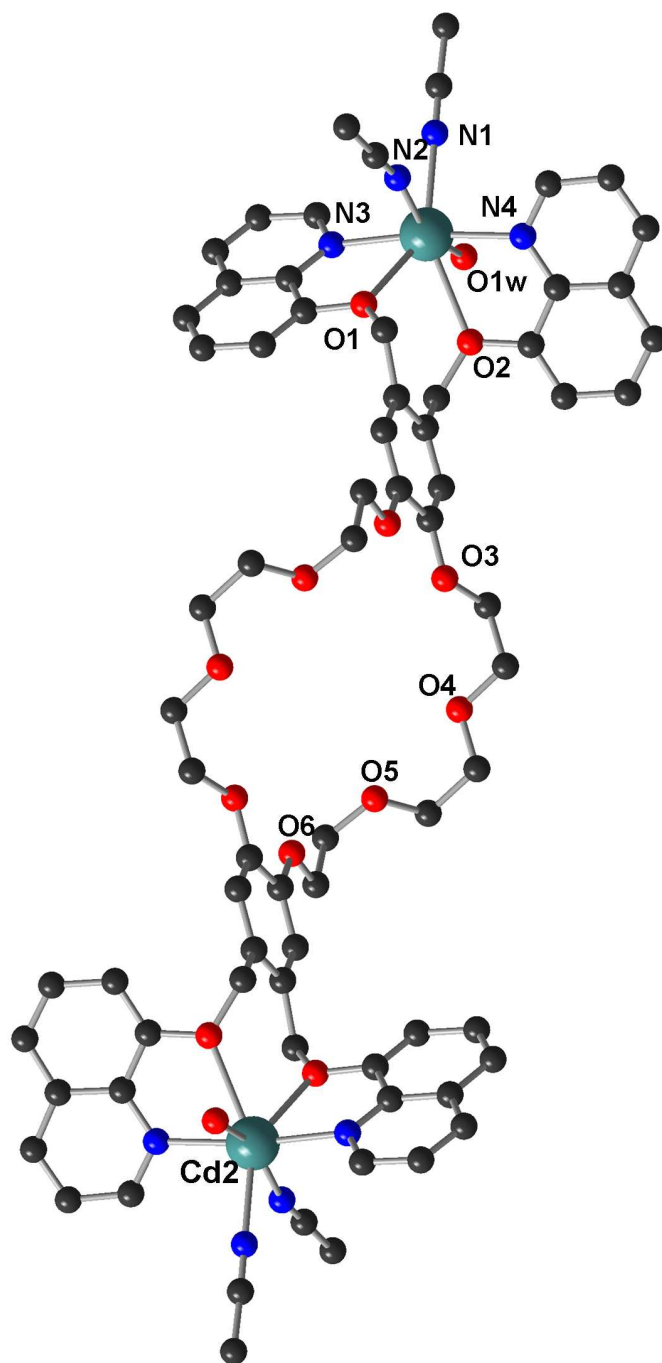


**Figure 5.5** The crown ether and the Cd(II) coordination sphere to emphasize the metal ligand bonding (the axle omitted for clarity).

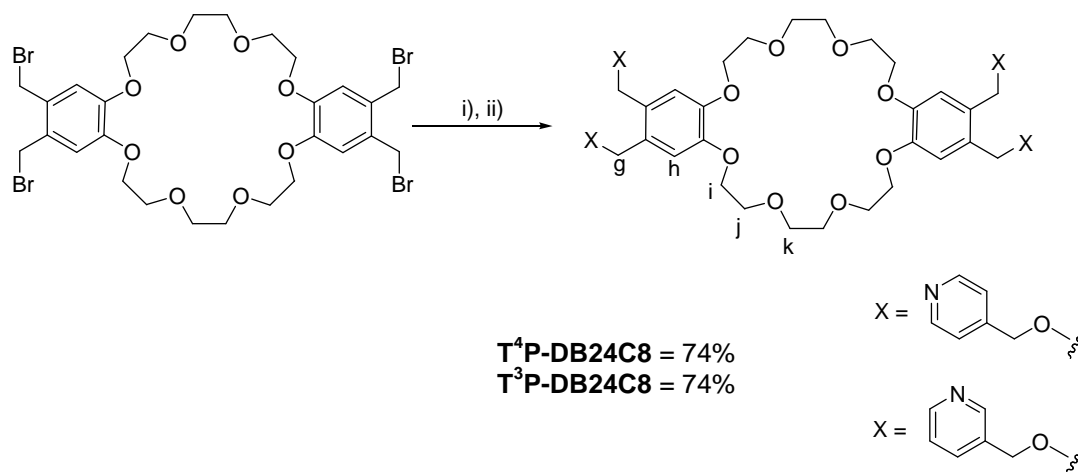
The ligand is coordinated to Cd(II) ions by both the nitrogen and oxygen donors of the oxine group. The Cd-N and Cd-O bonds are 2.28(7), 2.27(7) Å and 2.46(4), 2.58(4) Å,



respectively. The Cd(II) is seven-coordinated in a distorted pentagonal bipyramidal geometry. Besides the oxine ligand, the other sites are filled with two MeCN molecules with Cd-N distances of 2.39(7) and 2.43(7) Å and an H<sub>2</sub>O molecule, with a Cd-O distance of 2.34(6) Å. This single water molecule produces another non-covalent interaction between the axle and the wheel, as it is involved in hydrogen-bonding with the ester carbonyl oxygen atom of the stopper group, with HO-H...O bond of 1.96 (2) Å and an O-H-O angle of 164.8 (3)°.<sup>8</sup>

### 5.2.2 Polymeric rotaxane

Crown ethers with pyridyl donor atoms in either in the three or four position were synthesized by Williamson ether synthesis conditions seen in Scheme 5.3. The new crown ethers were isolated as yellow solids in good yields.



**Scheme 5.3** i) NaH, 3-py or 4-py, DMF, rt 2 h ii) **TB-DB24C8**, 60°C, 36 h.

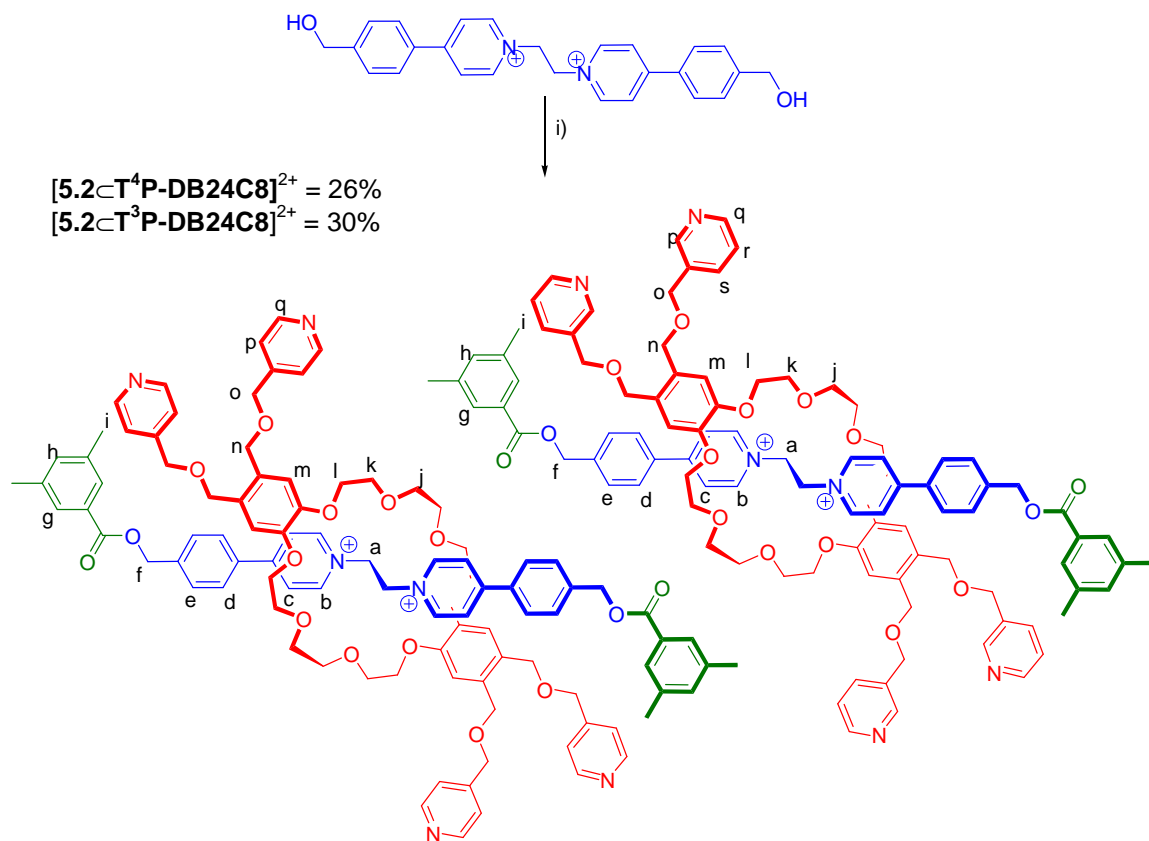
The <sup>1</sup>H NMR spectrum of compounds **T<sup>4</sup>P-DB24C8** or **T<sup>3</sup>P-DB24C8** shows the main core remains unchanged relative to the starting material **TB-DB24C8**. The main differences arise from the aromatic (**h**) and the benzylic protons (**g**). In both **T<sup>4</sup>P-DB24C8** and **T<sup>3</sup>P-DB24C8**, respectively **h** and **g** are shifted downfield due to the presence of the pyridinemethanol groups. Table 5.5 shows a comparison of these

chemical shift changes to **DB24C8**. The ESI-MS shows that four substitutions of pyridinemethanol groups are present on the crown ether.

**Table 5.5** Comparison of the chemical shifts of the wheels **TB-DB24C8**, **T<sup>4</sup>P-DB24C8**, and **T<sup>3</sup>P-DB24C8** in CD<sub>2</sub>Cl<sub>2</sub>.

Protons	TB-DB24C8	T <sup>4</sup> P-DB24C8	T <sup>3</sup> P-DB24C8
<i>j</i>	3.37	3.68 (0.31)	3.68 (0.31)
<i>k</i>	3.85	3.78 (-0.07)	3.78 (-0.07)
<i>i</i>	4.12	4.06 (-0.06)	4.06 (-0.06)
<i>g</i>	6.86	6.88 (-0.02)	6.91 (-0.07)
<i>h</i>	4.62	4.69 (-0.07)	4.51 (-0.11)

The [2]rotaxanes designed with bridging appendages were prepared under similar conditions used to synthesis the chelating [2]rotaxane (Scheme 5.4), and some of the major peaks are summarized in Table 5.6.



**Scheme 5.4** i) 3 eq. [5.1]<sup>2+</sup>, 1 eq. T<sup>4</sup>P-DB24C8 or T<sup>3</sup>P-DB24C8, 9 eq. 3,5-dimethylbenzoic anhydride, <sup>n</sup>Bu<sub>3</sub>P (cat.), MeCN/CH<sub>2</sub>Cl<sub>2</sub> for 72 h.

Evidence supporting the various supramolecular interactions such as hydrogen-bonding and  $\pi$ - $\pi$  stacking were apparent. Hydrogen-bonding between the ethylene (**a**) and  $\alpha$ -pyridinium (**b**) protons of the thread with the polyether oxygen atoms of the wheel is demonstrated by a downfield shift of the signals for **a** from 5.11 ppm in  $[\mathbf{5.2}]^{2+}$  to 5.46 ppm for  $\mathbf{T}^4\mathbf{P}\text{-DB24C8}$  and  $\mathbf{T}^3\mathbf{P}\text{-DB24C8}$ . The  $\alpha$ -pyridinium (**b**) proton signal is also shifted downfield from 8.65 ppm in  $[\mathbf{5.2}]^{2+}$  to 9.03 ppm for both  $\mathbf{T}^4\mathbf{P}\text{-DB24C8}$  and  $\mathbf{T}^3\mathbf{P}\text{-DB24C8}$ .

**Table 5.6** Comparison of the chemical shifts of the dumbbell  $[\mathbf{5.2}][\text{BF}_4]_2$ , and [2]rotaxane  $[\mathbf{5.2}\subset\mathbf{T}^4\mathbf{P}\text{-DB24C8}][\text{BF}_4]_2$ , and  $[\mathbf{5.2}\subset\mathbf{T}^3\mathbf{P}\text{-DB24C8}][\text{BF}_4]_2$  in  $\text{CD}_3\text{CN}$ .

Protons	$[\mathbf{5.2}]^{2+}$	$[\mathbf{5.2}\subset\mathbf{T}^4\mathbf{P}\text{-DB24C8}]^{2+}$	$[\mathbf{5.2}\subset\mathbf{T}^3\mathbf{P}\text{-DB24C8}]^{2+}$
<i>a</i>	5.11	5.46 (0.35)	5.46 (0.35)
<i>b</i>	8.65	9.03 (0.38)	9.03 (0.38)
<i>c</i>	8.33	7.97 (-0.36)	7.97 (-0.36)
<i>d</i>	7.98	7.57 (-0.41)	7.57 (-0.41)
<i>e</i>	7.73	7.50 (-0.23)	7.50 (-0.23)

The  $^1\text{H}$  NMR spectra also show changes in the wheel, which are summarized in Table 5.7. The differences arise from the single aromatic proton on the parent **DB24C8** unit (**m**), and the benzylic protons (**n**). As mentioned, the free crown ether,  $\mathbf{T}^4\mathbf{P}\text{-DB24C8}$ , shows a singlet at 6.96 ppm for **m** but this singlet shifts upfield to 6.68 ppm ( $\Delta\delta = 0.28$  ppm) for  $[\mathbf{5.2}\subset\mathbf{T}^4\mathbf{P}\text{-DB24C8}]^{2+}$ . Also, the benzylic protons for the free crown ether show a singlet at 4.51 ppm but this singlet shifts upfield to 4.28 ppm ( $\Delta\delta = 0.23$  ppm) for  $[\mathbf{5.2}\subset\mathbf{T}^4\mathbf{P}\text{-DB24C8}]^{2+}$ . Similarly, for crown ether  $\mathbf{T}^3\mathbf{P}\text{-DB24C8}$  the singlet at 6.96 ppm for **m** shifts upfield to 6.70 ppm ( $\Delta\delta = 0.26$  ppm) for  $[\mathbf{5.2}\subset\mathbf{T}^3\mathbf{P}\text{-DB24C8}]^{2+}$  while the benzylic protons **n** which shows a singlet at 4.51 ppm which shifts upfield to 4.29 ppm ( $\Delta\delta = 0.22$  ppm) in the [2]rotaxane. The ESI-MS also confirmed the interlocked nature of the complex, with the loss of two counter ions, and protonation of one of the pyridine

rings to give the molecular ions  $[5.2\text{C}(\text{H}+\text{T}^4\text{P-DB24C8})]^{3+}$  and  $[5.2\text{C}(\text{H}+\text{T}^3\text{P-DB24C8})]^{3+}$  at 531.9138 *m/e*.

**Table 5.7** Comparison of the chemical shifts of the [2]rotaxanes  $[5.2\text{C}\text{T}^4\text{P-DB24C8}][\text{BF}_4]_2$  and  $[5.2\text{C}\text{T}^3\text{P-DB24C8}][\text{BF}_4]_2$  in  $\text{CD}_3\text{CN}$ .

Proton	$\text{T}^4\text{P-DB24C8}$	$[5.2\text{C}\text{T}^4\text{P-DB24C8}]^{2+}$	$\text{T}^3\text{P-DB24C8}$	$[5.2\text{C}\text{T}^3\text{P-DB24C8}]^{2+}$
<i>j</i>	3.68	4.07 (0.39)	3.66	4.06 (0.40)
<i>k</i>	3.80	4.07 (0.27)	3.78	4.06 (0.28)
<i>l</i>	4.10	4.07 (0.03)	4.09	4.06 (0.03)
<i>m</i>	6.99	6.70 (-0.29)	6.96	6.68 (-0.28)
<i>n</i>	4.56	4.29 (-0.27)	4.49	4.28 (-0.21)
<i>o</i>	4.52	4.29 (-0.23)	4.51	4.28 (-0.23)

Single crystals of  $[5.2\text{C}\text{T}^4\text{P-DB24C8}][\text{BF}_4]_2$  were grown by the slow diffusion of isopropyl ether into a MeCN solution. The yellow crystal appeared as small block over a few days. Figure 5.6 shows a ball-and-stick representation of the cationic portion of  $[5.2\text{C}\text{T}^4\text{P-DB24C8}]^{2+}$ . The structure reveals typical features of **DB24C8** portion adopting a typical S-conformation while the  $\text{NCH}_2\text{CH}_2\text{N}$  unit exhibits an *anti* conformation.  $[5.2\text{C}\text{T}^4\text{P-DB24C8}]^{2+}$  is stoppered at both ends by a 3,5-dimethylphenyl group. As expected, the cationic axle interpenetrates the central cavity of the wheel allowing the electron-rich aromatic portion of the wheel to  $\pi$ -stack with the electron-deficient axle. The structure also reveals a high degree of C-H...O hydrogen bonding between the components. The four protons *ortho*- to N3- as well the four central protons attached to ethylene bridge form eight hydrogen bonds with the oxygens of the wheel with C-O distances ranging from 3.20(8) - 3.64(7) Å. The  $-\text{CH}_2\text{OCH}_2(\text{C}_5\text{H}_4\text{N})$  appendages flank the ester stopping groups and are pulled away from the core of the [2]rotaxane.<sup>9</sup> This conformation shows that it should be possible to use the pyridine donors for coordination.

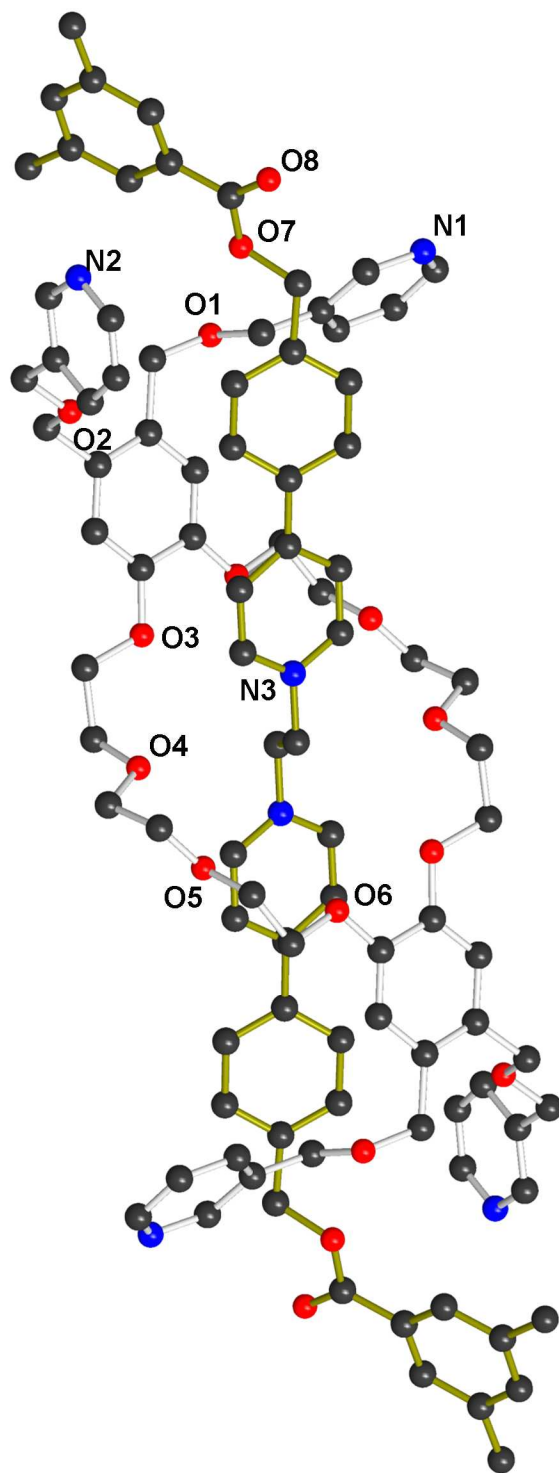


**Figure 5.6** Ball-and-stick representation of  $[5.2\text{C-T}^4\text{P-DB24C8}]^{2+}$  (anions and H-atoms are omitted for clarity. Colour key: O = red, N = blue, C = dark gray; axle = gold bonds, wheel = silver bonds).

The synthesis of bis(pyridyl) ligands in which the pyridyl groups are separated by spacer groups of varying flexibility can give rise either polymers or chelating complexes. The bis(pyridylether) ligand developed by Son<sup>9</sup> from the reaction of 4-pyridylethanol with  $\alpha,\alpha'$ -dibromo-o-xylene gave the ligand as seen Figure 5.7. This ligand forms either a polymer when reacted with Ag(I) or a monomeric complex when reacted with either Co(II) or Cu(II).

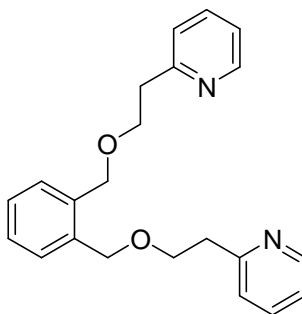


**Figure 5.7** Son's bis(pyridylether) ligand that can form polymers.<sup>9</sup>

It was predicted that with the increased flexibility of the pyridine methanol group, the polymeric system will be much more likely for  $[5.2\text{-T}^4\text{P-DB24C8}][\text{BF}_4]_2$  or  $[5.2\text{-T}^3\text{P-DB24C8}][\text{BF}_4]_2$

Single crystals of a metal complex were grown by slow diffusion of isopropyl ether into a saturated MeCN solution of  $[\text{Cd}(\text{H}_2\text{O})_6][\text{BF}_4]_2$  and  $[5.2\text{-T}^3\text{P-DB24C8}][\text{BF}_4]_2$ . After a few days crystals with the formula of  $[\text{Cd}_2\text{Cl}_4(\text{H}_2\text{O})_4(5.2\text{-T}^3\text{P-DB24C8})][\text{BF}_4]_2$  developed. The source of chloride ion was determined to be the residual anions from column chromatography where  $\text{NH}_4\text{Cl}(aq)$  was used (Figure 5.8).

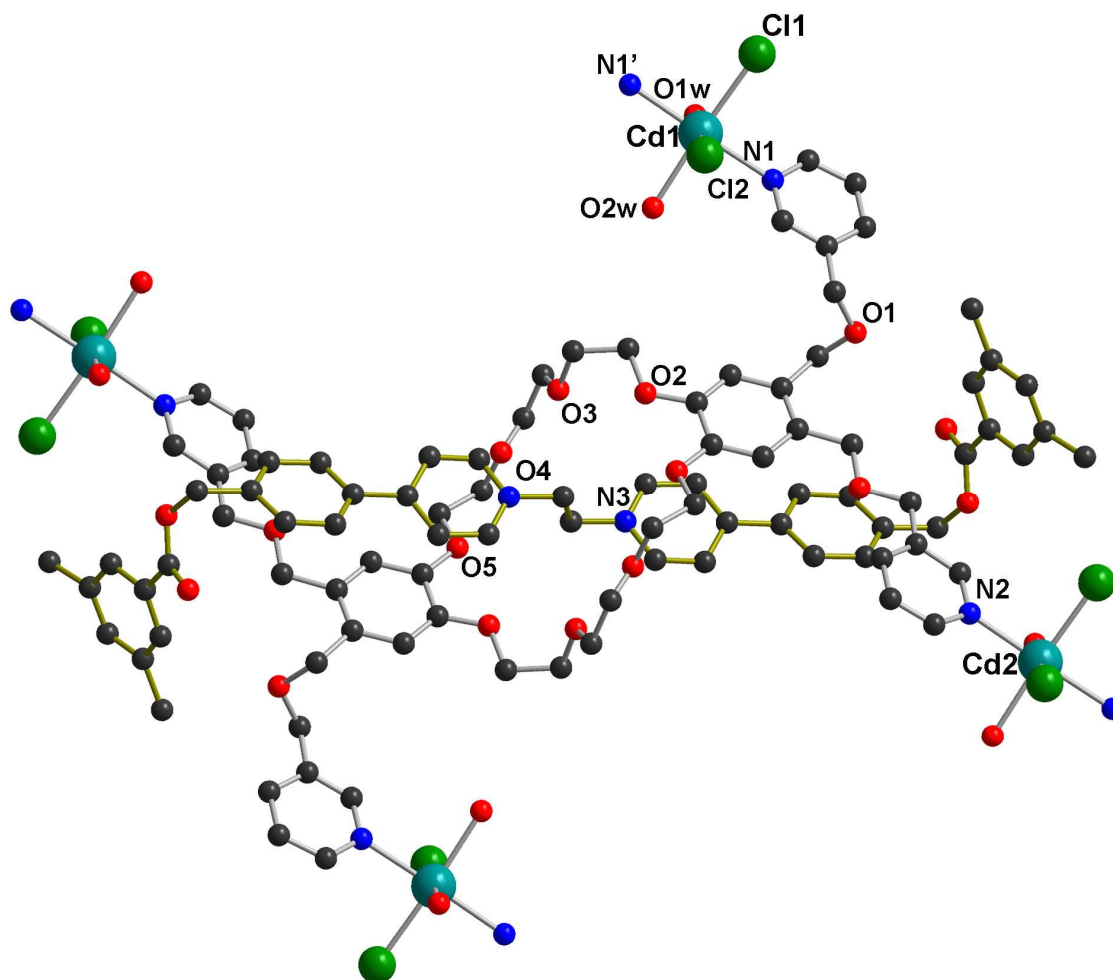


**Figure 5.8** Shows a ball and stick representation of  $[\text{Cd}_2\text{Cl}_4(\text{H}_2\text{O})_4(5.2\text{-T}^3\text{P-DB24C8})]^{2+}$  showing how the 3-pyridyl groups each coordinate to a different Cd(II) ion. All counterions and all solvent molecules have been omitted for clarity. (Colour key: Cd = teal, Cl = green, O = red, N = blue, C = dark gray; axle = gold bonds, wheel = silver bonds).

As was observed previously for the  $[5.2\text{-T}^3\text{P-DB24C8}]^{2+}$  the parent basic structure of the [2]rotaxane remains the same, except the pyridyl groups are extended to coordinate to four Cd(II) centres. The metal nodes consist of  $[(\text{H}_2\text{O})_2\text{Cd}(\mu\text{-Cl})_2\text{Cd}(\text{H}_2\text{O})_2]$  clusters with Cd...Cd distances across the  $\text{Cd}(\mu\text{-Cl})_2\text{Cd}$  linkage of 3.73(2) Å, while the closest Cd...Cd distance between nodes is 17.01(3) Å. The 3-pyridyl donors from different rotaxanes end up in the plane of the node, and *trans* to each other in the axial coordination sites, with N...Cd...N angle of 175.2(3)°. The Cd...N distances are 2.29(1) and 2.33(1) Å.<sup>8</sup>

The four different 3-pyridyl groups of one single crown ether are coordinated to four different Cd(II) ions resulting in a 2-periodic metal organic framework, with large holes through which the axle can be threaded as seen in Figure 5.9.

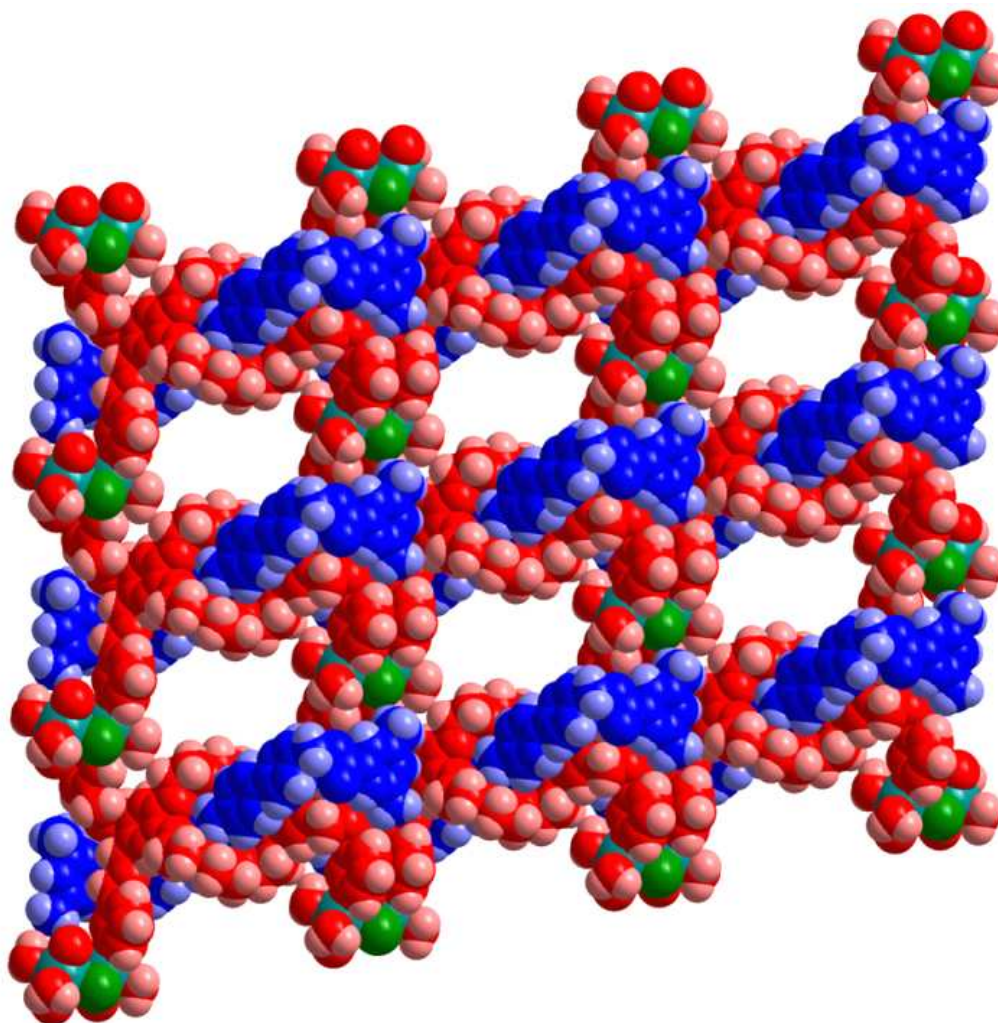


**Figure 5.9** A space filling model of the complete 2-periodic network. All non-coordinating anions have been omitted for clarity. (colour key: Cd = teal, Cl = green, axle = blue, wheel = red).



### 5.3 Conclusion

A new style of metal organic rotaxane framework material can be produced by inverting the metal coordinated roles of the rotaxane components – the axle and wheel. [2]Rotaxanes, [5.2-TO-DB24C8][BF<sub>4</sub>]<sub>2</sub>, containing the oxine wheel were able to coordinate to Cd(II) in a chelating mode for this ligand and also bind to two MeCN solvent molecules with hydrogen-bonds to a water molecule via the axle carbonyl group. The [2]rotaxane [5.2-T<sup>3</sup>P-DB24C8][BF<sub>4</sub>]<sub>2</sub> containing pyridyl groups can form a 2-periodic array of crown ethers and the metal ions, making a grid filled with large holes through which the axle can be threaded.

### 5.4 Experimental

#### 5.4.1 General Methods

Chemicals were obtained from Aldrich and used as received. Tetrakis(bromomethyl)dibenzo-24-crown-8 **TB-DB24C8**,<sup>10</sup> 3,5-dimethylbenzoic anhydride,<sup>11</sup> and 1,2-bis(4-pyridine-4ylphenylmethanol)ethane tetrafluoroborate [3.5][BF<sub>4</sub>]<sub>2</sub><sup>11</sup> and 1,2-Bis(3,5-dimethylbenzoate)benzyl-pyridinium))ethane tetrafluoroborate [5.2][BF<sub>4</sub>]<sub>2</sub><sup>12</sup> were synthesized using literature preparations. Solvents were dried using an Innovative Techniques Solvent Purification Systems. <sup>1</sup>H NMR spectra were obtained on a Bruker Avance 500 instrument operating at 500 MHz. Deuterated solvents were purchased from Cambridge Isotope Laboratories Inc. and used as received. High-resolution mass spectra were recorded in 50/50 MeCN/H<sub>2</sub>O on a Micromass LCT Electrospray TOF mass spectrometer.

### Synthesis **TO-DB24C8**

Oxine (0.798 g, 4.88 mmol) was added to a solution of NaH (132 mg, 5.50 mmol) in dry THF (30 mL) and was stirred for 2 h at room temperature. After which time **TB-DB24C8** (1.00 g, 1.21 mmol) and DMF (2 mL) were added, and the mixture was refluxed for 36 h. The reaction mixture was cooled to room temperature, and water (4 mL) was added. The THF was removed, the oil was dissolved in CH<sub>2</sub>Cl<sub>2</sub> (50 mL) and washed 1 M NaHCO<sub>3</sub> (3x50 mL) and H<sub>2</sub>O (50 mL), and then dried with MgSO<sub>4</sub>, filtered, and concentrated. The solid was recrystallized from CH<sub>3</sub>CN twice to give a reddish solid. Yield: 0.830 mg (63%). MP: 133-136. **ESI-MS**:  $m/z$  [**TO-DB24C8** + H]<sup>+</sup> calc. 1077.4286, found 1077.4332.

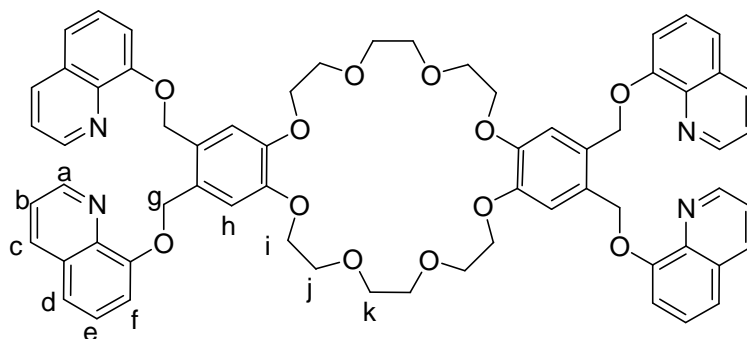


**Table 5.8** <sup>1</sup>H NMR spectroscopic data for **TO-DB24C8** in CD<sub>2</sub>Cl<sub>2</sub>.

Proton	$\delta$ (ppm)	Multiplicity	# protons	J (Hz)
<i>a</i>	8.85	d	4	$J_{ab}^3 = 2.5$
<i>b</i>	7.41	m	4	-
<i>c</i>	8.10	d	4	$J_{cb}^3 = 8.3$
<i>d,e</i>	7.37-7.35	m	8	-
<i>f</i>	7.14	d	4	$J_{ef}^3 = 6.9$
<i>g</i>	5.50	s	8	-
<i>h</i>	7.18	s	4	-
<i>i</i>	4.29	m	8	-
<i>j</i>	3.83	m	8	-
<i>k</i>	3.79	m	8	-

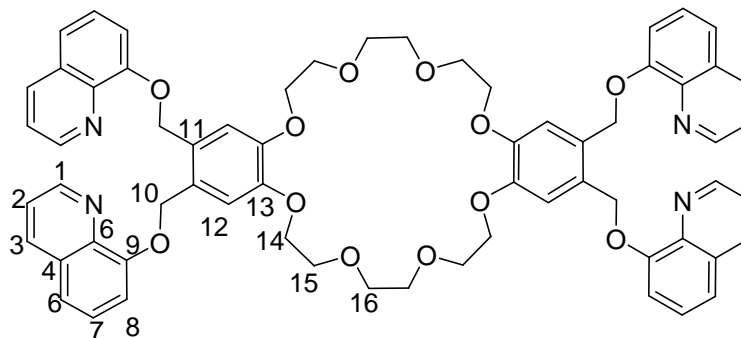


**Table 5.9**  $^{13}\text{C}$  NMR spectroscopic data for **TO-DB24C8** in  $\text{CD}_2\text{Cl}_2$ .

Carbon	$\delta$ (ppm)
1	149.7
2	122.1
3	136.2
4	129.2
5	141.2
6	120.5
7	127.1
8	110.7
9	155.1
10	69.4
11	130.0
12	116.3
13	149.3
14	70.0
15	70.3
16	71.6

#### Synthesis **T<sup>4</sup>P-DB24C8**

4-Pyridinemethanol (0.545 g, 4.99 mmol) was added to a solution of NaH (0.066 g, 2.74 mmol) and dry DMF (30 mL) and the mixture was stirred for 2 h at room temperature. After which time, **TB-DB24C8** (1.00 g, 1.21 mmol) was added and the mixture was refluxed for 36 h. The reaction mixture was then cooled to room temperature and water (4 mL) was added. The DMF was removed, the oil was dissolved in  $\text{CH}_2\text{Cl}_2$  (50 mL), and then washed with 1 M  $\text{NaHCO}_3$  (3x50 mL) and  $\text{H}_2\text{O}$  (50 mL), and then dried with

MgSO<sub>4</sub>, filtered, and concentrated. Yield: 0.837 g (74%). MP: 97-100°C. ESI-MS: *m/z*

[(T<sup>4</sup>P-DB24C8 + Na)<sup>+</sup> calc. 955.4099, found 955.4147.

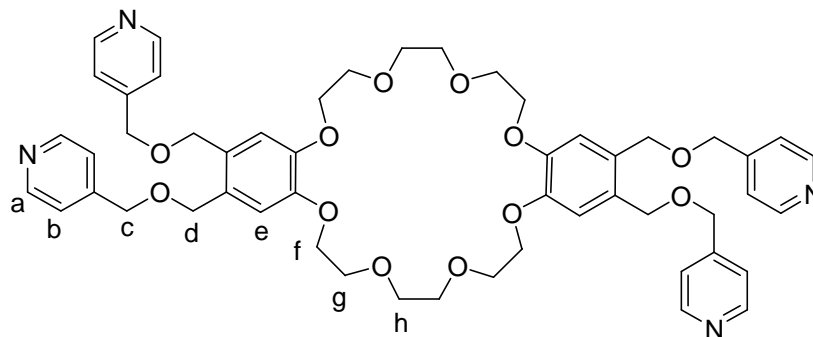


**Table 5.10** <sup>1</sup>H NMR spectroscopic data for T<sup>4</sup>P-DB24C8 in CD<sub>2</sub>Cl<sub>2</sub>.

Proton	δ (ppm)	Multiplicity	# protons	J (Hz)
<i>a</i>	8.44	d	8	$J_{ab}^3 = 4.5$
<i>b</i>	7.15	d	8	$J_{ba}^3 = 5.0$
<i>c</i>	4.43	s	8	-
<i>d</i>	4.69	s	8	-
<i>e</i>	6.88	s	4	-
<i>f</i>	4.06	m	8	-
<i>g</i>	3.78	m	8	-
<i>h</i>	3.68	m	8	-

**Table 5.11** <sup>1</sup>H NMR spectroscopic data for T<sup>4</sup>P-DB24C8 in CD<sub>3</sub>CN.

Proton	δ (ppm)	Multiplicity	# protons	J (Hz)
<i>a</i>	8.49	d	8	$J_{ab}^3 = 4.5$
<i>b</i>	7.28	d	8	$J_{ba}^3 = 5.0$
<i>c</i>	4.52	s	8	-
<i>d</i>	4.56	s	8	-
<i>e</i>	6.99	s	4	-
<i>f</i>	4.10	m	8	-
<i>g</i>	3.80	m	8	-
<i>h</i>	3.68	m	8	-

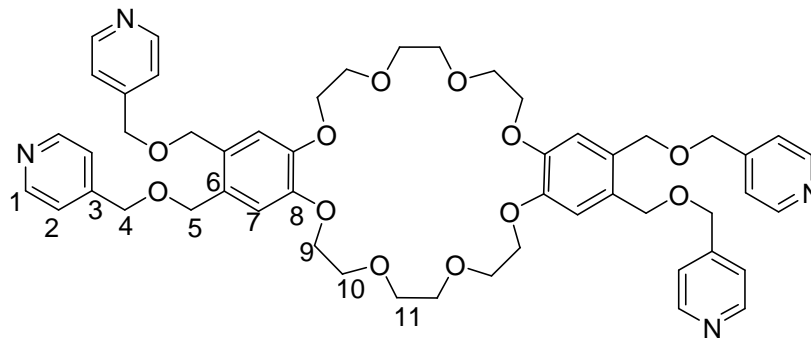


**Table 5.12**  $^{13}\text{C}$  NMR spectroscopic data for **T<sup>4</sup>P-DB24C8** in  $\text{CD}_2\text{Cl}_2$ .

Carbon	$\delta$ (ppm)
1	150.0
2	122.3
3	148.9
4	71.5
5	69.9
6	129.8
7	115.9
8	148.2
9	70.3
10	70.4
11	70.8

### Synthesis **T<sup>3</sup>P-DB24C8**

3-Pyridinemethanol (0.545 g, 4.99 mmol) was added to a solution of NaH (0.066 g, 2.74 mmol) and dry DMF (30 mL) and the mixture was stirred for 2 h at room temperature, after which time, **TB-DB24C8** (1.00 g, 1.21 mmol) was added and the mixture was refluxed for 36 h. The reaction mixture was then cooled to room temperature and water (4 mL) was added. The DMF was removed, the oil was dissolved in  $\text{CH}_2\text{Cl}_2$  (50 mL) and washed with 1 M  $\text{NaHCO}_3$  (3x50 mL) and  $\text{H}_2\text{O}$  (50 mL), and then dried with  $\text{MgSO}_4$ , filtered, and concentrated. Yield: 0.837 g (74%). MP: 82-85°C. **ESI-MS**:  $m/z$  [**T<sup>3</sup>P-DB24C8** +  $\text{Na}$ ] $^+$  calc. 955.4099, found 955.4147.

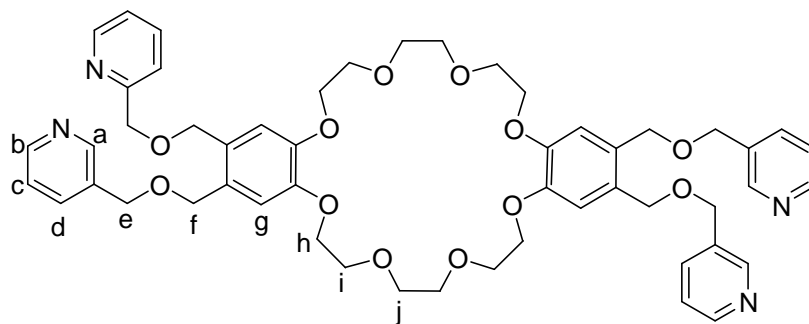


**Table 5.13**  $^1\text{H}$  NMR spectroscopic data for **T<sup>3</sup>P-DB24C8** in  $\text{CD}_2\text{Cl}_2$ .

Proton	$\delta$ (ppm)	Multiplicity	# protons	J (Hz)
<i>a</i>	9.04	s	4	-
<i>b</i>	8.54	d	4	$J^3_{bc} = 4.2$
<i>c</i>	7.24	dd	4	$J^3_{bc} = 5.1, J^3_{cd} = 7.4$
<i>d</i>	7.63	d	4	$J^3_{dc} = 7.6$
<i>e</i>	4.48	s	8	-
<i>f</i>	4.51	s	8	-
<i>g</i>	6.91	s	4	-
<i>h</i>	4.06	m	8	-
<i>i</i>	3.78	m	8	-
<i>j</i>	3.68	m	8	-

**Table 5.14**  $^1\text{H}$  NMR spectroscopic data for **T<sup>3</sup>P-DB24C8** in  $\text{CD}_3\text{CN}$ .

Proton	$\delta$ (ppm)	Multiplicity	# protons	J (Hz)
<i>a</i>	8.51	s	4	-
<i>b</i>	8.47	d	4	$J^3_{bc} = 4.2$
<i>c</i>	7.30	dd	4	$J^3_{bc} = 5.1, J^3_{cd} = 7.4$
<i>d</i>	7.67	d	4	$J^3_{dc} = 7.6$
<i>e</i>	4.51	s	8	-
<i>f</i>	4.49	s	8	-
<i>g</i>	6.96	s	4	-
<i>h</i>	4.09	m	8	-
<i>i</i>	3.78	m	8	-
<i>j</i>	3.66	m	8	-

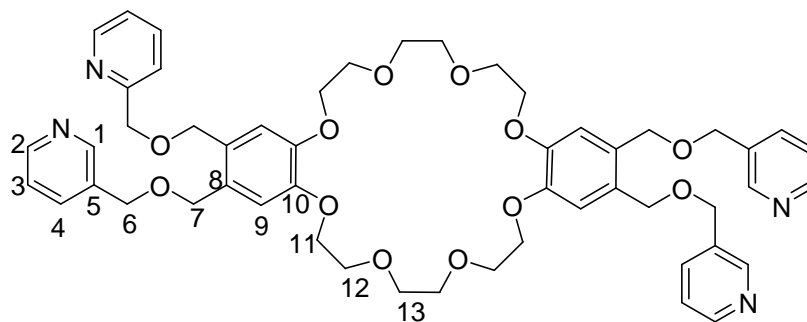


**Table 5.15**  $^{13}\text{C}$  NMR spectroscopic data for **T<sup>3</sup>P-DB24C8** in  $\text{CD}_2\text{Cl}_2$ .

Carbon	$\delta$ (ppm)
1	149.6
2	149.4
3	123.9
4	136.9
5	134.4
6	71.5
7	69.9
8	134.4
9	115.9
10	148.9
11	70.1
12	70.3
13	70.3

#### Synthesis [5.2-**TO-DB24C8**][ $\text{BF}_4$ ]<sub>2</sub>

[**3.5**][ $\text{BF}_4$ ]<sub>2</sub> (0.088 g, 0.154 mmol) was combined with **TO-DB24C8** (0.054 g, 0.050 mmol) and 3,5-dimethylbenzoic anhydride (0.390 g, 1.38 mmol) in acetonitrile/ $\text{CH}_2\text{Cl}_2$  (10 mL).  $^n\text{Bu}_3\text{P}$  (5 mol %) was added as a catalyst and the mixture was allowed to stir for 72 h at room temperature. The solvent was removed under reduced pressure and the product was stirred in anhydrous ethanol for 30 min. A column was done with  $\text{MeOH}/\text{CH}_2\text{Cl}_2$  (4:1), and solvent was removed. The product was dissolved in acetonitrile and isopropyl ether was allowed to diffuse into the solution. The product was yellow

solid. Yield 0.030 g (32%). ESI-MS:  $m/z$  [5.2cTO-DB24C8]<sup>2+</sup> calc. 869.3671, found 869.3685.

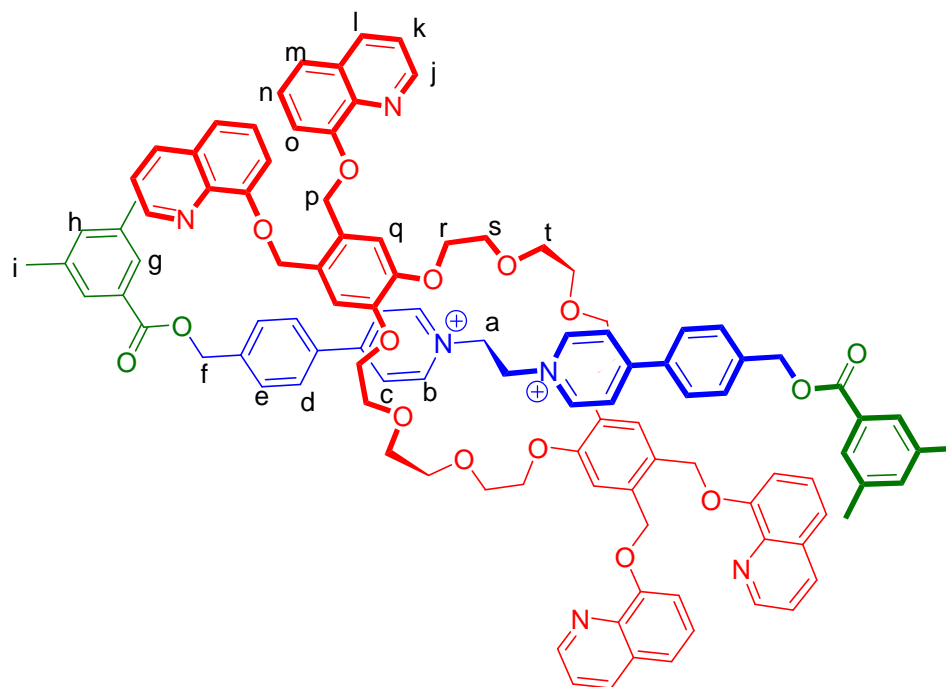


**Table 5.16** <sup>1</sup>H NMR spectroscopic data for [5.2cTO-DB24C8][BF<sub>4</sub>]<sub>2</sub> in CD<sub>3</sub>CN.

Proton	$\delta$ (ppm)	Multiplicity	# protons	J (Hz)
<i>a</i>	5.78	s	4	-
<i>b</i>	9.03	d	4	$J_{bc}^3 = 7.3$
<i>c</i>	8.20	d	4	$J_{cb}^3 = 6.7$
<i>d</i>	7.46	m	4	-
<i>e</i>	7.46	m	4	-
<i>f</i>	5.32	s	4	-
<i>g</i>	7.46	m	4	-
<i>h</i>	5.05	s	2	-
<i>i</i>	2.07	s	12	-
<i>j</i>	8.81	d	4	$J_{jk}^3 = 5.5$
<i>k</i>	7.37	t	4	$J_{kj}^3 = 7.7, J_{kl}^3 = 8.1$
<i>l</i>	8.03	d	4	$J_{lk}^3 = 6.7$
<i>m</i>	7.40	d	4	$J_{mn}^3 = 8.1$
<i>n</i>	6.67	d	4	$J_{nm}^3 = 8.2$
<i>o</i>	7.11	d	4	$J_{on}^3 = 7.5$
<i>p</i>	4.88	s	8	-
<i>q</i>	6.97	s	4	-
<i>r, s, t</i>	4.09 - 4.00	m	24	-



**Table 5.17**  $^1\text{H}$  NMR spectroscopic data for  $[\mathbf{5.2c}\text{-TO-DB24C8}][\text{BF}_4]_2$  in  $\text{CD}_2\text{Cl}_2$ .

Proton	$\delta$ (ppm)	Multiplicity	# protons	J (Hz)
<i>a</i>	5.50	s	4	-
<i>b</i>	9.08	d	4	$J_{bc}^3 = 7.3$
<i>c</i>	8.25	d	4	$J_{cb}^3 = 6.7$
<i>d</i>	7.43	m	4	-
<i>e</i>	7.43	m	4	-
<i>f</i>	5.25	s	4	-
<i>g</i>	7.57	m	4	-
<i>h</i>	7.13	s	2	-
<i>i</i>	2.21	s	12	-
<i>j</i>	8.71	d	4	$J_{jk}^3 = 5.5$
<i>k</i>	7.43	m	4	-
<i>l</i>	8.13	d	4	$J_{lm}^3 = 6.7$
<i>m</i>	7.43	d	4	$J_{mn}^3 = 8.1$
<i>n</i>	7.85	d	4	$J_{nm}^3 = 8.2$
<i>o</i>	7.17	d	4	$J_{on}^3 = 7.4$
<i>p</i>	5.01	s	8	-
<i>q</i>	7.03	s	4	-
<i>r, s, t</i>	4.15-3.96	m	24	-

Synthesis  $[\mathbf{5.2c}\text{-T}^4\text{P-DB24C8}][\text{BF}_4]_2$ 

$[\mathbf{3.5}][\text{BF}_4]_2$  (0.088 g, 1.54 mmol) was combined with  $\text{T}^4\text{P-DB24C8}$  (0.072 g, 0.077 mmol) and 3,5-dimethylbenzoic anhydride (0.032 g, 0.524 mmol) in acetonitrile/ $\text{CH}_2\text{Cl}_2$  (10 mL).  $^n\text{Bu}_3\text{P}$  (5 mol %) was added as a catalyst and the mixture was allowed to stir for 72 h at room temperature. The solvent was removed under pressure and the product was stirred in anhydrous ethanol for 30 min. The product was dissolved in acetonitrile and isopropyl ether was allowed to diffuse into the solution. The product was yellow solid. Yield 0.035 g (26%). **ESI-MS:**  $m/z$   $[\mathbf{5.2c}\text{-H}+\text{T}^4\text{P-DB24C8}]^{3+}$  calc. 531.9138, found 531.9134.

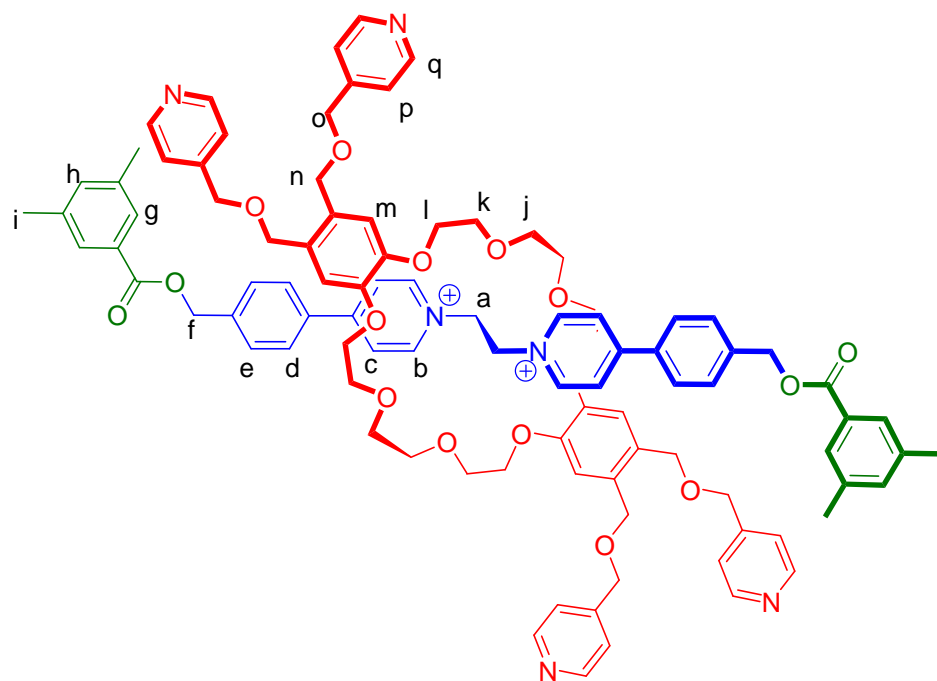


**Table 5.18**  $^1\text{H}$  NMR spectroscopic data for  $[5.2\text{-C-T}^4\text{P-DB24C8}][\text{BF}_4]_2$  in  $\text{CD}_3\text{CN}$ .

Proton	$\delta$ (ppm)	Multiplicity	# protons	J (Hz)
<i>a</i>	5.46	s	4	-
<i>b</i>	9.04	d	4	$J_{bc}^3 = 6.9$
<i>c</i>	7.98	d	4	$J_{cb}^3 = 7.0$
<i>d</i>	7.51	d	4	$J_{de}^3 = 8.3$
<i>e</i>	7.58	d	4	$J_{ed}^3 = 8.2$
<i>f</i>	5.36	s	4	-
<i>g</i>	7.69	s	4	-
<i>h</i>	7.22	s	2	-
<i>i</i>	2.36	s	12	-
<i>q</i>	8.48	d	8	$J_{jk}^3 = 5.0$
<i>p</i>	7.17	d	8	$J_{kj}^3 = 5.0$
<i>o</i>	4.29	s	8	-
<i>n</i>	4.29	s	8	-
<i>m</i>	6.70	s	4	-
<i>l,k,j</i>	4.16 – 4.03	m	24	-

Synthesis [5.2-**T<sup>3</sup>P-DB24C8**][BF<sub>4</sub>]<sub>2</sub>

[3.5][BF<sub>4</sub>]<sub>2</sub> (0.088 g, 1.54 mmol) was combined with **T<sup>3</sup>P-DB24C8** (0.072 g, 0.077 mmol) and 3,5-dimethylbenzoic anhydride (0.032 g, 0.524 mmol) in acetonitrile/CH<sub>2</sub>Cl<sub>2</sub> (10 mL). <sup>n</sup>Bu<sub>3</sub>P (5 mol %) was added as a catalyst and the mixture was allowed to stir for 72 h at room temperature. The solvent was removed under pressure and the product was stirred in anhydrous ethanol for 30 min. A column was done with MeOH/CH<sub>2</sub>Cl<sub>2</sub> (4:1), and solvent was removed. The product was dissolved in acetonitrile and isopropyl ether was allowed to diffuse into the solution. The product was yellow solid. Yield 0.040 g (30%). **ESI-MS**: *m/z* [5.2-**H+T<sup>3</sup>P-DB24C8**]<sup>3+</sup> calc. 531.9138, found 531.9134.

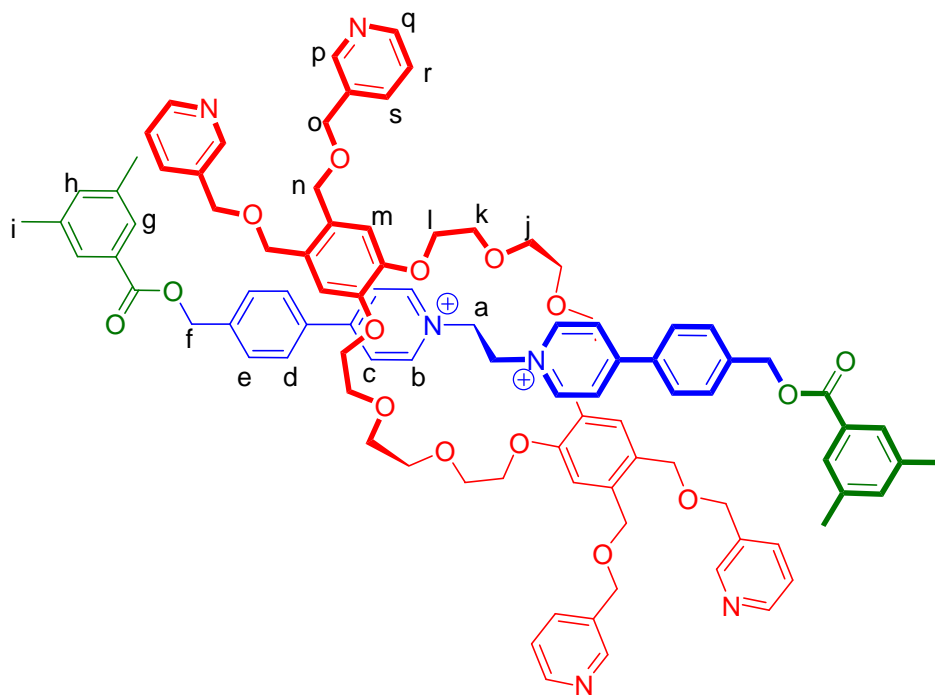


**Table 5.19**  $^1\text{H}$  NMR spectroscopic data for  $[\mathbf{5.2cT^3P-DB24C8}][\text{BF}_4]_2$  in  $\text{CD}_3\text{CN}$ .

Proton	$\delta$ (ppm)	Multiplicity	# protons	J (Hz)
<i>a</i>	5.46	s	4	-
<i>b</i>	9.04	d	4	$J_{bc}^3 = 6.8$
<i>c</i>	7.98	d	4	$J_{cb}^3 = 6.8$
<i>d</i>	7.58	d	4	$J_{de}^3 = 8.0$
<i>e</i>	7.58	d	4	$J_{ed}^3 = 8.0$
<i>f</i>	5.37	s	4	-
<i>g</i>	7.70	s	4	-
<i>h</i>	7.28	s	2	-
<i>i</i>	2.35	s	12	-
<i>p</i>	8.46	s	4	-
<i>q</i>	8.49	d	4	$J_{kl}^3 = 4.4$
<i>r</i>	7.29	m	4	-
<i>s</i>	7.49	d	4	$J_{lm}^3 = 8.2$
<i>m</i>	6.68	s	8	-
<i>o</i>	4.28	s	8	-
<i>n</i>	4.28	s	4	-
<i>l,k,j</i>	4.03 – 4.08	m	24	-

**Synthesis**  $[(\text{Cd}(\text{MeCN})_2(\text{H}_2\text{O})_2)(\mathbf{5.2cTO-DB24C8})][\text{BF}_4]_6$ 

To a solution of  $[\mathbf{5.2cTO-DB24C8}][\text{BF}_4]_2$  (30 mg) was dissolved in 1 mL of  $\text{CH}_3\text{CN}$  was added to  $\text{Cd}(\text{BF}_4)_2 \cdot 6 \text{H}_2\text{O}$  (9 mg) and the mixture was stirred at room temperature overnight. Slow diffusion of isopropyl ether into the solution gave brown crystals. Yield 0.054 g (99%). **ESI-MS:**  $m/z$   $[(\mathbf{5.2cTO-DB24C8})]^{2+}$  calc. 869.3670, found 869.3115.

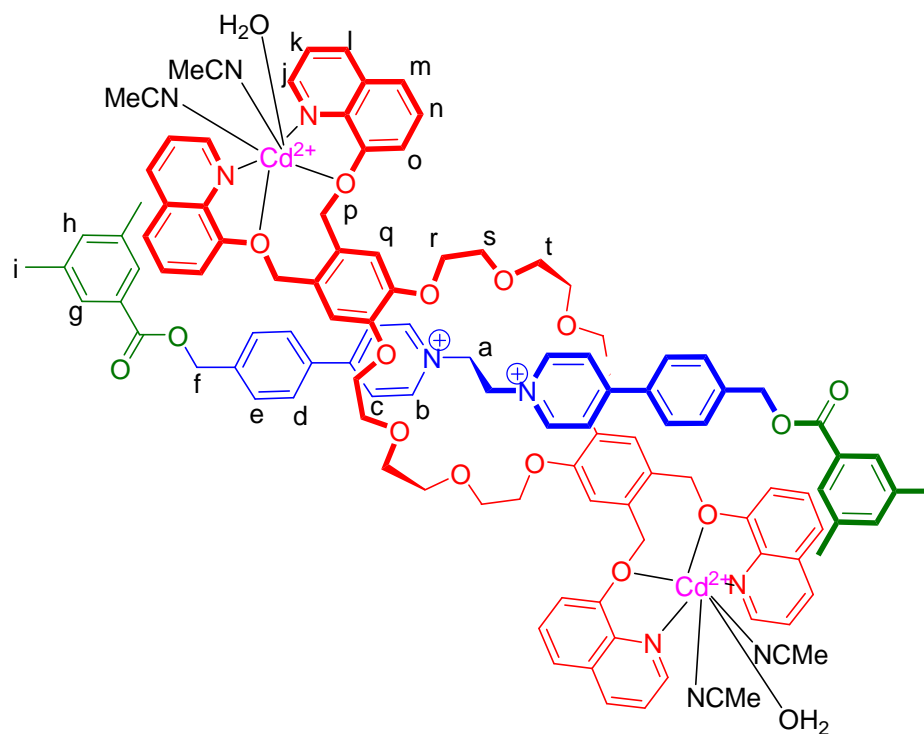


**Table 5.20**  $^1\text{H}$  NMR spectroscopic data for  $[(\text{Cd}(\text{MeCN})_2(\text{H}_2\text{O})_2(5.2\text{cTO-DB24C8}))]^{6+}$  in  $\text{CD}_3\text{CN}$ .

Proton	$\delta$ (ppm)	Multiplicity	# protons	J (Hz)
<i>a</i>	4.97	m	2	-
<i>b</i>	9.02	d	12	$J^3_{bc} = 5.4$
<i>c</i>	8.67	d	4	$J^3_{cb} = 7.9$
<i>d</i>	7.34	d	4	$J^3_{de} = 7.4$
<i>e</i>	7.41	d	4	$J^3_{ed} = 7.1$
<i>f</i>	4.97	s	4	-
<i>g</i>	7.50	s	4	-
<i>h</i>	7.16	s	4	-
<i>i</i>	2.26	s	4	-
<i>j</i>	9.13	d	4	$J^3_{jk} = 3.3$
<i>k</i>	7.67	t	4	$J^3_{kj} = 7.8, J^3_{kl} = 8.0$
<i>l</i>	7.88	m	4	-
<i>m</i>	7.73	d	4	$J^3_{mn} = 7.9$
<i>n</i>	7.88	m	4	-
<i>o</i>	7.00	d	4	$J^3_{on} = 6.6$
<i>p</i>	4.97	m	8	-
<i>q</i>	6.93	s	4	-
<i>r, s, t</i>	4.17-4.05	m	24	-

Synthesis  $[\text{Cd}_2\text{Cl}_4(\text{H}_2\text{O})_4(\mathbf{5.2cT^3P-DB24C8})][\text{BF}_4]_2$

To a solution of  $[\mathbf{5.2cT^3P-DB24C8}][\text{BF}_4]_2$  (30 mg) was dissolved in 1 mL of  $\text{CH}_3\text{CN}$  was added to  $\text{Cd}(\text{BF}_4)_2 \cdot 6 \text{H}_2\text{O}$  (9 mg) and the mixture was stirred at room temperature overnight. Slow diffusion of isopropyl ether into the solution gave yellow crystals in quantitative yield.

#### Reference:

1. a) Loeb, S. J. *Organic Nanostructure*; Wiley: Weinheim 2003, pp 33. b) Loeb, S. J. *Chem. Commun.* **2005**, 1511.
2. Logacheva, N. M.; Baulin, V. E.; Tsivadze, A. Y.; Pyatova, E. N.; Ivanova, I. S.; Velikodny, Y. A.; Chernyshev, V. V. *Dalton Trans.*, **2009**, 2482.
3. Han, M.; Zhang, H.; Yang, L.; Jiang, Q.; Liu, Y. *Org. Lett.* **2008**, *10*, 5557. b) Ding, Z.; Zhang, Y.; Teng, X.; Liu, Y. *J. Org. Chem.* **2011**, *76*, 1910.
4. Ballardini, R.; Balzani, V.; Clemente-Leon, M.; Credi, A.; Gandolfi, M. T.; Ishow, E.; Perkins, J.; Stoddart, J. F.; Tseng, H.; Wenger, S. *J. Am. Chem. Soc.* **2002**, *124*, 12786.
5. Lazarides, T.; Barbieri, A.; Sabatini, C.; Barigelletti, F.; Adams, H.; Ward, M. D. *Inorg. Chem. Acta*, **2007**, *360*, 814.
6. Ghosh, K.; Yang, H.; Northop, B. H.; Lyndron, M. M.; Zheng, Y.; Muddiman, D. C.; Stang, P. J. *J. Am. Chem. Soc.* **2008**, *130*, 5320.
7. Al-Mandhary, M. R.; A., Steel, P. J. *Eur. J. Inorg. Chem.*, **2004**, 329. b) Al-Mandhary, M. R. A.; Steel, P. J. *Inorg. Chem. Commun.*, **2002**, *5*, 954.
8. Mercer, D. J. W.; Vukotic, N.; Loeb, S. J., *Chem. Commun.* **2011**, *47*, 896.
9. Siaw-Lathey, C.; Zhang, H.; Son, D. Y. *Polyhedron*, **2005**, *24*, 785.
10. Nakamura, Y.; Asami, A.; Ogawa, T.; Inokuma, S.; Nishimura, J. *J. Am. Chem. Soc.* **2002**, *124*, 429.
11. a) Makita, Y.; Kilara, N.; Takata, T. *J. Org. Chem.* **2008**, *73*, 9245. b) Mercer, D. J. W.; Vella, S. J.; Guertin, L.; Sudan, N. D.; Tiburico, J.; Vukotic, N.; Wisner, J. A.; Loeb, S. J. *Eur. J. Org. Chem.* **2011**, *9*, 1763.
12. Guertin, L. B. Sc. Thesis, University of Windsor, Windsor, ON, 2008.

# Chapter 6

## [2]Rotaxane Ligands with Donors on Both the Axle and Wheel

### 6.1 Introduction

The focus of this chapter is to combine the “rotaxane as a ligand” concepts from chapters 2 and 5 to design a sophisticated [2]rotaxane with coordinating groups appended to *both* the axle and the wheel. This could, in an ideal metal-ligand system, give rise to two independent coordination networks linked only by the interpenetration of the ligand. In particular, the focus will be on a design in which the ligands on the axle could lead to a 1-periodic coordination polymer and the ligands on the wheel could form a 2-periodic coordination network. To date, there are no known examples of this type of coordination polymer or metal organic framework material.

Recently we have shown that a terpyridine ligand can be utilized as the stopper of a [2]rotaxane to form a 1-periodic coordination polymer.<sup>1</sup> However, due to unseen problems with synthesis such a chelating group could not be used in this case. In place of the terpyridine group, the bis(2-pyridylmethyl)amine ligand as a stopper was developed; Figure 6.1.

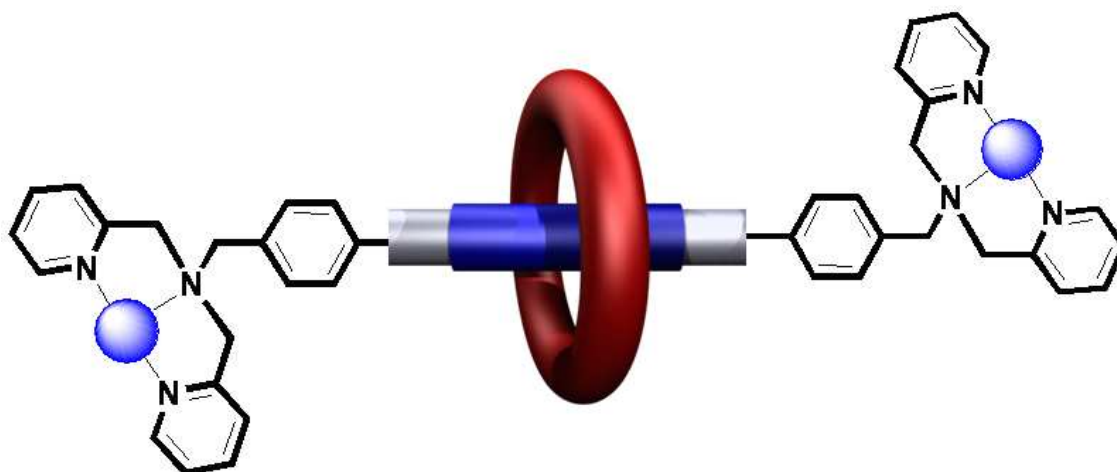


**Figure 6.1** The new stopper based [2]rotaxane with bis(2-pyridylmethyl)amine.

Recently, Leigh developed a [2]rotaxane that contains two bis(2-pyridylmethyl)amine (**BPMA**) chelating sites, one attached to the rotaxane macrocycle and one to the rotaxane thread. This was synthesized using a hydrogen bond-templated clipping strategy; Figure 6.2.<sup>2</sup>

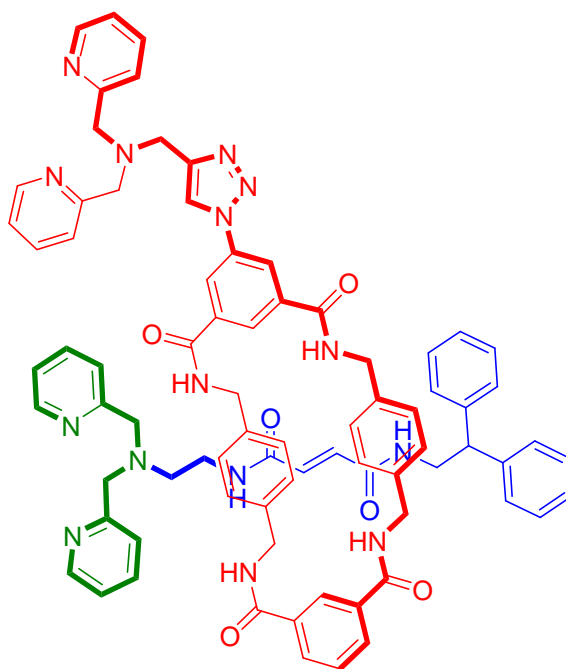


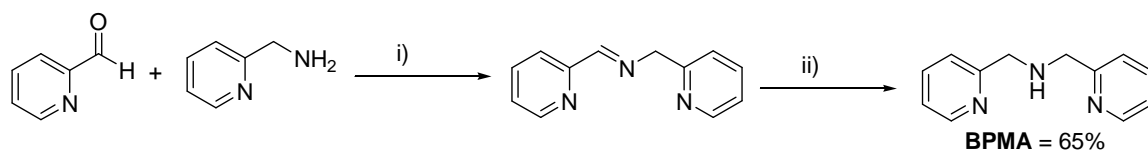
**Figure 6.2** Leigh “combo” chelating rotaxane.<sup>3</sup>

## 6.2 Results and Discussion

### 6.2.1 Synthesis of Bis(2-pyridylmethyl)amine

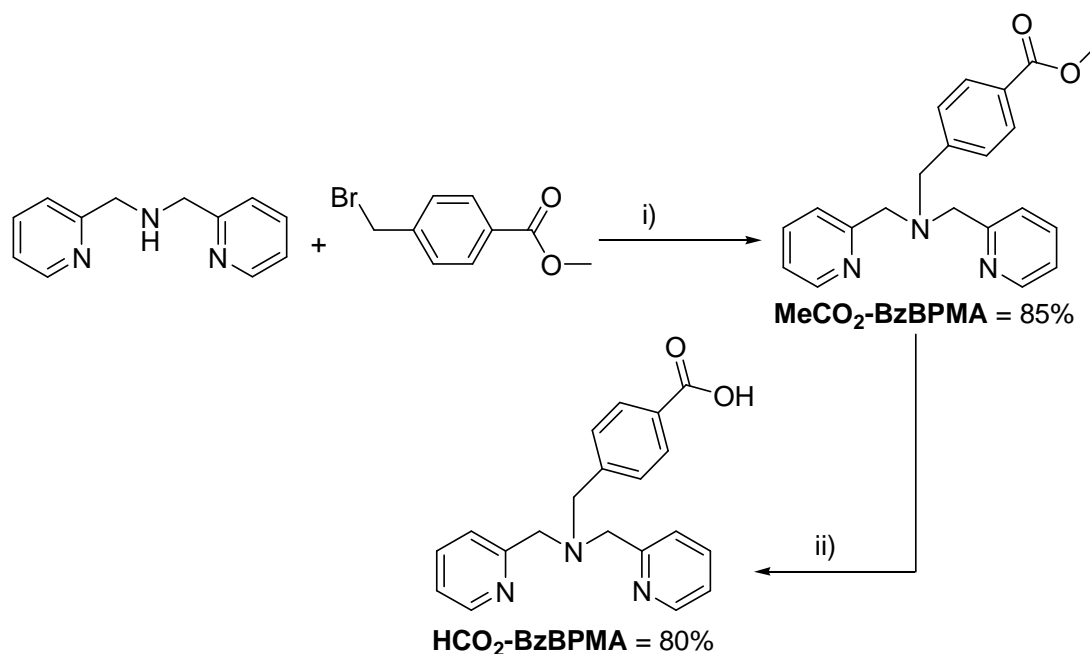
The ligand **BPMA** was chosen as the ligand unit for eventual inclusion as the stopper for these new type of [2]rotaxane ligands. The synthesis of **BPMA** proceeded smoothly via the condensation of pyridine-2-carboxaldehyde with 2-aminomethylpyridine, to form the imine. Subsequent reduction of the imine, *in situ* with NaBH<sub>4</sub> produced the desired compound **BPMA** as previously reported; Scheme 6.1.<sup>3</sup>





**Scheme 6.1** i) EtOH, ii) NaBH<sub>4</sub>, reflux.

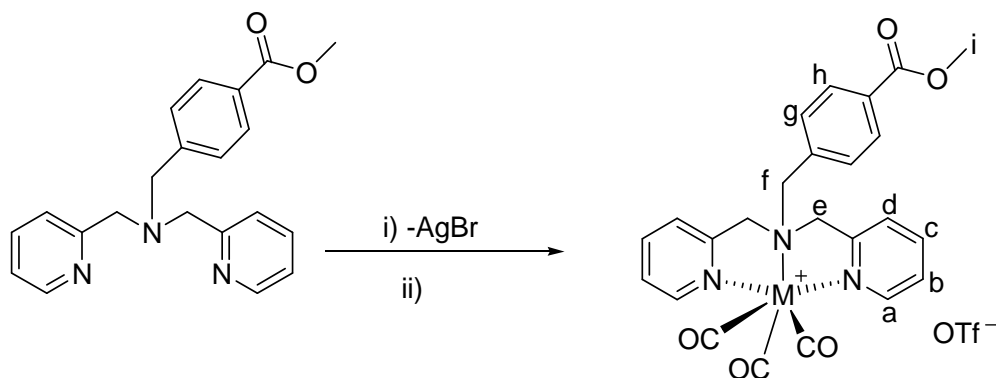
Alkylation of the secondary amine occurred via a literature procedure, in moderate yield with methyl *p*-(bromomethyl)benzoate, and triethylamine to produce ((*p*-methylbenzoyl)benzyl)bis(2-pyridylmethyl)amine (**MeCO<sub>2</sub>BzBPMA**). Hydrolysis of the ester was carried with NaOH in MeOH to produce *N*-(*p*-carboxybenzyl)bis(2-pyridylmethyl)amine (**HCO<sub>2</sub>-BzBPMA**), as previously reported; Scheme 6.2.<sup>4</sup>



**Scheme 6.2** i) Et<sub>3</sub>N, THF, reflux, 2h ii) 2M NaOH<sub>(aq)</sub>, MeOH.

Similar ligands have been studied in previous years to coordinate to number of metals such as ruthenium(II), osmium(II), and group 10 and 12 transition metals.<sup>5</sup> The methyl ester ligand was studied with Cu(II), Zn(II), and the metal carbonyl fragments Mo(CO)<sub>6</sub>,<sup>5</sup> Mn(CO)<sub>5</sub>Br and Re(CO)<sub>5</sub>Br. These complexes with **MeCO<sub>2</sub>-BzBPMA** were

generally prepared by reacting equimolar amounts of both  $M(\text{CO})_5\text{Br}$  ( $M = \text{Mn}$  or  $\text{Re}$ ) and  $\text{AgOTf}$  in refluxing methanol in the presence of the ligand; Scheme 6.3.<sup>5</sup>



**Scheme 6.3** i)  $M(\text{CO})_5\text{Br}$ ,  $\text{AgOTf}$ ,  $\text{MeOH}$ , 60 min ( $M = \text{Mn}$  or  $\text{Re}$ ) ii)  $[\text{Re}(\text{CO})_5(\text{MeOH})][\text{OTf}]$ ,  $\text{MeCO}_2\text{-BzBPMA}$ , 60 min.

The IR spectrum of  $[\text{Re}(\text{CO})_3(\text{MeCO}_2\text{-BzBPMA})][\text{OTf}]$  was recorded in a KBr pellet and showed the characteristic bands of the ligand as well as two bands of a nearly  $C_{3v}$ -symmetrical  $\text{Re}(\text{CO})_3$  fragment, with the doubly degenerate  $E$  band slightly split ( $2029, 1949 \text{ cm}^{-1}$ ).

The  $^1\text{H-NMR}$  spectrum of  $[\text{Re}(\text{CO})_3(\text{MeCO}_2\text{-BzBPMA})][\text{OTf}]$  in  $\text{CD}_3\text{CN}$  is summarized in Table 6.1. Metal coordination was observed by higher chemical shifts for the proton adjacent to the pyridine (**a**) and splitting of the methylene groups next to the amine nitrogen (**e**) by  $-0.31$  and  $-1.18/-0.46$  ppm respectively. The ESI-MS also confirmed coordination resulting in observation of the parent ion as  $[\text{Re}(\text{CO})_3(\text{MeCO}_2\text{-BzBPMA})]^+$  at  $618.1031 \text{ m/e}$ .

**Table 6.1** Comparison of the chemical shifts of free ligand MeCO<sub>2</sub>-BzBPMA and metal [Re(CO)<sub>3</sub>(MeCO<sub>2</sub>-BzBPMA)][OTf].

Proton	MeCO <sub>2</sub> -BzBPMA	[Re(CO) <sub>3</sub> (MeCO <sub>2</sub> -BzBPMA)] <sup>+</sup>
<i>a</i>	8.47	8.78 (-0.31)
<i>b</i>	7.20	7.28 (-0.08)
<i>c</i>	7.69	7.83 (-0.14)
<i>d</i>	7.57	7.79 (-0.22)
<i>e</i>	3.75	4.93 (-1.18), 4.31 (-0.46)
<i>f</i>	3.73	4.97 (-1.24)
<i>g</i>	7.54	7.34 (0.20)
<i>h</i>	7.94	8.14 (-0.20)
<i>i</i>	3.92	3.92 (0.00)

Single crystals of the Mn(I) complex were grown by slow diffusion of isopropyl ether into a solution of MeCN. The cationic portion of the structure, [Mn(CO)<sub>3</sub>(MeCO<sub>2</sub>-BzBPMA)]<sup>+</sup> is shown in Figure 6.3. The manganese centre is in a slightly distorted octahedral coordination environment, with the N<sub>3</sub> ligand and the three carbonyl ligands coordinating facially. The angles between the Mn(I) and the carbonyl ligands are bent towards each other such that the C(2)-Mn(1)-C(3) angle is only 86.3° and the other angles are significantly different less 180°; Table 6.2 shows selected bond lengths and angles. Although no related Mn(CO)<sub>x</sub> structures were found in the CCDC, a related Re(CO)<sub>3</sub> complex was found to have the bond angles in good agreement with this Mn(I) complexes.<sup>6,7</sup>

**Table 6.2** Bond lengths(Å) and bond angles(°) for [Mn(CO)<sub>3</sub>(MeCO<sub>2</sub>-BzBPMA)]<sup>+</sup>.

Mn-N(1)	2.06(2)	N(1)-Mn-N(2)	83.4(5)
Mn-N(2)	2.04(2)	N(2)-Mn-N(3)	82.3(6)
Mn-N(3)	2.12(2)	N(1)-Mn-N(3)	80.5(5)
Mn-C(1)	1.83(2)	C(1)-Mn-C(2)	88.7(6)
Mn-C(2)	1.82(2)	C(2)-Mn-C(3)	86.3(8)
Mn-C(3)	1.82(2)	C(1)-Mn-C(3)	91.7(6)
C(1)-O(1)	1.13(1)	Mn-C(1)-O(1)	178.2(9)
C(2)-O(2)	1.14(1)	Mn-C(2)-O(2)	173.4(11)
C(3)-O(3)	1.14(1)	Mn-C(3)-O(3)	176.5(12)

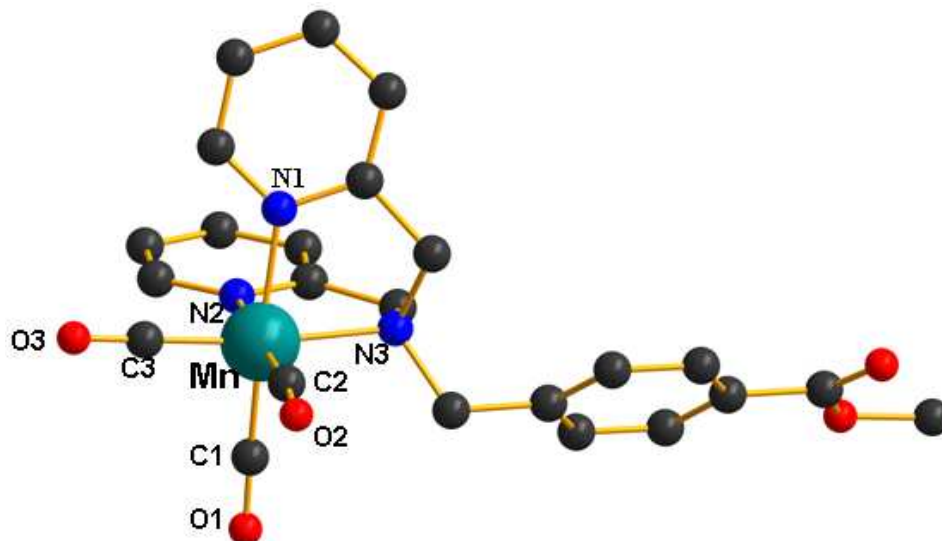
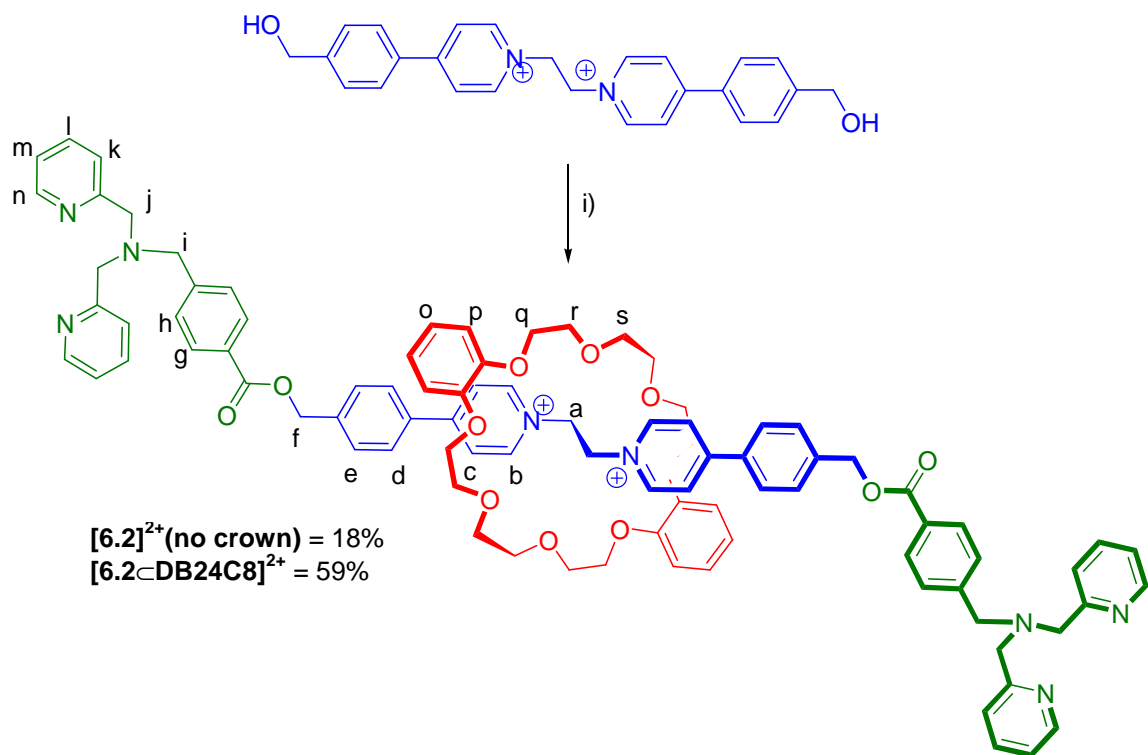


**Figure 6.3** A ball-stick representation of the cationic portion of the X-ray crystal structure of  $[(\text{Mn}(\text{CO})_3(\text{MeCO}_2\text{-BzBPMA}))]^+$ . All hydrogen atoms, all anions and all solvent molecules have been omitted for clarity. (Mn = blue-gray, O = red, N = blue, C = black, ligands bonds = gold).

### 6.2.2 Synthesis of a BPMA stoppered [2]rotaxane

The [2]rotaxane were synthesized in good yield through esterification of the [2]pseudorotaxane formed between  $[\mathbf{3.5}][\text{OTf}]_2$ , **DB24C8** with **HCO<sub>2</sub>-BzBPMA** and *N,N'*-Dicyclohexylcarbodiimide (DCC) in MeCN at room temperature; Scheme 6.4.<sup>8,9</sup>



**Scheme 6.4 i)** DB24C8, HCO<sub>2</sub>-BzBPMA, DCC, <sup>n</sup>Bu<sub>3</sub>P (cat.), MeCN, RT for 72 h.

The <sup>1</sup>H NMR spectrum of compounds [6.2][OTf]<sub>2</sub> and [6.2⊂DB24C8][OTf]<sub>2</sub> in CD<sub>3</sub>CN are shown in Figure 6.4 and some of the major peaks are summarized in Table 6.3. The spectrum of the [2]rotaxane showed evidence supporting the various supramolecular interactions such as hydrogen bonding and π-π stacking. Hydrogen bonding between the ethylene (**a**) and α-pyridinium (**b**) protons of the axle and the polyether oxygen atoms of the macrocycle is evidenced by a downfield shift of the signals for **a** and **b** of 0.32 and 0.18 respectively.

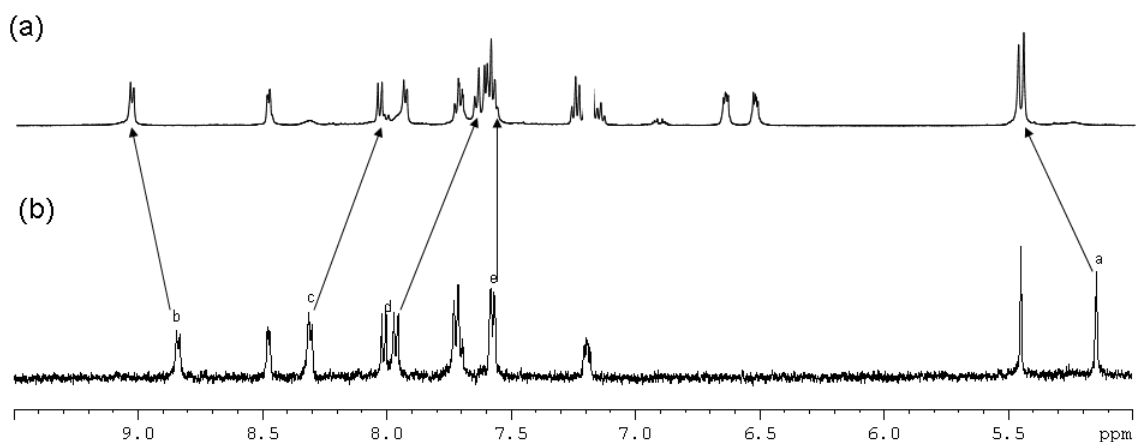


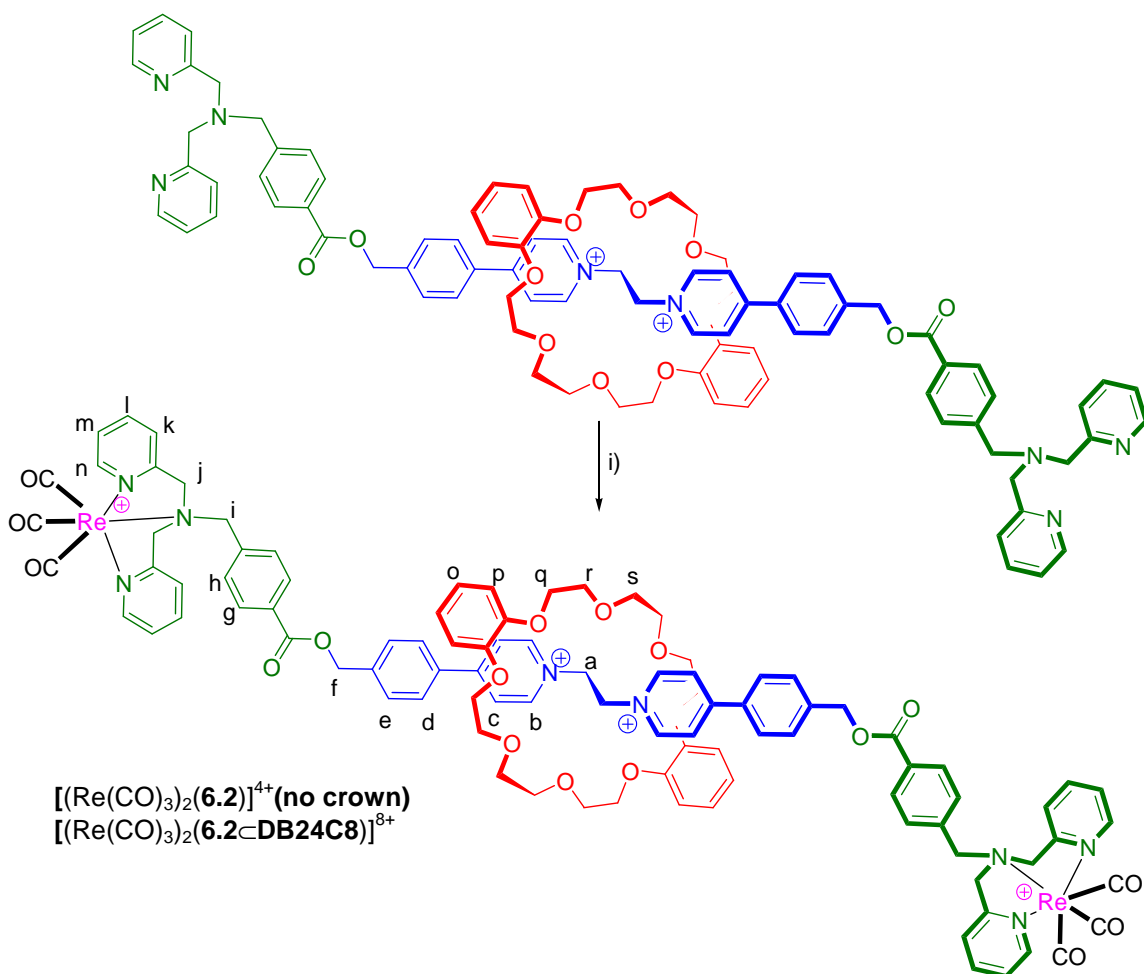
**Figure 6.4** Comparison of the  $^1\text{H}$  NMR shifts of (a)  $[\mathbf{6.2-DB24C8}][\text{OTf}]_2$ , and (b)  $[\mathbf{6.2}][\text{OTf}]_2$  in  $\text{CD}_3\text{CN}$  at 500 MHz.

**Table 6.3** Comparison of the chemical shifts of the dumbbell  $[\mathbf{6.2}][\text{OTf}]_2$  and the [2]rotaxane,  $[\mathbf{6.2-DB24C8}][\text{OTf}]_2$ .

Protons	$[\mathbf{6.2}]^{2+}$	$[\mathbf{6.2-DB24C8}]^{2+}$
<i>a</i>	5.15	5.44 (0.32)
<i>b</i>	8.84	9.02 (0.18)
<i>c</i>	8.31	8.03 (-0.28)
<i>d</i>	7.96	7.65 (-0.31)
<i>e</i>	7.58	7.60 (0.02)

In addition to resonances which are diagnostic of the capping process and rotaxane formation in general. The presence of the singlet at 5.47 ppm for **f** also indicated acylation of the alcohol had occurred. The  $^1\text{H}$  NMR spectra reveals the presence of two separate resonances for **o** and **p** at 6.65 and 6.56 ppm, compared to 6.93 ppm for free **DB24C8**, are indicative of  $\pi$ -stacking between pairs of electron-poor pyridinium and electron-rich crown aromatic rings. The ESI-MS confirmed the interlocked nature of the complex, with the loss of two counter ions,  $[\mathbf{6.2-DB24C8}]^{2+}$  at 738.3438 *m/e*.

To investigate the coordination ability of this unique ligand, a Re(I) complex was prepared. Scheme 6.5, shows generally how the monomer looks in solution when two equivalents of  $[\text{Re}(\text{CO})_5(\text{MeOH})][\text{OTf}]$  were reacted with  $[\mathbf{6.2-DB24C8}][\text{OTf}]_2$ .



**Scheme 6.5** i)  $[\text{Re}(\text{CO})_5(\text{MeOH})][\text{OTf}]$  in MeOH, reflux, 1 hr.

The  $^1\text{H}$  NMR spectrum of the Re(I) rotaxane complex was recorded in  $\text{CD}_3\text{CN}$  revealed upfield shifts of the protons **n-j**. Proton **n**, in complex  $[(\text{Re}(\text{CO})_3)_2(\mathbf{6.2}\text{-DB24C8})]^{4+}$  shifts from 8.78 ppm for the uncomplexed [2]rotaxane to 8.48 ppm when coordinated to a rhenium(I) centre. Also seen is the splitting of the methylene proton **j** at 4.94 and 4.32 ppm. Conventional 2D NMR techniques ( $^1\text{H} - ^1\text{H}$  COSY) were also employed to help assign the observed resonances. The differences between the [2]rotaxane ligand and the corresponding rhenium(I) complex are summarized in Table 6.4. The ESI-MS of the metal complex showed the loss of all the counter ions to give  $[(\text{Re}(\text{CO}_3))_2(\mathbf{6.2}\text{-DB24C8})]^{4+}$  at 504.6403  $m/e$ .

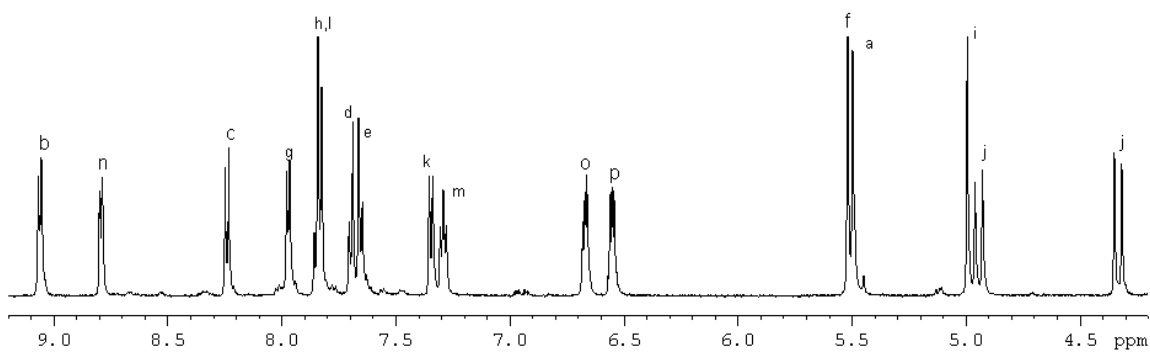


**Figure 6.5**  $^1\text{H}$  NMR spectrum of  $[(\text{Re}(\text{CO})_3)_2(\mathbf{6.2-DB24C8})][\text{OTf}]_4$  at 500MHz.

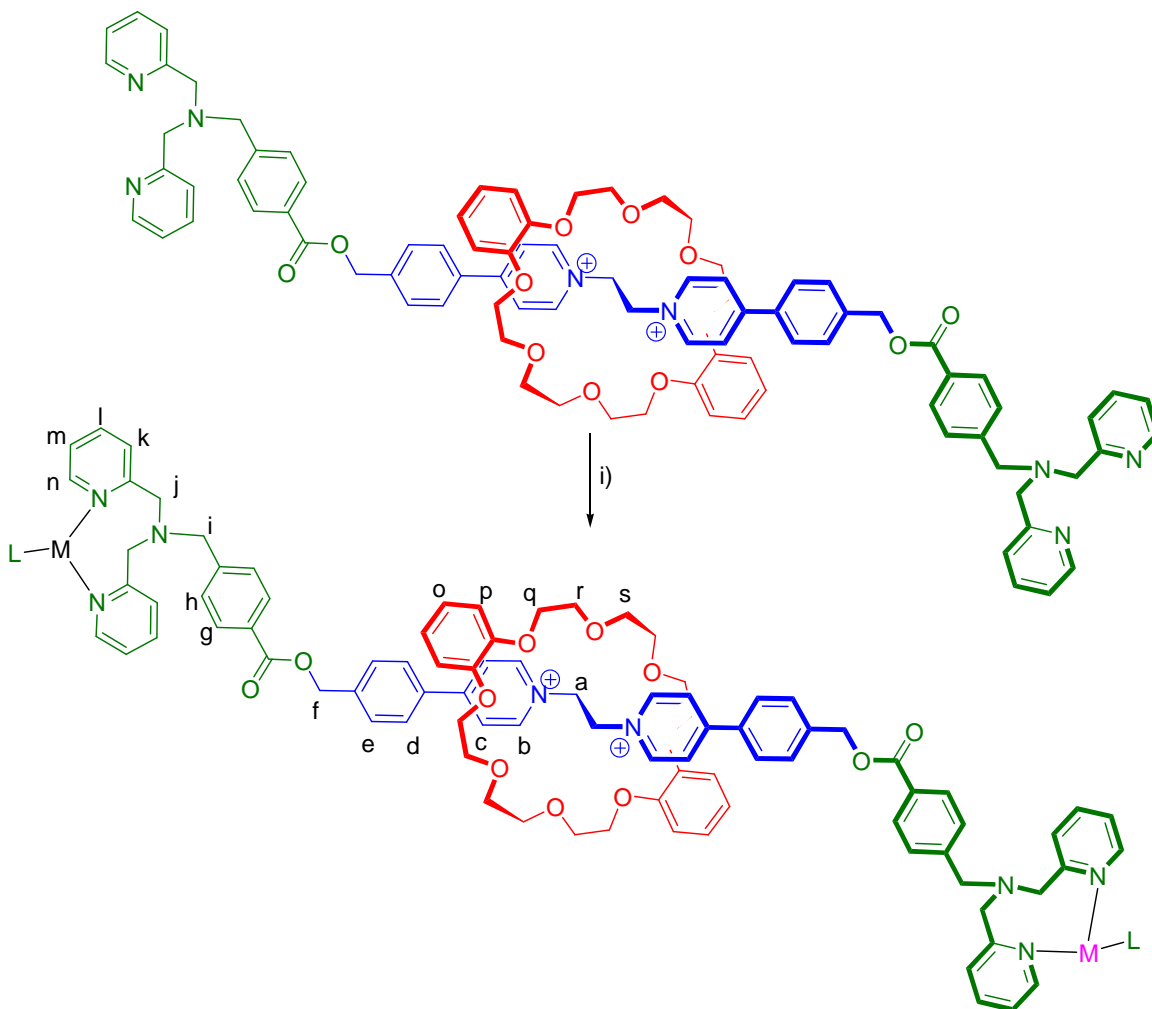
**Table 6.4** A comparison of the  $^1\text{H}$  NMR chemical shifts for dumbbell  $[\mathbf{6.2}][\text{OTf}]_2$ , [2]rotaxane ligand  $[\mathbf{6.2-DB24C8}][\text{OTf}]_2$  and complex  $[(\text{Re}(\text{CO})_3)_2(\mathbf{6.2})]^{4+}$ ,  $[(\text{Re}(\text{CO})_3)_2(\mathbf{6.2-DB24C8})][\text{OTf}]_4$ .

proton	$[\mathbf{6.2}]^{2+}$	$[(\text{Re}(\text{CO})_3)_2(\mathbf{6.2})]^{4+}$	$[\mathbf{6.2-DB24C8}]^{2+}$	$[(\text{Re}(\text{CO})_3)_2(\mathbf{6.2-DB24C8})]^{4+}$
<i>a</i>	5.15	5.12 (-0.03)	5.44	5.50 (0.06)
<i>b</i>	8.84	8.72 (-0.12)	9.02	9.06 (0.04)
<i>c</i>	8.31	8.35 (0.04)	8.03	8.24 (0.18)
<i>d</i>	7.96	8.01 (0.05)	7.65	7.70 (0.05)
<i>e</i>	7.58	7.77 (0.19)	7.60	7.66 (0.06)
<i>f</i>	5.45	5.52 (0.07)	5.47	5.52 (0.05)
<i>g</i>	8.01	8.22 (0.21)	7.94	7.97 (0.03)
<i>h</i>	7.71	7.82 (0.11)	7.60	7.83 (0.23)
<i>i</i>	3.75	4.98 (1.23)	3.79	4.99 (1.20)
<i>j</i>	3.75	4.93 (1.18), 4.31 (0.56)	3.79	4.94 (1.15), 4.33 (0.54)
<i>k</i>	7.58	7.33 (-0.25)	7.60	7.35 (-0.25)
<i>l</i>	7.71	7.82 (0.11)	7.73	7.83 (0.10)
<i>m</i>	7.20	7.28 (0.08)	7.21	7.29 (0.08)
<i>n</i>	8.48	8.79 (0.31)	8.49	8.79 (0.30)
<i>o</i>	-	-	6.65	6.67 (0.02)
<i>p</i>	-	-	6.53	6.55 (0.02)

To investigate the coordination ability of this unique rotaxane ligand, silver(I) and cadmium(II) were investigated as these metals are known to form complexes with this ligand.<sup>10,11</sup> Scheme 6.6 shows generally how the monomer would look in solution when two equivalents of  $[\text{Ag}][\text{OTf}]$ , or  $[\text{Cd}(\text{H}_2\text{O})_6][\text{BF}_4]_2$  in MeCN were added to  $[\mathbf{6.2-DB24C8}][\text{OTf}]_2$ . The coordination of Ag(I) with the **BPMA** results in the formation of a dimeric species with two Ag(I) coordinating to two **BPMA** ligands



through the pyridyl and amine groups and a Ag(I)⋯Ag(I) interaction.<sup>10</sup> A similar dimer still exists if the amine group is substituted, and does not depend on solvent or counter ions.<sup>10b</sup> NMR data supports that the dimer exists but with the loss of the amine coordination and the Ag(I)⋯Ag(I) interaction but is replaced with either solvent or counter-ion filling the coordination sphere.



**Scheme 6.6** i) 2 equivalents of Ag(OTf) or [Cd(H<sub>2</sub>O)<sub>6</sub>][BF<sub>4</sub>]<sub>2</sub> in MeCN for 24 h at RT.

The <sup>1</sup>H NMR spectrum for the Ag(I) complex revealed downfield shifts of the protons **n-j**. Proton **n**, in complex [(Ag)<sub>x</sub>(**6.2cDB24C8**)]<sup>4+</sup> shifts from 8.48 ppm for the uncomplexed [2]rotaxane to 8.55 ppm when coordinated to a silver(I) centre. The

resonances due to **j** and **i** in the uncomplexed [2]rotaxane both appear at 3.79 ppm but in the silver(I) complex shifts them upfield to 3.77 and 3.70 ppm respectively. The difference between the [2]rotaxane and the corresponding silver(I) complex was summarized in Table 6.5.

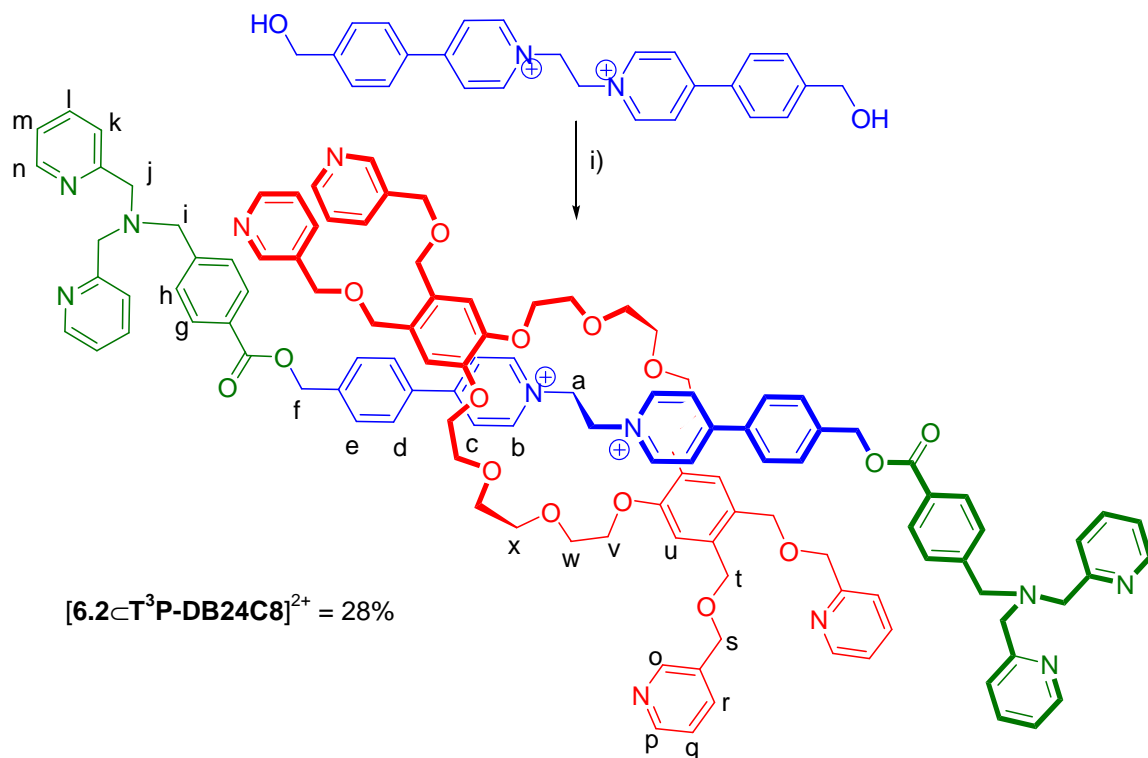
The coordination of Cd(II) with the **BPMA** results in a bis-ligand species with one Cd(II) coordinating to two **BPMA** ligands through the pyridyl and amine groups.<sup>12</sup> The <sup>1</sup>H NMR spectrum for the Cd(II) complex revealed downfield shifts of the protons **n-j**. Proton **n**, in complex [(Cd)<sub>x</sub>(**6.2-DB24C8**)]<sup>x+</sup> shifts from 8.48 ppm for the uncomplexed [2]rotaxane to 8.70 ppm when coordinated to a cadmium(II) centre. Proton **i**, in [(Cd)<sub>x</sub>(**6.2-DB24C8**)]<sup>x+</sup> shifts from 3.79 ppm for the uncomplexed [2]rotaxane, to 3.91 ppm when coordinated to the cadmium(II) centre. In addition, splitting of the methylene proton **j** from 3.79 ppm into downfield resonances at 3.76 and 4.13 ppm is observed upon complexation.

**Table 6.5** <sup>1</sup>H NMR chemical shifts for [2]rotaxane [**6.2-DB24C8**][OTf]<sub>2</sub> and complex [(Ag)<sub>x</sub>(**6.2-DB24C8**)]<sup>x+</sup> and [(Cd)<sub>x</sub>(**6.2-DB24C8**)]<sup>x+</sup> in CD<sub>3</sub>CN.

protons	[ <b>6.2-DB24C8</b> ] <sup>2+</sup>	[(Ag) <sub>x</sub> ( <b>6.2-DB24C8</b> )] <sup>x+</sup>	[(Cd) <sub>x</sub> ( <b>6.2-DB24C8</b> )] <sup>x+</sup>
<i>a</i>	5.44	5.43 (-0.01)	5.49 (0.05)
<i>b</i>	9.02	9.04 (0.02)	9.06 (0.04)
<i>c</i>	8.03	8.00 (-0.03)	8.14 (0.11)
<i>d</i>	7.65	7.62 (-0.03)	7.66 (0.01)
<i>e</i>	7.60	7.62 (0.02)	7.66 (0.06)
<i>f</i>	5.47	5.46 (-0.01)	5.49 (0.02)
<i>g</i>	7.94	7.94 (0.00)	7.97 (0.03)
<i>h</i>	7.60	7.48 (-0.12)	7.44 (-0.16)
<i>i</i>	3.79	3.70 (-0.09)	3.91 (0.12)
<i>j</i>	3.79	3.77 (-0.02)	4.13 (0.36), 3.76 (-0.03)
<i>k</i>	7.60	7.37 (-0.23)	7.53 (-0.07)
<i>l</i>	7.73	7.84 (0.11)	8.07 (0.34)
<i>m</i>	7.21	7.40 (0.19)	7.66 (0.45)
<i>n</i>	8.49	8.55 (0.06)	8.70 (0.21)
<i>o</i>	6.65	6.64 (-0.01)	6.66 (0.01)
<i>p</i>	6.53	6.50 (-0.03)	6.54 (0.01)

### 6.2.3 [2]Rotaxane ligand with donors on both the axle and wheel

The synthesis of a [2]rotaxane ligand with donor groups on *both* the axle and the wheel followed the same procedure as that used to prepare [6.2-DB24C8][OTf]<sub>2</sub> except that the crown used was **T<sup>3</sup>P-DB24C8**; Scheme 6.7. Some of the major <sup>1</sup>H NMR peaks are summarized in Table 6.6. The <sup>1</sup>H NMR spectrum of [6.2-T<sup>3</sup>P-DB24C8][OTf]<sub>2</sub> shows evidence supporting the various supramolecular interactions such as hydrogen bonding and  $\pi$ - $\pi$  stacking. Hydrogen-bonding between the ethylene (**a**) and  $\alpha$ -pyridinium (**b**) protons of the thread and the polyether oxygen atoms of the macrocycle is demonstrated by a downfield shift of the signals for **a** to 5.37 ppm, the shift of proton **b** to 9.02 ppm for [6.2-DB24C8][OTf]<sub>2</sub>.



Scheme 6.7 i) T<sup>3</sup>P-DB24C8, HCO<sub>2</sub>-BzBPMA, DCC, <sup>n</sup>Bu<sub>3</sub>P (cat.), MeCN for 72 h.

**Table 6.6**  $^1\text{H}$  NMR assignments for  $[\mathbf{6.2}][\text{OTf}]_2$ , and  $[\mathbf{6.2}\subset\text{T}^3\text{P-DB24C8}][\text{OTf}]_2$  in  $\text{CD}_3\text{CN}$ .

Protons	$[\mathbf{6.2}]^{2+}$	$[\mathbf{6.2}\subset\text{T}^3\text{P-DB24C8}]^{2+}$
<i>a</i>	5.11	5.37(0.26)
<i>b</i>	8.65	9.02(0.37)
<i>c</i>	8.33	8.02(-0.31)
<i>d</i>	7.98	7.55(-0.43)
<i>e</i>	7.73	7.70(-0.03)

The  $^1\text{H}$  NMR spectrum also shows changes for the wheel, which are summarized in Table 6.7. The differences occur at the singlet aromatic proton on the parent  $\text{T}^3\text{P-DB24C8}$  unit (**u**), and the benzylic protons (**t**). As mentioned, the free crown ether,  $\text{T}^3\text{P-DB24C8}$ , shows a singlet at 6.96 ppm for **u** but this singlet shifts upfield to 6.66 ppm ( $\Delta\delta = 0.30$  ppm) for  $[\mathbf{6.2}\subset\text{T}^3\text{P-DB24C8}]^{2+}$ . Also, the benzylic protons for the free crown ether show a singlet at 4.51 ppm but this singlet shifts downfield to 4.52 ppm ( $\Delta\delta = 0.01$  ppm). The ESI-MS of  $[\mathbf{6.2}\subset\text{T}^3\text{P-DB24C8}]^{2+}$  also confirmed the interlocked natures of the complex, with the loss of two counter ions resulting in observation of the parent ion  $[\mathbf{6.2}\subset\text{T}^3\text{P-DB24C8}]^{2+}$  at 980.4467 *m/e*.

**Table 6.7**  $^1\text{H}$  NMR assignments of  $\text{T}^3\text{P-DB24C8}$  and  $[\mathbf{6.2}\subset\text{T}^3\text{P-DB24C8}][\text{OTf}]_2$  in  $\text{CD}_3\text{CN}$ .

Protons	$\text{T}^3\text{P-DB24C8}$	$[\mathbf{6.2}\subset\text{T}^3\text{P-DB24C8}]^{2+}$
<i>o</i>	8.51	8.46(-0.05)
<i>p</i>	8.47	8.46(-0.01)
<i>q</i>	7.30	7.24(-0.06)
<i>r</i>	7.67	7.49(-0.18)
<i>s</i>	4.51	4.52(-0.01)
<i>t</i>	4.49	4.51(-0.02)
<i>u</i>	6.96	6.66(-0.30)

Upon coordination, it is possible that this new “combo” ligand rotaxane could form two independent frameworks, one created by linking axle to axle and another by linking of the wheels. Both of these metal ligand interactions have been observed in separate

systems containing only one of the donor sets. Figure 6.6 shows a schematic view of this concept.

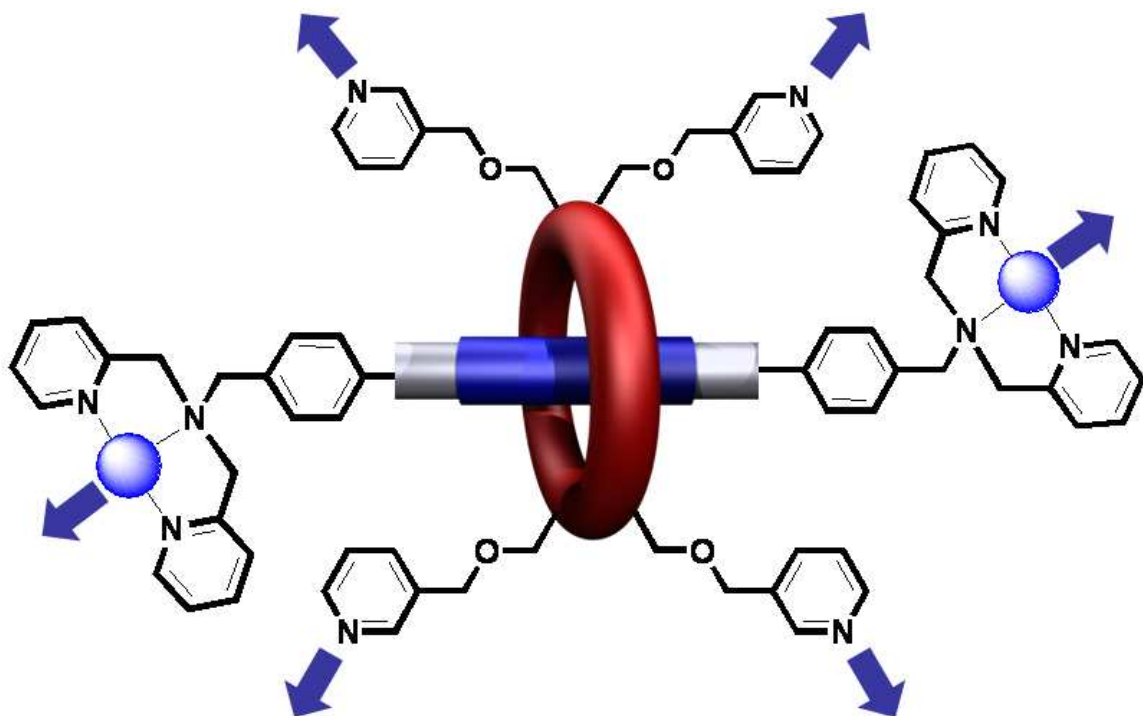


**Figure 6.6** Possible coordination of the “combo” rotaxane ligand.

### 6.3 Conclusion

An interlocked molecule with a new chelating group **BPMA** as a stopper was prepared and coordinated to a number of metals. Upon coordination to Mn(I) the ligand adopts a facial orientation around the metal as seen previously with related ligands of this type. The robust nature of this [2]rotaxane was confirmed by  $^1\text{H}$  NMR spectroscopy. The complex with Re(I) demonstrates a further example the “rotaxane as ligand” approach for preparing robust complexes that require harsh reactions conditions. The Ag(I) and Cd(II) complexes demonstrate the possibility of preparing coordination polymers.

The idea of creating a “combo” ligand rotaxane with donors appended to both axle and wheel was also presented and the successful preparation of such a ligand confirmed by  $^1\text{H}$  NMR spectroscopy and mass spectrometry. Future coordination studies on the

“combo” rotaxane ligand may provide solid state evidence that a MORF with independent networks derived from this design may be possible. To date, all attempts to grow X-ray quality crystals with different labile metal ions have failed.

## 6.4 Experimental

### 6.4.1 General Methods

Pyridine-2-carboxaldehyde, 2-aminomethylpyridine, NaBH<sub>4</sub>, triethylamine, methyl-*p*-(bromomethyl)benzoate, and AgOTf were purchased from Sigma-Aldrich and used as received. Re<sub>2</sub>(CO)<sub>10</sub> was obtained from Strem and used as received. Re(CO)<sub>5</sub>Br<sup>13</sup>, 1,2-bis(4-pyridine-4ylphenylmethanol)ethane<sup>9</sup> and [3.5][OTf]<sub>2</sub> were synthesized using literature methods. Solvents were dried using an Innovative Technology Solvent Purification System. <sup>1</sup>H NMR spectra were obtained on a Bruker Avance 500 instrument operating at 500 MHz. Deuterated solvents were purchased from Cambridge Isotope Laboratories Inc. and used as received. High-resolution mass spectra were recorded in 50/50 MeCN/H<sub>2</sub>O on a Micromass LCT Electrospray TOF mass spectrometer.

#### Synthesis **BPMA**

Pyridine-2-carboxaldehyde (8.0 g, 76.5 mmol) was dissolved in 30 mL of absolute ethanol in a 250 mL three-neck round bottom flask. 2-Aminomethylpyridine (8.27 g, 76.5 mmol) dissolved in 60 mL absolute ethanol and added dropwise via a constant addition funnel over a 15 min period to the carboxaldehyde solution. The reaction mixture was stirred for 30 min at room temperature. Sodium borohydride (5.80 g, 153 mmol) was then added to the solution. After complete addition, the reaction mixture was refluxed for 3 h and subsequently cooled in an ice bath and acidified to pH = 2 using 12M HCl. The white solid was filtered and the filtrate was evaporated to get rid of the ethanol. The resulting

oil was dissolved in 120 mL ethanol and 30 mL concentrated HCl and 70 mL diethyl ether was added. The clear solution was cooled in the freezer overnight, revealing white crystals. The crystals were filtered and dried, then dissolved in a minimal amount of H<sub>2</sub>O and made basic to pH = 10 by addition of 10% NaOH. The product was extracted with 3 x 20 mL of CH<sub>2</sub>Cl<sub>2</sub> and subsequently dried over anhydrous MgSO<sub>4</sub>. The CH<sub>2</sub>Cl<sub>2</sub> was removed by rotary evaporation to yield pale yellow oil. Yield = 9.62 g (65%)

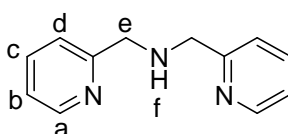


**Table 6.8** <sup>1</sup>H NMR spectroscopic data for **BPMA** in CDCl<sub>3</sub>

Proton	$\delta$ (ppm)	Multiplicity	# protons	J (Hz)
<i>a</i>	8.46	d	2	$J_{ab}^3 = 8.3$
<i>b</i>	7.07	dd	2	$J_{ba}^3 = 4.7, J_{bc}^3 = 7.0$
<i>c</i>	7.54	dd	2	$J_{cb}^3 = 1.6, J_{cd}^3 = 6.2$
<i>d</i>	7.27	d	2	$J_{dc}^3 = 6.5$
<i>e</i>	3.90	s	4	-
<i>f</i>	2.99	s	1	-

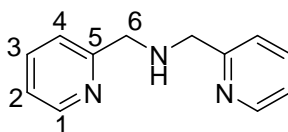


**Table 6.9** <sup>13</sup>C-NMR spectroscopic data for **BPMA** in CDCl<sub>3</sub>

Carbon	$\delta$ (ppm)
<i>1</i>	149.2
<i>2</i>	121.8
<i>3</i>	136.3
<i>4</i>	122.2
<i>5</i>	159.4
<i>6</i>	54.5

### Synthesis MeO<sub>2</sub>-BzBPMA

Triethylamine (0.69 mL, 5.00 mmol) was added to a solution of **BPMA** (1.0 g, 5.00 mmol) and methyl p-(bromomethyl)benzoate (1.15 g, 5.00 mmol) in THF (35 mL), and the mixture was refluxed for 2 h. The mixture was allowed to reach room temperature and filtered to remove a white precipitate. After removal of solvent under reduced pressure, the oily residue was redissolved in Et<sub>2</sub>O (40 mL) and filtered to remove a red solid. The Et<sub>2</sub>O was removed to yield orange oil. Yield = 1.49 g (85%)

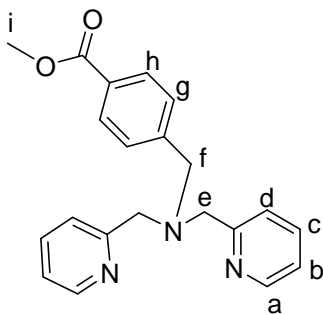


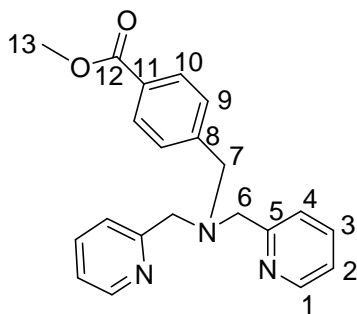
**Table 6.10** <sup>1</sup>H-NMR spectroscopic data for MeO<sub>2</sub>-BzBPMA in CDCl<sub>3</sub>

Proton	$\delta$ (ppm)	Multiplicity	# protons	J (Hz)
<i>a</i>	8.53	d	2	$J_{ab}^3 = 4.2$
<i>b</i>	7.16	dd	2	$J_{ba}^3 = 5.6, J_{bc}^3 = 6.7$
<i>c</i>	7.67	dd	2	$J_{cb}^3 = 7.7, J_{cd}^3 = 7.6$
<i>d</i>	7.56	d	2	$J_{dc}^3 = 7.9$
<i>e</i>	3.81	s	4	-
<i>f</i>	3.75	s	2	-
<i>g</i>	7.49	d	2	$J_{gh}^3 = 8.1$
<i>h</i>	7.99	d	2	$J_{hg}^3 = 8.1$
<i>i</i>	3.90	s	3	-



**Table 6.11**  $^1\text{H}$ -DMR spectroscopic data for **MeO<sub>2</sub>-BzBPMA** in CD<sub>3</sub>CN

Proton	$\delta$ (ppm)	Multiplicity	# protons	J (Hz)
<i>a</i>	8.47	d	2	$J_{ab}^3 = 4.2$
<i>b</i>	7.20	tt	2	$J_{ba}^3 = 5.6, J_{bc}^3 = 6.7$
<i>c</i>	7.69	dd	2	$J_{cb}^3 = 7.7, J_{cd}^3 = 7.6$
<i>d</i>	7.57	d	2	$J_{dc}^3 = 7.9$
<i>e</i>	3.75	s	4	-
<i>f</i>	3.73	s	2	-
<i>g</i>	7.54	d	2	$J_{gh}^3 = 8.1$
<i>h</i>	7.94	d	2	$J_{hg}^3 = 8.1$
<i>i</i>	3.92	s	3	-

**Table 6.12**  $^{13}\text{C}$ -NMR spectroscopic data for **MeO<sub>2</sub>-BzBPMA** in CDCl<sub>3</sub>

Carbon	$\delta$ (ppm)
<i>1</i>	149.5
<i>2</i>	122.1
<i>3</i>	136.5
<i>4</i>	122.8
<i>5</i>	159.3
<i>6</i>	60.1
<i>7</i>	58.2
<i>8</i>	144.5
<i>9</i>	128.7
<i>10</i>	129.6
<i>11</i>	128.9
<i>12</i>	167.0
<i>13</i>	52.0

Synthesis [Re(CO)<sub>3</sub>(MeCO<sub>2</sub>-BzBPMA)][OTf]

Under an inert atmosphere, AgOTf (0.139 g, 0.542 mmol) and Re(CO)<sub>5</sub>Br (0.200 g, 0.492 mmol) in methanol (1 mL) were heated to reflux for 60 min. The AgBr precipitate was removed by filtration through Celite. The MeCO<sub>2</sub>-BzBPMA (0.188 g, 0.542 mmol) was dissolved in methanol (5 mL) and the solution was refluxed for an additional 1 h. After cooling to room temperature, the solvent was removed in vacuo and the residue dissolved in a minimum of diethyl ether. The precipitate was filtered and recrystallized from CH<sub>3</sub>CN/Et<sub>2</sub>O. After standing for a day, a quantitative yield of brown solid [Re(CO)<sub>3</sub>(MeCO<sub>2</sub>-BzBPMA)][OTf] was obtained. **ESI-MS:** *m/z* [Re(CO)<sub>3</sub>(MeCO<sub>2</sub>-BzBPMA)]<sup>+</sup> calc. 618.1033, found 618.1031. IR(KBr)  $\nu$ (cm<sup>-1</sup>): 2029, 1949.

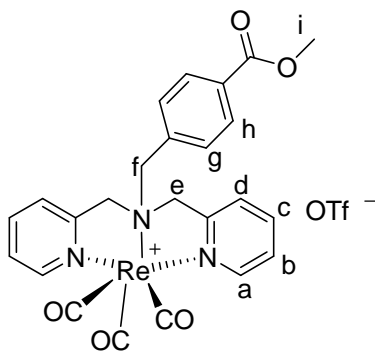
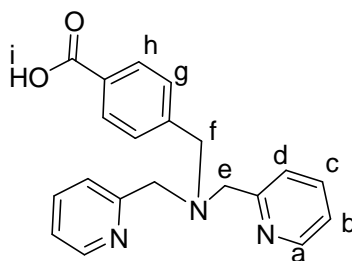


**Table 6.13** <sup>1</sup>H-NMR spectroscopic data for [Re(CO)<sub>3</sub>(MeCO<sub>2</sub>-BzBPMA)]<sup>+</sup> in CD<sub>3</sub>CN

Proton	$\delta$ (ppm)	Multiplicity	# protons	J (Hz)
<i>a</i>	8.78	d	2	$J_{ab}^3 = 5.3$
<i>b</i>	7.28	dd	2	$J_{ba}^3 = 6.0, J_{bc}^3 = 6.7$
<i>c</i>	7.83	dd	2	$J_{cb}^3 = 7.3, J_{cd}^3 = 7.6$
<i>d</i>	7.79	d	2	$J_{cd}^3 = 7.7$
<i>e</i>	4.93, 4.31	d	4	$J_{e,e'}^3 = 16.1$
<i>f</i>	4.97	s	2	-
<i>g</i>	7.34	d	2	$J_{gh}^3 = 7.7$
<i>h</i>	8.14	d	2	$J_{hg}^3 = 7.8$
<i>i</i>	3.92	s	3	-

### Synthesis **HCO<sub>2</sub>-BzBPMA**

A solution of NaOH (0.4 g, 20 mmol) in H<sub>2</sub>O (5 mL) was added to a solution **MeCO<sub>2</sub>-BzBPMA** (0.695 g, 2.0 mmol) in MeOH (20 mL), and the mixture was stirred for 2h at room temperature. The pH was adjusted to 7 by drop wise addition of 1M HCl (10 mL), followed by removal of the solvent under reduced pressure. The sticky white residue was stirred in CHCl<sub>3</sub> (100 mL), followed by filtration to remove NaCl. The CHCl<sub>3</sub> solution was dried with MgSO<sub>4</sub>. Yield: 0.534 g (80%).

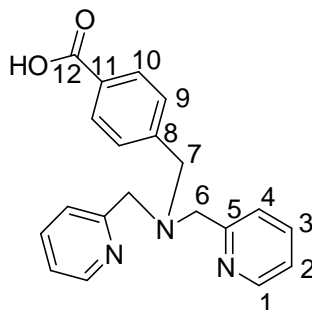


**Table 6.14** <sup>1</sup>H-NMR spectroscopic data for **HCO<sub>2</sub>-BzBPMA** in CDCl<sub>3</sub>

Proton	$\delta$ (ppm)	Multiplicity	# protons	J (Hz)
<i>a</i>	8.65	d	2	$J_{ab}^3 = 4.2$
<i>b</i>	7.23	tt	2	$J_{ba}^3 = 5.6, J_{bc}^3 = 6.7$
<i>c</i>	7.73	dd	2	$J_{cb}^3 = 7.7, J_{cd}^3 = 7.6$
<i>d</i>	7.64	d	2	$J_{dc}^3 = 7.9$
<i>e</i>	3.92	s	4	-
<i>f</i>	3.80	s	2	-
<i>g</i>	7.47	d	2	$J_{gh}^3 = 8.1$
<i>h</i>	8.02	d	2	$J_{hg}^3 = 8.1$

**Table 6.15**  $^1\text{H-NMR}$  spectroscopic data for **HCO<sub>2</sub>-BzBPMA** in CD<sub>3</sub>CN

Proton	$\delta$ (ppm)	Multiplicity	# protons	J (Hz)
<i>a</i>	8.47	d	2	$J_{ab}^3 = 4.2$
<i>b</i>	7.20	tt	2	$J_{ba}^3 = 5.6, J_{bc}^3 = 6.7$
<i>c</i>	7.69	dd	2	$J_{cb}^3 = 7.7, J_{cd}^3 = 7.6$
<i>d</i>	7.57	d	2	$J_{dc}^3 = 7.9$
<i>e</i>	3.75	s	4	-
<i>f</i>	3.73	s	2	-
<i>g</i>	7.54	d	2	$J_{gh}^3 = 8.1$
<i>h</i>	7.94	d	2	$J_{hg}^3 = 8.1$

**Table 6.16**  $^{13}\text{C-NMR}$  spectroscopic data for **HCO<sub>2</sub>-BzBPMA** in CDCl<sub>3</sub>

Carbon	$\delta$ (ppm)
<i>1</i>	148.5
<i>2</i>	122.5
<i>3</i>	137.2
<i>4</i>	123.6
<i>5</i>	158.6
<i>6</i>	59.1
<i>7</i>	58.0
<i>8</i>	142.7
<i>9</i>	129.1
<i>10</i>	130.8
<i>11</i>	130.0
<i>12</i>	169.3

Synthesis [6.2-DB24C8][OTf]<sub>2</sub>

[3.5][OTf]<sub>2</sub> (0.060 g, 0.105 mmol) was combined with **DB24C8** (0.141 g, 0.314 mmol), in acetonitrile (5 mL) and stirred over night. The reaction was cooled to 0 °C before **HCO<sub>2</sub>-BzBPMA** (0.140 g, 0.420 mmol) and DCC (0.173 g, 0.838 mmol) were added. <sup>n</sup>Bu<sub>3</sub>P (5 mol %) was added as a catalyst and the mixture was allowed to stir for 96 h at room temperature. The side-product was filtered. The solvent was removed under pressure and the product was stirred in toluene and isolated by filtration. Yield 0.090 g (59%). **ESI-MS**: *m/z* [6.2-DB24C8]<sup>2+</sup> calc. 738.3427, found 738.3438.

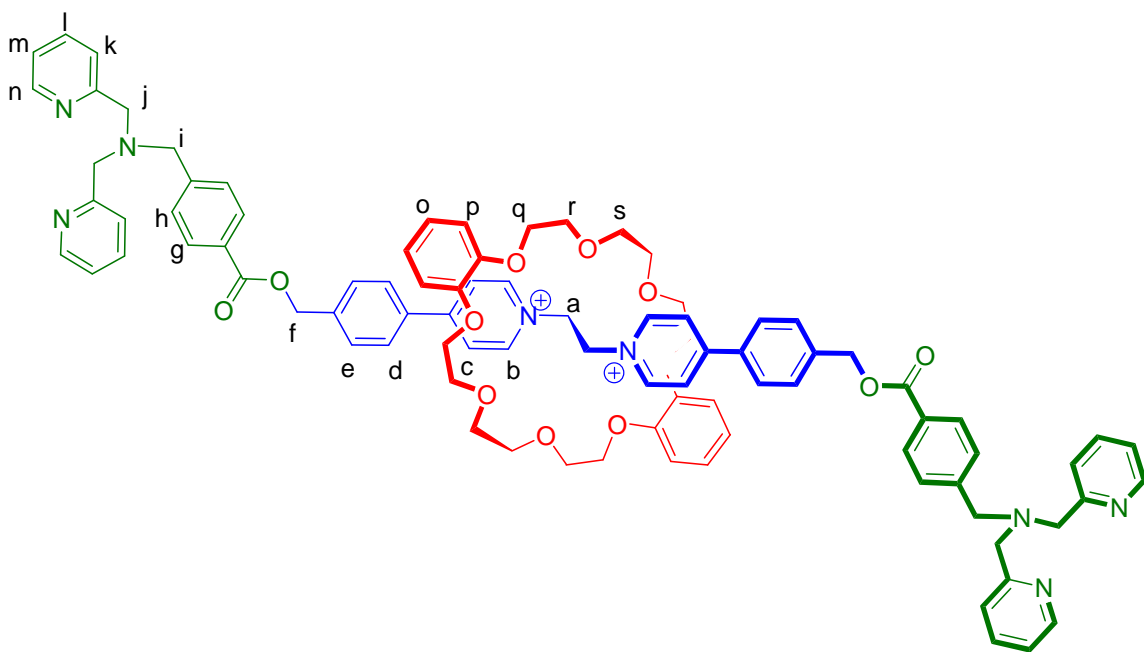


**Table 6.17**  $^1\text{H-NMR}$  spectroscopic data for  $[\mathbf{6.2-DB24C8}]^{2+}$  in  $\text{CD}_3\text{CN}$ 

Proton	$\delta$ (ppm)	Multiplicity	# protons	J (Hz)
<i>a</i>	5.45	s	4	-
<i>b</i>	9.04	d	4	$J_{bc}^3 = 6.5$
<i>c</i>	8.04	d	4	$J_{cb}^3 = 8.3$
<i>d</i>	7.65	d	4	$J_{de}^3 = 8.4$
<i>e</i>	7.60	m	4	-
<i>f</i>	5.47	s	4	-
<i>g</i>	7.94	d	4	$J_{gh}^3 = 6.4$
<i>h</i>	7.60	m	4	-
<i>i</i>	3.76	s	4	-
<i>j</i>	3.76	s	8	-
<i>k</i>	7.60	m	4	-
<i>l</i>	7.72	dd	4	$J_{lm}^3 = 7.7, J_{lk}^3 = 6.0$
<i>m</i>	7.24	m	4	-
<i>n</i>	8.49	d	4	$J_{nm}^3 = 4.1$
<i>o</i>	6.65	m	4	-
<i>p</i>	6.53	m	4	-
<i>q,r,s</i>	4.03-3.95	m	24	-

Synthesis  $[\mathbf{6.2}][\text{OTf}]_2$ 

$[\mathbf{3.5}][\text{OTf}]_2$  (0.060g, 0.105 mmol), the reaction was cooled to zero degrees before the addition of **HCO<sub>2</sub>-BzBPMA** (0.140 g, 0.420 mmol) and DCC (0.173 g, 0.838 mmol).  $^n\text{Bu}_3\text{P}$  (5 mol %) was added as a catalyst and the mixture was allowed to stir for 96 h at room temperature. The side-product was filtered. The solvent was removed under pressure and the product was stirred in hexanes. The solid was filtered, and stored in chloroform to remove any excess stopper leaving the capped thread as an off white solid. Yield 0.020 g (18%).

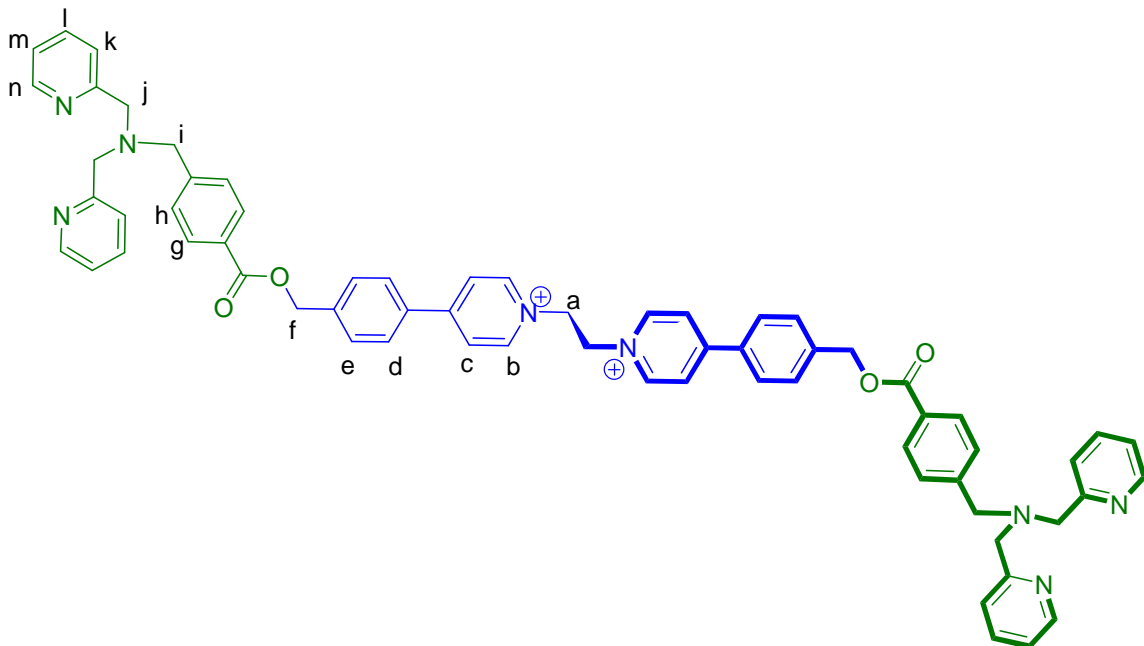


**Table 6.18**  $^1\text{H-NMR}$  spectroscopic data for  $[\mathbf{6.2}]^{2+}$  in  $\text{CD}_3\text{CN}$

Proton	$\delta$ (ppm)	Multiplicity	# protons	J (Hz)
<i>a</i>	5.15	s	4	-
<i>b</i>	8.84	d	4	$J^3_{bc} = 6.7$
<i>c</i>	8.31	d	4	$J^3_{cb} = 6.6$
<i>d</i>	7.96	d	4	$J^3_{de} = 8.5$
<i>e</i>	7.58	d	4	$J^3_{ed} = 6.3$
<i>f</i>	5.45	s	4	-
<i>g</i>	8.01	d	4	$J^3_{gh} = 8.3$
<i>h</i>	7.71	m	4	-
<i>i</i>	3.75	s	4	-
<i>j</i>	3.75	s	8	-
<i>k</i>	7.58	d	4	$J^3_{kl} = 6.3$
<i>l</i>	7.71	m	4	-
<i>m</i>	7.20	t	4	$J^3_{mn} = 3.8, J^3_{ml} = 7.3$
<i>n</i>	8.48	d	4	$J^3_{nm} = 3.2$

### Synthesis $[(\text{Re}(\text{CO}_3)_2)(\mathbf{6.2-DB24C8})][\text{OTf}]_4$

Under an inert atmosphere,  $\text{AgBF}_4$  (0.042 g, 0.218 mmol) and  $\text{Re}(\text{CO})_5\text{Br}$  (0.044 g, 0.109 mmol) in MeOH (1 mL) were heated to reflux for 60 min. The AgBr precipitate was removed by filtration through Celite. The  $[\mathbf{6.2-DB24C8}][\text{OTf}]_2$  (0.090 mg, 0.055 mmol) dissolved in methanol (5 mL) was added to the solution which was refluxed for an additional 1 h. After cooling to room temperature, the solvent was removed in vacuo and the residue dissolved in a minimum of diethyl ether and stirred for 30 min. The precipitate was filtered and recrystallized from  $\text{CH}_3\text{CN}/\text{Et}_2\text{O}$ . After standing for a day, a brown solid was isolated. Yield 0.130 g (98%). **ESI-MS:**  $m/z$   $[(\text{Re}(\text{CO}_3)_2)(\mathbf{6.2-DB24C8})]^{4+}$  calc. 504.6406, found 504.6402. IR(KBr)  $\nu(\text{cm}^{-1})$ : 2036, 1940.

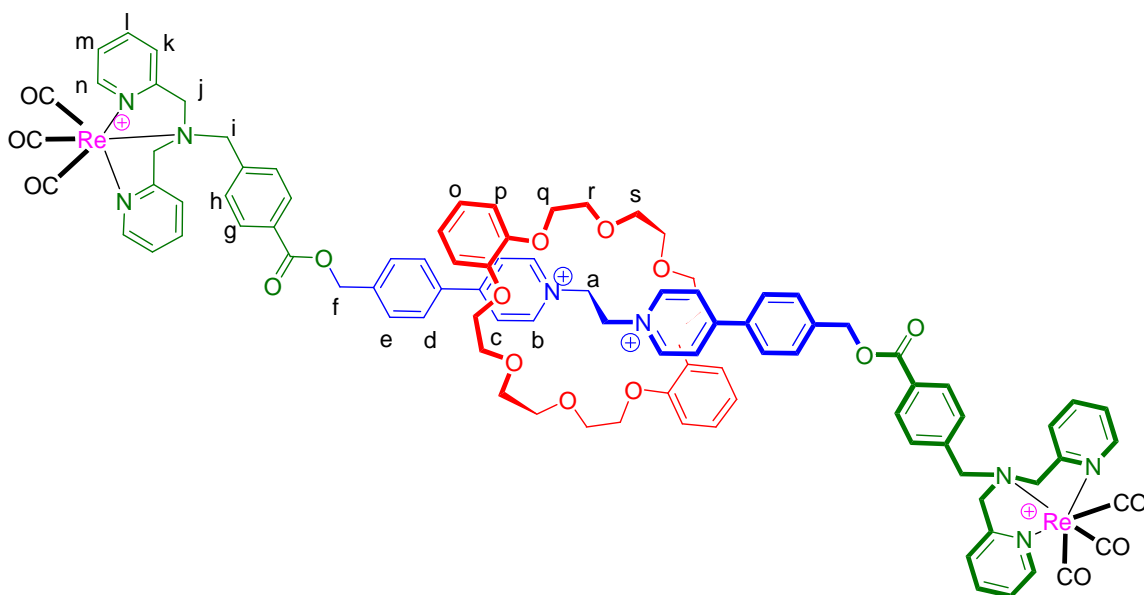




**Table 6.19**  $^1\text{H-NMR}$  spectroscopic data for  $[(\text{Re}(\text{CO}_3))_2(\mathbf{6.2-DB24C8})]^{4+}$  in  $\text{CD}_3\text{CN}$ 

Proton	$\delta$ (ppm)	Multiplicity	# protons	J (Hz)
<i>a</i>	5.50	s	4	-
<i>b</i>	9.06	d	4	$J_{bc}^3 = 6.7$
<i>c</i>	8.23	d	4	$J_{cb}^3 = 8.2$
<i>d</i>	7.69	d	4	$J_{de}^3 = 8.4$
<i>e</i>	7.65	d	4	$J_{ed}^3 = 8.4$
<i>f</i>	5.49	s	4	-
<i>g</i>	7.96	d	4	$J_{gh}^3 = 6.8$
<i>h</i>	7.34	m	4	-
<i>i</i>	4.99	s	4	-
<i>j</i>	4.94, 4.33	d	8	$J_{ij}^3 = 16.1$
<i>k</i>	7.83	m	4	-
<i>l</i>	7.83	m	4	-
<i>m</i>	7.27	m	4	-
<i>n</i>	8.78	d	4	$J_{nm}^3 = 5.0$
<i>o</i>	6.66	m	4	-
<i>p</i>	6.54	m	4	-
<i>q,r,s</i>	4.03-3.98	m	24	-

Synthesis  $[(\text{Re}(\text{CO}_3)_2)(\mathbf{6.2})][\text{OTf}]_4$ 

Under an inert atmosphere,  $\text{AgOTf}$  (0.030 g, 0.117 mmol) and  $\text{Re}(\text{CO})_5\text{Br}$  (0.024 g, 0.059 mmol) in  $\text{MeOH}$  (1 mL) were heated to reflux for 60 min. The  $\text{AgBr}$  precipitate was removed by filtration through Celite. The  $[\mathbf{6.2}][\text{OTf}]_2$  (0.020 g, 0.015 mmol) dissolved in  $\text{MeOH}$  (1 mL) and the solution was refluxed for an additional 1 h. After cooling to room temperature, the solvent was removed in vacuo and the residue dissolved in a minimum of diethyl ether and stirred for 30 min. The precipitate was filtered and recrystallized from  $\text{CH}_3\text{CN}/\text{Et}_2\text{O}$ . After standing for a day, a brown solid was isolated. Yield 0.030 g (98%). IR(KBr)  $\nu(\text{cm}^{-1})$ : 2035, 1917.

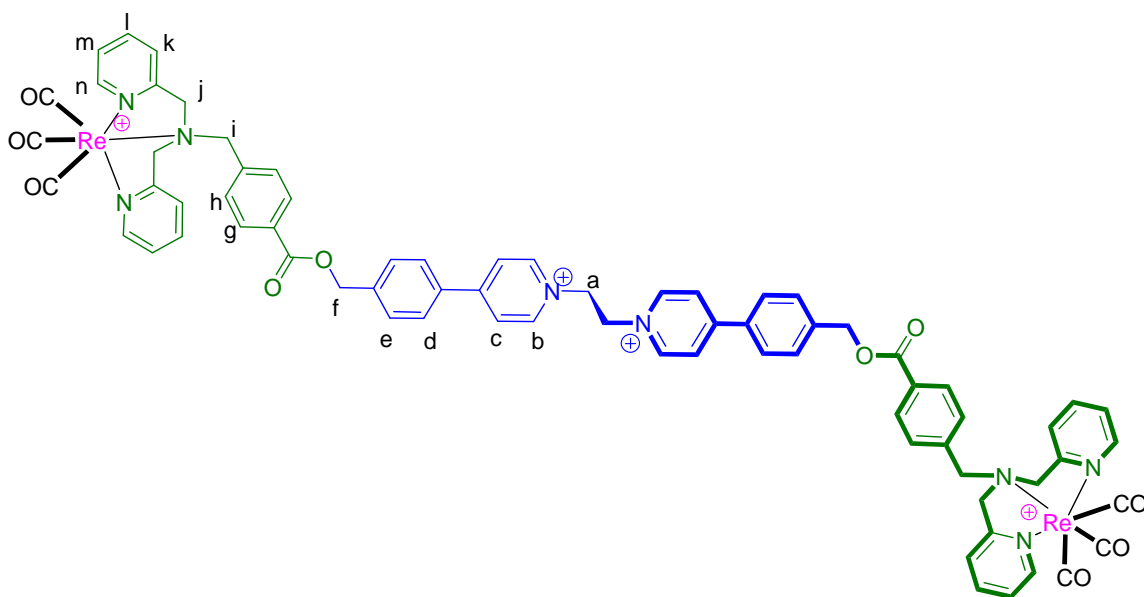


**Table 6.20**  $^1\text{H-NMR}$  spectroscopic data for  $[(\text{Re}(\text{CO})_2)(\mathbf{6.2})]^{4+}$  in  $\text{CD}_3\text{CN}$

Proton	$\delta$ (ppm)	Multiplicity	# protons	J (Hz)
<i>a</i>	5.12	s	4	-
<i>b</i>	8.79	d	4	$J_{bc}^3 = 5.1$
<i>c</i>	8.35	d	4	$J_{cb}^3 = 7.0$
<i>d</i>	8.01	d	4	$J_{de}^3 = 8.4$
<i>e</i>	7.77	d	4	$J_{ed}^3 = 8.4$
<i>f</i>	5.52	s	4	-
<i>g</i>	8.22	d	4	$J_{gh}^3 = 8.2$
<i>h</i>	7.82	m	4	-
<i>i</i>	4.98	s	4	-
<i>j</i>	4.93, 4.31	d	8	$J_{jj'}^3 = 16.1$
<i>k</i>	7.33	d	4	$J_{kl}^3 = 7.9$
<i>l</i>	7.82	m	4	-
<i>m</i>	7.28	dd	4	$J_{mn}^3 = 6.7, J_{ml}^3 = 6.5$
<i>n</i>	8.72	d	4	$J_{nm}^3 = 7.0$

Synthesis [(Ag)<sub>x</sub>(6.2-DB24C8)][OTf]<sub>x</sub>

To a solution of [6.2-DB24C8][OTf]<sub>2</sub> (0.030 g, 0.0148 mmol) dissolved in CH<sub>3</sub>CN (1 mL) was added AgOTf (9 mg, 0.0350 mmol) and the mixture stirred at room temperature overnight. Isopropyl ether was slowly diffused into the solution to give a yellow solid. Yield 0.130 g (98%).

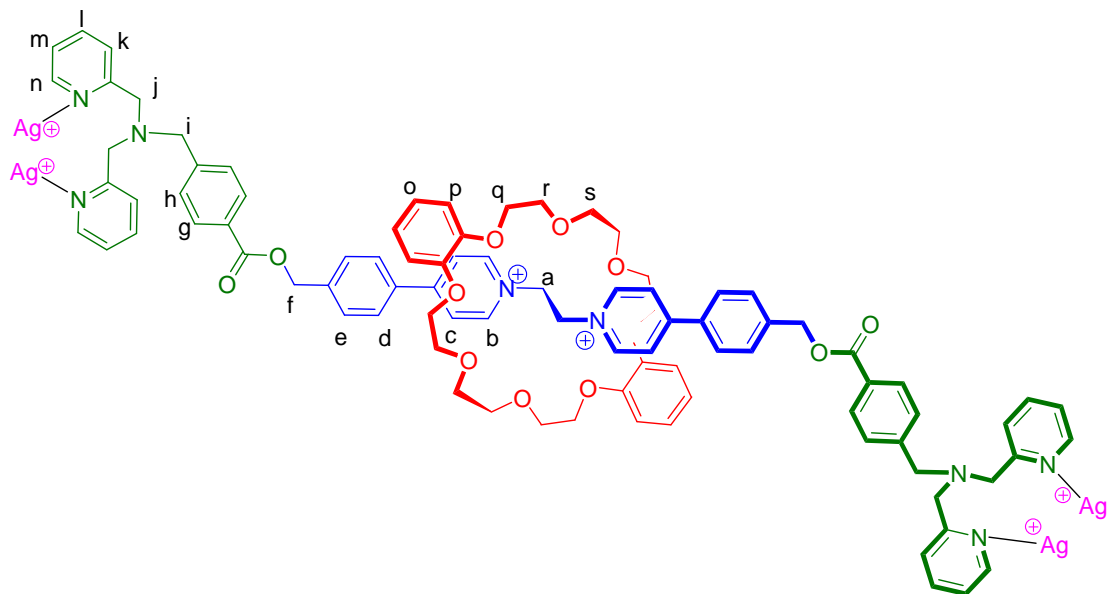


**Table 6.21**  $^1\text{H-NMR}$  spectroscopic data for  $[(\text{Ag})_x(\mathbf{6.2-DB24C8})]_x^+$  in  $\text{CD}_3\text{CN}$ 

Proton	$\delta$ (ppm)	Multiplicity	# protons	J (Hz)
<i>a</i>	5.43	s	4	-
<i>b</i>	9.04	d	4	$J_{bc}^3 = 6.9$
<i>c</i>	8.00	d	4	$J_{cb}^3 = 8.3$
<i>d</i>	7.62	m	4	-
<i>e</i>	7.62	m	4	-
<i>f</i>	5.46	s	4	-
<i>g</i>	7.94	d	4	$J_{gh}^3 = 6.9$
<i>h</i>	7.37	d	4	$J_{hg}^3 = 7.8$
<i>i</i>	3.70	s	4	-
<i>j</i>	3.77	s	8	-
<i>k</i>	7.48	d	4	$J_{kl}^3 = 8.3$
<i>l</i>	7.84	dd	4	$J_{lm}^3 = 7.7, J_{lk}^3 = 7.8$
<i>m</i>	7.40	m	4	-
<i>n</i>	8.55	d	4	$J_{nm}^3 = 4.2$
<i>o</i>	6.64	m	4	-
<i>p</i>	6.50	m	4	-
<i>q,r,s</i>	4.03-3.96	m	24	-

**Synthesis**  $[(\text{Cd})_x(\mathbf{6.2-DB24C8})][\text{OTf}]_x$ 

To a solution of  $[\mathbf{6.2-DB24C8}][\text{OTf}]_2$  (0.030 g, 0.020 mmol) dissolved  $\text{CH}_3\text{CN}$  (1 mL) was added to  $[\text{Cd}(\text{H}_2\text{O})_6][\text{BF}_4]_2$  (5 mg, 0.127 mmol) and the mixture stirred at room temperature overnight. Isopropyl ether was slowly diffused into the solution to give a yellow solid.

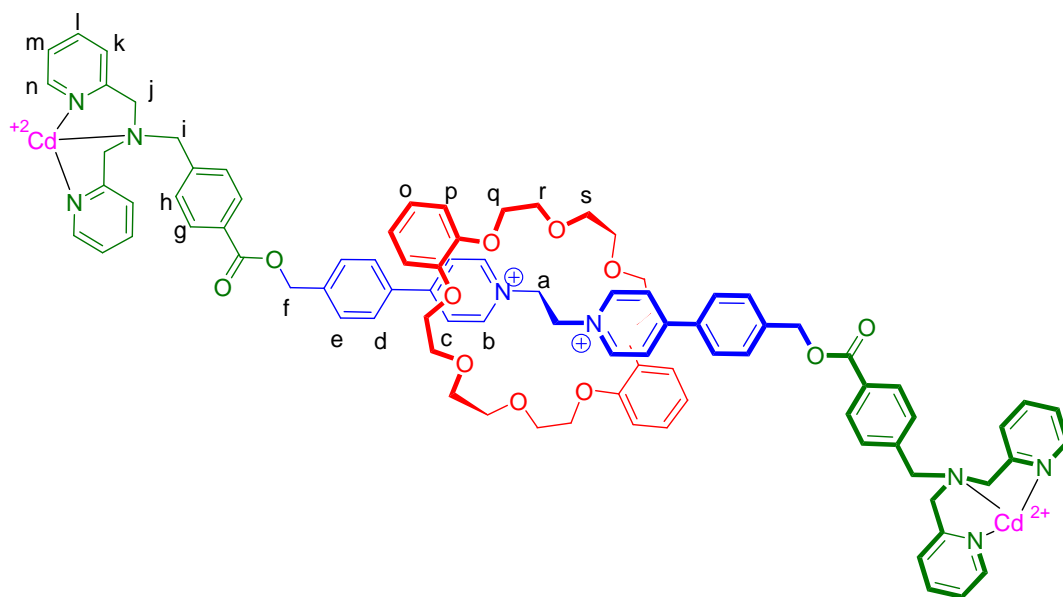


**Table 6.22**  $^1\text{H-NMR}$  spectroscopic data for  $[(\text{Cd})_x(\text{6.2-DB24C8})]_x^+$  in  $\text{CD}_3\text{CN}$

Proton	$\delta$ (ppm)	Multiplicity	# protons	J (Hz)
<i>a</i>	5.49	s	4	-
<i>b</i>	9.06	d	4	$J_{bc}^3 = 6.9$
<i>c</i>	8.14	d	4	$J_{cb}^3 = 8.3$
<i>d</i>	7.66	m	4	-
<i>e</i>	7.66	m	4	-
<i>f</i>	5.49	s	4	-
<i>g</i>	7.97	d	4	$J_{gh}^3 = 6.9$
<i>h</i>	7.44	d	4	$J_{hg}^3 = 7.8$
<i>i</i>	3.91	s	4	-
<i>j</i>	4.13, 3.76	s	8	$J_{ij}^3 = 15.7$
<i>k</i>	7.53	d	4	$J_{kl}^3 = 8.3$
<i>l</i>	8.07	dd	4	$J_{lm}^3 = 7.7, J_{lk}^3 = 7.8$
<i>m</i>	7.66	m	4	-
<i>n</i>	8.70	d	4	$J_{nm}^3 = 4.3$
<i>o</i>	6.66	m	4	-
<i>p</i>	6.54	m	4	-
<i>q,r,s</i>	4.04-3.98	m	24	-

Synthesis [6.2cT<sup>3</sup>P-DB24C8][OTf]<sub>2</sub>

[3.5][OTf]<sub>2</sub> (0.060 g, 0.105 mmol) was combined with T<sup>3</sup>P-DB24C8 (0.294 g, 0.315 mmol), in acetonitrile (5 ml) and stirred overnight. The reaction was cooled to zero degree before HCO<sub>2</sub>-BzBPMA (0.140 g, 0.420 mmol) and DCC (0.173 g, 0.838 mmol). <sup>n</sup>Bu<sub>3</sub>P (5 mol %) was added as a catalyst and the mixture was allowed to stir for 96 h at room temperature. The side-product was filtered. The solvent was removed under pressure and the product was stirred in ethyl acetate to remove the excess crown. The solid was filtered giving us the product as [6.2cT<sup>3</sup>P-DB24C8][OTf]<sub>2</sub> adducted. Yield 0.093g (28%). **ESI-MS:** *m/z* [6.2cT<sup>3</sup>P-DB24C8]<sup>2+</sup> calc. 980.4467, found 980.4487.

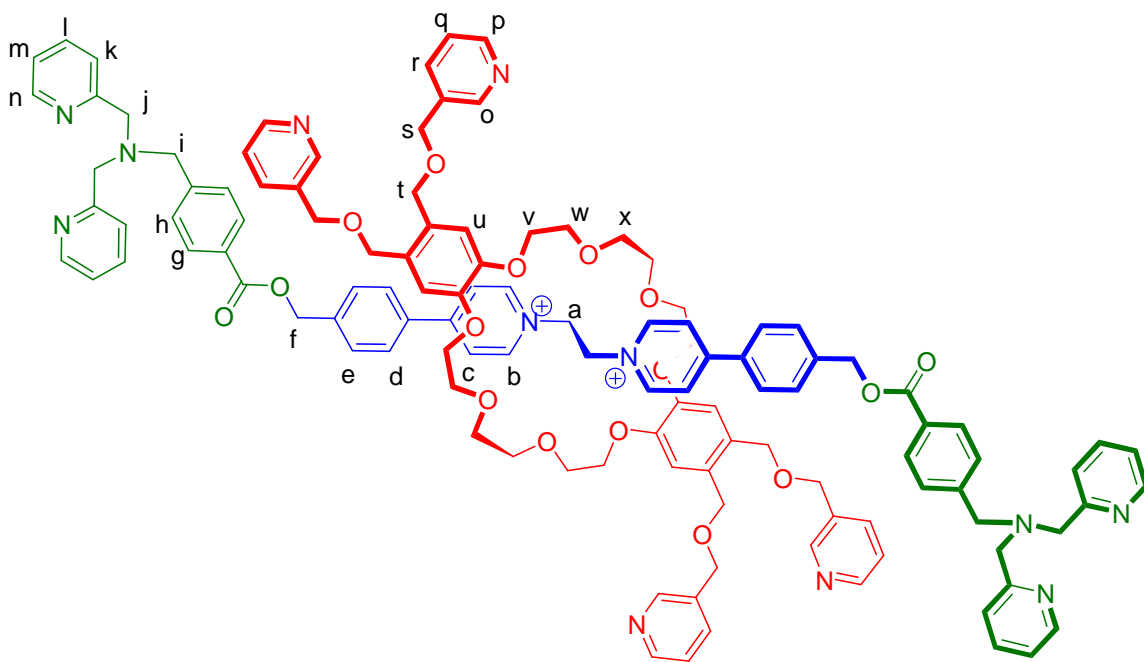


**Table 6.23**  $^1\text{H-NMR}$  spectroscopic data for  $[\text{6.2-C}^{\text{T}^3\text{P-DB24C8}}]^{2+}$  in  $\text{CD}_3\text{CN}$

Proton	$\delta$ (ppm)	Multiplicity	# protons	J (Hz)
<i>a</i>	5.37	s	4	-
<i>b</i>	9.02	d	4	$J^3_{bc} = 6.9$
<i>c</i>	8.02	d	4	$J^3_{cb} = 8.7$
<i>d</i>	7.55	m	4	-
<i>e</i>	7.69	m	4	-
<i>f</i>	5.44	s	4	-
<i>g</i>	7.92	d	4	$J^3_{gh} = 6.9$
<i>h</i>	7.55	m	4	-
<i>i</i>	3.72	s	4	-
<i>j</i>	3.72	s	8	-
<i>k</i>	7.55	m	4	-
<i>l</i>	7.69	m	4	-
<i>m</i>	7.21	m	4	-
<i>n</i>	8.48	m	4	-
<i>o</i>	8.48	m	4	-
<i>p</i>	8.48	m	4	-
<i>q</i>	7.25	m	4	-
<i>r</i>	7.49	d	4	$J^3_{rg} = 8.6$
<i>s</i>	4.52	s	4	-
<i>t</i>	4.51	s	8	-
<i>u</i>	6.66	s	4	-
<i>v,w,x</i>	3.77-3.71	m	24	-

**Reference:**

1. Mercer, D. J.; Loeb, S. J. *Dalton Trans.* **2011**, 40, 6385.
2. Gonzalez, D.; Kovivisto, B. D.; Leigh, D. A. *Chem. Commun.*, **2007**, 4218.
3. Larsen, S.; Michelsen, K.; Pedersen, E. *Acta Chem. Scand. A*, **1986**, 40, 63.
4. a) Staversen, D. R.; Bothe, E.; Weyhermuller, T.; Motzler-Nolte, N. *Eur. J Inorg. Chem.* **2002**, 1518. b) Kirin, S. I.; Dubon, P.; Weyhermuller, Y.; Bill, E.; Motzler-Nolte, N. *Inorg. Chem.* **2005**, 44, 5405
5. a) Bebout, D. C.; Stokes, S. W.; Butcher, R. J. *Inorg Chem.* **1999**, 38, 1126. b) Bebout, D. C.; DeLanoy, A. E.; Ehmann, D. E.; Kastner, M. E.; Parrish, D. A.; Butcher, R. J. *Inorg. Chem.* **1998**, 37, 2952. c) Glerup, J.; Goodson, P. A.; Hodgson, D. J.; Michelsen, K.; Nielsen, K. M.; Weible, H. *Inorg. Chem.* **1992**, 31, 4611. d) Jenkins, H. A.; Yap, G. P. A.; Puddephatt, R. J. *Organometallics* **1997**, 16, 1946. e) Mola, J.; Romero, I.; Rodriguez, M.; Bozoglian, F.; Poater, A.;

- Sola, M.; Parella, T.; Benet-Buchholz, J.; Fontrodona, X.; Llobet, A. *Inorg. Chem.* **2007**, *46*, 10707.
6. Kunz, P. C.; Bruckmann, N. E.; Spingler, B. *Eur. J. Inorg. Chem.* **2007**, 394.
  7. a) Mullice, L. A.; Laye, R. H.; Harding, L. P.; Buurma, N. J.; Pope, S. J. A. *New J. Chem.* **2008**, *32*, 2140. b) Moore, A. L.; Bucar, D. K.; MacGillivray, L. R.; Benny, P. D. *Dalton Trans.* **2010**, *39*, 1926. c) Patra, M.; Gasser, G.; Bobukhov, D.; Merz, K.; Shtemenko, A. V.; Motzler-Nolte, N. *Dalton Trans.* **2010**, *39*, 5617.
  8. Mercer, D. J. W.; Vella, S. J.; Guertin, L.; Sudan, N. D.; Tiburico, J.; Vukotic, N.; Wisner, J. A.; Loeb, S. J. *Eur. J. Org. Chem.* **2011**, *9*, 1763.
  9. Makita, Y.; Kihara, N.; Takata, T. *Chem. Lett.* **2007**, *36*, 102.
  10. Piero, S. D.; Fedele, R.; Melchior, A.; Portanova, R.; Tolazzi, M.; Zangrando, E. *Inorg. Chem.* **2007**, *46*, 4683. b) Mercer, D. J.; Jenkins, H. A. *Inorg. Chem. Acta* **2007**, *360*, 3091.
  11. Piero, S. D.; Bernardo, P. D.; Fedele, R.; Melchior, A.; Polese, P.; Tolazzi, M. *Eur. J. Inorg. Chem.* **2006**, 3738.
  12. Schmidt, S. P.; Trogler, W. C.; Basolo, F. *Inorg. Synth.* **1990**, *28*, 160.



# Chapter 7

## Future Directions

The build up of the whole thesis has to lead to the development of new so-called “combo” rotaxane ligands. From the initial studies involving ligands as stoppers and appending ligand groups to crown ethers, the idea of being to form a “double” set of independent frameworks appears, at least, plausible. Even though there are many different possible coordination outcomes using  $[6.2\text{-T}^3\text{P-DB24C8}][\text{OTf}]_2$  as a ligand, the most likely metal-ligand self-assembly interactions are those that link axle to axle and wheel to wheels as pictured in Figure 7.1.

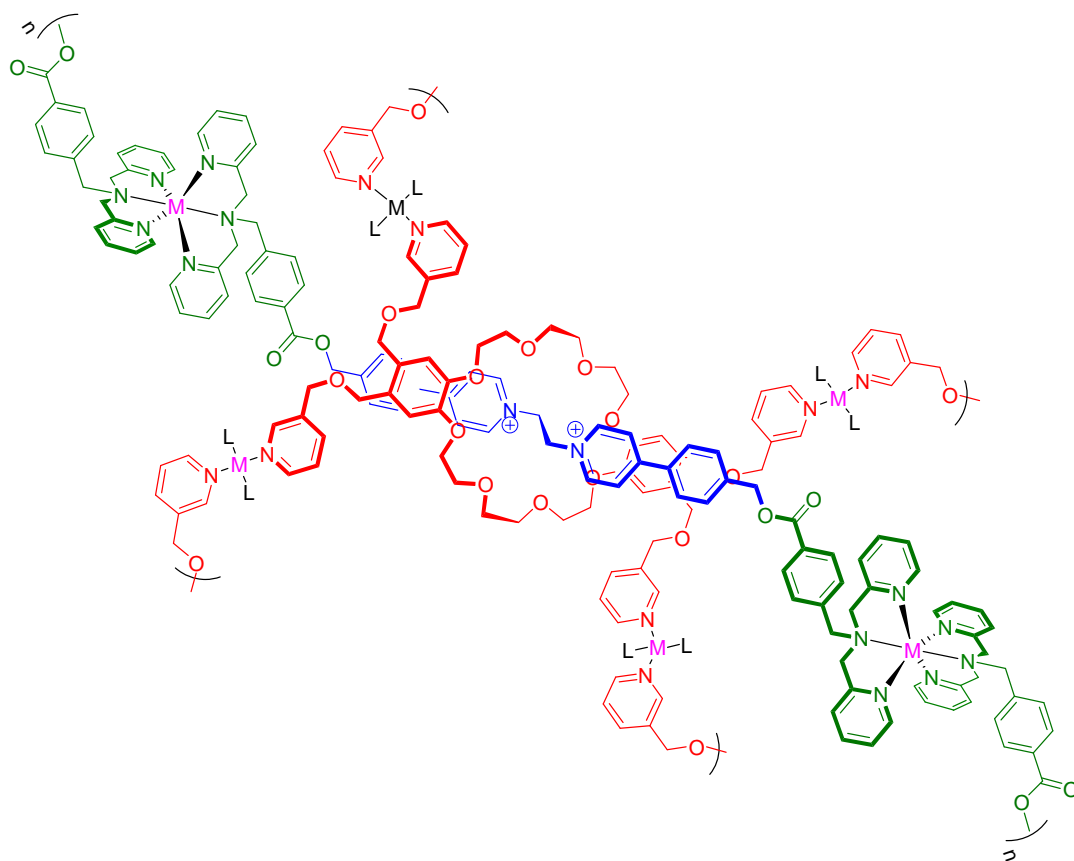


**Figure 7.1** Possible “double” network that  $[6.2\text{-T}^3\text{P-DB24C8}][\text{OTf}]_2$  will form upon coordination where  $M = \text{Cd(II)}$  or  $\text{Ag(I)}$ .

Besides using nitrogen based donors there are many different donors available such as sulfur donors that can be used in the construction of MORFs; Figure 7.2, where R is any aryl or alkyl group, and R' being a bulky aryl group that can as a stopper.

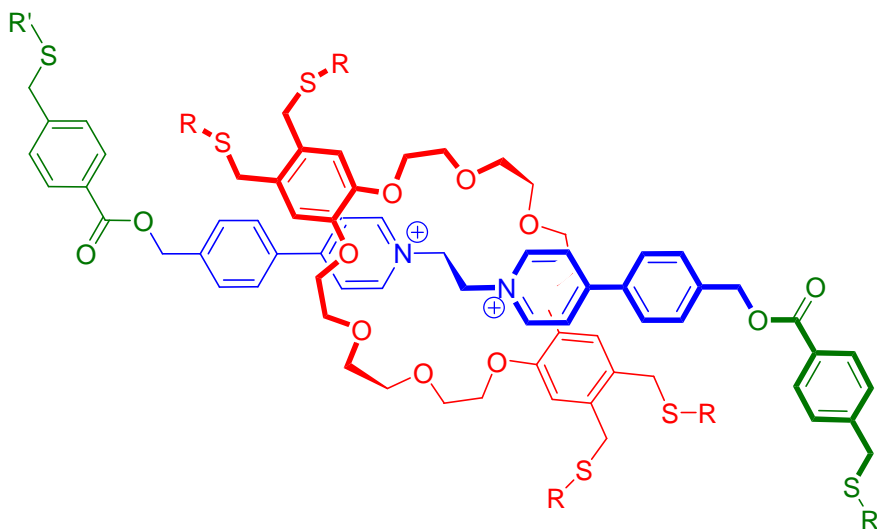


**Figure 7.2** Sulfur donor “combo” rotaxane ligand.

Besides just forming the “combo” rotaxane ligand with the same donor ligands, we could mix and match the donor ligands with each other; Figure 7.3.

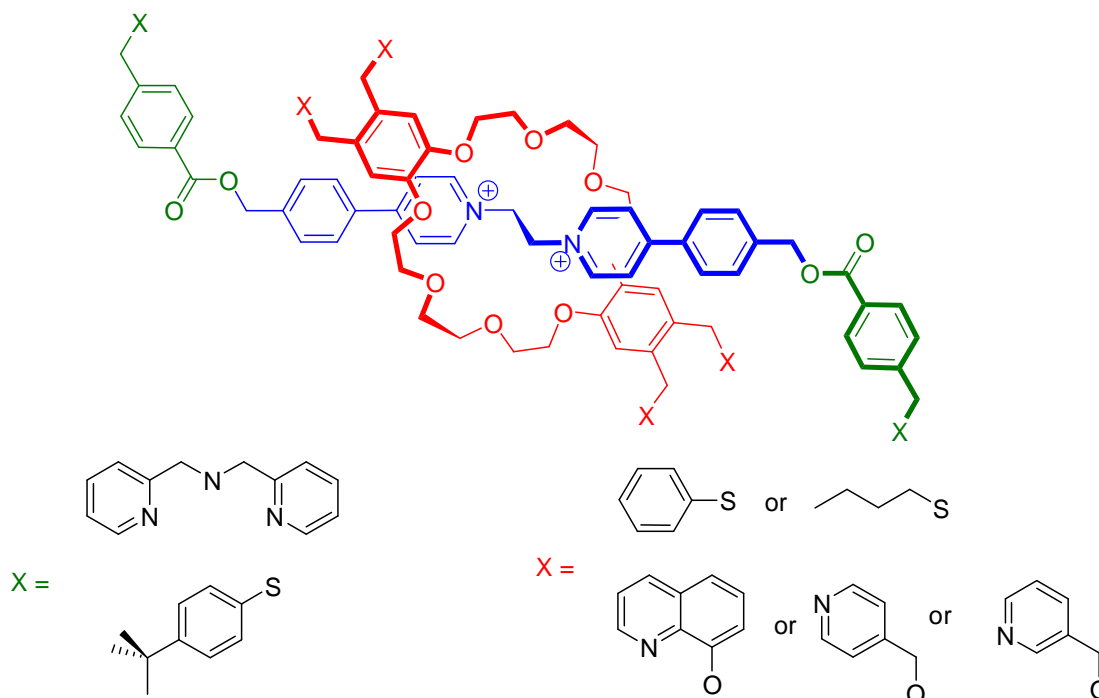


**Figure 7.3** Possible mixed donor [2]rotaxane system that could be made.

The generation of a mixed donor “combo” rotaxane ligand may allow for the generation of mixed metal MORF by considering the hardness and softness of the donors and metals.

## Vita Auctoris

Name	Darren J. W. Mercer
Date of Birth	August, 1982
Place of Birth	Carbonear, Newfoundland, Canada
Citizenship	Canadian
Education	Ph. D., Chemistry, 2011 University of Windsor Windsor, Ontario, Canada  B. Sc., Honours: Chemistry Co-op, 2005 Saint Mary's University Halifax, Nova Scotia, Canada
Professional Work History	Research Assistant University of Windsor, Windsor, Ontario, Canada Sept., 2005 – present  Teaching Assistant University of Windsor, Windsor, Ontario, Canada Sept., 2005 – present  Research Assistant Saint Mary's University, Halifax, Nova Scotia, Canada Sept., 2004 – Aug., 2005
Scholarships and Awards	90th Canadian Society for Chemistry Conference Inorganic Division Graduate Student Poster Prize (2007)  University of Windsor Tuition Scholarship (2005-2006)  William A Redmond Bursary (2006)
Publications	Darren. J. W. Mercer and Stephen J. Loeb “Complexes of [2]rotaxane ligand with terminal terpyridine groups”, <i>Dalton Trans.</i> , <b>2011</b> , 40, 6385.  Darren J. Mercer, Sarah J. Vella, Lianne Guertin, V. Nicholas Vukotic and Stephen J. Loeb “Rotaxane based on the 1,2-bis(pyridinio)ethane -24-crown-8 Templating Motif”, <i>Eur. J. Org. Chem.</i> <b>2011</b> , 2011(9), 1763-1770.

- Darren J. W. Mercer, V. Nicholas Vukotic and Stephen J. Loeb, "Linking [2]rotaxane wheels to create a new type of metal organic rotaxane Framework" *Chem. Commun.* **2011**, 47(3), 896-898.
- Darren. J. W. Mercer and Stephen J. Loeb "Metal-based Anion Receptors: An Application of Second-sphere Coordination" *Chem. Soc. Rev.* **2010**, 39(10), 3612-3620. Special issue
- Darren J. W. Mercer and Hilary A. Jenkins, "Cationic ligands for Ag(I): Organometallic polymers versus unimolecular complexes" *Inorg. Chim. Acta.*, **2007**, 360(9), 3091-3098.
- Conference Presentation "Effect of Substituted Crown Ethers in the Synthesis of Metal Organic Rotaxane Frameworks" Darren J. Mercer, S. J. Loeb, 1<sup>st</sup> French/Canadian Workshop in Supramolecular Chemistry Montreal QC/Paris, Fr, July 15 – July 17, 2009.
- "Chelating Crown Ethers in the Synthesis of Metal Organic Rotaxane Framework (MORF)s" Darren J. Mercer, S. J. Loeb, 92<sup>nd</sup> CSC Hamilton, ON, May 30 – June 3, 2009.
- "Metal Organic Rotaxane Framework (MORF)s" Darren J. W. Mercer, G. J. E. Davidson, D. J. Hoffart, S. J. Loeb 41<sup>st</sup> IDW St. Catharine's, ON, Nov. 28 – 30, 2009.
- Conference Posters "New Metal-Organic Rotaxane Framework; the *Inverse* Approach to *i*-MORFs" Darren J. Mercer, S. J. Loeb 43<sup>rd</sup> IDW Windsor, ON, Nov. 5 – Nov. 7, 2010.
- "Rotaxanes containing Functional Crown Ethers: The Synthesis of *Inverse* Metal-Organic Rotaxane Frameworks (*i*-MORF)" Darren J. Mercer, S. J. Loeb 93<sup>rd</sup> CSC Toronto, ON, May29-June 2, 2010.
- "Templating New Metal Organic Rotaxane Framework (MORFs) with Substituted Crown Ethers" Darren J. W. Mercer, S. K. Loeb, S.J. Loeb 91<sup>st</sup> CSC Edmonton, AB, May 24 – 28, 2008.
- "Substituted Crown Ethers for Building [2]Rotaxanes and Metal Organic Rotaxane Frameworks (MORFs)" Darren J. W. Mercer, S. J. Loeb. 40<sup>th</sup> IDW Toronto, ON, Nov 2 – 4, 2007.
- "Substituted Crown Ethers for Building Metal Organic Rotaxane Frameworks (MORFs)" Darren J. W. Mercer, S. J. Loeb 90<sup>th</sup> CSC Winnipeg, MB, May 26 – 30, 2007 (Graduate Student Poster Prize).

“New Rotaxane Linkers for Metal Organic Rotaxane Frameworks (MORFs)” Darren J. W. Mercer, S. J. Loeb 89<sup>th</sup> CSC Conference Halifax, NS, May 27 – 31, 2006.